

PENETRANT TRANSPORT IN COAL NETWORK STRUCTURES  
BETWEEN 35°C AND 150°C

Jorge M. Olivares and Nikolaos A. Peppas\*  
School of Chemical Engineering  
Purdue University  
West Lafayette, Indiana 47907

Keyword: coal network, penetrant transport, Case-II transport

## INTRODUCTION

The dynamics of penetrant swelling of macromolecular coal systems can provide important information about the structure of the coal itself and its interactions with vapors and liquids. For example, it is possible to identify the thermodynamic state of the coal network. Inflections or dips in the time-sorption curve may be attributed to specific relaxations of the macromolecular coal system. If the coal is in the glassy state, one can determine whether the sorption is due to Fickian diffusion and/or due to relaxations of the macromolecular coal chains and estimate values of the diffusion coefficient and of the relaxation constants.

Increased concentration of penetrant in a macromolecular coal system has the same effect as increase of the temperature. As sorption continues, the density of the coal decreases thus allowing increased bond rotations and mobility. In addition, the favorable energetics involved in sorption provide the energy required for motion. Thus the glass transition temperature is lowered by the presence of the penetrant.

In previous work from our laboratory (1-7) we have examined the mechanism of penetrant transport in coal networks at low temperatures using pyridine (1-6) and various other amines (7). We have concluded that at low temperature (below 50°C) the mechanism of pyridine transport is non-Fickian or Case-II and that the size of the samples tested may shift the overall coupling of the diffusional and relaxational mechanisms.

Analysis of the sorption data can be accomplished by various means. For example, a convenient method of analysis involves fitting of the sorption data (4) to the empirical equation,

$$\frac{M_t}{M_\infty} = kt^n \quad (1)$$

Here,  $M_t$  is the mass of solvent imbibed at time  $t$ ,  $M_\infty$  is the mass of solvent imbibed at long times, and  $k$  is a constant which depends on the structural characteristics of the material and on the solvent/material interactions. The exponent,  $n$ , is used to indicate the type of diffusion and to infer state changes in the macromolecular systems. For a thin slab, when  $n$  equals 0.5, the diffusion is Fickian. When  $n$  is 1.0, Case II transport occurs. Finally, values of  $n$  between 0.5 and 1.0 indicate anomalous transport. If  $n > 1.0$ , the swelling material is likely to craze and fracture due to the tremendous osmotic pressure differences at the accelerating and advancing front. This type of transport mechanism is known as Super Case II transport.

\* Correspondence

Up to now only one research contribution from our laboratory (8) has examined the change in temperature as a method to decouple the diffusion and relaxation phenomena. In the present work we examine the transport of various penetrants in coal sections at moderate temperatures.

## EXPERIMENTAL PART

Coal samples were supplied by the Pennsylvania State University Coal Bank (PSU). Table 1 includes pertinent information provided by PSU for the coals used in this investigation.

Table 1. Analysis of Coal Samples Used

PSOC Code No.	County, State	Rank	%C (dmmf)	%H (dmmf)	%MM (dry)
418	Titus, TX	LigA	69.9	6.1	27.5
791	Titus, TX	LigA	72.2	5.3	20.7
247	Burke, ND	LigA	75.5	4.8	12.7
312	Navajo, AR	HVC	78.3	5.7	7.5
853	Delta, CO	HVC	80.1	5.0	3.7
402	Craig, OK	HVA	82.4	5.6	18.4
341	Jefferson, PA	HVA	86.0	5.7	14.5
384	Sullivan, PA	SAn	94.1	3.5	24.1

The techniques presented here for preparing uncontaminated thin section specimens of coal are based on the method of preparation employed by Brenner (9). Uncontaminated coal samples were prepared using a paraffin-based adhesive which could be completely removed from the sample. A chunk of coal was ground flat in a direction parallel to the geographic bedding plane on a horizontal diamond grinding wheel using progressively finer diamond grits. The flat surface of the coal was then heat cemented to a pre-conditioned microscope slide. When the hexane-soluble, paraffin-based, thermoplastic adhesive (Paraplast, American Scientific Products) had hardened, the coal chunk was cut with a diamond saw leaving approximately a two millimeter thick slab of coal mounted on the glass slide. The slab was then ground using a vertical diamond grinding wheel to the desired final thickness. The thin section specimens of coal were removed from the glass slide by soaking in n-hexane for several hours. Hexane did not swell the coal sample. After a few days of immersion, the solvent was removed, the samples were oven-dried at 60°C and stored in a dry nitrogen atmosphere at room temperature until use. The uncontaminated samples obtained ranged in thickness from 100  $\mu\text{m}$  to 1500  $\mu\text{m}$ . Thin coal sections, 200  $\mu\text{m}$  to 1200  $\mu\text{m}$  thick, of 1 mg to 10 mg were dried and cut in squares. They were introduced to one of the chambers of a thermogravimetric analyzer (TGS-2, Perkin Elmer, Norwalk, Connecticut) and the whole system was calibrated. The electrobalance system of the TGS-2 was purged with a continuous stream of nitrogen passing through three traps filled with N,N-dimethyl formamide (DMF) or pyridine. By adjusting the flow rate of nitrogen it was possible to control the evaporation rate of DMF or pyridine and, therefore, the ratio in the gaseous phase. Therefore, it was possible to conduct dynamic DMF uptake experiments at different activities. In addition, because of the microfurnace available in the thermogravimetric system, it was possible to carry out experiments at various temperatures.

## RESULTS AND DISCUSSION

Selected data of pyridine and DMF uptake as a function of time and temperature are presented in Figures 1 through 6. In all cases, the diffusion time has been normalized with respect to the square of the sample thickness,  $t/l^2$ . In addition, all graphs present the amount of penetrant adsorbed per gram of dry coal,  $M_t/M_c$ .

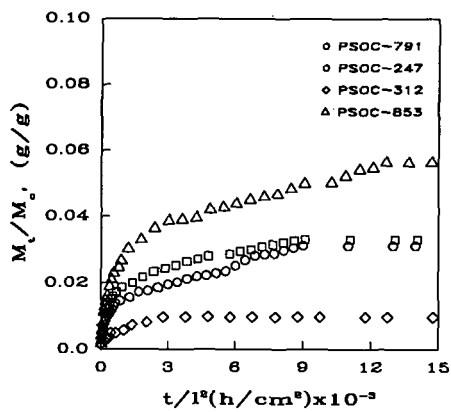


Fig. 1. Pyridine uptake in thin coal sections at 35°C.

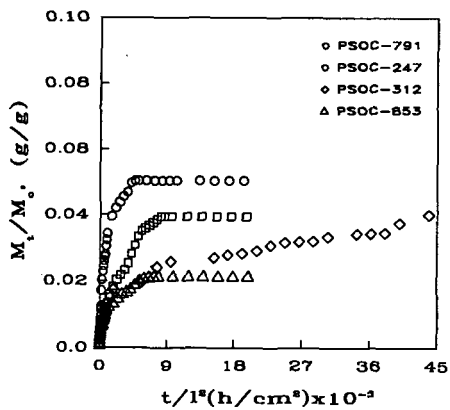


Fig. 2. Pyridine uptake in thin coal sections at 100°C.

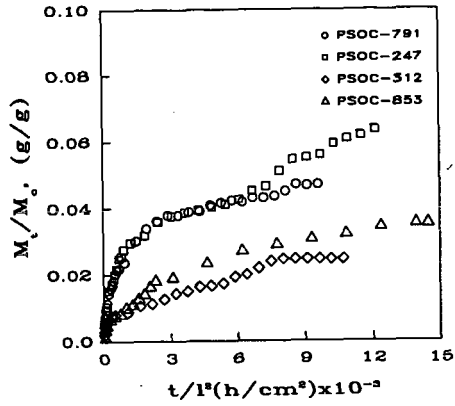


Fig. 3. Pyridine uptake in thin coal sections at 150°C.

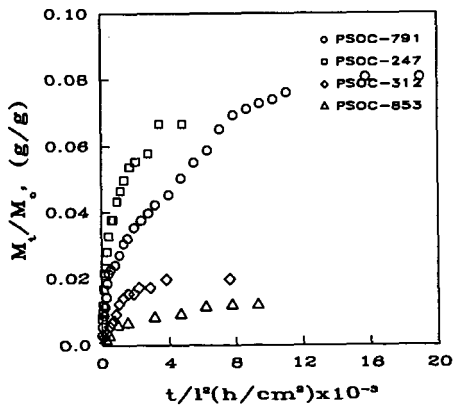


Fig. 4. DMF uptake in thin coal sections at 35°C.

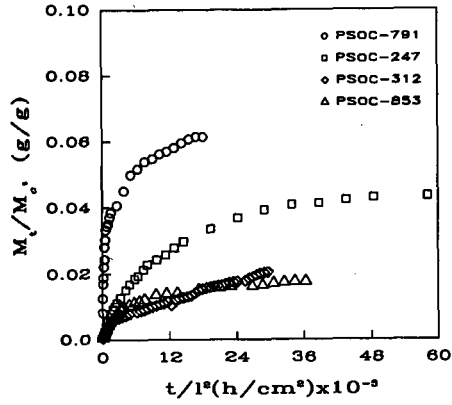


Fig. 5. DMF uptake in thin coal sections at 100°C.

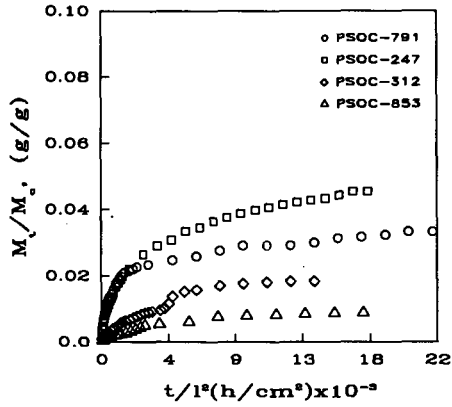


Fig. 6. DMF uptake in thin coal sections at 150°C.

These results were analyzed using equation (1) and the value of k and n are reported in Tables 2 and 3, respectively.

Table 2  
Analysis of Pyridine Uptake by Coal Samples Using Equation (1)

PSOC	Temperature (°C)	n	95% CI for n	k	95% CI for k
791	35	0.42	0.06	$8.6 \times 10^{-4}$	$2.3 \times 10^{-4}$
247	35	0.56	0.05	$4.3 \times 10^{-4}$	$1.1 \times 10^{-4}$
312	35	0.34	0.12	$5.1 \times 10^{-4}$	$2.6 \times 10^{-4}$
853	35	0.61	0.09	$4.6 \times 10^{-4}$	$2.0 \times 10^{-4}$
-	-	-	-	-	-
791	100	0.47	0.04	$1.2 \times 10^{-3}$	$2.4 \times 10^{-4}$
247	100	0.61	0.03	$1.8 \times 10^{-4}$	$3.3 \times 10^{-5}$
312	100	0.32	0.04	$1.4 \times 10^{-3}$	$3.5 \times 10^{-4}$
853	100	0.68	0.09	$1.2 \times 10^{-4}$	$4.4 \times 10^{-5}$
-	-	-	-	-	-
791	150	0.41	0.02	$1.4 \times 10^{-3}$	$1.4 \times 10^{-4}$
247	150	0.58	0.08	$6.9 \times 10^{-3}$	$2.8 \times 10^{-3}$
312	150	0.32	0.04	$4.2 \times 10^{-2}$	$9.1 \times 10^{-3}$
853	150	0.61	0.09	$4.2 \times 10^{-3}$	$2.0 \times 10^{-3}$

Table 3  
Analysis of DMF Uptake by Coal Samples Using Equation (1)

PSOC	Temperature (°C)	n	95% CI for n	k	95% CI for k
791	35	0.49	0.05	$8.8 \times 10^{-4}$	$2.4 \times 10^{-4}$
247	35	0.51	0.04	$1.5 \times 10^{-3}$	$2.9 \times 10^{-4}$
312	35	0.74	0.13	$6.5 \times 10^{-5}$	$3.6 \times 10^{-5}$
853	35	0.62	0.29	$6.6 \times 10^{-5}$	$5.6 \times 10^{-5}$
-	-	-	-	-	-
791	100	0.47	0.07	$1.6 \times 10^{-3}$	$5.5 \times 10^{-4}$
247	100	0.67	0.03	$5.7 \times 10^{-5}$	$1.0 \times 10^{-5}$
312	100	0.52	0.03	$9.6 \times 10^{-5}$	$1.7 \times 10^{-5}$
853	100	0.70	0.04	$3.3 \times 10^{-5}$	$8.3 \times 10^{-6}$
-	-	-	-	-	-
791	150	0.59	0.06	$3.2 \times 10^{-4}$	$9.5 \times 10^{-5}$
247	150	0.55	0.03	$3.9 \times 10^{-4}$	$7.1 \times 10^{-5}$
312	150	0.61	0.02	$6.7 \times 10^{-5}$	$9.9 \times 10^{-6}$
853	150	0.65	0.04	$2.4 \times 10^{-5}$	$5.2 \times 10^{-6}$

These results indicate that anomalous transport is observed in some samples of coal, especially at the higher degree of crosslinking, exemplified by the high carbon content of the coal samples. No Case-II transport was observed, and the results indicate a slight decoupling of diffusion and relaxation at higher temperatures.

This work was supported by a grant from the Department of Energy (PETC).

#### REFERENCES

1. N.A. Peppas and L.M. Lucht, *Chem. Eng. Commun.*, *37*, 333 (1985).
2. B.D. Barr-Howell, N.A. Peppas and D.N. Winslow, *Chem. Eng. Commun.*, *43*, 301 (1986).
3. B.D. Barr-Howell, N.A. Peppas and T.G. Squires, *J. Appl. Polym. Sci.*, *31*, 39 (1986).
4. P.L. Ritger and N.A. Peppas, *Fuel*, *66*, 815 (1987).
5. L.M. Lucht and N.A. Peppas, *J. Appl. Polym. Sci.*, *33*, 1552 (1987).
6. B.D. Barr-Howell, J.M. Howell and N.A. Peppas, *Energy and Fuels*, *1*, 181 (1987).
7. P.L. Ritger and N.A. Peppas, *Fuel*, *66*, 1379 (1987).
8. B.D. Barr-Howell, J.M. Howell and N.A. Peppas, *Thermoch. Acta*, *116*, 153 (1987).
9. D. Brenner, *Nature*, *306*, 772 (1983).

## The Relationships Between Coal Macromolecular Structure and Solvent Diffusion Mechanisms

Peter J. Hall, Harry Marsh and K. Mark Thomas  
Northern Carbon Research Laboratories  
University of Newcastle-upon-Tyne  
Newcastle-upon-Tyne NE1 7RU  
United Kingdom

**Key Words:** Macromolecular structure, diffusion, viscoelastic properties

### Introduction

The diffusion of solvents through coal is the limiting step of many coal processes and measurement of the mechanism and kinetics of solvent diffusion has been the subject of numerous investigations<sup>1,2</sup>. It is generally accepted that solvent diffusion through coal is analogous to the diffusion of solvents through conventional glassy polymers and much of the formalism of the latter has been applied to coal<sup>3</sup>. The diffusion of solvents may vary between two extrema. If the diffusion is controlled by the concentration gradient between the center and the outside of the particle the diffusion mechanism is Fickian and, for diffusion into a sphere, the kinetics are expressed by the following expression<sup>4</sup>:

$$\frac{M(t)}{M_e} = 1 - \frac{6}{\pi^2} \sum_{n=1}^{\infty} \frac{1}{n^2} \exp(-Dn^2\pi^2 t/a^2) \quad 1$$

where  $M(t)$  is the mass uptake at time  $t$ ,  $M_e$  is the equilibrium mass uptake,  $a$  is the particle radius and  $D$  is the diffusion coefficient. However, the mechanism of diffusion can deviate significantly from the Fickian mode when the diffusing solvent changes the viscoelastic properties of the glassy solvent. In the limit the diffusion of solvents is completely controlled by polymer relaxation and the solvent advances through the polymer with a well defined front such that ahead of the front the solvent concentration is zero and behind the front the solvent is at equilibrium concentration. Furthermore, ahead of the front the polymer is glassy and behind the front the solvent is rubbery. This kind of diffusion is referred to as "relaxation" or "Case II" diffusion and is characterized either by a polymer relaxation constant or the front velocity. Simple integration of the mass uptake at time  $t$  gives the following kinetic expression<sup>5</sup>:

$$\frac{M(t)}{M_e} = 1 - (1 - k_0 t / C_0 a)^3 \quad 2$$

where  $k_0$  is the relaxation constant and  $C_0$  is the equilibrium solvent concentration. The

front velocity is  $k_0/C_0$ .

Diffusion mechanisms for solvents through coals has been shown to vary between these limits<sup>2</sup>. However, the structural features of the coal macromolecular structure or the details of the macromolecular/solvent interactions which determine diffusion mechanisms remain undefined and are the subject of this paper.

The method used to monitor the amount of solvent that has diffused into the solvent is Dynamic Volumetric Swelling (DVS). Essentially, the amount of volumetric swelling is monitored as a function of time. Only solvent that has diffused into the "bulk" structure can cause coal to swell so that this technique is insensitive to occluded solvent. At any time  $T$ , the amount of solvent that has diffused into the bulk is proportional to the amount of volumetric swelling, so that:

$$\frac{M(t)}{M_e} = \frac{Q(t)}{Q_e} \quad 3$$

where  $Q(t)$  is the amount of volumetric swelling at time  $t$  and  $Q_e$  is the equilibrium swelling. Graphically, to distinguish between the extremal modes of diffusion it is conventional to plot the normalized mass (or swelling) uptake as a function of root normalized time,  $(t/t_e)^{1/2}$ . Figure 1 shows the normalized plots for the theoretical Fickian and Relaxation diffusion modes. It can be seen that under this regime the normalized Fickian curve increases monotonically whereas the Relaxation controlled mode has an inflexion at low  $(t/t_e)^{1/2}$ .

### Experimental

The apparatus was adapted from a design by Aida and Squires<sup>6</sup>. Essentially it consists of a glass cylinder 2 cm in diameter in which coal, supported by a quartz frit, interacts with the solvent. A light PTFE piston is placed on top of the coal and the increase in the height of the coal sample is monitored by a linear transducer connected to a microcomputer. The piston was of such a size as to allow a gap of about 1/4mm between the itself and the outer cylinder. The reaction chamber was surrounded by a constant temperature water bath, kept at 313K for these experiments. The coals were ground to between 60 and 30 Tyler mesh. With this particle size the diffusion of solvents through the coal bed was at least two orders of magnitude faster than diffusion into the particles. Coal was placed into the cylinder and the upper surface levelled. The initial height of the coal sample was measured and the piston and transducer placed on the coal. Solvent was introduced into the chamber to just below the frit and allowed to come to thermal equilibrium. Further solvent was added until the coal and piston were covered. The increase in sample height was monitored as a function of time. Since the approach to equilibrium swelling was asymptotic, the equilibrium time was chosen as the time to reach 99.5% of the equilibrium swelling value.

The coals were obtained from the coal bank of the Northern Carbon Research Laboratories and are described in Table 1. Two solvent sets were chosen, a set of

substituted pyridine molecules and a set of straight chain amines. The former were chosen because the steric properties of the molecules are similar but the basicity depends upon the substitution. In the latter, the molar volume increases with amine chain length whereas the basicity is relatively constant with amine chain length. The  $pK_b$  values and molar volumes of these solvent sets are given in Table 2.

### Results and Discussion

Figure 2 shows the swelling curves for Gedling coal as a function of time. As would be expected, the time to equilibrium swelling (as defined above) increases as a function of amine chain length or molar volume. The amount of swelling also increases with amine molar volume, as observed by Green and West<sup>7</sup>. However, Figure 3 shows that when the swelling is normalized and plotted against root normalized time the curves have the same trajectory. Therefore all of the amines have the same swelling mechanism, regardless of molar volume.

Figure 4 shows the normalized DVS data for the substituted pyridine set. The diffusion changes from an anomalous mode for the pyridine and 2-methylpyridine to Fickian for the 2-fluoropyridine.

The principal mechanism of swelling for bases such as the amine and substituted pyridine sets appears to involve the disruption of inter chain hydrogen bonds<sup>8,9</sup>. Coal hydrogen bonds have a range of bond energy<sup>9</sup>. One result of this is that weaker bases, such as the 2-fluoropyridine, are able to disrupt only the weakest hydrogen bonds, stronger hydrogen bonds act as *de facto* crosslinks. As solvent basicity increases in the substituted pyridine set the solvents are able to disrupt increasing numbers of hydrogen bonds. Eventually a point is reached at which all of the hydrogen bonds are disrupted. This is manifested as a plateau in swelling/basicity curves<sup>9</sup>.

One explanation of the progressive change from anomalous diffusion to Fickian diffusion could be that as the bases disrupt hydrogen bonds so the viscoelastic properties of the coals change from glassy to increasingly rubbery in the presence of the solvents. However, Figure 4 shows that pyridine and 2-methylpyridine have the same diffusion mechanism, even though their basicities are significantly different. This can be rationalized by noting that pyridine and 2-methylpyridine swell Gedling coal to the same extent<sup>9</sup> and, by hypothesis, disrupt the same number of hydrogen bonds.

Further corroborative evidence for the above theory comes from the diffusion mechanisms of the straight chain amine set. The amine chain length has little effect on molecular basicity and the observed increase in swelling with chain length has been attributed to the presence of increasingly larger molecules within the coal structure<sup>7</sup>. Green and West<sup>7</sup> have presented evidence to suggest that the molar amount of amine is absorbed per unit weight of coal is independent of amine size. This is consistent with the idea of

solvent basicity determining the number of hydrogen bonds disrupted.

From the above a consistent picture can be made of the factors which determine diffusion mechanisms for basic solvents. In its usual state Gedling coal is glassy at room temperature. When hydrogen bonds are disrupted by basic solvents the effective crosslink density decreases. There is an associated change of the coal viscoelastic properties as the coal becomes more rubbery. The degree to which coal becomes rubbery is a function of the density of hydrogen bonds disrupted. No assumptions are made about the mechanism by which basic solvents disrupt hydrogen bonds. However, the disruption of hydrogen bonds in itself may not be sufficient to change coal viscoelastic properties. Lucht *et al.*<sup>10</sup> have shown that  $T_g$  is reduced only to a limiting value of about 410K following sorption of pyridine vapor. There is a certain amount of evidence from work by Brenner<sup>11</sup> to suggest that solvent which makes coal rubbery is weakly associated in the coal structure. This may imply some sort of a solvent plasticization effect. These observations are not inconsistent with the picture presented above because during the uptake of liquids, for the Anomalous and Relaxation controlled diffusion, the concentration of solvent behind the solvent front must be sufficiently large to cause the rubbery behavior. In summary, the above picture only seeks to stress that an essential part of the glass to rubber conversion is the disruption of hydrogen bonds. Recent, unpublished, work suggests that solvents which would be expected to have a plasticization effect similar to pyridine (such as chlorobenzene) in themselves do not change coal viscoelastic properties.

With the preceding in mind, an attempt can now be made to interpret the diffusion properties of a rank range of coals. The diffusion mechanisms are presented in Figure 5 with pyridine as the diffusing solvent. The lignite displays a Fickian diffusion and the diffusional mode becomes increasingly Relaxation controlled as rank increases. The diffusional mode for Cortonwood is well outside of the theoretical Relaxation controlled limit. Now, if the change in viscoelastic properties were simply a function of the density of hydrogen bonds disrupted then relaxation controlled behavior would be expected for coals with high oxygen contents. In fact the opposite is true. This can be rationalized by assuming that the change in viscoelastic property is, *ceteris paribus*, a function of the ratio of crosslink density before and after solvent diffusion *i.e.*  $(M_c/M_c + M_h)$ . Where  $M_c$  is the covalent crosslink density and  $M_h$  is the hydrogen bond crosslink density. If this is indeed the case then the ratio of hydrogen bond to covalent (and other non-scissile) crosslinks increases as a function of coal rank in the range 50-87% carbon content. supportive evidence for this hypothesis comes from a body of data, derived from a variety of coal chemical and physical properties, which suggests that the crosslink density of coal reaches a minimum at about 87% carbon content<sup>3,8</sup>.

There is no easy explanation in this framework for the behavior of Cortonwood coal. The swelling appeared to be a two-stage process with a quasi-equilibrium followed by a very slow approach to swelling equilibrium. A detailed picture of the factors influencing

coal diffusion mechanism requires more work. The role of solvent plasticization is unexplored.

### Conclusions

The mechanism of diffusion of a solvent through a coal is, in part, determined by the degree to which the diffusing solvent changes the coal viscoelastic properties. One factor which influences this is the density of hydrogen bonds disrupted by the solvent in ratio to the non-scissile coal crosslinks. Solvent steric properties influence the kinetics, but not the mechanism of diffusion.

### References

1. Hseih, S.T. and Duda, J.L., *Fuel*, **66**, 170, 1987.
2. Peppas, N.A. and Lucht, *Chem. Eng. Comm.*, **37**, 334, 1984.
3. Thomas, K.M. in *Carbon and Coal Gasification*, Eds Figureido, J.L. and Moulijn, J.A., NATO ASI Series E, 105, Martinus Nijhoff, Netherlands, 1986.
4. Crank, J., *The Mathematics of Diffusion*, Clarendon Press, UK, 1975.
5. Ensore, D.J., Hopfenberg, H.B. and Stannett, V.T., *Polymer*, **18**, 793, 1977.
6. Aida, T. and Squires, T.G., *ACS Fuel Division Preprints*, **30**, 95, 1985.
7. Green, T.K. and West, T.A., *Fuel*, **61**, 65, 1986.
8. Green, T.K., Kovac, J., Brenner, D. and Larsen, J.W., in *Coal Structure*, Ed Meyer, R.A., Academic Press, NY, 1982.
9. Hall, P.J., Thomas, K.M. and Marsh, H., *Fuel*, **67**, 863, 1988.
10. Lucht, L.M., Larson, J.M. and Peppas, N.A., *Energy and Fuels*, **1**, 56, 1987.
11. Brenner, D., *Fuel*, **63**, 1324, 1984.

Table 1

Coal	%C	%H	%O*	%N	%Mineral
ND Lignite	50.0	4.3	45.7	-	-
Gedling	81.6	5.2	9.4	1.7	2.8
Cresswell	84.5	5.5	5.9	1.9	3.0
Cortonwood	87.2	5.6	3.9	1.7	2.7

\* by difference

**Table 2**

Solvent	pK <sub>b</sub>	Molar Volume (cm <sup>3</sup> /mol)
Propylamine	3.3	82.2
Butylamine	3.2	98.8
Propylamine	3.4	115.9
Hexylamine	3.4	132.1
2-methylpyridine	8.0	98.8
Pyridine	8.6	80.9
2-chloropyridine	13.5	94.6
2-fluoropyridine	14.4	86.1

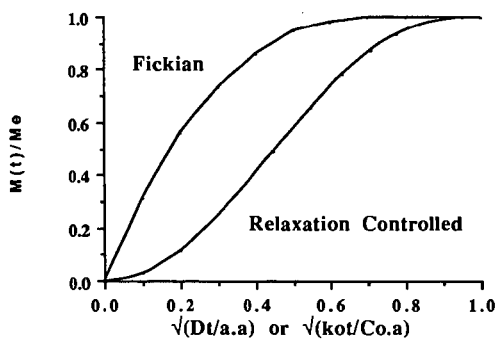


Figure 1. The normalized, theoretical, modes for Fickian and Relaxation-controlled diffusion into a sphere.

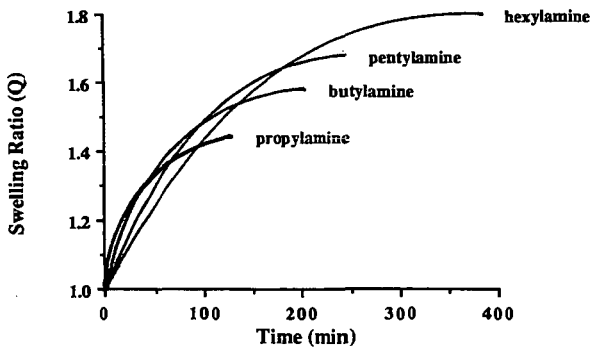


Figure 2. The dynamic volumetric swelling for straight chain amines in Gedling

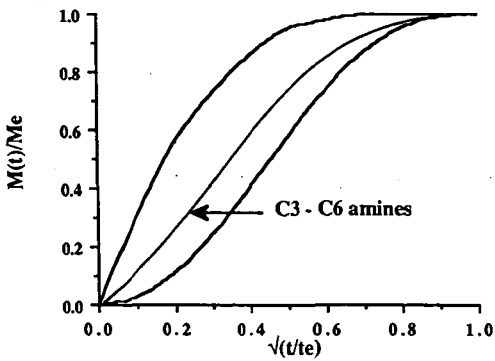


Figure 3. The diffusion mechanism for straight chain amines into Gedling coal at 313K as deduced from dynamic volumetric swelling.

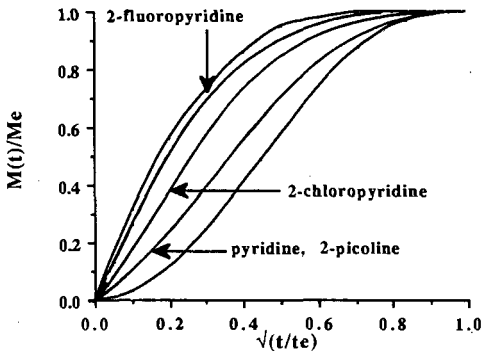


Figure 4. The diffusion mechanisms for substituted pyridines into Gedling coal at 313K, as deduced from dynamic volumetric swelling.

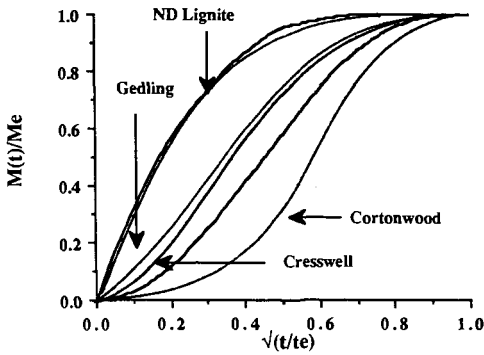


Figure 5. The diffusion mechanisms for pyridine into a range of coals at 313K, as deduced from dynamic volumetric swelling.

## COAL SOLUBILITY AND SWELLING

Paul Painter, Yung Park, John Graf,  
Maria Sobkowiak and Mike Coleman  
Polymer Science Program  
The Pennsylvania State University  
University Park, PA 16802

Key Words: Coal solubility, coal swelling, hydrogen bonding

### INTRODUCTION

The characterization of coal as a macromolecular network has resulted in a significant advance in our understanding of this complex material. By applying the theories of Paul Flory (1,2), the solubility (or, more accurately, extractability) and swelling of a coal can be used as a probe of structure (3-11). It is widely recognized however, that the original theories are flawed, particularly the Flory-Rehner treatment of the swelling of polymer networks (although it apparently benefits from the cancellation of errors (12)), and their application to coals is further limited by the presumed non-Gaussian behaviour of the "chains" and the realization that coal segments interact with each other and solvent through the formation of hydrogen bonds. Strong, specific interactions such as these are not accounted for in Flory's original equations describing the free energy of mixing and the contribution of the chemical potentials to the balance of forces involved in the swelling of a cross-linked network. We have recently developed an association model that can account for hydrogen bonding in polymer mixtures (13-16). The result is a Flory-Huggins equation accounting for the entropy of mixing and the dispersive (and other) non-hydrogen bonding forces described by a  $\chi$  parameter, with an addition free energy term  $\Delta G_H$  that accounts for the change in the number and type of hydrogen bonds that occur as a function of composition;

$$\frac{\Delta G_M}{RT} = \frac{\phi_A}{x_A} \ln \phi_A + \frac{\phi_B}{x_B} \ln \phi_B + \phi_A \phi_B \chi + \frac{\Delta G_H}{RT} \quad (1)$$

where  $\phi_A, \phi_B$  are volume fractions and  $x_A, x_B$  are "degrees of polymerization", or, more accurately, the ratio's of the molar volumes of the components relative to a reference molar volume. The crucial points concerning this equation are:

- 1) The  $\Delta G_H$  term is negative and favourable to mixing
- 2) The quantities used to calculate  $\Delta G_H$  are determined experimentally and there are no adjustable parameters in this term
- 3) Phase behaviour is determined by the balance between the positive and unfavourable to mixing  $\chi$  term and the favourable to mixing entropic and  $\Delta G_H$  terms and the contribution of these terms to the derivatives of the free energy with respect to composition.

The equations for  $\Delta G_H$  and its derivatives and the details of their specific application to coal have been presented elsewhere (17,18). Here we will concern ourselves with a brief outline of some of our most important recent results. Space does not permit a detailed description of the calculations, which will be presented in a set of three papers that are about to be submitted for publication (19-21). Our discussion will touch upon;

- a) The determination of  $\chi$  from solubility parameters.
- b) The calculation of "hypothetical" phase diagrams for coal solutions
- c) The calculation of the molecular weight between cross-link points from swelling measurements
- d) The formulation of a new model for the description of coal swelling and its relationship to structure.

## COAL SOLUBILITY PARAMETERS

If we are limiting its application to non-specific and (relatively) weak interactions, then the value of the Flory  $\chi$  parameter can be estimated from solubility parameters using

$$\chi = \frac{V_B}{RT} (\delta_c - \delta_s)^2 + 0.34 \quad (2)$$

where  $V_B$  is a reference volume and  $\delta_c$  and  $\delta_s$  are the solubility parameters of the coal and solvent, respectively. For an insoluble network the solubility parameter ( $\delta_c$ ) has been determined in one of two ways: from group contributions using, for example, the methods of van Krevelen (4,22) Hoy (23) or Small (24), or from swelling measurements. Unfortunately, both these methods involve difficulties and for coals lead to the prediction of very different solubility parameters, even when the effect of hydrogen bonding is minimized or excluded. For example, Larsen et al. (7) carefully examined the swelling of acetylated coals in non-hydrogen bonding solvents. An Illinois No. 6 and a Bruceton coal both gave a maximum degree of swelling for solvents with solubility parameters in the range 9-10 (cal/cm<sup>3</sup>)<sup>1/2</sup>. This value would then normally be taken as the proper value for coal, as it would give the minimum value for  $\chi$ . However, a calculation of the corresponding solubility parameters using the atomic contribution method proposed by van Krevelen (4) gives values in the range 11-12 (cal/cm<sup>3</sup>)<sup>1/2</sup>, depending upon the precise value of the fraction aromaticity assumed for these samples. We found it difficult to understand precisely how van Krevelen obtained his parameters, as his methodology is not described, but on the basis of our calculations we believe it to be prone to large errors and fully of broad and perhaps unjustifiable assumptions, as we will discuss in detail elsewhere in a separate publication (19). The obvious choice would therefore seem to be the experimentally determined values. Paradoxically, we believe that van Krevelen's result is at least in the right range and the value obtained from maximum swelling is not the value for coal. This is not because of any problem with the experiments, but one that has its origins in free volume or compressibility effects that are ignored in simple theories of mixing.

In resolving the differences in the values of  $\delta_c$  given by group contributions and swelling measurements we first observe that this problem is not unique to coal. Bristow and Watson (26) found that certain rubbers with solubility parameter values of the order of 9-10, gave maximum swelling in a series of n-alkanes with heptane,  $\delta=7.4$ . This difference was demonstrated to be due to so-called free volume effects by Biros et al. (27), who applied Flory's equation-of-state theory (2). It is a relatively straightforward matter to show that such effects also account for the observed maximum in the swelling of coal. We have applied the lattice fluid model of Sanchez and Lacombe (28-30) rather than Flory's theory, however.

The association formalism we use to describe hydrogen bond interactions and the Sanchez-Lacombe theory are both simple lattice models, so for future application it is more appropriate to combine these approaches, as we will report elsewhere (31), than to somehow graft an association model onto Flory's equation-of-state. Accordingly, using the equations of Sanchez and Lacombe (28-29) the Flory  $\chi$  parameter can be written as:

$$\chi = \frac{\bar{p}\Delta\epsilon^*}{RT} + \frac{1}{\phi_2} \left[ \bar{T}_1 (\bar{p}_1 - \bar{p}) + \frac{(1-\bar{p})}{\bar{p}} \ln(1-\bar{p}) - \frac{(1-\bar{r})}{\bar{r}} \ln(1-\bar{r}) + \frac{1}{\bar{r}} \ln(\bar{p}/\bar{p}_1) \right] \quad (3)$$

or, more simply

$$\chi = \frac{\bar{\rho} \Delta \epsilon^*}{kT} + \beta^1 \quad (4)$$

where  $\bar{\rho}$ ,  $T$  are the reduced density and temperature (see references 27-29) and the subscripts 1 and 2 refer to components 1 and 2 of the mixture. The term  $\Delta \epsilon^*$  is given by

$$\Delta \epsilon^* = \epsilon_{11}^* + \epsilon_{22}^* - 2\epsilon_{12}^* \quad (5)$$

and is the usual difference in the energy of 1-2 contacts relative to 1-1,2-2 contacts. If we make the geometric mean assumption

$$\epsilon_{12}^* = (\epsilon_{11}^* \epsilon_{22}^*)^{1/2} \quad (6)$$

then

$$\chi = \frac{\bar{\rho}}{kT} \left[ (\epsilon_{11}^*)^{1/2} - (\epsilon_{22}^*)^{1/2} \right]^2 + \beta^1 \quad (7)$$

The correspondence of this equation to the solubility parameter approach can then be seen immediately by rewriting equation 1 on the basis of numbers of molecules rather than moles and transforming the subscripts:

$$\chi = \frac{V_1}{kT} (\delta_1 - \delta_2)^2 + \beta \quad (8)$$

The solubility parameters are related to the cohesive energy densities (CED) and hence the lattice fluid parameters (28,29) through

$$\delta = (\text{CED})^{1/2} = \left( \frac{\Delta E_v}{V} \right)^{1/2} = \left( \frac{\epsilon^*}{v^*} \right)^{1/2} \bar{\rho} \quad (9)$$

where  $v^*$  is the average close packed volume of a segment and generally varies with composition (i.e.,  $v_1^* \neq v_2^*$ ). If we assume there is no dependence of the energies of interaction ( $\epsilon_{11}^*$  etc.) on composition and use the identity  $V_1 = v_1^* / \bar{\rho}_1$ , then equation (8) can be obtained directly from equation 7. Accordingly, in the solubility parameter approach we can identify the parameter  $\beta$  with so-called free volume or compressibility effects, while the  $(\delta_1 - \delta_2)^2$  term reflects exchange interaction energies that are assumed independent of composition. We must now face the following question: for coal is the value of  $\beta$  of the order of 0.34, as in many polymer systems, or are free volume differences such that there is a larger deviation? It is a relatively straightforward matter to use equation 3 to calculate  $\chi$  for various coal/solvent mixtures. The necessary parameters for the solvents used by Larsen et al. (7) were obtained from Sanchez and Lacombe (28), while the parameters for coal were calculated from its coefficient of thermal expansion ( $\alpha = 1 \times 10^{-5}$ , from van Krevelen (34) and an assumed value of the solubility parameter of  $\delta_c = 11.8$ , a value estimated from van Krevelen's method (4). Coal-solvent interactions were also assumed to be given by the usual geometric mean assumption. The equations necessary for these calculations are given elsewhere (19) and here we simply present the result in Figure 1, a plot of  $\chi$  vs  $\delta_s$ . A coal with a solubility parameter of  $11.8 \text{ (cal/cm}^3)^{1/2}$  has a minimum value of  $\chi$  and hence a predicted maximum swelling with a solvent that has a solubility parameter of

about  $10 \text{ (cal/cm}^3)^{1/2}$ . A value of  $\delta$  for an Illinois #6 coal of 11.4, as we estimate from a revised methodology (19) gives a predicted maximum swelling with non-hydrogen bonding solvents that have a solubility parameter in the range 9-10, corresponding to the value determined experimentally by Larsen et al. (7).

### THE PHASE BEHAVIOUR OF SOLUTIONS OF COAL MOLECULES

An understanding of the solubility of a coal in various solvents can be obtained by a calculation of hypothetical phase diagrams. They are hypothetical in the sense that we assume that the coal is not cross-linked, but is simply a macromolecule. This macromolecule could be highly branched and with an extremely high molecular weight, but within the limitations of the simple lattice model applied here its equilibrium properties can be determined. This, in turn, allows an understanding of why a particular solvent is capable of extracting more (or less) soluble material than another and, as we will see, provides some fundamental insight into the variation of swelling behavior with temperature.

In a preliminary communication of this work (18) we calculated theoretical phase diagrams as a function of coal rank. the value of  $\chi$  was estimated using van Krevelens method (4). As we will discuss in detail in a separate paper (19), we have little confidence in the precise value so calculated for any particular coal, but the trend with rank makes sense in terms of what we know about the structure of coal and the value appears to be in the right range. The calculation of the  $\Delta G_H$  term and the derivatives of the free energy are described in previous publications (13-18). here we will discuss the calculated spinodals for three coals, an Illinois #6, PSOC 207 and PSOC 402, shown in Figures 2-4, as these results bear on the interpretation of swelling measurements.

For Illinois #6 coal we illustrate the spinodals obtained for mixing with three different solvents, pyridine, THF and benzene. For pyridine, we predict a typical inverted "U" shaped stability curve with an upper critical solution temperature near 25°C. Mixtures with THF and benzene are predicted to be far less miscible, with the stability limits calculated to be near the two composition extremes. An examination of Table 1, which lists the solvent parameters utilized here, together with some values for other solvents, immediately demonstrates why. Pyridine forms much stronger hydrogen bonds than the other solvents listed (as measured by the equilibrium constant  $K_A$ ) and, in addition, its solubility parameter is closer to the range we estimate represents the most likely value for this coal (11-12  $(\text{cal/cm}^3)^{1/2}$ ). Thus, favorable interactions (coal solvent hydrogen bonds) are maximized and  $\chi$  is minimized. This is a crucial point, correlation of coal swelling to a single parameter, chosen so as to represent  $\chi$  or some measure of the strength of favorable interactions, can be misleading. It is the balance of favorable and unfavorable forces that is crucial.

The calculated spinodals for PSOC 207 and PSOC 402 in pyridine show progressively increasing values of the upper critical solution temperature (maximum value of the inverted "U") relative to Illinois #6 coal, a trend that largely reflects the increasing value of  $\chi$  calculated for this coal-pyridine series. To reiterate, although the precise positions of these curves are obviously affected by the errors in calculating  $\delta_c$ , we believe that this predicted trend in behavior should be reasonably accurate.

The calculated phase behaviours indicates that if these coals were not cross-linked they would be completely soluble in pyridine at elevated temperatures. This remains true even if we assume very high molecular weights for the coal molecules (the contribution of the combinatorial entropy from the coal is very small for the degree of polymerization  $x_B$  assumed in these calculations ( $x_B=100$ ); changing this value to 1000 or 10,000 has only a minor effect on the calculated spinodals, as illustrated in our preceding publications (17,18)). Accordingly, we believe that these results strongly support the present generally held view that at least up to a certain carbon content, coals are cross-linked networks

### THE SWELLING OF COAL

Hydrogen bonding affects the swelling of coal through its contribution to the chemical potential of the solvent ( $\Delta G_H$ )<sub>A</sub>. The Flory Rehner equation, as modified by Kovac (32) and applied to coal by Larsen et al. (7), can then be written

$$\bar{M}_c = \frac{\rho_B V_A \phi_B^{1/3} + \rho_B V_A / N \phi_B^{1/3}}{\left[ \ln(1 - \phi_B) + \phi_B + \chi \phi_B^2 + \frac{(\Delta G_H)_A}{RT} \right]} \quad (10)$$

where  $\bar{M}_c$  is the number average molecular weight between cross link points and  $N$  represents the number of "clusters" between cross link points. Larsen et al. (7) studied the swelling of an extracted but otherwise unreacted Illinois #6 coal in pyridine. Using the reported swelling ration of about  $Q=2.4$ , we obtained the plots of  $\bar{M}_c$ , the number average molecular weight between cross link points against  $M_0$ , the assumed molecular weight of a coal cluster, shown in Figure 5. In this initial plot we put  $(\Delta G_H)_A = 0$ , i.e., we ignored hydrogen bonding. Results were obtained for four different assumed values of  $\delta_{\text{coal}}$ , ranging from 9 to 12 and display the large sensitivity to  $\chi$  noted by Lucht and Peppas (8). These results are dramatically altered if we now include the effect of hydrogen bonding, using equation 10. The effect of variations in  $\chi$  is now greatly reduced, as can be seen from Figure 6, and the calculated values of  $\bar{M}_c$  are now much smaller. This is a consequence of the large contribution of hydrogen bonding to the chemical potential of the solvent, i.e., the  $(\Delta G_H)_A$  term dominates the  $\chi$  term. A calculated molecular weight of about 500, or "degree of polymerization" of about 2 clusters, between cross-link points is determined. This appears to be too small to be reasonable, but we will defer a discussion of this point until after we consider some additional data.

Lucht and Peppas (9) have also studied the swelling of various coals in pyridine, including PSOC 207 and PSOC 402. These swelling measurements were conducted at three different temperatures, 35, 60 and 80°C, and the results of applying equation 10 to their data is shown in Figures 7 and 8. It can be seen that there are distinct differences in the calculated values of the molecular weight between cross-link points with much larger values being determined at high temperatures. Unlike Lucht and Peppas (8), we allowed  $\chi$  to have its usual  $1/T$  dependence, while the variation of the values of the equilibrium constants, and hence  $(\Delta G_H)_A$ , with temperature was determined through the usual vant Hoff relationship (14). Accordingly, it is not the temperature dependence of the solvent chemical potential that is responsible for such large differences. Only small variations might be expected due to the errors inherent in the various assumptions that are made concerning the form of the temperature dependence of the parameters over this fairly limited range. An explanation is immediately apparent if we examine the calculated solution phase diagrams shown in Figures 3 and 4, however. PSOC 207 and 402 are predicted to have upper critical solution temperatures near 75 and 125°C, respectively, these values being subject to the significant errors involved in estimating  $\chi$  (19). Clearly, if the swollen network is at a temperature above this transition, in the single phase region, the coal should swell to the limit imposed by the nature of the network. Below this transition, however, there is a two phase region that is predicted for the coal primary chains in pyridine. The precise position of this transition for the network would be affected by the elastic forces between cross-link points, but clearly at some critical temperature solvent would be expelled leading to the phenomenon of gel collapse. The plots shown in Figures 7 and 8 suggest that this is precisely what we are observing in coal. PSOC 207 shows a large change in swelling and hence calculated molecular weight on going from 35°C to 60°C, but a small difference on going from 60°C to 80°C. In contrast, the major change for PSOC 402 appears to occur between 60°C and 80°C. We believe that these discontinuities in behaviour are due to expulsion of solvent from the swollen coal network. Our association model predicts this trend remarkably well; an examination of the calculated solution phase behaviours, shown in Figures 4 and 5, indicates that PSOC 402 has a higher UCST than PSOC 207. The absolute values of the transition are off by approximately 40°C, but this is not bad considering the errors in calculating  $\chi$  and the probability that we should include a chain extension term in accounting for the phase behaviour of the gel.

If we now consider the values of the molecular weight obtained at the highest swelling temperature to be the most accurate, the predicted molecular weight between cross links is now more reasonable, but still small in terms of the inherent limitations of the model. If we further assume that the molecular weight of an average "cluster" is of the order of 200, this model predicts that the number of such

clusters between cross links is of the order of three for these coals. We must therefore, question whether it is at all appropriate to apply Flory's theory to coal, even in the modified form expressed by equation 10. We will suggest an alternative in the following section.

### SWELLING BY DISINTERSPERSION

Even if we discount the flaws perceived by various authors in the original Flory-Rehner theory, its application to coal, even using the modified Gaussian statistics proposed by Kovac (32) and accounting for the contribution of hydrogen bonding, must be considered highly suspect. The results suggest that the number of aromatic "clusters" between crosslinks is small and such chains are certainly stiff. Nevertheless, we believe that it is possible to construct a simple model that provides at least a rough estimate of the molecular weight between cross-link points, although we do not formulate it in those terms.

This model is based on the very important observations of Bastide et al. (33) that the radius of gyration of the chains of a swollen polystyrene gel were equal, within the limits of experimental error, to that of the free chains in the same solvent, and did not vary when the degree of swelling was altered. On this basis it was proposed (34) that swelling was associated with a topological reorganization of the network, where the cross link points essentially rearrange their positions with only minor perturbations to the chain dimensions, a process that these authors labeled disinterspersion. We assume that the stiff molecules in coal essentially unfold in this manner and that the degree of swelling is then limited by the geometry of the system. A more complete account of our arguments is given in reference 1, but a schematic view of this process is illustrated in Figure 9. Strangely enough, we will argue that the coal "chains" are not straight rods, as shown in this figure, but follow random walk or perhaps self avoiding walk statistics. This is a second crucial point in the development of our simple model. It is important to realize that we are not making this claim on the basis of any argument concerning chain flexibility. Instead, we propose that this is a consequence of the heterogeneity of linkages that must occur in coal. A two dimensional view of simple aromatic units (benzene and naphthalene rings), linked by -CH<sub>2</sub>- and -O- groups, is shown in Figure 10. Even if we require on steric grounds that bonds in the ortho position are unlikely, the variety of other possibilities result in a chain that can be modeled by a set of virtual bonds, in this example shown linking the centers of the aromatic clusters, such that they trace out a (more-or-less) random walk or random flight. If the network then simply swells to the limit permitted by the "unfolding" of these chains, which behave as stiff, bent wires, then the relationship between the degree of swelling and the contour length of these chains follows from simple geometry. If we let the functionality of the network be equal to  $f$  and the average end-to-end distance between cross link points be equal to  $R_0$  ( $=\langle r^2 \rangle^{1/2}$ ), then we can pick a cross-link point in the swollen network at random and determine the volume of the chains in the volume  $(4/3)\pi R_0^3$  following Bastide et al. (34). This is equal to  $fV_s N$ , where  $V_s$  is the volume occupied by each "repeat" unit and  $N$  is the number of repeat units in each primary chain. It then follows that the volume fraction of polymer in the swollen gel is given by

$$\phi = \frac{3fV_s N}{4N\pi R_0^3} \quad (11)$$

The quantity  $R_0$  is related to  $N$  by the general relationship

$$R_0 = aN^v \quad (12)$$

where  $a$  is the length of an average unit and  $v$  has a value in the range 0.5 to 1 (for a random walk  $v = 0.5$ , a self avoiding walk  $v = 0.6$  and for a rigid rod  $v = 1$ ).

The parameter  $a$ ,  $V_s$  and  $N$  are not easily defined for any particular coal, but, as we show in more detail in a separate publication (21), by defining these quantities on a per carbon atom basis we obtain

$$N_c^{(3v-1)} = \frac{3fV_c}{4\pi\phi a_c^3} n_c^{3(v-1)} \quad (13)$$

where  $N_c$  is the number of carbon atoms between cross-link points,  $V_c$  is the molar volume per carbon atom (which can be determined from the elemental composition and density), and  $a_c$  is the length of such a cluster (or virtual bond in Figure 10) divided by the number of carbon atoms ( $n_c$ , in that cluster. If we assume that as a result of the heterogeneities of the cross-link points and the limited degree of chain flexibility that can occur in a good solvent,  $v = 0.6$ , then plots of  $N_c$  vs  $n_c$  for various values of  $a_c$  can be constructed, as shown in Figure 11 (a value of  $f = 3$  was assumed). The data used to obtain these plots was that of the Illinois #6 coal studied by Larsen et al. (7). If we assume an average of 8-9 carbon atoms per repeat or cluster, corresponding to a mixture of substituted benzene and naphthalene rings, with the former predominating, then it follows from known bond length and bond angle geometries that  $a_c$  is in the range 0.5 to 0.6, so that  $N_c$  would have a value somewhere between 25 and 45 carbon atoms, corresponding to approximately 3-5 clusters between each cross-link point. For a network with  $f = 4$ , this increases to a value between 4 and 7 (19).

## CONCLUSIONS

We believe a number of important conclusions follow from this analysis, amongst the most significant of which are:

- 1) Solubility parameters for coal are not accurately determined from swelling measurements because of free volume effects.
- 2) The phase behaviour of the coal network/solvent has to be taken into account when conducting swelling measurements.
- 3) We predict that the phenomenon of gel collapse could occur in coal.
- 4) A simple model for coal swelling based on disinterspersion has been proposed, following the work of Bastide et al. (33,34).

## ACKNOWLEDGEMENTS

We gratefully acknowledge the support of the Office of Basic Energy Sciences, Division of Chemical Sciences, Department of Energy, under Grant No. DE-FG02-86ER13537.

## REFERENCES

1. Flory, P. J. Principles of Polymer Chemistry; Cornell University Press: Ithaca: NY, 1953.
2. Flory, P. J. Selected Works of Paul J. Flory; Mandelkern, L., Mark, J. E., Suter, U. W., Yoon, Do. Y., Eds.; Stanford University Press: Stanford, CA, 1985; Vol. I-III.
3. van Krevelen, D. W. Coal; Elsevier: New York, 1981.
4. van Krevelen, D. W. Fuel 1966, 45, 229.
5. Green, T.; Kovac, J.; Brenner, D.; Larsen, J. W. In Coal Structure; Meyers, R. A., Ed.; Academic: New York, 1982.
6. Larsen, J. W. In Chemistry and Physics of Coal Utilization; AIP Conference Proceedings, 70; Cooper, B. R., Petrakis, L., Eds.; AIP: New York, 1981.
7. Larsen, J. W.; Green, T. K.; Kovac, J. J. Org. Chem. 1985, 50, 4729.
8. Lucht, L. M.; Peppas, N. A. In chemistry and Physics of Coal Utilization, AIP Conference Proceedings 18; Cooper, B. R., Petrakis, L., Eds.; AIP: New York, 1981.
9. Lucht, L. M.; Peppas, N. A. Fuel 1987, 66, 803.
10. Lucht, L. M.; Peppas, N. A. J. Appl. Polym. Sci. 1987, 33, 2777.
11. Brenner, D. Fuel 1985, 64, 167.

12. DeGennes, P. G., *Scaling concepts in Polymer Physics*, Cornell University Press, Ithaca, NY, (1979).
13. Painter, P. C.; Park, Y.; Coleman, M. M., *Macromolecules*, 1988, 21, 66.
14. Painter, P. C.; Park, Y.; Coleman, M. M., *Macromolecules*, 1989, 22, 570.
15. Painter, P. C.; Park, Y.; Coleman, M. M., *Macromolecules*, 1989, 22, 580.
16. Painter, P. C., Graf, J. and Coleman, M. M. *J. Chem. Phys.* (submitted for publication).
17. Painter, P. C., Park, Y. and Coleman, M. M., *Energy and Fuels*, 1988, 2, 693.
18. Painter, P. C., Park, Y., Sobkowiak, M. and Coleman, M. M., *ACS Fuel Chem. Div. Preprints*, 1989, 34(2), 559.
19. Painter, P. C., Graf, J. and Coleman M. M., (to be submitted to *Energy and Fuels*).
20. Painter, P. C., Park, Y., Sobkowiak, M. and Coleman, M. M. (to be submitted to *Energy and Fuels*).
21. Painter, P. C., Graf, J., and Coleman, M. M. (to be submitted to *Energy and Fuels*).
22. van Krevelen, D. W. *Fuel* 1966, 45, 229.
23. van Krevelen, P. W., *Properties of Polymers*; Elsevier: Amsterdam, 1972.
24. Hoy, K. L., *J. Paint Technol.*, 1970, 42, 76.
25. Small, P. A., *J. Appl. Chem.*, 1953, 3, 71.
26. Bristow, G. M. and Watson W. F., *Trans. Faraday, Soc.*, 1958, 54, 1731.
27. Birois, J. Zeman, L. and Patterson, D. *Macromolecules*, 1971, 4, 30.
28. Sanchez, I. C. and Lacombe, R. H. *J. Phys. Chem.* 1976, 80, 2352, 2568.
29. Sanchez, I. C. and Lacombe, R. H. *Macromolecules*, 1978, 11, 1145.
30. Sanchez, I. C. and Lacombe, R. H. *J. Pol. Sci. Poly Letters Ed*, 1977, 15, 71.
31. Painter, P. C., Graf, J. and Coleman, M. M., to be published.
32. Kovac, J. *Macromolecules*, 1978, 11, 362.
33. Bastide, J., et al., as reported by Candau, S., Bastide, J. and Delsanti, M., *Advances in Polymer Science*, 1982, 44, 27.
34. Bastide, J., Picot, C., Candau, S., *J. Macromol. Sci., Phys.* 1981, B19, 13.

Table 4. Parameters for Solvents at 25°C

SOLVENTS	$V_s$ ( $\text{cm}^3 \text{mol}^{-1}$ )	$K_A$ ( $\text{kcal mol}^{-1}$ )	$h_s$ ( $\text{kcal mol}^{-1}$ )	$\delta_s$ ( $\text{cal cm}^{-3}$ ) <sup>1/2</sup>
PYRIDINE	81	284.87	8.9	10.6
THF	74.3	89.54	5.76	9.9
ACETON	74.3	58.9	4.03	9.9
DIETHYL ETHER	101.7	45.24	5.76	7.5
ACETONITRILE	55.4	23.56	2.03	11.8
BENZENE	82.2	1.41*	1.25	9.1

\* Weak H-bonds between OH groups and  $\pi$  electrons have been proposed.

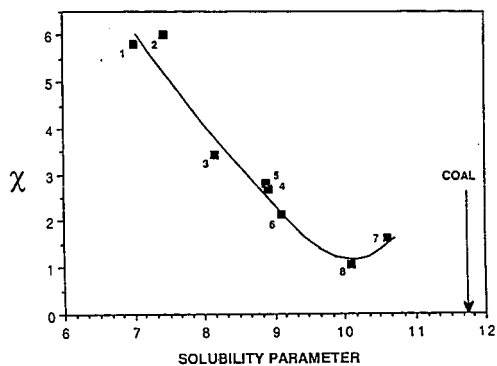


Figure 1. Plot of  $\chi$  vs solubility parameters for the Illinois #6 coal and solvents studied by Larsen et al. (7).

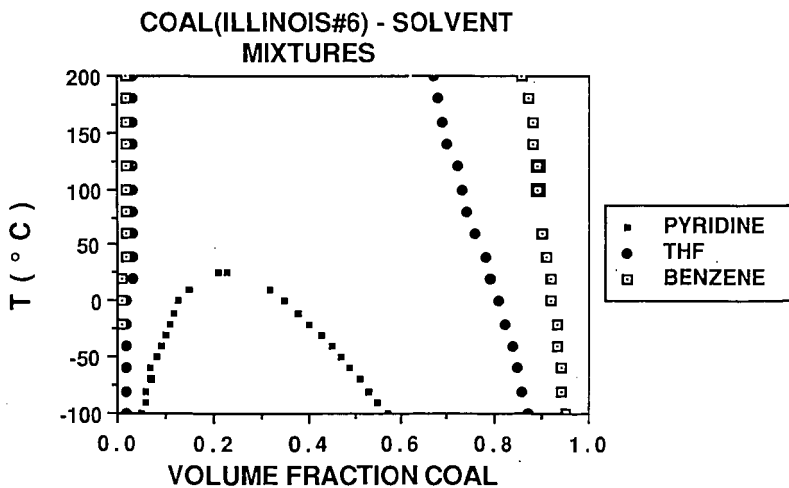


Figure 2. Phase diagram (spinodals) for an Illinois #6 coal mixed with various solvents.

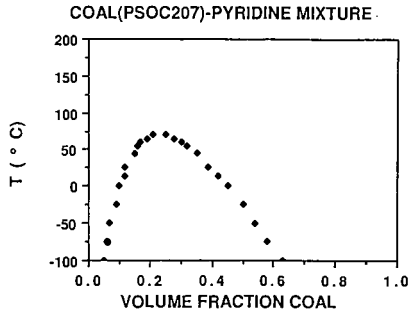


Figure 3. Phase diagram (spinodal) for PSOC 207-pyridine mixtures.

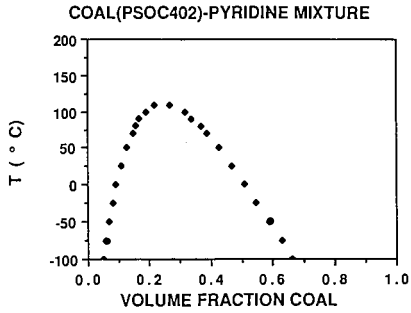


Figure 4. Spinodal for PSOC 402/pyridine mixtures.

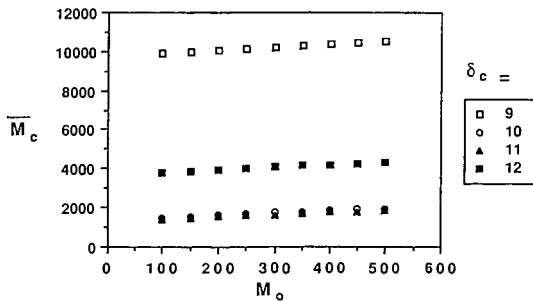


Figure 5. Plot of  $\overline{M}_c$  vs  $M_o$  (see text) for Illinois #6 coal, ignoring hydrogen bonds.

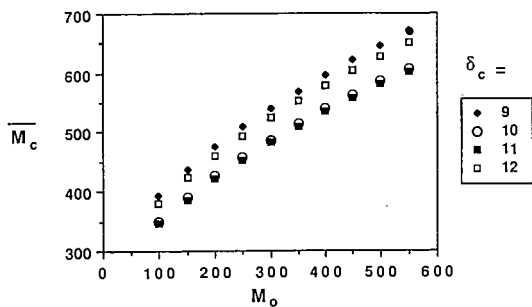


Figure 6. Plot of  $\bar{M}_c$  vs  $M_o$  for Illinois #6 coal when hydrogen bonding is included.

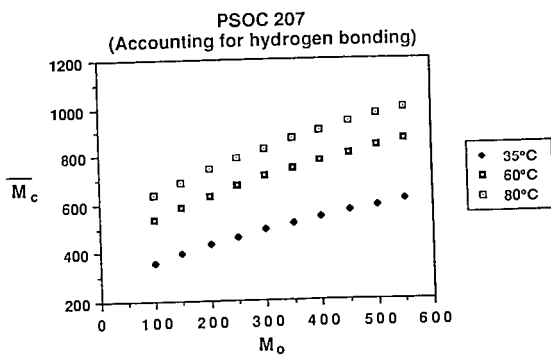


Figure 7.  $\bar{M}_c$  vs  $M_o$  for PSOC 207.

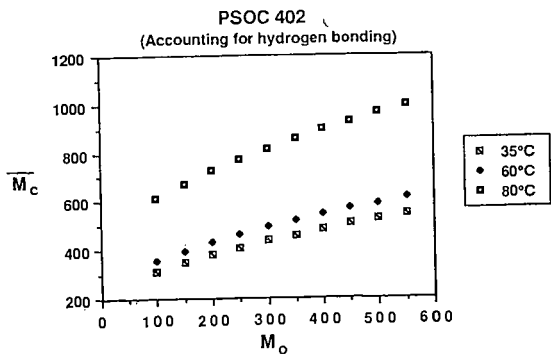


Figure 8.  $\bar{M}_c$  vs  $M_o$  for PSOC 402

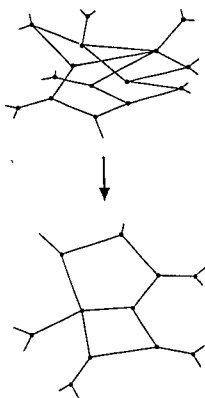


Figure 9. Disinterspersion for a network of rigid rods.

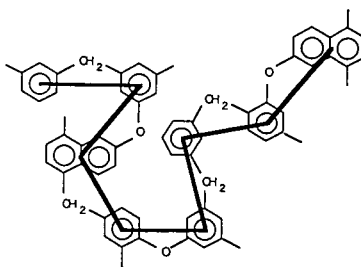


Figure 10. A random walk imposed by a pattern of substitution in a rigid chain.

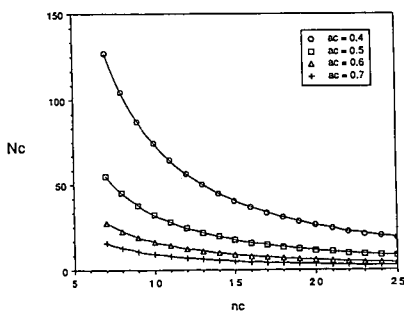


Figure 11. Plot of  $N_c$  (number of carbon atoms between cross link points) vs  $n_c$  (the number of carbon atoms per cluster).

## SOLVENT-INDUCED ASSOCIATIONS OF HIGH-VOLATILE BITUMINOUS COALS

Masaharu Nishioka\* and John W. Larsen

Corporate Research Science Laboratories  
Exxon Research and Engineering Company  
Clinton Township, Annandale, NJ 08801  
(\*Present address: BCR National Laboratory,  
500 William Pitt Way, Pittsburgh, PA 15238)

Keywords: association; soaking; hydrogen bonds

### INTRODUCTION

It is known that solvent-induced crystallization of amorphous polymers can occur below their glass transition temperatures. This conformational change of the polymer chains into a lower free energy state is facilitated by the presence of the solvent. We recently reported a similar solvent-induced association between coal macromolecules. This is analogous to the solvent-induced crystallization of amorphous polymers in that the amorphous coal macromolecules are altered to increase relatively strong intermolecular interactions leading to a lower free energy state.

It was previously observed that the pyridine extractability and optical anisotropy of Pittsburgh No. 8 coal decreased after heating at 115°C in chlorobenzene under nitrogen for seven days. Immersion in pyridine at room temperature for one day, followed by eliminating pyridine, had the same effect on pyridine extractability as exposure to hot chlorobenzene for a week. Treatment of the pyridine extract from the same coal with chlorobenzene (115°C, 1 week) resulted in about half of the formerly soluble extract becoming pyridine-insoluble. The physical interactions responsible for the solvent-induced conformational changes of coal macromolecules are relatively strong, because some of these interactions cannot be overcome by solvation with pyridine.

In this paper, the solvent-induced associations of several high-volatile bituminous coals were investigated in several solvents for various times. The scope and magnitude of the phenomenon in bituminous coals was investigated in several solvents for various times. The scope and magnitude of the phenomenon in bituminous coals was explored, though not exhaustively. Additional structural information on the changes occurring in these samples was obtained using FT-IR and X-ray diffraction.

### EXPERIMENTAL SECTION

ACS reagents and HPLC grade solvents were used. Tetrahydrofuran (THF) was distilled before use, and the other solvents were used without further purification. The coal samples were obtained from Exxon Research and Engineering Co. and the Pennsylvania State University Coal Bank. Their elemental

analyses were given in the previous paper.<sup>2</sup> Coal samples were ground and sifted under a nitrogen atmosphere. Minus 60-mesh size coal particles were used in the experiments.

Samples (two-gram) were extracted with 200 mL of pyridine for 24 hours in a Soxhlet apparatus under nitrogen atmosphere. The coal extracts were dried to constant weight in a vacuum oven at 50°C after evaporation of the pyridine.

Approximately 5 grams of each coal sample was placed in 100 mL of solvent in a 250 mL flask or a 300 mL autoclave and magnetically stirred under nitrogen. The mixture was either stirred at room temperature, heated, or mildly refluxed in an oil bath or in an autoclave heater. The cooled mixture was dried using a rotary evaporator, mixed with methanol, and filtered, while being rinsed with methanol several times. The coal was dried to constant weight in the vacuum oven at 50°C.

O-methylation was carried out following the method of Liotta.<sup>3</sup> Two different O-methylated Pittsburgh No. 8 coals were prepared. One was obtained using normal conditions (exhaustive alkylation), and the other was partially alkylated by using a limited amount of alkylation reagents. For the latter reaction, 5 grams of coal samples was placed in 100 mL of THF, and 1.5 cm<sup>3</sup> of 1M tetrabutylammonium hydroxide in methanol and 0.2 cm<sup>3</sup> of iodomethane were used in the reactions.

Infrared spectra were obtained on an IBM 97/IR Series Fourier Transform Photoacoustic Infrared Spectrometer. Spectra were recorded from 256 scans at 8 cm<sup>-1</sup> resolution against a reference of carbon black. Samples for infrared spectra were further evacuated for 12 hours at 100°C.

X-ray diffraction studies were carried out at ambient temperatures on a Phillips APD 3600 Automated Powder Diffractometer (Phillips Electronics Instruments, Inc., Mahwah, NJ) using CuK radiation (1.5418 Å) at 45 kV, 40 ma. The diffractometer was equipped with a graphite monochromator, theta-compensating slit, scintillation counter, and pulse-height selector. The X-ray data were collected, stored, and displayed using the APD 3600 data system.

## RESULTS

Pittsburgh No. 8 coal was immersed or mildly refluxed in the following hot solvents for times as long as 28 days: chlorobenzene, toluene, toluene/ethanol (95/5 vol %), and H<sub>2</sub>O. O-methylated Pittsburgh No. 8 coals were similarly treated in toluene for one week. These solvent-treated coals were dried and Soxhlet extracted with pyridine. The pyridine extraction yields are plotted in Figure 1. Figure 2 shows the changes in pyridine extractability (Soxhlet) with time for various high-volatile bituminous coals heated at 115°C in chlorobenzene. The solvent treatment resulted in decreasing amounts of pyridine extracts for all coals studied. Table I shows the change in pyridine Soxhlet extractability for Illinois No. 6 coal treated in chlorobenzene at different temperatures for 24 hours.

Structural differences between the original and the solvent-treated coals were investigated using photoacoustic Fourier transform infrared spectroscopy.

Absorptions due to hydrogen bonds in these samples were slightly different. Figure 3 shows overlay spectra (2810-3740  $\text{cm}^{-1}$ ) of the original, two-day, and four-week chlorobenzene-treated Pittsburgh No. 8 coals. No absorbance change between 3200-3516  $\text{cm}^{-1}$  was observed for the untreated coal after soaking in methanol and drying. The four-day, one-week and two-week chlorobenzene-treated coals gave spectra almost identical to that of the two-day treated coal.

Changes in aromatic parallel stacking due to solvent treatment were surveyed using the X-ray diffraction [002] band.<sup>4</sup> The X-ray [002] diffraction peak of the Pittsburgh No. 8 coal is very weak, and no change resulted from chlorobenzene treatment. A pyridine extract from Pittsburgh No. 8 coal was treated with chlorobenzene at 115°C for a week, and the portion rendered insoluble by this treatment was isolated and subjected to X-ray analysis. No [002] band was observed.

#### DISCUSSION

One of the major secondary interactions in coals is hydrogen bonds.<sup>5,6</sup> Toluene and chlorobenzene cannot break hydrogen bonds in coals at room temperature.<sup>5,7</sup> However, it is possible that weak hydrogen bonds are broken thermally at higher temperatures, because such solvents swell coals more at higher temperatures. The ability of chlorobenzene to disrupt the weak secondary interactions in coals is expected to be slightly greater than that of toluene, because of its greater interaction with coals as revealed by its higher solvent-swelling values. The ability of toluene containing ethanol to disrupt the weak secondary interactions should be greater than pure toluene since ethanol can participate in and break coal-coal hydrogen bonds while toluene cannot. Pyridine can break most, if not all, hydrogen bonds in coals at room temperature and so thoroughly disrupts these interactions.<sup>5,7</sup>

The relative rates of decrease in pyridine Soxhlet extraction yield of Pittsburgh No. 8 coal after solvent treatment (Figure 1) are consistent with the ability of the solvents to disrupt hydrogen bonds. The decrease was most rapid when the treating solvent was pyridine, slowest with toluene, and slightly faster with the toluene/ethanol mixed solvent than with pure toluene. The effect of chlorobenzene treatment was faster and larger than that of toluene over the 30-day period of the experiments. Hydroxyl groups can be capped by O-methylation, eliminating hydrogen bonds.<sup>3</sup> This treatment enhanced the rate of decrease of the pyridine Soxhlet extractability of toluene-treated coals.

The effect of solvent treatment on the hydrogen bonds present in this coal were studied by FT-IR using the band assignments recently reported by Painter et al. There are four general types of hydrogen-bonded structures<sup>-1</sup> involving hydroxyl groups in coal. These are found between 3200 and 3516  $\text{cm}^{-1}$ . In this study, the absorbance between 3200 and 3516  $\text{cm}^{-1}$  was examined. The intensity of the aliphatic C-H stretching band at 2930  $\text{cm}^{-1}$  was used as the reference in comparing the spectra. Weak hydrogen bonds were reduced after the solvent-induced conformational changes (Figure 3) as revealed by a decrease in the intensity of the IR peaks. Similar absorbance changes in hydrogen bonds have been observed for other coals used in this study. This loss is ascribed to a reduction in hydrogen bonding as a result of conformational changes.

It is proposed that solvent-induced conformational changes occur and that they require breaking secondary interactions. Direct structural evidence for hydrogen bond disruption has been obtained. Evidence for participation of other non-covalent interactions is indirect.

Pittsburgh No. 8 coal heated in boiling pyridine gave almost the same pyridine extraction yield as that of the starting coal if the pyridine was not removed from the treated coal.<sup>2</sup> Strong secondary interactions seem not to be produced in the pyridine-swollen state, but are formed during the pyridine-removal step. Probably, pyridine solvates the sites which can generate the strong secondary bonds so they form as pyridine is removed.

Anisotropic solvent swelling of coals has been studied using thin sections.<sup>7,9</sup> Coals swell more perpendicular to the bedding plane than parallel to it. After swelling with pyridine and removing it with a nitrogen flow, the coal shrank parallel to the bedding plane and expanded perpendicular to it. Similarly, the coal initially shrinks parallel to the bedding plane and expands perpendicular to it when thin sections are<sup>10</sup> treated with hot chlorobenzene or toluene and then dried with nitrogen.

Optical anisotropy in coals is well known.<sup>11</sup> Birefringence in coal thin sections and swollen thin sections was observed by Brenner. The loss of optical anisotropy in solvents at room temperature<sup>9,12</sup> coincided with the solvent's ability to break secondary interactions. The Birefringence of high-volatile bituminous coals apparently stems from a low degree of molecular orientation.<sup>12</sup> When macromolecules are in the glassy state, all large molecular chain motions are restricted, but segmental motion is not necessarily restricted.<sup>13</sup> The presence of a solvent in the coal macromolecules lowers the glass transition temperature.<sup>14</sup> Coal macromolecules may not be completely in the glassy state in cold pyridine, hot chlorobenzene or toluene, and some movement of coal can occur. The optical anisotropy of Pittsburgh No. 8 coal diminished after soaking in hot chlorobenzene.<sup>2</sup> The observed loss of optical anisotropy of Pittsburgh No. 8 coal after exposure to hot chlorobenzene provides additional evidence for conformational rearrangements in the swollen coal.

Pyridine breaks most or all of the hydrogen bonds in coals. Therefore, coal-coal hydrogen bonding will give no or a small effect on pyridine extractability. Since the pyridine extractability of the solvent-treated coal is smaller than that of the starting coal, it is likely that strong secondary interactions which are not hydrogen bonds are produced during the solvent-induced conformational change. An X-ray study of the effects of solvent treatment on the [002] band reveal no changes. The enhanced association does not include increased amounts of parallel face-to-face aromatic stacking. These imply that unknown complexes are involved in the new interactions.

A number of lines of evidence point to the solvent-induced association of coal molecules to a lower free energy state. Mined coals are in a metastable, strained state.<sup>7</sup> The existence of coals in a non-equilibrium state was shown by swelling and vapor uptake hysteresis.<sup>15,16</sup> These observations are presumably concerned with the initial movement of coal macromolecules during relaxation of the strained state as the coal is swollen by solvents. In high-volatile bituminous coals, physical interactions which cannot be broken by boiling pyridine are formed during pyridine removal, but are hardly formed in

the coal while it is fully pyridine swollen. The pyridine extract can aggregate during hot chlorobenzene treatment. These results demonstrate that the solvent-induced conformational change of coal macromolecules occurs with the coal achieving a lower free-energy state after relaxation. Secondary interactions originally present in the coal are broken and other secondary interactions are generated by the solvent-treatment. One view of this is schematically shown in Figure 4. The rates of disruption and formation of these secondary interactions will be dependent upon original coal properties, the interaction between the coal and the solvents used, and system conditions.

#### ACKNOWLEDGMENTS

We thank G. D. Cody, Jr. and M. Siskin for helpful discussions. The effort of J. C. Scanlon for making X-ray measurements is gratefully acknowledged.

#### REFERENCES

1. Jameel, H., Waldman, J., and Regenfeld, L., J. Appl. Polym. Sci., 1981, 26, 1975-1811, and references cited in the paper.
2. Nishioka, M. and Larsen, J. W., Energy & Fuels, submitted.
3. Liotta, R., Fuel, 1979, 58, 724-728.
4. Hirsh, P. B., Proc. Royal Soc. (London), 1954, A226, 143-169.
5. Larsen, J. W. and Baskar, A. J., Energy & Fuels, 1987, 1, 230-232.
6. Painter, P. C., Sobkowiak, M., and Youtcheff, J., Fuel, 1987, 66, 973-978.
7. Cody, G. D., Jr., Larsen, J. W., and Siskin, M., Energy & Fuels, 1988, 2, 340-344.
8. Sanada, Y. and Honda, H., Fuel, 1966, 45, 451-456.
9. Brenner, D., Fuel, 1985, 64, 167-456.
10. Jeffreys, H. E. and Cody, G. D., Jr., unpublished data.
11. van Krevelen, D. W., Coal; Elsevier: New York, 1961, Chapter 17.
12. Cody, G. D., Jr., Larsen, J. W., and Siskin, M., unpublished data.
13. Barr-Howell, B. D., Howell, J. M., and Peppas, N. A., Energy & Fuels, 1987, 1, 181-1186.
14. Lucht, L. M., Larson, J. M., and Peppas, N. A., Energy & Fuels, 1987, 1, 56-58.
15. Ritger, P. L. and Peppas, N. A., Fuel, 1987, 66, 1379-1388, and the preceding series of papers.
16. Hsieh, S. T. and Duda, J. L., Fuel, 1987, 66, 170-178.

TABLE I. PYRIDINE SOXHLET EXTRACTION YIELDS (WT %) OF ILLINOIS NO. 6 COAL  
AFTER SOAKING IN CHLOROBENZENE AT DIFFERENT TEMPERATURES FOR 24 HOURS

<u>Temperature</u> (°C)	<u>Extraction Yield</u> (wt %)
23	27
115	19
200	16
300	24 + tar (20)*

\*Tar was recovered during methanol rinsing.  
The yield is wt % of the coal.

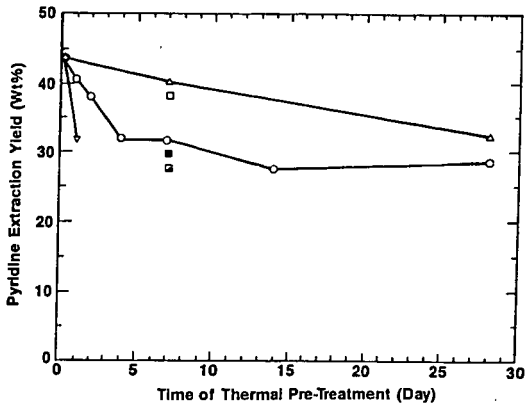


Figure 1. Change of pyridine extractability (Soxhlet) of Pittsburgh No. 8 coal immersed in solvents and dried, (V) room temperature pyridine, (O) 115°C chlorobenzene, (Δ) 100°C toluene, (□) 107°C toluene/ethanol (95/5 vol %) and 100°C toluene for completely (◻) and partly (◼) 0-methylated coal.

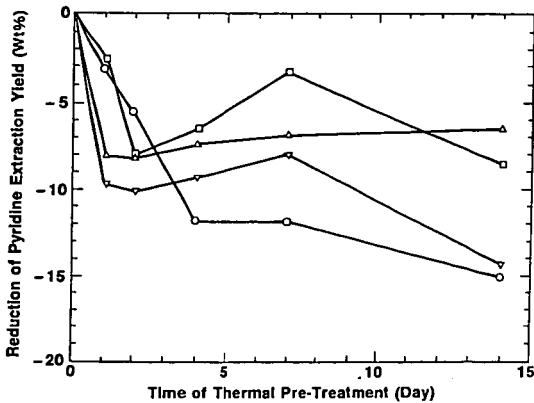


Figure 2. Difference of pyridine extraction (Soxhlet) yields between chlorobenzene-treated coals and starting coals for various ranks of high volatile bituminous coals. Key: (Δ) Wandoan, (V) Illinois No. 6, (O) Pittsburgh No. 8, and (□) PSOC-1336.

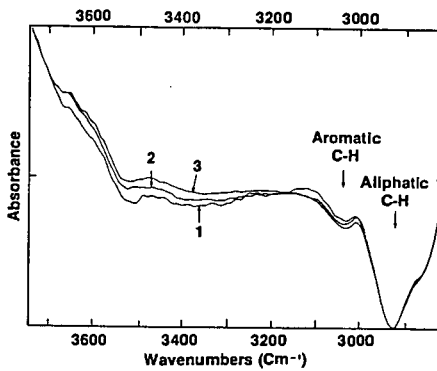


Figure 3. Overlay photoacoustic infrared Fourier transform spectra of (1) starting, (2) 2-day chlorobenzene-treated, and (3) 4-week chlorobenzene-treated Pittsburgh No. 8 coals.

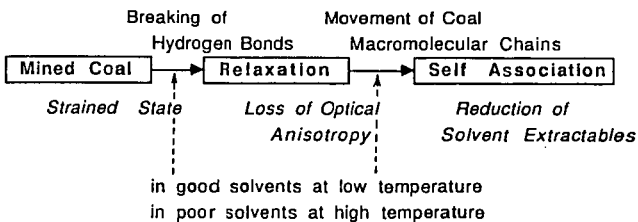


Figure 4. Schematic diagram for solvent-induced conformational changes of macromolecules in high-volatile bituminous coals.

## RANK DEPENDENCE OF ASSOCIATIVE EQUILIBRIA OF COAL MOLECULES IN SOLVENTS

M. Nishioka\*

Exxon Research and Engineering Company, Clinton Township, Annandale, NJ 08801

\*Present address: BCR National Laboratory  
500 William Pitt Way  
Pittsburgh, PA 15238

Keywords: associative equilibrium; extraction rate; intermolecular interaction

### Introduction

Solvent-induced association (a conformational change) of several high-volatile bituminous coals was observed in hot toluene, hot chlorobenzene, and cold pyridine.<sup>1,2</sup> It was proposed that the solvent-induced conformational change is due to two concerted processes: breaking secondary interactions originally present and forming new secondary interactions in a lower free energy state. This implies that associative equilibria between coal molecules will exist in solvents. In this paper, the rank dependence of the associative equilibria and intermolecular interactions is investigated.

### Experimental Section

All ACS and HPLC grade chemicals were used without further purification. The coal samples were obtained from Exxon Research and Engineering Co., and the Pennsylvania State University Coal Bank. Their elemental analyses were reported in the previous paper.<sup>1</sup> Coal samples were ground and sifted under a nitrogen atmosphere. Minus 60 mesh particles were used in the experiments.

Approximately 2 to 5 g of each coal sample were placed in a 250 mL flask in 100 mL of pyridine and either stirred at room temperature or refluxed (115°C) under dry N<sub>2</sub> in an oil bath. One series of cooled samples was dried using a rotary evaporator, mixed with methanol, filtered, and rinsed with methanol several times. The coal was then dried to constant weight in the vacuum oven at 50°C. Another series of samples was filtered and the wet residues promptly Soxhlet-extracted.

The Diels-Alder reaction has been reported.<sup>1</sup> Maleic anhydride adducts formed using phenol solvent were precipitated in methanol, filtered, and then Soxhlet-extracted with methanol for 24 hrs. in order to eliminate by-products formed by reactions of maleic anhydride and phenol before removal of non-reacted maleic anhydride by Soxhlet extraction with H<sub>2</sub>O. The by-products were easily extracted with methanol, which was verified by using a blank experiment without coal. The major molecular masses of by-products from coal, and those obtained using the blank experiment, were the same: 270, 322, and 362. Infrared spectra and X-ray diffraction studies were carried out as previously described.<sup>2</sup>

### Results and Discussion

Pyridine extractability rectilinearly increases up to ca. 87 wt% C coal (named here as A-region), then decreases sharply with rank (87-90 wt% C: B-region).<sup>3</sup> At still higher rank (>90 wt% C: C-region), only a few percent is extracted.

Pyridine extraction rate was compared for each region coal, and selected results are shown in Figure 1. A-region coal was promptly extracted within one or two days, while more than seven days were required for the extraction of B-region coal to be completed under the same conditions. C-region coal yields extract slowly, and the ultimate extractability is very small.

Pyridine extractability of the A-region coal was greater at the boiling point (115°C) than at room temperature,<sup>1</sup> but extraction yields of the A-region coal at 115°C and at 180°C were similar.<sup>3,4</sup> However, pyridine extractability of the B-region coal at 180°C is much greater than that at 115°C.<sup>4</sup>

Since it was first reported by Harger and Illingworth<sup>5,6</sup> that coals preheated at 200 to 400°C in an inert atmosphere give much higher yields of extract than unheated coals, the preheating effect has been investigated by several groups, and recently reviewed.<sup>7</sup> Solvent extractability increases with preheating temperature, reaches a maximum, and then declines.<sup>3,8</sup> However, the pyridine and chloroform extraction yields of the A-region coal were only slightly increased by preheating to 300°C, while the B-region coal was much more extractable after preheating at temperatures below 300°C.<sup>3</sup> The dependence of the preheating effect on coal rank was recently studied by preheating at 250°C for 24 hrs.<sup>7</sup> The effect was highly rank-dependent. Tetrahydrofuran extraction yields of higher-rank coals increased after preheating, while those of lower-rank coals decreased. These data show that A and B-region coals differ in their response to heating.

Heating the A-region coal at 115°C in chlorobenzene for seven days caused a decrease in pyridine extractability.<sup>1</sup> The same solvent treatment was given to a B-region coal, PSOC-1300 (89.9% C), in this study, but the pyridine extraction yield (24 hrs) of this treated coal increased to 18 wt% from 7 wt%. Figure 2 shows the change in pyridine extraction yields caused by soaking coal in pyridine at the boiling point for seven days for various A- and B-region coals. The pyridine extractabilities of coals dried after soaking in pyridine at room temperature for one day are also included in this figure. Pyridine extractabilities of the B-region coals significantly increased after soaking in pyridine at the boiling point for seven days contrary to those of the A-region coals. Pyridine extractabilities of the coals dried after soaking in pyridine at room temperature decreased for the A-region coals, but slightly increased for the B-region coals. These data show that the pyridine extractabilities of the A- and B-region coals after treatment with pyridine and chlorobenzene result in opposites.

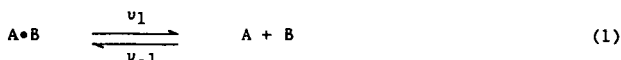
Aggregations are seen in phase separation phenomena such as precipitation, gelation, and crystallization. Dormans and van Krevelen<sup>3</sup> studied precipitation from a pyridine soluble Soxhlet-extract at room temperature. Pyridine extracts from the A-region coal did not form precipitates after 240 hrs, while those from the B- and C-region coals yielded precipitates amounting to between 10 and 30 wt% of the extract. In the present study, the pyridine extract of an A-region coal, PSOC-1336 (84.1% C), was concentrated, filtered, and held at room temperature under nitrogen. The extract with concentration of 13.4 mg/cm<sup>3</sup> showed no precipitate after 14 days, while the extract with concentration of 55.3 mg/cm<sup>3</sup> precipitated 0.5 wt% of the extract after 5 days. The precipitate could be easily seen at the bottom of a flask. Concentrated pyridine extracts of other A-region coals, Illinois No. 6 (79.9% C) and Pittsburgh No. 8 (83.8% C), also formed precipitates if their concentration were more than 100 mg/cm<sup>3</sup>. van Krevelen's work suggests that high temperature (Soxhlet extraction) extracts of the B- and

C-region coals easily associate at low (room) temperature. The present work shows that high temperature extracts of the A-region coal do not associate at low temperature when diluted, but concentrated extracts do tend to associate.

All of the above data are summarized in Table I. These data can be understood as the result of change of the equilibrium state of coal molecules in solvents. The associative equilibria seem to be highly rank-dependent.

From the above results, it is suggested that extractability may be controlled by the equilibrium state between a solvent and coal. This is amendable to a quantitative treatment.

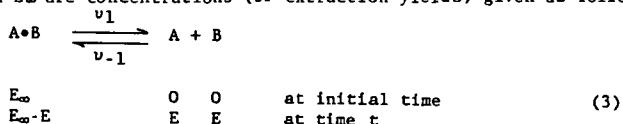
Assume that a complex A·B equilibrates with each component A and B in a solvent.



If the complex A·B is not extractable, components A and B are extractable with a solvent, and the rate  $v_1$  is much greater than the rate  $v_{-1}$ , the extraction rate of each component is given as

$$\frac{dE}{dt} = k_1 (E_\infty - E) \quad (v_1 \gg v_{-1}) \quad (2)$$

where  $E$  and  $E_\infty$  are concentrations (or extraction yields) given as follows



Therefore, an extraction yield at given time is

$$E = E_\infty (1 - e^{-k_1 t}) \quad (4)$$

where  $E_\infty$  and  $k_1$  are regarded as an ultimate extraction yield and an extraction rate constant, respectively. A similar equation was derived by Oele *et al.*<sup>9</sup> for the extractive disintegration of bituminous coals at high temperatures (150 to 350°C) in an anthracene oil and  $\beta$ -naphthol. They assumed a zero order process for a forward disintegration at the initial step and additionally a first order process for a backward integration when extraction proceeds. Equation (4) is a first order rate. The rate constant  $k_1$  is determined by extraction yields  $E_1$  and  $E_2$  at two different times  $t_1$  and  $t_2$ ,

$$k_1 = \frac{\ln \frac{E_\infty - E_1}{E_\infty - E_2}}{t_2 - t_1} \quad (5)$$

or by measurement of increment of extraction by half ( $\tau$ )

$$k_1 = \frac{\ln 2}{\tau} \quad (6)$$

Calculated values using Equation (4) are shown in Figure 1 as well as experimental results for extractability versus extraction time. Extraction rate can be approximated by using Equation (4). Therefore, the dissociation of the coal-coal interactions can be thought of the major rate determining step in an extraction process. The slow rate of Soxhlet extraction is attributed to the slow dissociation (small  $k_1$ ) of aggregated clusters. The stronger the physical interactions are, the smaller will be the rate constants  $k_1$ . The poorer solvents are for the extract, the smaller rate constants  $k_1$  will be. In the case of very small rate constants, high temperature could be required to overcome the activation energy to allow dissociation of components.

Since high temperatures and good solvents are apparently needed to dissociate the aggregated clusters in the B- and C-region coals (Table I), chemical reactivity for these coals should be promoted at the higher temperatures and good solvents which lead to dissociation, while that for the A-region coal should not be enhanced even at the same condition. The Diels-Alder reaction has been utilized to weaken the interaction between polynuclear aromatics in coals.<sup>1,10</sup> In this work, maleic anhydride was reacted with each region coal in phenol at 115 and 180°C, and the product was pyridine-extracted.<sup>1,10</sup> Increased extractability at 180°C was observed for all coals, but the increases for B- and C-region coals were much greater than that of the A-region coal. A-region extractability increased by 1/3, while the B- and C-region extractabilities increased by factors of 7 and 15, respectively. The enhancements of pyridine extractabilities for the B- and C-regions coals were particularly remarkable as compared with the results obtained by using a chlorobenzene solvent (115°C).

The IR absorptions between 1700 and 1750  $\text{cm}^{-1}$  assigned to carbonyl vibrations in maleic anhydride adducts are shown in Figure 3 for a starting C-region coal, PSOC-688 (92.0ZC), and its maleic anhydride adducts reacted under various conditions. These results demonstrate more maleic anhydride incorporation at higher temperature, although the Diels-Alder reaction is reversible and low temperatures are preferred for adduct formation. Pyridine is a good solvent but cannot be used for this reaction, because this solvent catalyzes the polymerization of maleic anhydride.<sup>10</sup> These results suggest that the intermolecular interaction dissociable at high temperature play an important structural role in the B- and C-region coals and is responsible for the differences in behaviors shown in Table I for each region coal.

Figure 4 shows the change in the X-ray diffraction [002] band caused by reaction with maleic anhydride. This band is due to the parallel stacking of aromatic systems.<sup>11</sup> The magnitude and half-width of the maleic anhydride adduct of the PSOC-688 reacted in chlorobenzene at 115°C was identical with that of starting coal. The parallel stacking was obviously reduced after the maleic anhydride reaction in phenol at 180°C. This result implies that the incorporation of maleic anhydride decreases the number of face-to-face aromatic stacks, and that the face-to-face interaction may be responsible, in part, for the association in high-rank coal.

### References

1. Nishioka, M.; Larsen, J. W. Energy & Fuels in press.
2. Nishioka, M.; Larsen, J. W. Prepr. Am. Chem. Soc. Div. Fuel Chem. 1990.
3. Dormans, H. N. M.; van Krevelen, D. W. Fuel 1960, 39, 273-292.
4. Illingworth, S. R. Fuel 1922, 24, 213-219.
5. Harger, J. J. Soc. Chem. Ind. 1914, 33, 389-392.
6. Illingworth, S. R. J. Soc. Chem. Ind. 1920, 39, 111-118.
7. Nishioka, M.; Larsen, J. W. Energy & Fuels 1988, 2, 351-355.
8. Wynne-Jones, W. F. K.; Blayden, H. E.; Shaw, F. Brennstoff-Chem. 1952, 33, 201-206.
9. Oele, A. P.; Waterman, H. I.; Goedkoop, M. L.; van Krevelen, D. W. Fuel 1951, 30, 169-178.
10. Quinga, E. M. Y.; Larsen, J. W. Energy & Fuels 1987, 1, 300-304.
11. Hirsh, P. B. Proc. Royal Soc. (London) 1954, A226, 143-169.

Table I. Differences in Behaviors in Extraction, Soaking, and Sitting Extract for Each Region Coal.

%C (daf)	A <87	B 87-90	C <sup>a</sup> >90
1. Pyridine extraction rate	fast	slow	
2. Temperature (115°C & 180°C) effect on pyridine extraction	small	large	
3. Preheating (200-400°C) effect on pyridine extraction	small	large	
4. Immersion in pyridine and removal of the solvent before pyridine extraction	decrease in extractability	increase in extractability	
5. Soaking in hot toluene or chlorobenzene before pyridine extraction	decrease in extractability	increase in extractability	
6. Precipitation of Soxhlet pyridine extracts at room temperature	no precipitation <sup>b</sup>	precipitation	

<sup>a</sup>Differences are very small because of very small ultimate extractability.

<sup>b</sup>Precipitation occurs only at high concentration.

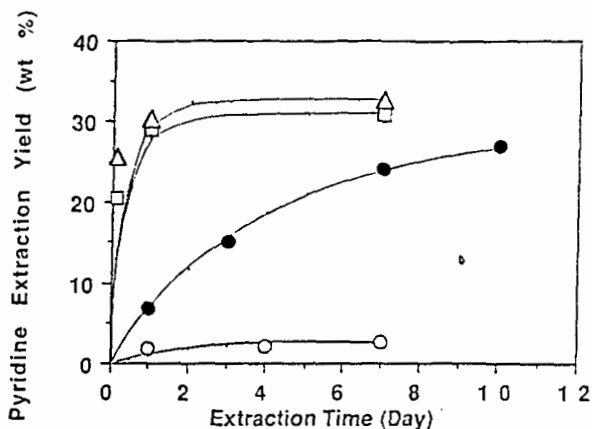


Figure 1. Pyridine extractability versus extraction time. Key: (□) Illinois No. 6 (79.9% $C$ ) ( $E_{\infty} = 31.2$ ,  $k_1 = 2.3$ ), ( $\Delta$ ) PSOC-1336 (84.1% $C$ ) ( $E_{\infty} = 32.8$ ,  $k_1 = 2.3$ ), ( $\bullet$ ) PSOC-1300 (89.9% $C$ ) ( $E_{\infty} = 29.0$ ,  $k_1 = 0.26$ ), and ( $\circ$ ) PSOC-688 (92.0% $C$ ) ( $E_{\infty} = 2.7$ ,  $k_1 = 0.43$ ).

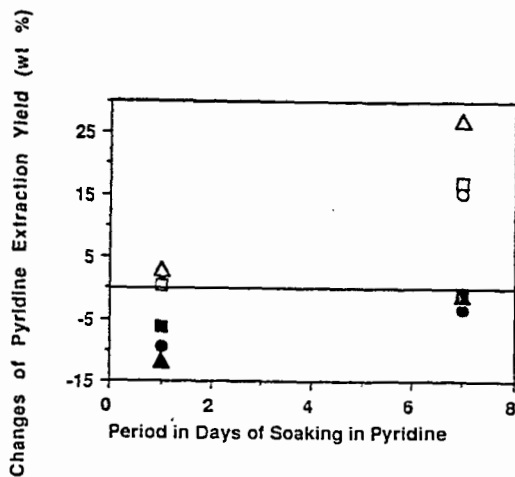


Figure 2. Changes of pyridine extractabilities of the A and B-region coals immersed in pyridine at the boiling point for seven days and their dried coals after immersing in pyridine at room temperature for one day. Key: ( $\Delta$ ) PSOC-991 (89.4% $C$ ), ( $\square$ ) PSOC-1300 (89.9% $C$ ), ( $\circ$ ) PSOC-721 (88.5% $C$ ), ( $\blacksquare$ ) Illinois No. 6 (79.9% $C$ ), ( $\bullet$ ) PSOC-1336 (84.1% $C$ ), and ( $\triangle$ ) Pittsburgh No. 8 (83.8% $C$ ).

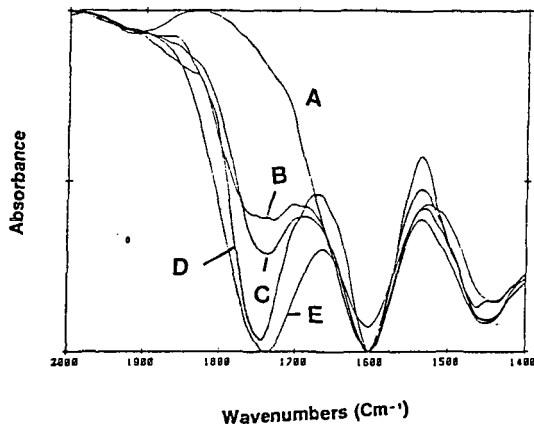


Figure 3. Overlay photoacoustic infrared Fourier transform spectra assigned to the carbonyl groups of (A) starting coal and maleic anhydride adducts of PSOC-688 reacted under selected solvents and temperature. Conditions of Diels-Alder reaction: (B) in chlorobenzene at 115°C, (C) in phenol at 115°C, (D) in phenol at 180°C, and (E) in 1,2-dichlorobenzene at 180°C.

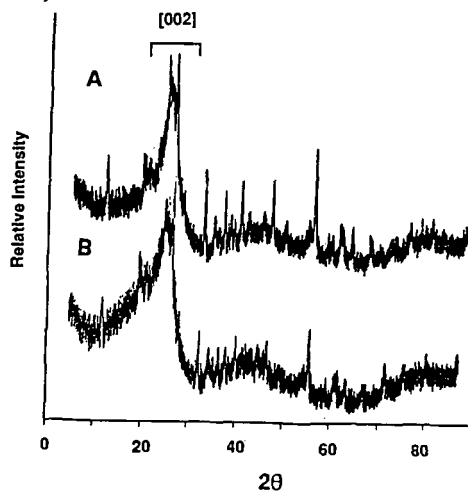


Figure 4. X-ray diffraction patterns of [002] band of maleic anhydride adducts of PSOC-688 reacted (A) in chlorobenzene at 115°C and (B) in phenol at 180°C.

## COAL ANALYSIS BY TG-FTIR

P.R. Solomon, M.A. Serio, R.M. Carangelo, and R. Bassilakis  
Advanced Fuel Research, Inc.  
87 Church Street, East Hartford, CT 06108 USA

**KEYWORDS:** Coal, Analysis, Pyrolysis, Combustion, TGA, FTIR

### INTRODUCTION

Thermogravimetric analysis has been employed in coal science to perform a number of characterizations including: proximate analysis (1), kinetics of weight loss (2,3) char reactivity (4-9) and gas adsorption measurements (10). A complimentary technique, evolved product analysis, has been employed to study pyrolysis product distributions and kinetics (11-18) functional group compositions (14,19-21), and temperature programmed desorption (22-24).

We have developed a TG-FTIR instrument which combines thermogravimetric analysis (TGA) with evolved product analysis by Fourier Transform Infrared (FT-IR) spectroscopy. FT-IR analysis of evolved products has advantages over mass spectroscopy in allowing analysis of very heavy products, and over gas chromatography in speed. To analyze coal, a sequence of drying, pyrolysis and combustion is employed to obtain: proximate analysis, volatiles composition, volatiles kinetics, and relative char reactivity. The application of TG-FTIR to coal and petroleum source rock has recently been described (25,26). The purpose of this paper is to describe the most recent improvements in the apparatus.

### EXPERIMENTAL

**Apparatus** - A schematic of the instrument is presented in Fig. 1. Its components are as follows: a DuPont™ 951 TGA; a hardware interface (including a furnace power supply); an Infrared Analysis 16 pass gas cell with transfer optics; a MICHELSON 110 FT-IR; (Resolution: 4  $\text{cm}^{-1}$ , Detector: MCT). A helium sweep gas is employed to bring evolved products from the TGA directly into the gas cell. This instrument package is now available commercially as the TG/plus from Bomem, Inc.

The most difficult volatiles to analyze are the heavy decomposition products which condense at room temperature, such as tars from coal. In the TG/plus, the high conductivity helium sweep gas and the rapid cooling causes these products to form an aerosol which is fine enough to follow the gas through the analysis cell. The cell is connected without restrictions to the sample area. The aerosol is also fine enough that there is little scattering of the infrared beam and it is thus attenuated as though the tar was in the gas phase.

**Procedure** - As an example of the analysis procedure, the pyrolysis and oxidation of a lignite is described. More detail can be found in Refs. 25 and 26. Figure 2a illustrates the weight loss from this sample and the temperature history. A 35 mg sample of Indian Head Zap lignite, loaded in the sample basket of the DuPont™ 951, is taken on a 30°C/min temperature excursion in the helium sweep gas, first to 150°C where it is held for 4 minutes to dry, then to 900°C for pyrolysis. The temperature is held at 900°C for 3 minutes. After cooling to 250°C, a small flow of  $\text{O}_2$  is added to the furnace at the 57 minute mark and the temperature is ramped at 30°C/min to 700°C (or higher) for oxidation.

During this excursion, infrared spectra are obtained once every thirty seconds. As discussed previously (25,26), the spectra show absorption bands for  $\text{CO}$ ,  $\text{CO}_2$ ,  $\text{CH}_4$ ,  $\text{H}_2\text{O}$ ,  $\text{SO}_2$ ,  $\text{COS}$ ,  $\text{C}_2\text{H}_4$ , olefins,  $\text{HCl}$ , and  $\text{NH}_3$ . The spectra above 400°C also show aliphatic, aromatic, hydroxyl, carbonyl and ether bands from tar. The evolution of gases derived from the IR absorbance spectra are obtained by a quantitative analysis program which employs a database of integration regions and calibration spectra for different compounds. The routine decides which regions of each calibration spectrum to use for best quantitation with the least interferences. The routine is fast so the product analysis is displayed during the actual experiment.

Figure 2b illustrates the integral of the evolution curves to obtain cumulative evolved product amounts. Because the data are quantitative, the sum of these curves match the weight loss as

determined by the TGA balance. Discrepancies occur in this match because of missing components such as  $H_2$  which cannot be seen by IR and  $H_2S$  which is very difficult to see. Secondly, when  $O_2$  is introduced, the balance shows a net gain in weight due to  $O_2$  chemisorption.

**Calibration** - To calibrate the instrument, known flows for calibration gases were mixed with a fixed flow of sweep gas and passed through the gas cell. Reference spectra were collected and the flow rate was varied to provide spectra over the range of expected concentrations. The quantitative analysis program employs the spectrum which most closely matches the experimental amplitudes since Beer's law (absorption is proportional to concentration) is not valid for many light gases.

Calibration spectra cannot be employed in the same way for tar since the absorptivity of any band varies with the tar compositions. Instead, the evolution of tar is derived by using the spectrum of a Pittsburgh Seam coal tar as a calibration standard. This coal tar has all the functional group features (but at different intensities) characteristic of coal tars. Its use as a reference spectrum determines the important tar functional group regions whose amplitudes provide a qualitative tar evolution profile for other coals. The tar's evolution determined in this manner typically exhibits a sharply peaked function with increasing temperature as shown in Fig. 3a.

To quantitatively determine the tar loss, it is assumed that the qualitative tar evolution profile is proportional to the rate of loss of tar. This will be true when the functional group compositions of the tar does not change with temperature, a condition which holds over most of the tar evolution profile as indicated by examining the infrared spectra at various times during its evolution. To determine the constant of proportionality for each sample, the tar loss profile is compared to the rate of weight loss from the balance minus the rate of weight loss for all the gases. This quantity is presented in Fig. 3b. The proportionality constant is picked by performing a least squares fit between the two curves over the region of tar evolution, except for parts where other gases are evolving quickly and might introduce error. The proportionality constant varies systematically from 0.86 times the absorptivity for Pittsburgh Seam coal for Zap lignite to 1.56 times Pittsburgh Seam coal for Pocahontas in agreement with the lower absorptivity of the aromatic components in the higher rank coals.

Routine calibration of the instrument is performed on a monthly basis using calcium oxalate. A typical evolution profile is presented in Fig. 4. The calcium oxalate has three weight loss regions yielding  $H_2O$ ,  $CO_2$ , and  $CO$ . The agreement between the sum of gases and weight loss shows that the calibration and the sweep gas flow rate are accurate. The positions of peaks compared to a known reference validates the accuracy of the thermocouple temperature measurement. To check for possible leaks in the system and the absence of oxygen in the helium sweep gas, graphite is run periodically. If there are no leaks and the helium is of high purity, no appreciable weight loss or  $CO_2$  evolution is experienced during the pyrolysis cycle.

**Samples** - The coals analyzed were Argonne premium coal samples. The characterization of these samples has appeared elsewhere (27). In addition, demineralized coals were produced using the technique of Bishop and Ward (28). This technique removes both discrete minerals as well as organically bound alkali or alkaline earth metals. Oxidized samples were prepared in an oven at  $100^\circ C$  or at room temperature in air.

## RESULTS AND DISCUSSION

**Analysis of Argonne Coals** - Analyses were performed for eight Argonne coals at both  $3^\circ C/min$  and  $30^\circ C/min$ . Results for three coals for the pyrolysis cycle ( $30^\circ C/min$ ) are presented in Figs. 5 to 7. Figures 5a to 7a presents the weight losses and temperature profiles. Also presented (dashed line) is the sum of species (tar,  $CH_4$ ,  $H_2O$ ,  $CO_2$ ,  $CO$ ,  $SO_2$ , and  $NH_3$ ). In general, the sum of species is within a few percent of the weight loss.

The evolution of tar and aliphatic gases is presented in Figs. 5c to 7c. These tar evolution profiles typically consist of a low temperature peak or shoulder followed by a narrow larger peak. The low temperature peak is believed to be due to the evaporation of unattached "guest" molecules (the molecular phase). The higher temperature peak is due to the release of coal fragments by bond breaking, evaporation and transport (29). In Fig. 5c, these peaks are labeled 1 (molecular phase) and 2 (pyrolysis).

Methane evolution is presented in Figs. 5e to 7e. Methane evolution occurs in two closely spaced peaks. The low temperature peak is initiated coincident with the initiation of tar evolution, but reaches a maximum at a slightly higher temperature than the maximum tar peak. The temperature for the maximum evolution varies little with rank but the temperature of initiation of methane evolution decreases with decreasing rank. The second peak appears as a shoulder on the high temperature side of the first peak. In Fig. 5e, these peaks are labeled 1 (methane loose) and 2 (methane tight).

Water evolution is presented in Figs. 5b to 7b. Water appears first at low temperature when the coal's moisture is evolved. For all coals, a prominent water peak also occurs simultaneously with the tar peak. This suggests that the chemistry responsible for this peak is either related to the free radicals produced, or the increase in fluidity (and hence mobility for bi-molecular interactions), both of which occur during tar formation. Burnham et al. (17) report the coincidence of the tar peak with the low temperature peaks for CO<sub>2</sub> and H<sub>2</sub>S, which supports the idea that tar evolution is associated with the decomposition of heteroatom functionalities. There is also a higher temperature H<sub>2</sub>O peak and a lower temperature peak or shoulder accompanying CO<sub>2</sub> evolution in low rank coals. In Fig. 7b, these peaks are labeled 1 (moisture), 2 (water extra loose, associated with early CO<sub>2</sub> evolution), 3 (water loose, associated with tar evolution), and 4 (water tight).

Figures 5d to 7d present the results for CO<sub>2</sub>. Wyodak (Fig. 7d) which is typical of low rank coals, shows three peaks between 200 and 900 °C labeled 2 (extra loose associated with H<sub>2</sub>O), 3 (loose associated with tar evolution and H<sub>2</sub>O evolution) and 4 (CO<sub>2</sub> tight). There is also a very low temperature peak labeled 1 (occurring only for the lowest rank coals) whose origin is presently unknown. Higher rank coals usually have peaks 3 and 4 but not peak 2 unless they are oxidized. Peak 2 is one of the regions affected most by oxidation. In addition, the evolution of CO<sub>2</sub> is often complicated in high rank coals by the evolution of CO<sub>2</sub> from carbonates such as calcite (Fig. 6d) and siderite.

The evolution of CO is presented in Figs. 5f to 7f. Low rank coals exhibit three peaks labeled 3, 4, and 5 as shown in Fig. 7f. Peaks 3 and 4 coincides with the CO<sub>2</sub> peaks 3 and 4, while peak 5 has no accompanying peaks for H<sub>2</sub>O or CO<sub>2</sub>. CO peaks also can be seen accompanying the CO<sub>2</sub> calcite peak (see Fig. 6). High rank coals appear to have only the high temperature peak 5.

Results for other gases are presented in parts g to i of Figs. 5 to 7. The C<sub>2</sub>H<sub>2</sub> yield shown in Figs. 5g to 7g occurs in a narrow evolution peak which lags the tar peak but precedes the methane. The ammonia evolution in Fig. 5h to 7h appear to coincide with the start of CO evolution (Figs. 5f to 7f). The SO<sub>2</sub> peak near 28 minutes (Figs. 5i to 7i) appears to coincide with one of the COS peaks (Figs. 5j to 7j).

Sample results for the combustion cycle are presented in Fig. 8. Since oxygen is added, the reported weight loss is for the elements C, H, S, not the oxide. This will make the sum of the elements (C, H, and S) lost less than the total measured weight loss, the difference being the oxygen in the char. The combustion cycle is dominated by the evolution of CO<sub>2</sub>, CO, and SO<sub>2</sub>. The sum of the C, H, and S in these species is in reasonable agreement with the weight loss.

**Analysis of Minerals** - The identification of evolution peaks due to minerals was made by performing TG/plus analysis of reference minerals and demineralized coals. An important contributor is calcite. The major reaction is the evolution of CO<sub>2</sub> near 800 °C. There are also small amounts of CO and H<sub>2</sub>O evolved. The CO<sub>2</sub> peak is almost identical in shape and position to that exhibited by the Illinois No. 6 coal in Fig. 6e. When the Illinois coal was demineralized (dashed line) the 800 °C CO<sub>2</sub> peak disappears. The demineralized coal also shows a small increase in the tar yield and little moisture, but no other major changes.

Several high rank coals (Pocahontas, Upper Freeport, and Pittsburgh) showed CO<sub>2</sub> peaks at about 525 °C which disappeared with demineralization. The 520 °C peak appears to be due to siderite based on the discussion by Raask (30).

**Volatile Kinetics** - The TG-FTIR analysis can be used to study product evolution kinetics. We have compared in Fig. 19, the temperature for the maximum hydrocarbon evolution rate for the Argonne coals as a function of rank at 0.05 and 0.5 °C/sec. Duplicate runs were all within ±4 °C. The peak temperatures as well as the shape of the tar peaks are in good agreement with the results of

Burnham et al. obtained using a Rock-Eval analyzer (17) and a Triple-Quadrupole Mass Spectrometer (TQMS). The 50 to 65°C shift in temperatures with heating rate corresponds to activation energies approximately between 45 and 60 Kcal/mole. The variation in the rate of thermal decomposition is in part responsible for the variation of ignition behavior with rank (31).

**Functional Group Composition** - The TG-FTIR analysis provides information on the coal's functional group composition since it is the functional group composition which gives rise to the variation in gas yields. Figure 9b shows the variation in oxygen containing products with rank. Low rank coals have a high content of oxygen functional groups.

Figure 9c presents the data for tar and CH<sub>4</sub> yields. Methane increases systematically with increasing rank. High volatile bituminous coals have the most tar. Tar yields are related to soot formation in combustion (31) to fluidity (32), and to yields in liquefaction (33) or mild gasification (34). The tar functional group composition can also be obtained from the infrared spectra during tar evolution.

**Char Properties** - The TG-FTIR analysis provides two measurements related to char reactivity. The first is the weight gain of the char which occurs when oxygen is added early in the combustion cycle (see Fig. 2b). This weight gain is proportional to the concentration of active sites which are accessible to O<sub>2</sub>. The second measurement is of the temperature required to produce a specified rate of weight loss during the oxidation cycle. As discussed previously, this critical temperature T<sub>cr</sub> is related to the reactivity (4-7). The higher the reactivity, the lower T<sub>cr</sub>.

Figure 9d compares both the oxygen chemisorbed and T<sub>cr</sub> as functions of the oxygen in the coal. There is a systematic decrease in T<sub>cr</sub> and an increase in oxygen chemisorbed with increasing oxygen. The interplay of decomposition kinetics and reactivity control the ignition behavior and burnout in combustion or gasification (31).

## CONCLUSIONS

A single TG-FTIR analysis provides an extensive coal characterization with regard to the decomposition kinetics, char reactivity, functional group compositions and conversion behavior.

## ACKNOWLEDGEMENT

Work was supported by the U.S. Department of Energy, Morgantown Energy Technology Center under Contract No. DE-AC21-86MC23075 and under NSF SBIR Grant No. ISI-8703520.

## REFERENCES

1. Ottaway, M., *Fuel*, **61**, 713-716, (1982).
2. Ciuryla, V.T., Weimer, R.F., Bivans, A., and Motika, S.A., *Fuel*, **58**, 748, (1979).
3. van Krevelen, D.W., van Heerden, C., and Huntjens, F.J., *Fuel*, **30**, 253, (1951).
4. Solomon, P.R., Serio, M.A., and Heninger, S.G., *ACS Div. of Fuel Chem. Preprints*, **31**, (3), 200-209, (1986).
5. Best, P.E., Solomon, P.R., Serio, M.A., Suuberg, E.M., Mott, W.R, Jr., and Bassilakis, R., *ACS Div. of Fuel Chem. Preprints*, **32**, (4), 138-146, (1987).
6. Serio, M.A., Solomon, P.R., Bassilakis, R., and Suuberg, E.M., *ACS Div. of Fuel Chem. Preprints*, **34**, (1), 9-21, (1989).
7. Serio, M.A., Solomon, P.R., Bassilakis, R., and Suuberg, E.M., The Effects of Minerals on Coal Reactivity, Int. Conf. on Coal Science, Japan, (10/89).
8. Jenkins, R.G., Nandi, S.P., and Walker, P.L., Jr., *Fuel*, **52**, 288, (1973).
9. Sahu, R., Levendis, Y.A., Flagan, R.C., and Gavalas, G.R., *Fuel*, **67**, 275-283, (1988).
10. Suuberg, E.M., Calo, J.M., and Wojtowicz, W., *ACS Div. of Fuel Chem. Preprints*, **31**, (3), 186-193, (1986).
11. Juntgen, H. and van Heek, K.H., *Fuel Proc. Tech.*, **2**, 261, (1979).
12. Winans, R.E., McBeth, R.L., and Neill, P.H., *ACS Div. of Fuel Chem. Preprints*, **33**, (3), 85-90, (1988).
13. Chakravarty, T., Windig, W., Hill, G.R., and Meuzelaar, H.L.C., *Energy & Fuels*, **2**, (4), 400-405, (1988).
14. Solomon, P.R. and Hamblen, D.G., Finding Order in Coal Pyrolysis Kinetics, Topical Report

- submitted to U.S. Department of Energy under Contract No. DE-AC21-FE05122, 1983, also *Progress in Energy and Combustion Science*, **9**, 323-361, (1983).
15. Fitzgerald, D. and van Krevelen, D.W., *Fuel*, **38**, 17, (1959).
  16. Campbell, J.H., *Fuel*, **57**, 217, (1978).
  17. Burnham, A.K., Oh, M.S., Crawford, R.W., and Samoun, A.M., *Energy & Fuels*, **3**, (1), 42-55, (1989).
  18. Weimer, R.F. and Ngan, D.Y., *ACS Div. of Fuel Chem. Preprints*, **24**, (3), 129-140, (1979).
  19. Attar, A. and Dupuis, F., *ACS Div. of Fuel Chem. Preprints*, **23**, (2), 44-53, (1978).
  20. Attar, A. and Hendrickson, G.G., *Coal Structure*, (R.A. Meyers, Ed.), Academic Press, NY, Chapter 5, p. 131, (1982).
  21. LaCount, R.B., Anderson, R.R., Friedman, S., and Blaustein, B.D., *Fuel*, **66**, 909-913, (1987).
  22. Hall, P.J. and Calo, J.M., *Energy & Fuels*, **3**, (3), 370-376, (1989).
  23. Zhang, Z.G., Kyotani, T., and Tomita, A., *Energy & Fuels*, **3**, 566-571, (1989).
  24. Kyotani, T., Zhang, Z.G., Hayashi, S. and Tomita, A., *Energy & Fuels*, **2**, 1136, (1988).
  25. Carangelo, R.M., Solomon, P.R., and Gerson, D.G., *Fuel*, **66**, 960-967, (1987).
  26. Whelan, J.K., Solomon, P.R., Deshpande, G.V., and Carangelo, R.M., *Energy and Fuels*, **2**, 65, (1988).
  27. Vorres, K.S., "Users Handbook for the Argonne Premium Coal Sample Program", Supported by US DOE, Contract No. W-31-109-ENG-238; (1989).
  28. Bishop, M. and Ward, D.L., *Fuel*, **37**, 191, (1958).
  29. Solomon, P.R., Hamblen, D.G., Carangelo, R.M., Serio, M.A., and Deshpande, G.V., *Energy & Fuels*, **2**, 405, (1988).
  30. Raask, E., *Mineral Impurities in Coal Combustion; Behavior, Problems, and Remedial Measures*, Hemisphere Publishing Corp., NY, (1985).
  31. Solomon, P.R., Chien, P.L., Carangelo, R.M., Best, P.E., and Markham, J.R., *22nd Symposium (Int) on Combustion*, The Combustion Institute, Pittsburgh, PA, 211, (1988).
  32. Solomon, P.R., Best, P.E., Yu, Z.Z., and Deshpande, G.V., *ACS Div. of Fuel Chem. Preprints*, **34**, (3), 895-906, (1989).
  33. Serio, M.A., Solomon, P.R., Kroo, E., Basilakis, R., Malhotra, R., and McMillen, D., "Fundamental Studies of Retrograde Reactions in Direct Liquefaction", Proceedings of the Direct Liquefaction Contractor's Meeting, (Oct. 2-4, 1989).
  34. Khan, M.R., Serio, M.A. Malhotra, R., and Solomon, P.R., *ACS Div. of Fuel Chem. Preprints*, **34**, (4), 1054-1061, (1989).

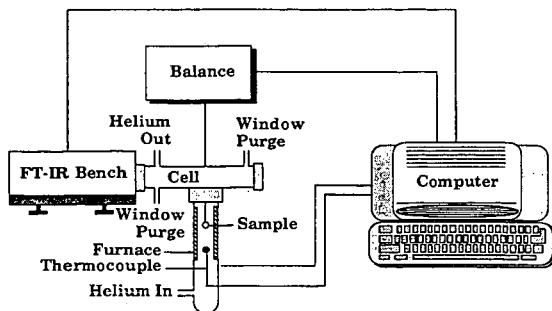


Figure 1. Schematic of TG/plus.

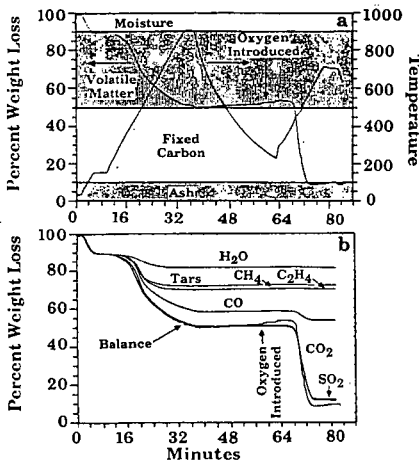


Figure 2. TG-FTIR Analysis of a Lignite. a) Temperature History and Weight Loss. b) Species Contributions to Weight Loss.

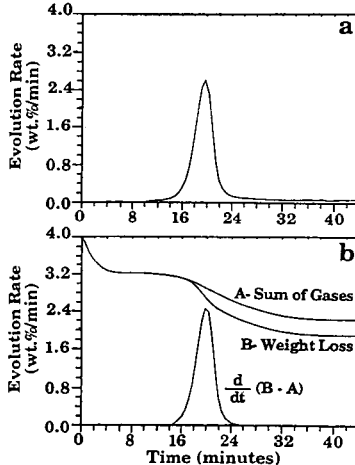


Figure 3. Calibration of Tar Absorptivity. a) Tar Absorption Profile. b) Weight Loss Minus the Sum of Gases.

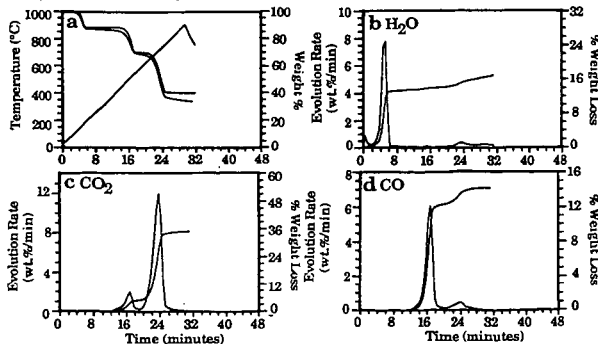


Figure 4. Pyrolysis of Calcium Oxylate. a) Weight Loss (solid), Sum of Evolved Products (dashed), and Temperature Profile. b)  $H_2O$  Evolution, c)  $CO_2$  Evolution, and d)  $CO$  Evolution.

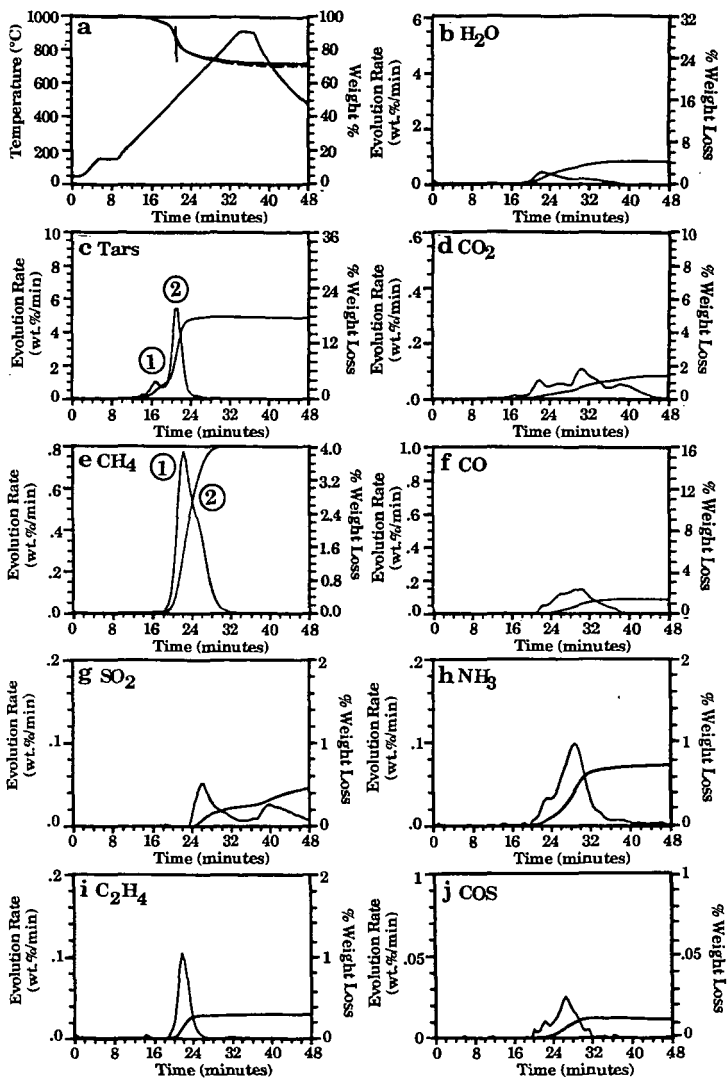


Figure 5. TG-FIIR Analysis of Upper Freeport Bituminous Coal during the Pyrolysis Cycle. a) Weight Loss (solid), Sum of Evolved Products (dashed), and Temperature Profile. b) H<sub>2</sub>O Evolution Rate and Integrated Amounts Evolved, c) Tar Evolution Rate and Integrated Amounts Evolved, d) CO<sub>2</sub> Evolution Rate and Integrated Amounts Evolved, e) Methane Evolution Rate and Integrated Amounts Evolved, f) CO Evolution Rate and Integrated Amounts Evolved, g) SO<sub>2</sub> Evolution Rate and Integrated Amounts Evolved, h) NH<sub>3</sub> Evolution Rate and Integrated Amounts Evolved, i) C<sub>2</sub>H<sub>4</sub> Evolution Rate and Integrated Amounts Evolved, and j) COS Evolution Rate and Integrated Amounts Evolved.

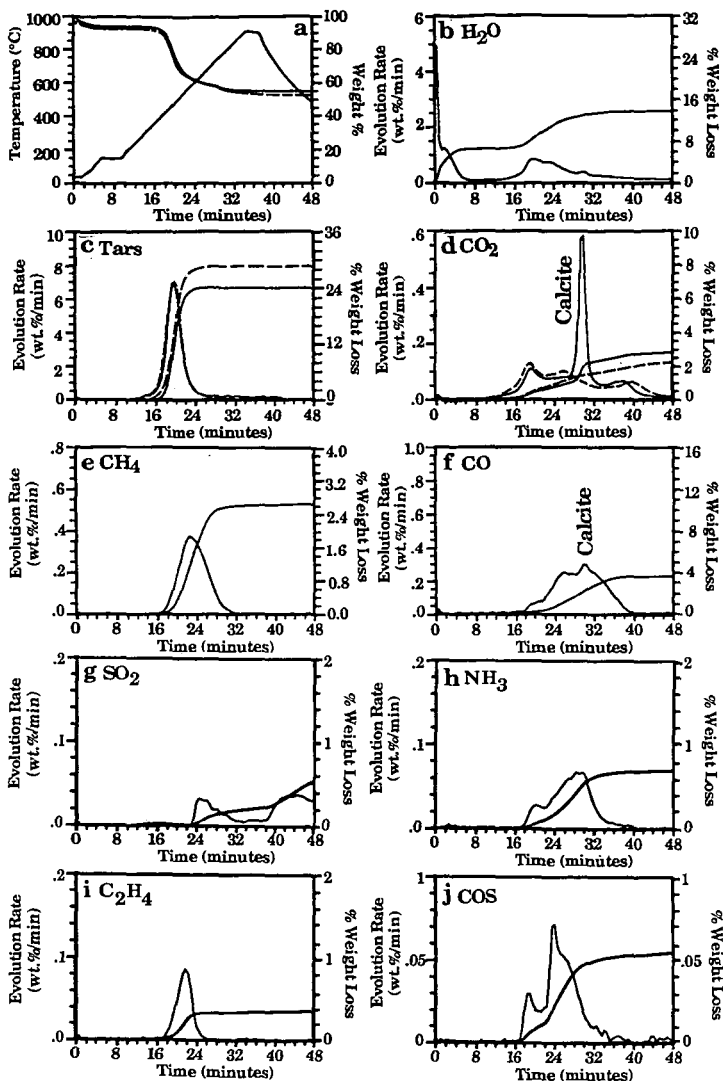


Figure 6. TG-FTIR Analysis of Illinois No. 6 Bituminous Coal during the Pyrolysis Cycle. a) Weight Loss (solid), Sum of Evolved Products (dashed), and Temperature Profile. b) H<sub>2</sub>O Evolution Rate and Integrated Amounts Evolved, c) Tar Evolution Rate and Integrated Amounts Evolved (raw coal (solid line) demineralized coal (dashed line)), d) CO<sub>2</sub> Evolution Rate and Integrated Amounts Evolved (raw coal (solid line) demineralized coal (dashed line)), e) Methane Evolution Rate and Integrated Amounts Evolved, f) CO Evolution Rate and Integrated Amounts Evolved, g) SO<sub>2</sub> Evolution Rate and Integrated Amounts Evolved, h) NH<sub>3</sub> Evolution Rate and Integrated Amounts Evolved, i) C<sub>2</sub>H<sub>4</sub> Evolution Rate and Integrated Amounts Evolved, and j) COS Evolution Rate and Integrated Amounts Evolved.

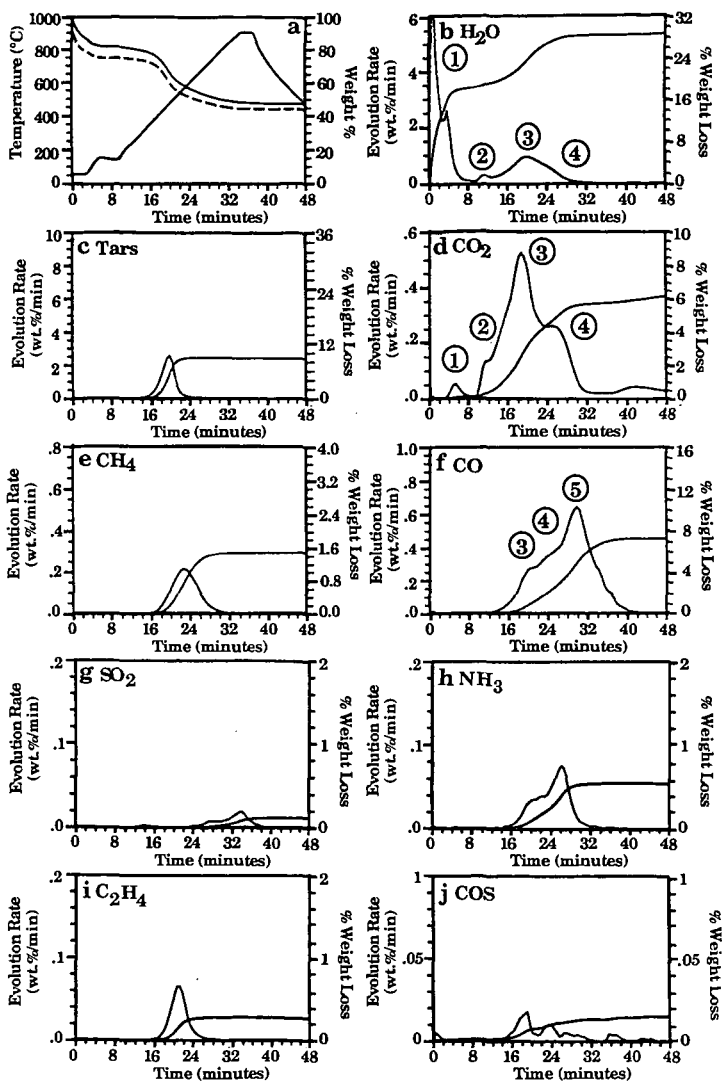


Figure 7. TG-FTIR Analysis of Wyodak Subbituminous Coal during the Pyrolysis Cycle. a) Weight Loss (solid), Sum of Evolved Products (dashed), and Temperature Profile. b) H<sub>2</sub>O Evolution Rate and Integrated Amounts Evolved, c) Tar Evolution Rate and Integrated Amounts Evolved, d) CO<sub>2</sub> Evolution Rate and Integrated Amounts Evolved, e) Methane Evolution Rate and Integrated Amounts Evolved, f) CO Evolution Rate and Integrated Amounts Evolved, g) SO<sub>2</sub> Evolution Rate and Integrated Amounts Evolved, h) NH<sub>3</sub> Evolution Rate and Integrated Amounts Evolved, i) C<sub>2</sub>H<sub>4</sub> Evolution Rate and Integrated Amounts Evolved, and j) COS Evolution Rate and Integrated Amounts Evolved.

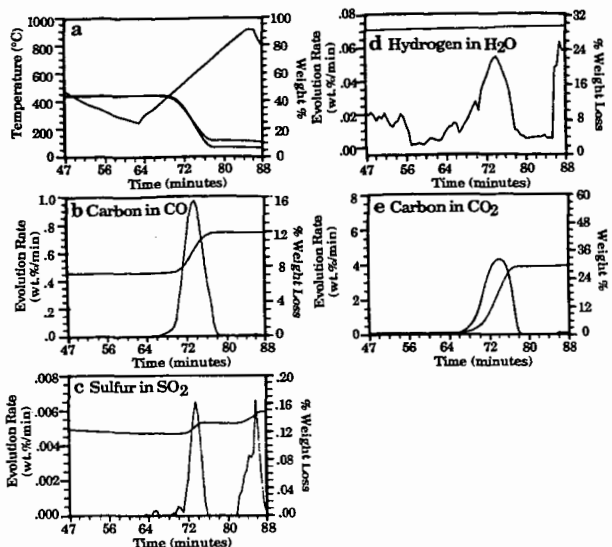


Figure 8. TG-FTIR Analysis of Wyodak Subbituminous during the Combustion Cycle. a) Weight Loss (solid), Sum of Evolved Products (dashed), and Temperature Profile. b) Carbon in CO Evolution Rate and Integrated Amount Evolved. c) Sulfur in SO<sub>2</sub> Evolution Rate and Integrated Amount Evolved. d) Hydrogen in H<sub>2</sub>O Evolution Rate and Integrated Amount Evolved. e) Carbon in CO<sub>2</sub> Evolution Rate and Integrated Amount Evolved.

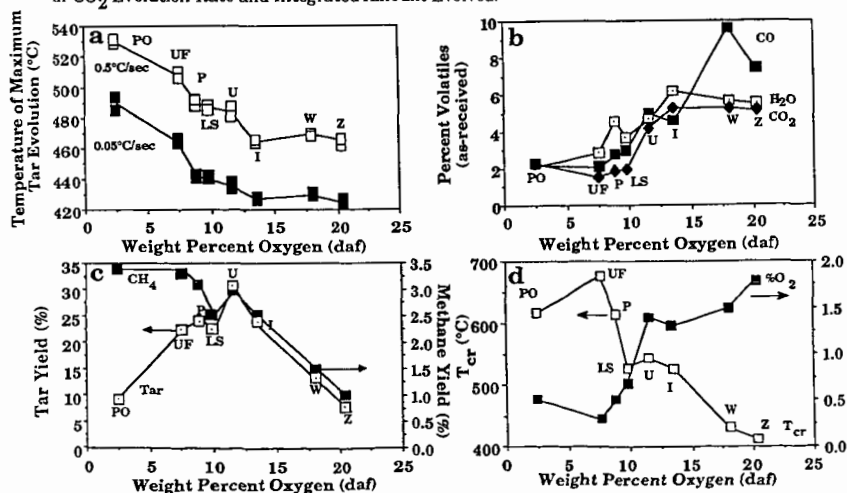


Figure 9. Variation of Coal Pyrolysis Properties with Rank. a) Rank Variation of Tar Evolution Temperature, b) Rank Variation of Oxygenated Gases c) Rank Variation of CH<sub>4</sub> and Hydrocarbons and d) Rank Variation of T<sub>cr</sub> and Oxygen Chemisorption.

## AGING STUDIES OF BITUMINOUS COAL BY ESCA AND FTIR

Cara L. Weitzsacker, James J. Schmidt  
Joseph J. Gardella, Jr.\*  
Department of Chemistry and Surface Science Center  
University of Buffalo, SUNY, Buffalo, NY 14214

Keywords: ESCA of coal, FTIR of coal, coal aging

### ABSTRACT

Electron Spectroscopy for Chemical Analysis (ESCA or XPS) and transmission Fourier Transform Infrared Spectroscopy (FTIR) were used to examine aged bituminous coals. The coals were obtained from the Illinois #6, Kentucky #9, Pittsburgh and Upper Freeport seams. The coals were stored under either ambient air, mine site tap water or nitrogen as they were exposed first to cold weather (10 C), warm weather (25 C) and the following cold season. Samples over the time periods were analyzed as raw, milled and processed coals. Emphasis was placed on changes in C, O, N and S functionalities on the surface by ESCA analysis, and in the bulk by transmission FTIR.

### INTRODUCTION

The aging of coal is of interest both to the fuel and coking industry due to the physical and chemical changes aging causes. The changes can affect the behavior and properties of coal, and therefore affect the coal as it is processed and utilized. In the majority of cases, the effects are negative. Oxidation, a major mechanism in the aging process, can decrease the fuel value of coal. Processing can become more problematic as aging occurs. (1-3)

Storage of coal is where significant oxidation can occur as coal ages. (1,2) Coal is commonly stored in large stockpiles open to weather conditions. In this study, storage conditions were modified to investigate what effects they may have on controlling or inhibiting aging. (4) Samples were stored under nitrogen gas, tap water or ambient air.

### EXPERIMENTAL

Coal samples, obtained by Otisca Industries, Ltd., were collected as they were brought up out of the mine. Coal was collected from the Illinois #6, Kentucky #9, Pittsburgh and Upper Freeport seams. The coal was placed under one of three atmospheres upon collection: nitrogen, ambient air or local mine site tap water.

Upon arrival at Otisca, the samples were riffled and crushed to 30m x 0 following ASTM methods, and returned to their respective environments. The coal was stored in 5 gallon pails holding approximately 17 lbs. each, and exposed to local weather during cold weather (10 C), the following

warm season (25 C) and another cold season. Individual samples were taken after each weather extreme. Samples were analyzed as raw samples, milled samples, and milled and processed samples. Raw coal was reduced to 60m x 0. Milled samples were ball milled to 15 m x 0. Processed samples were first milled and then agglomerated using pentane. At this point mineral matter was removed.

Initially a set of samples from each seam was analyzed before exposure to weather to establish a baseline for the aging study. The handling, analysis, and results of these analyses were presented in a previous preprint.(5)

The samples received from Otisca were handled as previously described (5). Analysis was done using a Perkin - Elmer Physical Electronics 5100 ESCA spectrometer using a non - monochromatized Mg K $\alpha$  X - ray source under the conditions 300W, 20mA and 15kV. Transmission FTIR spectra were collected on a Nicolet 7199A FTIR spectrometer with an MCT detector, taking 1000 scans, and a Mattson Alpha Centauri FTIR spectrometer with DTGS detector, taking 32 scans.

#### RESULTS AND DISCUSSION

In the previous study (5), the baseline samples were analyzed to establish what information can be obtained from the ESCA and FTIR analyses. In that study it was shown that as the samples went from raw to milled to processed there was a decrease in mineral matter. In the milled samples, mineral surfaces were generally covered by a thin film of organic matter. In the processed samples, most mineral matter was separated from the coal during agglomeration. It was also shown there was no significant difference in the baseline samples due to differing storage conditions.

In this study, the trends from raw to milled to processed coal were observed throughout the storage period, as would be expected. No major differences due to storage conditions were observed, but some difference was seen in the nitrogen stored samples.

As the coal aged (see Table 1), changes in the surface percent atomic concentration (%AC), oxygen to carbon ratios (O/C), and peak shape changes were examined. Changes in %AC carbon and oxygen would be an indication of oxidation, as would peak shape changes. Peak shape changes were examined in the FTIR spectra.

As the coal aged, trends were investigated in percent atomic concentrations. The inorganic elements such as Al and Si showed no notable changes over the storage period. Sulfur also remained consistent throughout aging, and nitrogen exhibited only minor fluctuations over the aging period. The largest change was seen in %AC carbon of the raw samples. There was an increase of up to 10 %AC between the baseline and first aged samples in all 4 seams. See Figure 1. There were slight variations through to the 7th batch, with only Illinois showing a significant decrease in %AC C. See Figure 2.

The milled samples showed a slight decrease in %AC from

the baseline to 1st aged sample. Slight decreases were seen in batch 4 or 5 in all seams, with the largest seen in the Pittsburgh samples.

In the processed samples, The %AC C was consistent through batch 1 - 7 except for the Kentucky seam, where a decrease was seen over batch 4 - 6, with an increase in the 7th batch.

Looking at what effect the storage conditions had, very little change was observed. In all four seams, no significant change in %AC C was seen in the air or water stored. Differences due to nitrogen storage was only significant in the Upper Freeport seam.

The trend in %AC total oxygen decreased through the processed samples due to the removal of minerals. Surface organic oxygen was calculated using the method of Perry and Grint (3), by subtracting oxygen as  $\text{SiO}_2$  and  $\text{Al}_2\text{O}_3$ . There were fluctuations in %AC surface organic oxygen as the samples aged. The least fluctuation was seen in the Pittsburgh seam, the most in the Upper Freeport seam.

The calculated %AC surface organic oxygen was used to calculate O/C ratios. An increase in this ratio would indicate oxidation of the coal was occurring. The largest difference in O/C ratio between treatments was seen in the Illinois and Upper Freeport seams, the least in Kentucky and Pittsburgh. No trend of increasing O/C ratio was seen except in Illinois raw samples. See Figure 3.

Peak shape changes were only notable for C, O, N and S. The C 1s envelope exhibited no gross changes as the samples aged. Slight increases in the shoulder and tailing towards the high binding energy side were observed over all treatments through batch 7. This would indicate a slight increase in the oxidized carbon functionalities and possibly a slight increase in aromatic carbon. See Figure 4.

The O 1s envelope has contributions from both organic and inorganic species. It is a broad slightly asymmetric peak. As the coal aged, a more distinct shoulder was seen towards low binding energy. The most severe case was seen in the processed samples. The inorganic matter was largely removed at this point. The shoulder was due to organic (carbon - bound) oxygen. See Figure 5.

The S 2p peak shape didn't vary much over the storage period. The presence of one or two peaks and the relative intensities of these two peaks varied. No solid trends were seen between the seams. In the Kentucky seam raw samples, there was one peak in the water stored sample and baseline nitrogen stored, but two peaks in the air stored and last nitrogen stored. The relative intensity of these two peaks varied as well. In the water stored milled baseline samples, the inorganic/oxidized organic species peak (5) was more intense than the organic species peak. In the 3rd batch sample, the relative intensities were reversed. See Figure 6. In the Upper Freeport samples, the trend was reversed for the respective samples. No definite trend was seen in or

between the seams.

The infrared results reflected the removal of the mineral matter with decreases in intensity of inorganic peaks. There was little difference between raw and milled samples, but there was significant difference between raw and processed samples. There were some differences in general between the seams, particularly in the 1400 - 700  $\text{cm}^{-1}$  region where bands corresponding to clay mineral matter appears. Kentucky and Pittsburgh had less of this matter than Illinois and Upper Freeport. This was most evident in the raw and milled samples.

No major changes were obvious from the infrared spectra. Over the four seams there was one trend in the 1800 - 1650  $\text{cm}^{-1}$  region. In the early samples there was a small peak at approximately 1730  $\text{cm}^{-1}$  or a shoulder between 1800 - 1650  $\text{cm}^{-1}$ . As the coal aged this small peak became less intense or the shoulder less prominent. This indicates there may be a decrease in carbonyl as the coal aged. See Figure 7.

#### CONCLUSIONS

This study shows that no major oxidation, either in the bulk or at the surface, was evidenced in these studies over the time period and temperature range they were stored at based on these analyses.

#### ACKNOWLEDGEMENTS

Support for this work has been provided by the Department of Energy under Contract # DE - AC22 - 87PC79880 DOE Pittsburgh Energy Technology Center with a subcontract to Otisca Industries, Ltd.

#### REFERENCES

1. Gethner, Jon S., FUEL 1987, 66, 1091
2. Huffman, Gerald P.; Huggins, Frank E.; Dunmyre, George R.; Pignocco, Arthur J.; Lin, Mon - Ching, FUEL 1985, 64, 849
3. Perry, David L.; Grint, Alan, FUEL 1983, 62, 1024
4. Fred Simmons, private communications
5. Weitzsacker, Cara L.; Schmidt, James J.; Gardella, Jr., Joseph A., ACS Fuel Div. Preprint, 1989, 34, 545

Batch #	Storage History
1	baseline
2,3	1st cold season
4,5	warm season
6,7	2nd cold season

FIGURE 1

KENTUCKY #9 (AIR) - ALL TREATMENTS  
SURFACE CARBON AS COAL AGED

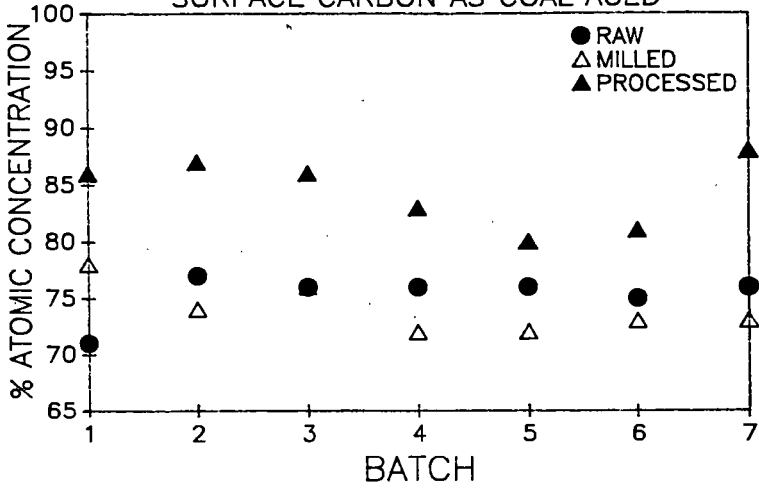


FIGURE 2

ILLINOIS #6 (AIR) - ALL TREATMENTS  
SURFACE CARBON AS COAL AGED

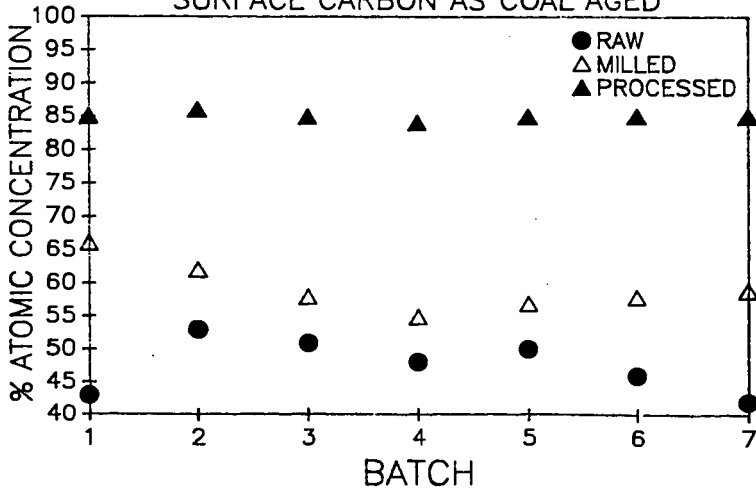


FIGURE 3

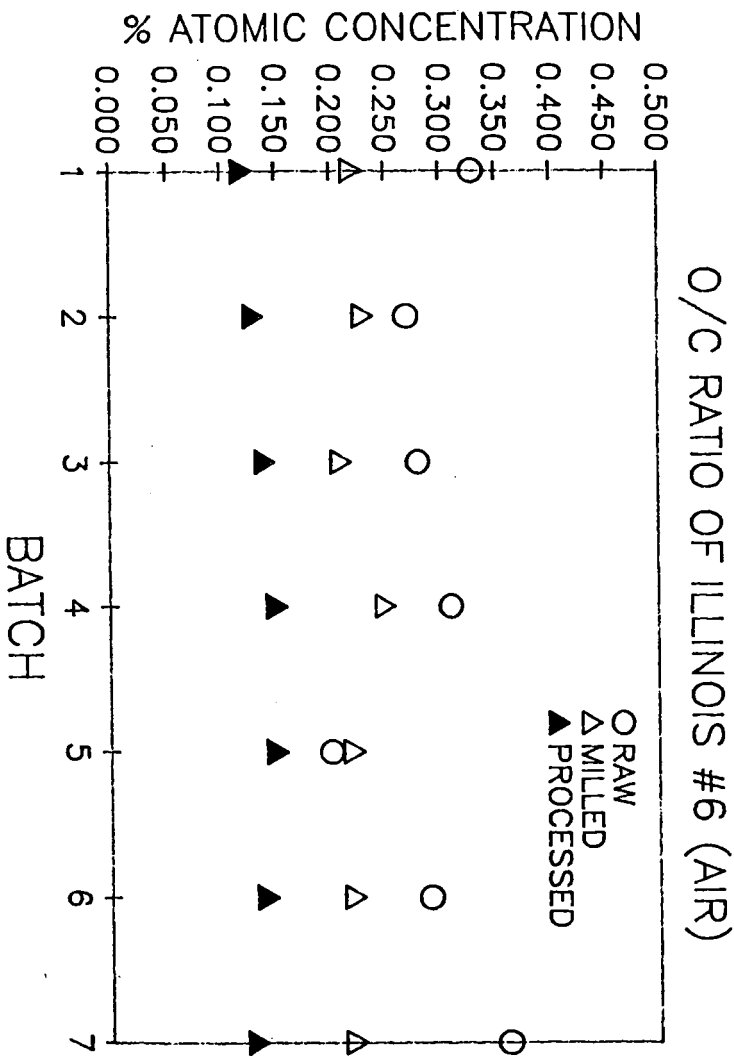


FIGURE 4

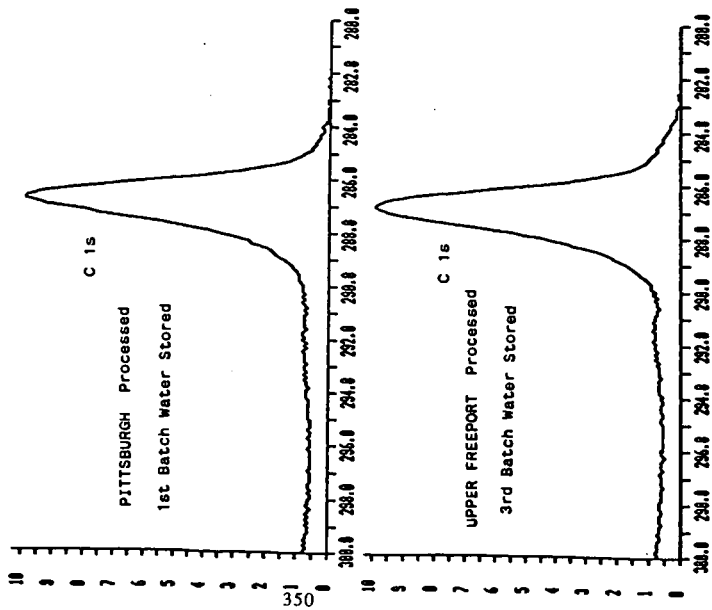
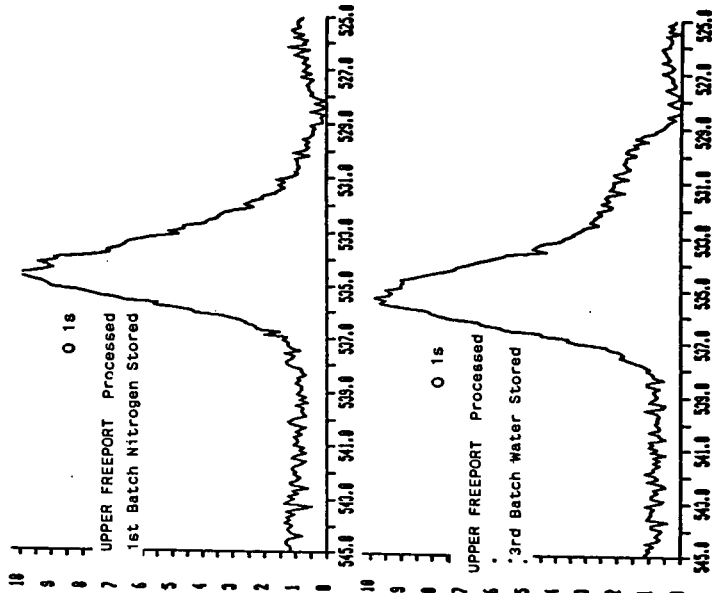


FIGURE 5



350

FIGURE 7

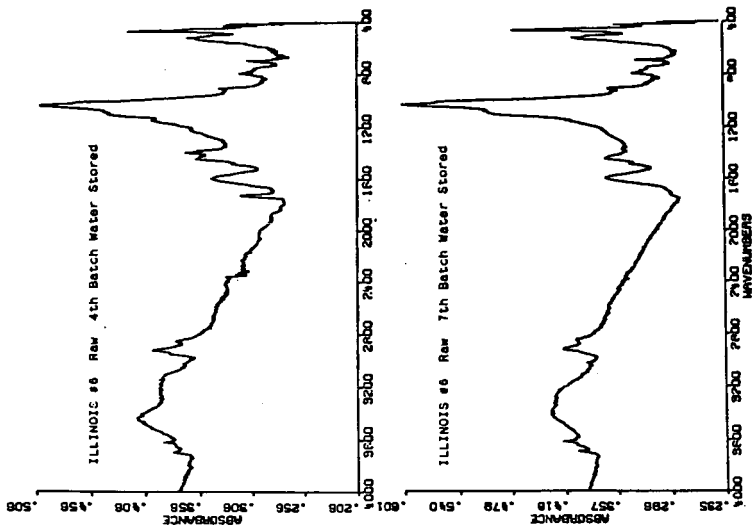
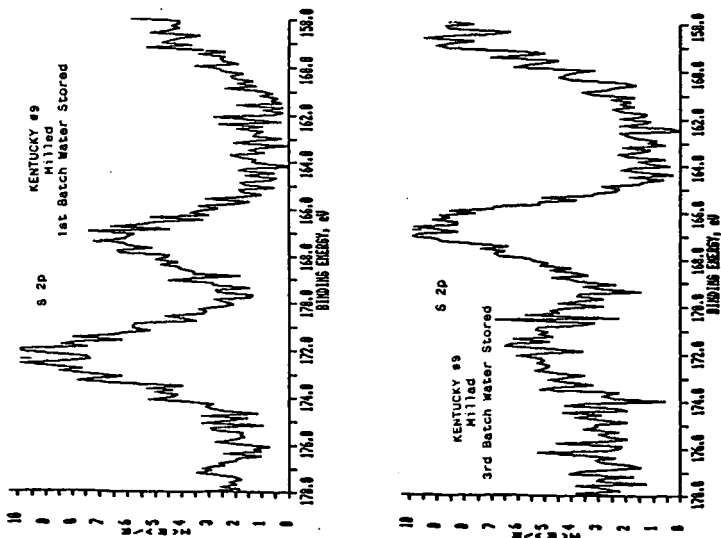


FIGURE 6



## THE EFFECTS OF HYDROTHERMAL TREATMENT ON WYODAK COAL

David S. Ross, Albert S. Hirschon, Doris S. Tse, and Bock H. Loo  
SRI International  
Menlo Park, CA 94025

Keywords: hydrous pyrolysis, hydrothermal treatment, Wyodak

### INTRODUCTION

There are a number of accounts of the treatment of coal with steam, including the recent work of Beinkowski et al.,<sup>1</sup> Brandes and Graff,<sup>2,3</sup> and Kahn, et al.<sup>4</sup> These efforts sought benefits to liquefaction and pyrolytic tar yields, and described changes in both the composition and the behavior of the coals. In other work Rozgonyi et al. described ash and sulfur reductions in steam-treated coal,<sup>5</sup> and some of our recent work with Illinois No. 6 coal in hot liquid water is described in a paper elsewhere in these preprints.<sup>6</sup>

The hydrothermal conditions used in these efforts are reminiscent of the hydrous pyrolysis studies conducted in research dealing with the accelerated maturation of oil shale.<sup>7,8</sup> Source rocks are heated in liquid water at temperatures in the 300-350°C range, resulting in the net production of alkanes and other hydrocarbons, in contrast to the case for dry pyrolysis where olefins are produced. The claim that hydrous pyrolysis actually mimics the natural process has been questioned recently,<sup>9,10</sup> but the phenomenology is unquestioned.

The work described here is an attempt to bridge the two areas. We are seeking to understand the changes brought about in Wyodak coal by liquid water in the range 150-350°C in terms of its structure. We expect the results of this work to provide some insight into any benefits such treatment provides liquefaction and volatiles production.

### EXPERIMENTAL

Our work was conducted with Wyodak samples from the Argonne Premium Coal Bank. In most cases the starting coal was dried in an oven at 60°C/1 torr/20 hr, a pretreatment that resulted in a loss of water representing about 30% of the coal mass. In some runs the as received coal was used, and we found no difference in behavior following hydrothermal treatment. The as received coal was used as well in a control run where the treatment was conducted with no added water. In that case the water in the coal may have contributed to the subsequent pyrolytic behavior, as described below.

The hydrothermal treatment was conducted in a 45 ml stainless steel reactor with a tightly fitting Pyrex insert. Sufficient water was used to assure in each case that a liquid phase was present at temperature, and the reactor was charged with 33-50 atm (500-750 psi) nitrogen (cold). The run temperatures (°C) and respective vapor pressures of water (atm) were 150/4.6, 250/38, and 350/160. After treatment the coal/water mixture was centrifuged directly in the insert, most of the water removed by pipette and saved for later analysis, and the coal removed in an N<sub>2</sub>-purged glove bag. The remaining superficial water was then removed in a stream of dry nitrogen.

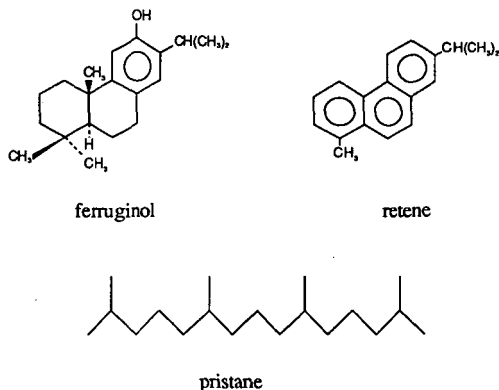
The bulk of the analysis was conducted by pyrolysis field ionization mass spectrometry (py-FIMS). The heating rate used throughout was 2.5°C/min, and spectra were recorded at nominally 30° intervals from ambient to 500°C. In some cases quantities of volatiles from the treated coal were transferred at 120°C via vacuum transfer to bulbs for analysis by conventional mass spectrometry. In addition to the parent-peak spectra, py-FIMS output included volatility data, and values for the weight average molecular weights ( $M_w$ ) of the fractions.

Analysis of the water fractions were conducted by first saturating the aqueous phase with NaCl, and then extracting with methylene chloride. The extracts were then analyzed by gas chromatography, and identification confirmed by comparison with authentic samples.

## BACKGROUND

Bienkowski et al. reported on the abundance of alkylated phenols and dihydroxybenzenes both in the pyrolysis tars of Wyodak coal, and in the water collected following steam treatment.<sup>1</sup> Kahn et al. similarly identified a large collection of phenols in the treatment water.<sup>2</sup> These results are expected based on the lignin residues present in this rank of coal.<sup>11</sup>

There is also a wide range of biomarkers reported for the extracts of Wyodak coal in work by Baset, et al. who studied benzene/ethanol extracts and pyrolysates evolved directly from the heated coal.<sup>12</sup> The extracts included ferruginol and retene, and they sought but found no pristane. The presence of the



corresponding olefin pristene in the pyrolysate, however, suggested that the alkane or a precursor was bound to the coal, and then released as the olefin when the coal was heated.

The geochemical studies on oil shale could be related to these findings, with the account by Hoering of specific interest.<sup>8</sup> In that work the treatment of preextracted Messel shale in liquid water at 330°C/3 days generated petroleum hydrocarbons including long chain normal alkanes, aromatics, and biomarkers. When D<sub>2</sub>O was used, deuterium was heavily incorporated into the hydrocarbons. Hoering's control results and the distributions of isotopic isomers essentially ruled out preexisting, trapped hydrocarbons, and the results suggested that the hydrocarbons were not merely freed, but rather generated in some manner by the water.

## RESULTS

We conducted a number of experiments with hydrothermal treatments at 150° and 250°C, with the majority of the work at 350°C. Analyses of the recovered coals included py-FIMS and simple analyses of recovered water and volatiles samples.

## Recovered Water, Direct Volatiles Analyses, and Elemental Analysis

As expected, analysis of the recovered water from 350°C treatment runs showed the presence of phenols and dihydroxybenzenes. The most prominent products were catechol (*o*-(OH)<sub>2</sub>Ph) and phenol in a ratio of about 2/1. Other products found in smaller quantities were resorcinol (*m*-(OH)<sub>2</sub>Ph) and hydroquinone (*p*-(OH)<sub>2</sub>Ph), with the ratio catechol/(resorcinol + hydroquinone) = 6/1.

The same materials were pulled from the coal heated to 120°C in a vacuum line transfer, and identified by conventional mass spectrometry. In this case phenol was the most prominent material; however we were surprised to find acetone as a major volatile product, present in quantities similar to those for phenol.\* Smaller quantities of simple ketones including butanone and a pentanone were also identified. These findings are discussed further below.

The elemental analyses from the work at 350°C are presented in Table 1. The %-oxygen values are by direct O-analysis. The final columns in the table show calculated compositions based on specific loss of the elements of CO<sub>2</sub> and H<sub>2</sub>O, and values for the net loss of OH are also shown for comparison. Clearly CO<sub>2</sub> loss is not significant, and water loss fits rather well. Curiously loss of OH fits the measured values even better, although the accuracy of the measured values may not warrant our modeling the results to such a degree. The product coals from the 150° and 250°C work showed no O-loss.

Thus at 350°C we see about a 30% loss of oxygen, but significantly the loss is independent of the presence of added water. Kahn et al recorded about a 20% O-loss for Wyodak coal with steam at 304-320°C,<sup>4</sup> and we have noted that about half the oxygen in Illinois No. 6 coal is lost in water/N<sub>2</sub> at 400°C.<sup>13</sup> The present results show that at least for Wyodak coal the loss is strictly thermally promoted and does not require added water. *However it is notable that the loss of water in the hydrothermal case occurs at a partial pressure of water of 160 atm.* The process is thus highly irreversible, and obviously does not involve bound or sorbed molecular water. One candidate water source are coal clays, which dehydrate at elevated temperatures.<sup>14</sup> However that process is reversible, and at any rate is very highly suppressed below around 475°C under just a few torr of water vapor.<sup>15</sup>

We conclude that the water loss must involve the dehydration specifically of chemically bound elements of water in the organic phase of the coal. The dehydration may be tied to the fact that catechol is a prominent thermal product. And as we have shown in other work, catechol thermally dehydrates and forms oligomers at 300°-400°C in the presence of kaolinite, one of the clays in coal. We expect to develop a better understanding of this process in further work.

## Volatilities

Several different py-FIMS measurements were made of separate samples of the as received coal on different days to establish the reproducibility of the method and the stability of the instrument, and the results of those runs (points) along with those for 150° and 250°C treatments (curves) are presented in Figure 1. The data for the as received coal fall essentially upon one another, demonstrating a satisfactory precision. The similar alignment of the data from the treated coal shows that little change in the coal takes place at 150°, while some activity is seen at the 250° level. The volatile fractions in these cases and in those below was consistently 25-30%.

The shape of the curves for the as received coal demonstrates two regions of activity. Below 300°-320°C the small quantities of preexisting volatile material in the coal are evaporated into the instrument. Then at higher temperatures pyrolytic fragmentation of the coal occurs, and products of that process are recorded. Thus for the as received coal and the 150° sample, no more than about 10% of the ultimately volatile material emerges in the first region. For the 250° treatment, since that temperature was below the point of substantial thermolysis, the increased volatiles for that run must be due specifically to the action of water in the treatment.

\* The possibility of adventitious acetone was considered. However the presence of acetone solely in runs from the 350°C treatment confirmed its formation in the process.

This point is demonstrated more clearly for the 350° work in Figure 2. The figure presents the curves for 30 min runs at 350°C both with added water (2 runs) and without added water, with some data for the as received coal are shown again for comparison. In this case to assure no confusion from possible thermal effects from oven drying, the as received coal was used for the run with no water.

The effects tied specifically to the hydrothermal conditions are evident from the profiles. They are emphasized by comparing the %-volatile values at an abscissa value of 350°C, the temperature at which the coal was treated, and for the as received, no water, and hydrothermal samples the volatilities are respectively 22%, 37% and 52%. The jump from 22 to 37% reflects a thermal effect that can be anticipated since the treatment temperature was in the pyrolysis range, although we cannot rule out some action by the water driven out of the coal. (Work with dried samples is in progress.) The remaining increase to 52%, however, must be due specifically to the presence of water.

Recognizing that the treatment involves holding coal samples at temperature for 30 min, and that the py-FIMS heating rate is 2.5°C/min, another useful comparison can be made over the interval 350° to ~425°C (i.e. 350°C to ~[350° + 2.5 x 30]). The pertinent data are presented in Table 2, which shows that the weight average molecular weights ( $M_w$ ) for the tars from the hydrothermally treated coal are consistently greater than those for both the as received and thermally heated samples, a result in turn consistent with the view that added water specifically affects the subsequent pyrolytic properties.

An effect is apparent as well from inspection of the Pyrex inserts after the runs. For the hydrothermal treatment they showed considerable quantities of tar deposited on the walls. For the thermal treatment case, however, the walls were clean, except for droplets of water which was driven from the coal during the treatment. Some insight into these effects can be developed with inspection of the various FIMS spectra, with attention to the effects of treatment on individual compound classes.

### FIMS Spectra and Coal Tars

Treatment at 350°C. FIMS spectra are presented in Figure 3 for the as received coal and for the 350° treatment both with and without water. Each spectrum is the accumulated signal for each sample up to a py-FIMS temperature of 300°C, and the differences in volatilities shown in Figure 2 are evident here.

Specific effects of the addition of water can be gathered from the difference spectrum shown in Figure 4. The figure represents [hydrothermally treated] minus [thermally treated], and is derived from the respective spectra for the full volatiles fractions evolved to 500°C. The data from the two runs have been normalized, so that the differences reflect changes in the compositions. Thus the addition of water shifts the thermolytic behavior of the coal so that the volatiles are richer in dihydroxybenzenes and a broad range of coal tar material at  $m/z$  values 200-500 amu, and depleted in phenols.

Also very prominent in both spectra is  $m/z = 58$ , identified as acetone by vacuum line isolation and analysis. The difference spectrum shows that its levels are elevated relatively in the pyrolysate from the thermally treated coal, probably due to its solubility in water. Other simple ketones in smaller quantities were also identified as noted above. We are not aware of accounts of acetone or other simple ketones as products of coal thermolysis, although such compounds are identified in wood tars and are derived from cellulose.<sup>16</sup> This finding could reflect the presence cellulose residues in Wyodak coal, and we expect to look further into this matter in future studies.

The profiles for the generation of acetone, phenol and dihydroxybenzene as a function of temperature are shown in Figure 5. For the as received coal the activity is almost solely in the pyrolysis region, and dihydroxybenzene (most likely catechol) is the most prominent product, with its production peaking at around 400°C. Both the thermal and hydrothermal treatments shift the production of all three materials to lower temperatures, but the presence of added water does not appear to affect the phenol and acetone release. The addition of water clearly affects dihydroxybenzene evolution, however, moving it to lower temperatures.

The assignments in the figure are probably satisfactory to py-FIMS temperatures up to 300°C, and for  $m/z = 90$  and 110 perhaps all the way to 500°C. However  $m/z = 58$  above 300°C probably represents butane rather than acetone, although as the figure shows the point is moot since it is not significant in that region. On the other hand it is prominent at lower temperatures for the thermally and hydrothermally treated coal, its peaking coinciding closely with that for phenol. Given that all three compounds are volatile, it is surprising that the maximum in their lower temperature evolution falls at around 140°C. For the hydrothermally treated coal there is some immediate evolution which then declines, and we assign this behavior to some material fully released by the water, and thus simply "sitting" on coal and readily pumped into the FIMS instrument. However the delayed, common peaking temperature for much of the phenol, dihydroxybenzene, and acetone suggests that they are present together in a nonvolatile, complexed form generated in initial thermal or hydrothermal treatment. We expect to continue work in this system to develop a better understanding of the sources of these materials.

Treatment at 250°C. Just as for the 350° work, treatment at 250°C promoted the production of coal tar, albeit at a lower level. The fact that tar was produced with treatment at a temperature below the pyrolysis region is another reflection of the specific action of water in the treatment. However there were significant differences between the 350° and 250° results. First, as shown in Figure 6, the phenols and benzenediols for the treated coal emerge fully in the pyrolysis region, and no acetone is seen. In this regard the treated coal acts like the as received coal, and the result is not surprising since from the 350° work we learned that the phenols and acetone were pyrolytically produced.

Second, several prominent peaks appear in the FIMS of the tars of the treated coal, but are present in neither the as received nor the 350°-treated coal. These compounds emerge at py-FIMS temperatures around 100°C, with  $m/z$  values corresponding to the parent masses of some biomarkers. They include peaks at 234, 268 and 270 amu, which correspond respectively to retene, pristane, and ferruginol. A prominent peak also appears a  $m/z = 252$ , and we are aware of no corresponding biomarker.

We emphasize that while these parent masses correspond to the biomarkers, at present we have no additional information on the structures. However with this caveat, it appears that there is some hydrolytic release of biomarkers. The mechanism of that action is of interest, particularly in the case of hydrocarbons such as retene and pristane which have no "handles" for the action of water. The question of the role of mineral matter in these processes must be raised, including aspects of coal structure which might provide substantial and widely ranging interaction between the organic and mineral components in coal.

## DISCUSSION

Our accumulated evidence thus far shows that there are both water-independent and water-promoted modes of release of tars and specific compounds. Phenols and acetone are evolved thermally at temperatures above 300°C, while hydrothermal conditions affect the dihydroxybenzene evolution. The question remains as to what features in the structure are responsible for this behavior. The production of acetone and other simple ketones may reflect the presence of some cellulose-related residue in the coal.

The water-promoted evolution of tars and biomarkers seems similar to the observations from the hydrous pyrolysis studies of oil shale. For oil shale such chemistry probably involves interfacial chemistry at the boundary joining the organic and mineral surfaces. In the case of coal, Allen and VanderSande have estimated that ultrafine mineral matter in the organic phase may represent up to 15% of the total quantity of mineral material in coal,<sup>17</sup> and the distribution of such a fine mineral material throughout the organic phase would lead to a significant interfacial volume. Our results may thus mirror the existence of such a volume, and specific interfacial chemistry generating and/or liberating volatile materials.

Finally, a possible parallel between oil shale and coal structure leads to an interesting surmise regarding the distribution of heteroatom components in coal. The heteroatom-containing fractions of oil shale are concentrated at the mineral surfaces,<sup>18</sup> presumably migrating over geologic time to acid/base sites in the clays. Were such a condition to exist in coal, we would then expect a nonrandom distribution of

heteroatom components, localized at the mineral inclusions within the organic phase. Such a picture of coal is considerably different from the structures commonly considered, and could be significant to the processing coal.

#### ACKNOWLEDGEMENT

We acknowledge support of the US DOE on Contract No. DE-AC22-89PC89880. We also are pleased to acknowledge helpful discussions with R. Malhotra and D. McMillen of SRI, and T. Milne of SERI.

#### REFERENCES

1. P. R. Beinkowski, R. Narayan, R. A. Greenkorn, and K-C Chao, *Ind. Eng. Chem. Res.*, **26**, 202-205 (1987).
2. S. D. Brandes and R. A. Graff, *Am. Chem. Soc. Div. of Fuel Chemistry Preprints*, **32**(3), 385-393 (1987).
3. R. A. Graff and S. D. Brandes, *Energy and Fuels*, **1**, 84-88 (1987).
4. M. R. Kahn, W-Y. Chen and E. Suuberg, *Energy and Fuels*, **3**, 223-230.
5. T. G. Rozgonyi, M. S. Mohan, R. A. Zingaro, and J. H. Zoeller, Jr., in *Proceedings of the 2nd International Conference on Processing and Utilization of High Sulfur Coals*, Y. Chugh, R. Caudle, C. Muchmore, and A. Sinha, Dds. (Elsevier, New York, 1988)
6. David S. Ross and Albert Hirschon, *Am. Chem. Soc. Div. of Fuel Chemistry Preprints*, **35**, 000-000 (1990).
7. a) M. D. Lewan, J. C. Winters, and J. H. McDonald, *Science*, **203**, 897-899 (1979)..
8. T. C. Hoering, *Organic Geochemistry*, **5**, 267-278, (1984).
9. M. Monthieux, P. Laniais, and J-C. Monin, *Organic Geochemistry*, **8**, 275-292 (1985).
10. E. Tannenbaum and I. R. Kaplan, *Nature*, **317**, 708-709 (1985)
11. P. G. Hatcher, H. E. Lerch, III, R. K. Korta, and T. V. Verhayen, *Fuel*, **67**, 1069-1075 (1988).
12. Z. H. Baset, R. J. Pancirov, and T. R. Ashe in *Adv. Org. Geochem. 1979*, A. G. Douglas and J. Maxwell, eds., Pergamon Press, Oxford, pp. 619-630.
13. D. S. Ross, T. K. Green, R. Mansani, and G. P. Hum, *Energy and Fuels*, **1**, 292-294, (1987).
14. J. Unsworth, C. Fowler, N. Heard, V. Weldon and V. McBrierty, *Fuel*, **67**, 1111-1119, (1988).
15. R. L. Stone, *J. Am. Ceram. Soc.*, **35**, 96-99, (1952); G. W. Brindley and J. Jemaitre in *Chemistry of Clays and Clay Minerals*, A. Newman, ed., Longman Scientific and Technical, London, 1987, pp. 327-329
16. R. J. Evans and T. A. Milne, *Energy and Fuels*, **1**(2), 123-137, (1987).
17. R. M. Allen and J. B. VanderSande, *Fuel*, **3**, 24-29 (1984).
18. J. J. McKay and R. S. Blanche, *Liquid Fuels Technology*, **3**(4), 489-521, (1985).

**Table 1**  
**Analyses of As Received and 350°C-Treated**  
**Wyodak Coal**

	Starting Coal	Treated Coal		Calculated For Loss Of <sup>a</sup>		
		With Water	No Water	CO <sub>2</sub>	H <sub>2</sub> O	"OH"
%C	66.47 67.60	71.56	72.17	70.45	71.67	71.34
%H	5.10 5.02	4.89	4.99	5.62	4.61	5.04
%N	0.85 0.86	0.95	0.94	0.93	0.91	0.91
%O	20.92 21.63	14.92	15.88	15.48	15.49	15.41
% ash	8.23 8.58	9.04	9.08	9.08	8.87	8.88

a. Calculated for loss of elements of CO<sub>2</sub>, H<sub>2</sub>O and OH from the starting coal, to match a final O-content of 15.4-15.5%.

**Table 2**  
**Weight Average Molecular Weights of Tars from**  
**As Received, Thermally Treated, and Hydrothermally**  
**Treated Wyodak Coal**

py-FIMS Temperature Interval (°C)	Sample <sup>a</sup>	$\bar{M}_w$
332-359	As received	458
	Thermal	434
	Hydrothermal	518
362-389	As received	455
	Thermal	449
	Hydrothermal	516
392-419	As received	431
	Thermal	427
	Hydrothermal	507
422-449	As received	366
	Thermal	356
	Hydrothermal	403

a. Thermal and hydrothermal samples heated at 350°C/30 min.

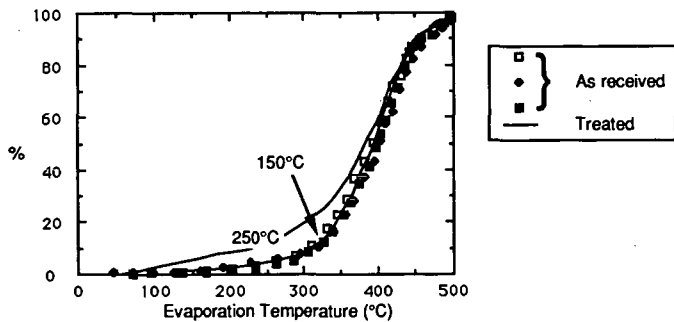


Figure 1. Evaporation curves for the as received coal and the 150° and 250°C coal products.

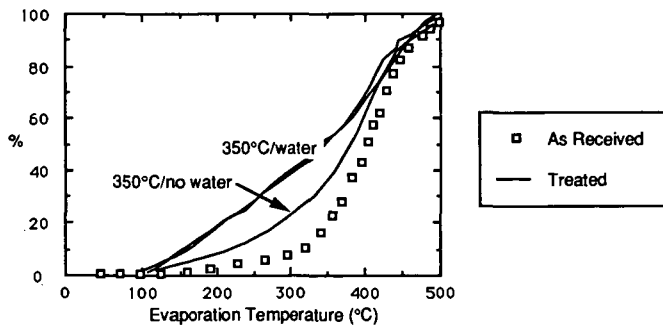


Figure 2. Evaporation curves for the as received coal, and products from 350°C runs both with (2 runs) and without water.

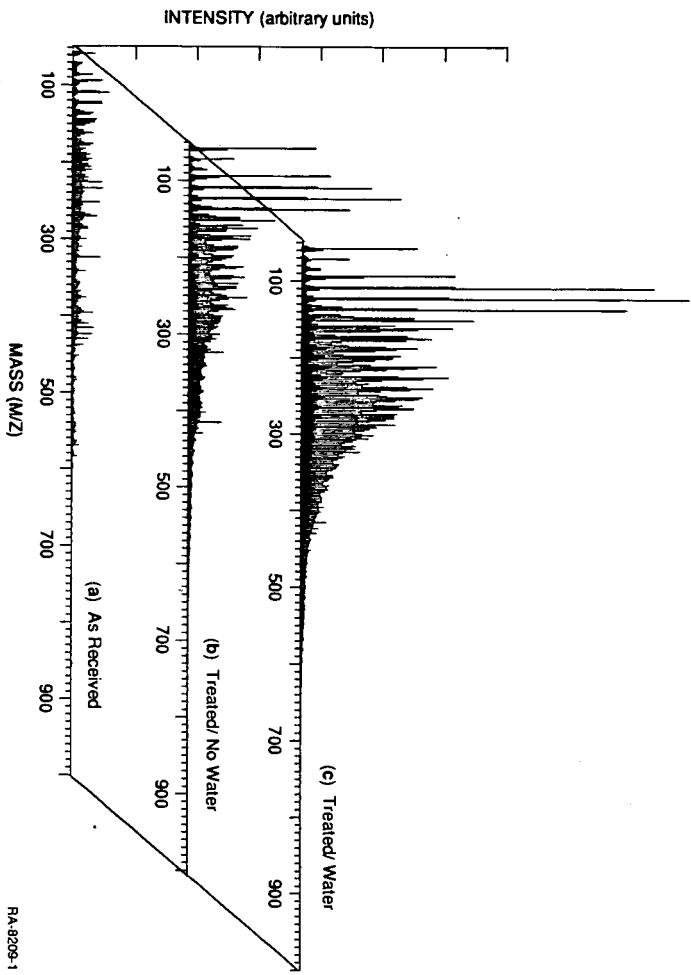


Figure 3. FIMS spectra for the as received coal, and for the coals treated at 350°C both thermally and hydrothermally.

RA-8209-1

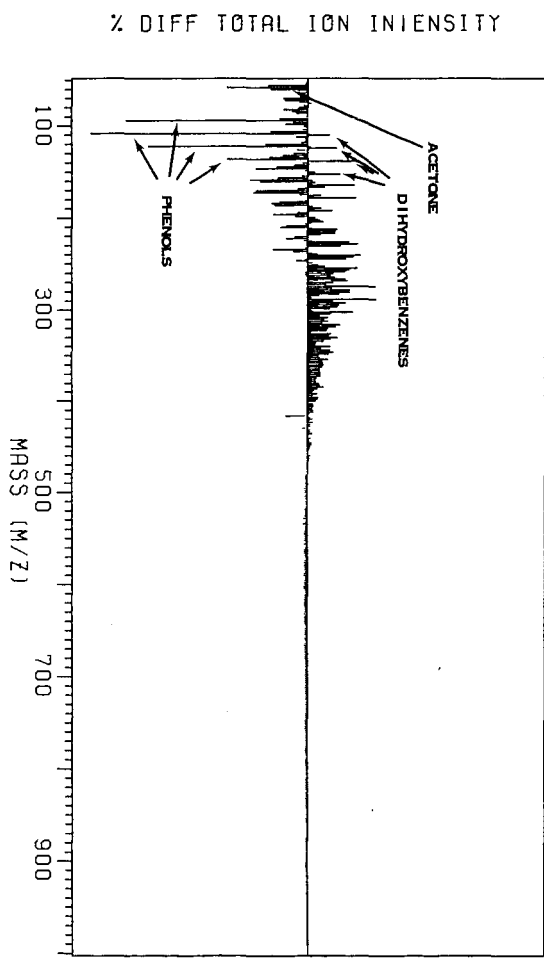


Figure 4. FIMS difference spectrum representing [hydrothermally treated] minus [thermally treated] for the volatiles evolved from ambient to 500°C.

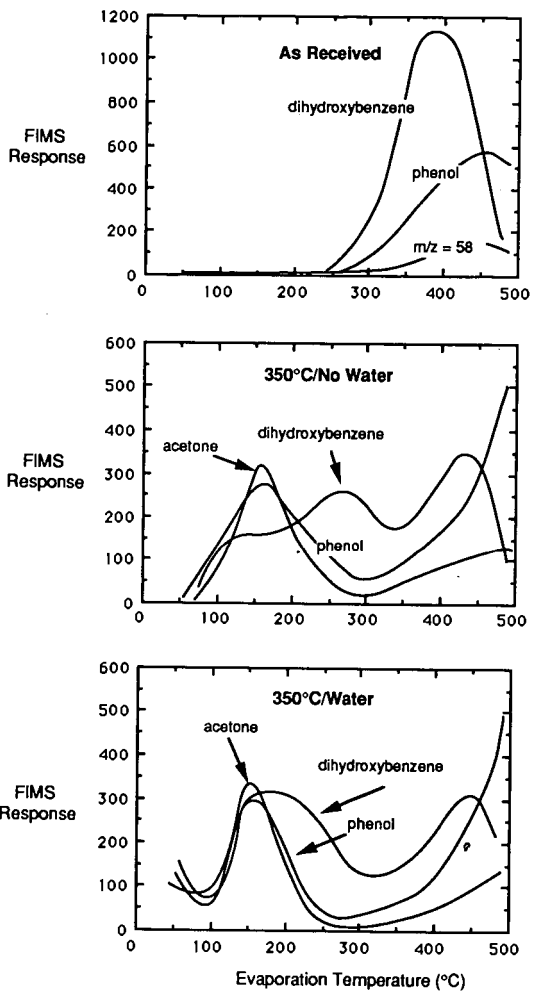


Figure 5. FIMS-derived profiles for acetone, phenol and dihydroxybenzene for runs at 350°C. The dihydroxybenzene is primarily catechol.

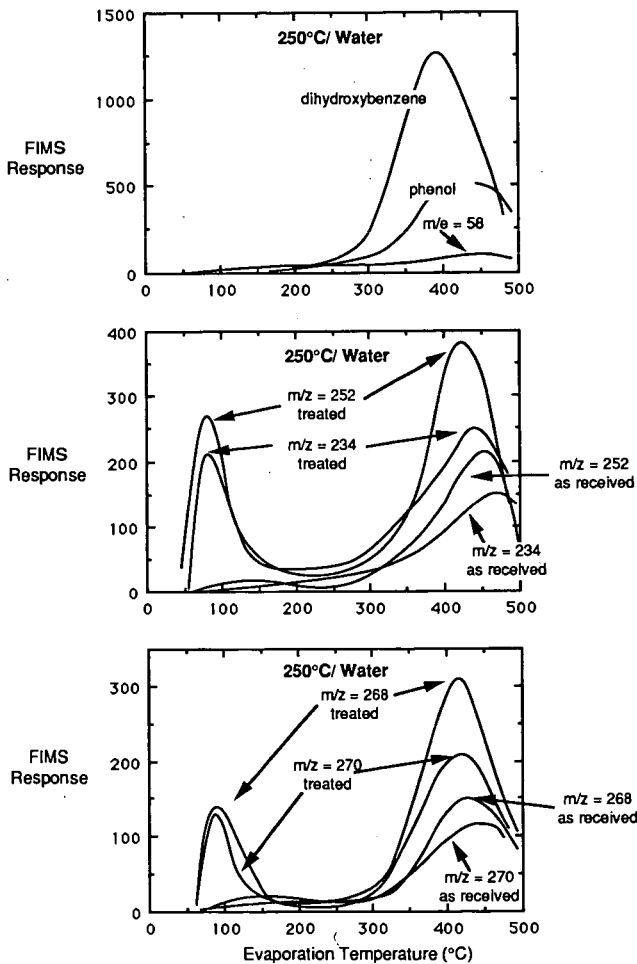


Figure 6. FIMS-derived profiles for several products from runs at 250°C. The m/z values at 234, 268, and 270 correspond to the parent masses for retene, pristane and ferruginol respectively.

## INVESTIGATION OF ORGANIC SULFUR STRUCTURE AS A FUNCTION OF COAL RANK

S.Mitra, F.E.Huggins, N.Shah, and G.P.Huffman  
Consortium for Fossil Fuel Liquefaction Science  
University of Kentucky, Lexington, KY 40506-0107

Keywords: Sulfur, Coal Rank, XAFS Spectroscopy

### INTRODUCTION

X-Ray Absorption Fine Structure (XAFS) spectroscopy is proving to be a very promising method by which information on the electronic bonding state and atomic environment of dilute elements in complex samples can be readily obtained. Of especial importance to coal science, is the technique's demonstrated ability to provide detailed information on organic sulfur in coal<sup>1,5</sup>. In this paper, we present the results of an XAFS investigation into the occurrence of various forms of sulfur present in a series of coals and maceral separates of different ranks.

### EXPERIMENTAL PROCEDURE

Samples were selected for this study on the basis that they contain predominantly organic sulfur. A large number of the samples were maceral separates prepared by density gradient centrifugation (DGC), which effectively removed inorganic sulfur forms. A detailed description of the DGC methods can be found elsewhere<sup>6,8</sup>. Other samples were whole coals or coal extracts with very little inorganic sulfur contents. Samples were prepared for XAFS spectroscopy by grinding representative samples to less than 100 mesh. The samples were then cold-pressed into pellets of boric acid of approximately 2.5 cm diameter or placed in thin Mylar bags for the XAFS experiments.

Some of the sulfur K-edge XAFS measurements on the coals were performed at the Stanford Synchrotron Radiation Laboratory on wiggler beam-lines VII-3 and IV-1. Electron energies were 3.0 and 3.3 GeV and beam currents were typically in the range 40 to 80 mA. Other XAFS measurements were conducted at the National Synchrotron Light Source at Brookhaven National Laboratory on beam-line X19-A, with electron energies 2.53 GeV and beam currents 90-200 mA. At both synchrotron facilities, Si (111) double crystal monochromators were used to vary the X-ray energy from about 100 eV below to as much as 600 eV above the sulfur K-shell absorption energy (2472 eV). An all-helium pathway was used to minimize absorption of the X-rays. Thin Mylar windows (6 $\mu$ m) were also used for the same reason. Fluorescent experiments were performed for this study with a Stern-Heald type detector.

Complementary studies with Mössbauer and X-Ray Photoelectron spectroscopies (XPS) were also performed on some of the samples to ascertain the amounts of pyritic sulfur, iron sulfates, and oxygen-bonded sulfur compounds that might be present in the samples.

### RESULTS AND DISCUSSION

The XAFS structure can be divided into two regions: the near edge structure, known as XANES, within about  $\pm 30$  eV of the edge, and the extended region, the EXAFS, from about 30 eV to 300-400 eV above the edge. The XANES region of the spectrum provides information on the

bonding and oxidation state of the sulfur atoms. The EXAFS region, on the other hand, gives information about the local structural environment of the atoms.

In this study, we have concentrated on the XANES region of the spectra. The XANES structure typically consists of one or more peaks superimposed upon an absorption step. The peaks in the XANES region are derived either from transitions to vacant, bound levels, or from low energy scattering resonances. The first large peak in the XANES of all sulfur compounds, the white line, arises from the electronic transition from the 1s level to vacant np, or ns levels. A least-squares analysis of the XANES structure can be made by fitting the data to the sum of an arctangent edge step, which represents the transition of the photoelectron to the continuum, and a number of lorentzian peaks, which represent transitions to vacant bound states or scattering resonances. Each different sulfur compound exhibits one or more peaks and an edge step. Hence, the sulfur K edge of a coal sample that has a number of distinct organic sulfur forms, should exhibit a number of 1s to np/ns transitions and a corresponding number of transitions to the continuum. In practice, however, we have found that in the least-squares analysis at most only two arctangent steps are needed to obtain an adequate fit. The lower energy step represents the transition to the continuum for the sulfur bonded to carbon and the other step represents the corresponding transition for sulfur bonded to oxygen. The relative areas under the peaks can then be used in a semi-quantitative manner to show the variation of organic sulfur forms from sample to sample. However, it should be emphasized that there is at present no direct relationship between peak area and the abundance of a given organic form of sulfur, because of our lack of knowledge concerning transition moments, selection rules, etc. for the transitions in different sulfur compounds. Such relationships remain to be established in future work.

In the analysis procedure, the zero point of energy for the sulfur XANES spectra is defined as the major peak in the differential of the elemental sulfur spectrum. Relative to this point, pyritic sulfur has its white line at about 1.5 eV, and organic sulfides, such as dibenzyl sulfide, have white lines at about 2.2 eV. Thiophenic sulfur compounds, such as dibenzothiophene, have their major peaks at about 2.8 eV. Among sulfur-oxygen compounds, organic sulfoxides and sulfones have white lines at about 4.9 and 9.9 eV, respectively, whereas inorganic sulfates have white lines at around 11.4 eV. The edge step for these different compounds also exhibit similar displacements. The positive shift with increasing sulfur oxidation state is because of decreased screening of the nuclear charge for the 1s level electrons as valence electrons are transferred to the oxygen anions. In various coal spectra, fitted peaks at about the correct positions can be associated with all the sulfur forms listed above.

Coals and maceral separates of high rank appear to have little or no sulfur-oxygen bound components and the relatively small peak at 8-12 eV is believed to be principally a scattering resonance<sup>9,10</sup>. Such samples were fit with only one arctangent function, as shown in Figure 1. Other samples, principally of lower rank, did need a second step for a better fit and exhibited a much larger peak at 8-12 eV, as shown by the XANES spectrum of leonardite in Figure 2. Virtually all of the sulfur in this sample is thought to be organic as all common inorganic forms-of-sulfur, namely pyrite, iron sulfates, and gypsum, were not detected by iron Mössbauer spectroscopy or calcium K-edge XAFS spectroscopy.

A tabulation of the areas under the different peaks for the samples examined in this study is shown in Table 1. Weight percent carbon (dry, ash-free) from ultimate analyses is used as an approximate measure of the rank of the coals. A systematic variation with coal rank is found in the relative amounts of higher energy peaks compared to the lower energy peak components. The lower rank coals show very pronounced peaks at 8-12 eV, suggestive of the increasing amounts of sulfur-oxygen forms, and the percentages of the areas under these peaks are considerably higher, as shown in Table 1. Figure 3 shows how the peak intensities vary for three coals of different ranks.

#### CONCLUSIONS

The sulfur K-edge XANES data obtained to date on coals of low inorganic sulfur abundances show a variation in both type and abundance of organic sulfur forms that was not expected. Low-rank coals appear to contain appreciable amounts of sulfur-oxygen compounds and such compounds appear to increase relative to sulfides and thiophenes as rank decreases. It should be emphasized that the percentages quoted in Table 1 are merely for areas under peaks in the least-squares fit. It remains to be established what the relationship is between peak areas and abundances for the different sulfur species and further studies are planned towards this end.

#### ACKNOWLEDGMENTS

The work described in this paper is supported in part by the Electric Power Research Institute through contract No. RP-8803-20 and in part by the Department of Energy through contract No. DE-FC22-89PC89852.

#### REFERENCES

1. Spiro C.E., Wong J., Lytle F., Greegor R.B., Maylotte D., Lampson S.; Science, (1984), **48**, 226.
2. Huffman G.P., Huggins F.E., Shah N., Bhattacharyya D., Pugmire R.J., Davis B., Lytle F.W., Greegor R.B.; ACS Div. Fuel Chem. Preprints, (1988), **33(1)**, 200.
3. Huffman G.P., Huggins F.E., Shah N., Bhattacharyya D., Pugmire R.J., Davis B., Lytle F.W., Greegor R.B.; Processing and Utilization of High Sulfur Coals II; Chugh Y.P., Caudle R.D., Eds., Elsevier, Amsterdam, (1987), 3.
4. George G.N., Gorbaty M.L.; J. Am. Chem. Soc., (1989), **111**, 3182.
5. Stock L.M., Wolny R., and Bal B.; Energy & Fuels, (1989), **3(6)**, 652.
6. Karas J., Pugmire R.J., Woolfenden W.R., Grant D.M., Blair S.; Int. J. Coal Geol., (1985), **5**, 315.
7. Keogh R., Poe S., Chawla B., Davis B.; Coal Science and Technology, Vol. II, 289.
8. Cooperative Research in Coal Liquefaction Infratechnology and Generic Technology Development, Final Report, DOE Contract No. DE-FC22-86PC90017, Consortium for Fossil Fuel Liquefaction Science, Lexington, KY, (1988).
9. Huffman G.P., Huggins F.E., Mitra S., Shah N., Pugmire R.J., Davis B., Lytle F.W., Greegor R.B.; Energy & Fuels, (1989), **3**, 200.
10. Huffman G.P., Huggins F.E., Mitra S., and Shah N.; International Conference on Coal Science (Tokyo), in press, (1989).

Table 1. XANES peak areas for various coals investigated.

Sample	%C, daf Whole Coal	% Area of Xanes peaks					
		1	2	3	4	5	6
PSOC 733, WV							
Exinite	87.4	0	60	20	6	14	0
Vitrinite	87.4	0	49	22	9	20	0
Inertinite	87.4	0	52	14	7	27	0
UKCAER 71155, KY							
Vitrinite	84.2	5	48	23	17	5	0
OHIO #5							
Vitrinite	83.5	4	52	20	5	20	0
OHIO #6							
Vitrinite	83.5	0	62	17	16	6	0
UKCAER 91864, KY							
NMP Extract	82.2	4	59	17	6	13	0
UKCAER 71094, KY							
Vitrinite	80.0	6	44	22	15	13	0
Inertinite	80.0	11	41	15	9	24	0
Exinite	80.0	5	44	24	17	10	0
Coal	80.0	7	46	26	11	11	0
PSOC 1110, Utah							
Exinite	72.5	10	30	13	25	14	8
Vitrinite	72.5	10	27	13	31	14	5
PSOC 1108, Utah							
Vitrinite	68.0	5	25	11	30	20	9
Leonardite							
Sample-A	60.1	4	23	21	39	11	2
Sample-B	60.0	5	20	18	24	33	0

Peaks occur in the following energy ranges:

Peak 1: 1.0- 2.2 eV, Peak 2: 2.0- 3.1 eV, Peak 3: 4.5- 4.9 eV,  
Peak 4: 9.3-10.3 eV, Peak 5: 11.5-12.0 eV, Peak 6: 15.0-17.5 eV.

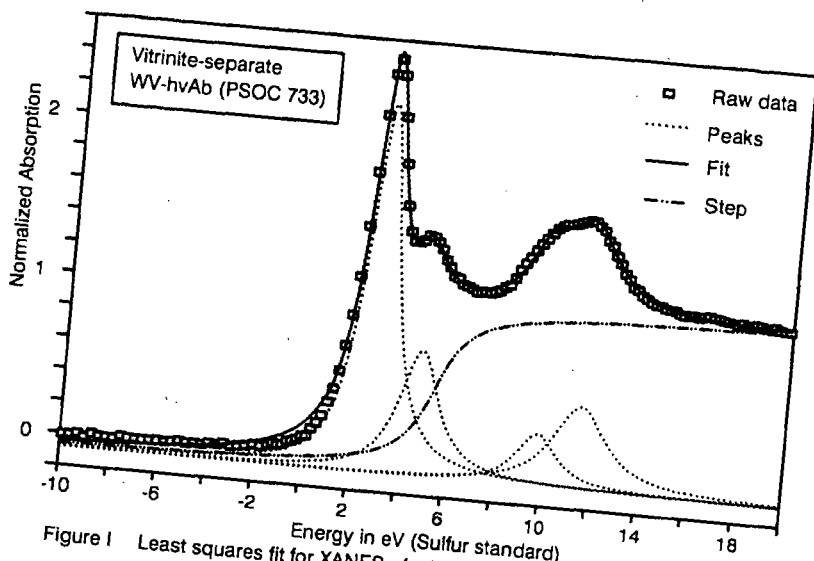


Figure 1 Least squares fit for XANES of a higher rank coal maceral with one step

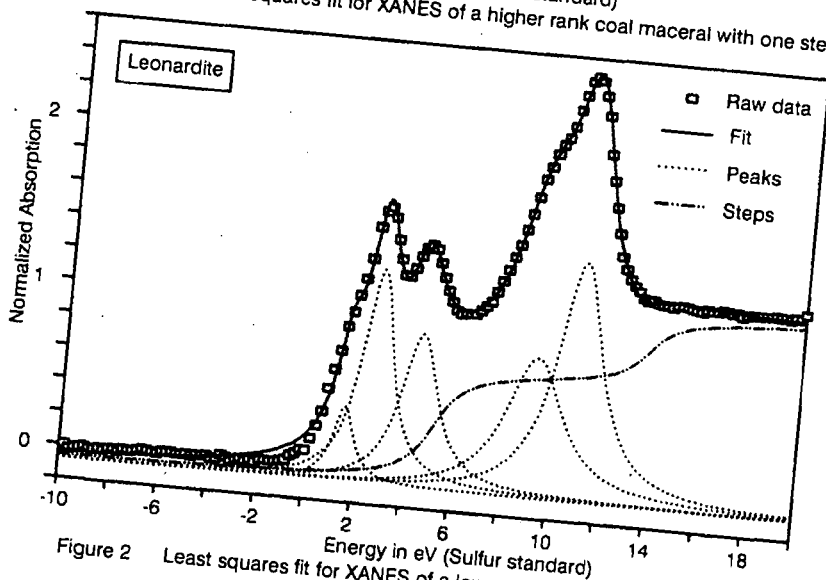


Figure 2 Least squares fit for XANES of a lower rank coal with two steps

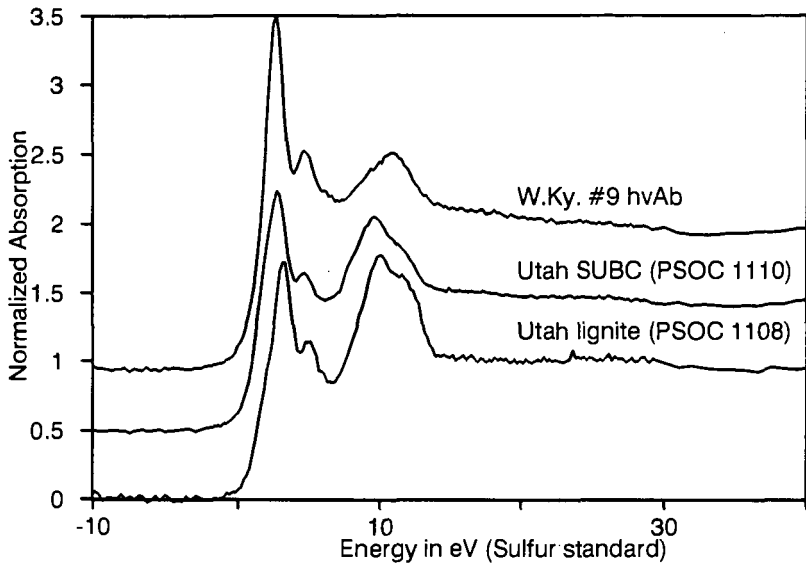


Figure 3 Sulfur XANES of coals of different ranks

Iron K-Edge EXAFS Investigation of  
Ash Deposits From Coal Combustion

Muthu S. Sundaram, Thomas A. Butcher,  
C. R. Krishna and Bernard M. Manowitz  
Department of Applied Science  
Brookhaven National Laboratory  
Upton, New York 11973

and

Melvin L. Zwillenberg  
Public Service Electric & Gas Company  
80 Park Plaza, T16  
Newark, New Jersey 07101

INTRODUCTION

The formation and buildup of the slag deposits on wall tubes is one of the most serious problems in pulverized coal combustion for power generation. This phenomenon, traditionally called wall slagging, is known for its undesirable effects on heat and mass transfer. Many empirical formulations based on the silica percentage and acid/base ratio have been developed in the past to describe the slag characteristics. Unfortunately, due to variation of several factors such as flame pattern turbulence, residence time, temperature distribution, gas velocity, etc. within the boiler, these empirical formulations are of limited use in the prediction of the behavior of the slag. In addition, these formulations do not take into consideration of the interaction between the constituents of the coal mineral matter. Another problem in this area is the lack of information on the transition of fluid slag to a solid form and the mechanism of formation of sticky deposits.

Further work in understanding the chemical "structure" of the slags should be profitable in relating the major issue of the influence of coal mineral matter on the operational characteristics of the commercial boilers. Application of Synchrotron-Induced X-Ray Absorption Fine Structure (EXAFS) in such studies was explored and an understanding of the local structure of the iron atoms in the slags derived from a commercial boiler forms the scope of this study.

EXAFS has now become a standard tool for structural determinations. Through EXAFS, it is possible to study the local environment of specific atomic species regardless of the physical state of the material under investigation and one could derive radial structure functions for the short range order near an absorbing element. In simpler terms, EXAFS represents the oscillatory structure due to interference between the outgoing photoelectron wave propagating from the x-ray absorbing atom and the incoming wave backscattered by the neighboring atoms. The EXAFS structure is observed over several hundred electron volts past the absorption edge and many excellent review articles are available on the theory and practice of EXAFS (1-4).

## EXPERIMENTAL PROCEDURE

The slag samples for EXAFS analysis were taken from the upper furnace wall of the Mercer Station of Public Service Electric & Gas company, Newark, New Jersey. This is a "wet bottom" unit which means that ash is removed from the furnace bottom as molten slag. This type of furnace design is commonly used with coal which have lower fusion temperatures.

The slag deposits were derived from a Virginia Pocohontas No. 5 bituminous coal. Three samples were analyzed by EXAFS technique: (1) an ASTM ash of the original coal, (2) an inner part of the slag deposit close to the tube wall, and (3) an outer part of the deposit thought to be formed at a higher temperature. The EXAFS materials were sampled from a large block of several feet long slag deposit which was about 6-in. to 8-in. thick.

The EXAFS measurements were made at room temperature on beamline X-19A, in the National Synchrotron Light Source (NSLS), at Brookhaven National Laboratory. The X-19A beamline is equipped with a NSLS boomerang-type double-drift fixed-exit monochromator. An Si(III) crystal with a Bragg angle range of  $8^\circ$  to  $15.5^\circ$ , corresponding to an energy range of 2.12 to 7.93 keV was employed in this study. The electron energy was 2.5 GeV and the beam current was within the range of 90 to 125 mA. The vertical beam height was 0.5 mm and the energy resolution was in the order of 0.7 eV. An Fe foil, obtained from Alpha Products, Danvers, Massachusetts, was used for energy calibration, and the first inflection point in the spectra was noticed at 7111.3 eV. This value was used as energy shift in plotting the spectral data contained in this paper.

A fluorescent ionization detector was employed. The direct beam detector, in front of the sample, was filled with He gas and the ionization detector was filled with a gentle stream of Ar gas. A 6  $\mu\text{m}$  thick manganese filter was used to improve the fluorescent detection.

The raw data was analyzed using EXASCAN data analysis program, originally developed at the University of Washington, Seattle, Washington, and later modified by Mark Eglinton of the University of West Virginia, Morgantown, West Virginia. The principles underlying complicated EXAFS data analysis were discussed in detail by Teo (5).

## RESULTS AND DISCUSSION

Figure 1(a) shows an example of the expanded version of the raw spectrum of standard  $\alpha\text{-Fe}_2\text{O}_3$ , -100 eV to +200 eV from the first point of inflection. This spectrum is indicative of the x-ray absorption near edge structure (XANES) which contains information about the chemical environment of the absorbing element. The structure in the XANES region (-20 eV to +50 eV from the absorption edge) is believed to be due to electronic density of the states and is not caused by interference effects from backscattering.

The pre-edge feature has been assigned to a  $1s \rightarrow 3d$  transition and the shoulder in the absorption edge, just prior to the edge crest, is considered to be due to  $1s \rightarrow 4s$  transition. Even though the observed spectral features are explainable on the basis of electronic transitions, it has been suggested that there is a strong possibility of them to be due to "shape resonances" which are much more sensitive to the ligand geometry and coordination number (6).

Figure 1(b), (c) and (d) shows the expanded version of the raw spectra of the ASTM ash, inner deposit (FETUBA) and outer deposit (FESLAG), respectively. All of these spectra contain a clearly resolved pre-edge peak due to the  $1s \rightarrow 3d$  transition as in the case of the standard  $\alpha\text{-Fe}_2\text{O}_3$ .

The intensity of the pre-edge peak is typical of iron in its +3 oxidation state ( $\text{Fe}^{3+}$ ). The magnitude of the intensity of  $1s \rightarrow 3d$  transition has been correlated to the degree of the site distortion from a perfect octahedron on the basis of Mossbauer studies (7).

In comparison with the  $\alpha\text{-Fe}_2\text{O}_3$  spectrum, the  $1s \rightarrow 4s$  feature was broadened out in all the samples derived from coal. All spectra clearly showed a sharp edge crest in identical position within the limits of experimental error. Since the  $\text{Fe}^{3+}$  in  $\alpha\text{-Fe}_2\text{O}_3$  is highly symmetrical and 6-coordinated, this may be true of the other samples investigated. However, the effect of other nearest neighbor bonding with  $\text{Fe}^{3+}$  on the XANES feature is not known at this time. Additional standards, incorporating (alkali, alkaline earth metals and Fe) -O bonding have to be evaluated.

Figure 2 shows the Fourier transforms (FT) of  $K^3$ -weighted K-edge EXAFS of Fe in the above samples without taking into consideration of the phase shift. There are two major peaks in the FT's corresponding to two different shells: the first peak at  $\sim 1.5 \text{ \AA}$  is attributed to Fe-O atom pair correlation. Considering the fact that EXAFS derived bond-lengths are accurate to  $0.02 \text{ \AA}$ , there are only minor variations in the pseudo radial distribution functions (PRDF), which is representative of the actual bond length in the absence of phase shift corrections, of the samples studied. The coordination (N) of Fe by oxygen decreased to 5.0, 4.5 and 4.0, respectively, for the ASTM ash, inner deposit and outer deposit, respectively, in comparison with  $N = 6$  for  $\alpha\text{-Fe}_2\text{O}_3$ .

The second peak around  $r = 2.7 \text{ \AA}$  corresponds to Fe-Fe atom pair correlation and none of the samples from the PSE&G boiler showed intensity similar to that of  $\alpha\text{-Fe}_2\text{O}_3$ . Furthermore, there is considerable variation in the shape of this peak. Whereas this peak was a triplet in the case of  $\alpha\text{-Fe}_2\text{O}_3$ , ASTM ash and the inner deposit, it was a singlet in the case of the outer deposit. It appears that the nature of the deposit formed in the boiler may be related to the second peak in the FT. The shape of the peak may be correlated to the type of the neighboring atom and the intensity of the peak may be used to determine the aggregation of the Fe atoms. The inner part of the deposit, which is close to the relatively cool tube, may be expected to be enriched with volatile alkalis which condense from the gas phase and the iron from the boiler tube. In any case, the

results show that the chemical nature of iron in the boiler deposits is different from that of  $Fe_2O_3$ , and there is a continuous variation in its nature across the deposit as additional layers are formed. This characteristic feature can be employed to establish the relationship between the processing conditions and the nature of ash deposits.

#### CONCLUSIONS

Slagging of ash and fouling of heat exchange tubes are two major problem areas in combustion of coal and other carbonaceous feedstock containing appreciable amounts of mineral matter in it. From the results of this study, employing samples generated in a large-scale utility boiler, it appears that XANES/EXAFS can be used as a structural problem of the materials that cause slagging and fouling, in order to obtain greater insight into the mechanism of their production. The EXAFS study of several other key elements such as Na, K, Ca, Al and S will be required to obtain a clear picture of the slag formation characteristics. The results can be applied to other emerging clean coal technologies such as fluidized bed combustion, coal-fueled gas turbines, etc.

#### ACKNOWLEDGEMENT

This research was supported by the U.S. Department of Energy under Contract No. AC02-76CH00016.

#### REFERENCES

1. Koningsberger, D. C. and Prins, R. X-ray Absorption: Principles, Applications and Techniques of EXAFS, SEXAFS and XANES. John Wiley & Sons, New York, New York 1988.
2. Fay, M. J., Proctor, A., Hoffmann, D. P. and Hercules, D. M. Anal. Chem. 60(21), 1225A (1988).
3. Lees, P. A., Citrin, P. H. Eisenberger, P. and Kincaid, B. M., Rev. Mod. Phys., 53(4), 769 (1981).
4. Hayes, T. M., and Boyce, J. B. Solid State Phys., 37, 173 (1982).
5. Teo, B. K. EXAFS: Basic Principles and Data Analysis. Springer-Verlag, New York, New York (1986).
6. Dehmer, J. L., and Dill, D. J. Chem. Phys., 65, 5327 (1976).
7. Bancroft, G. M., Maddock, A. G. and Burns, R. G. Geochem. Cosmochem. Acta, 31, 2219 (1967).

ORIGINAL COPY NOT CLEAR

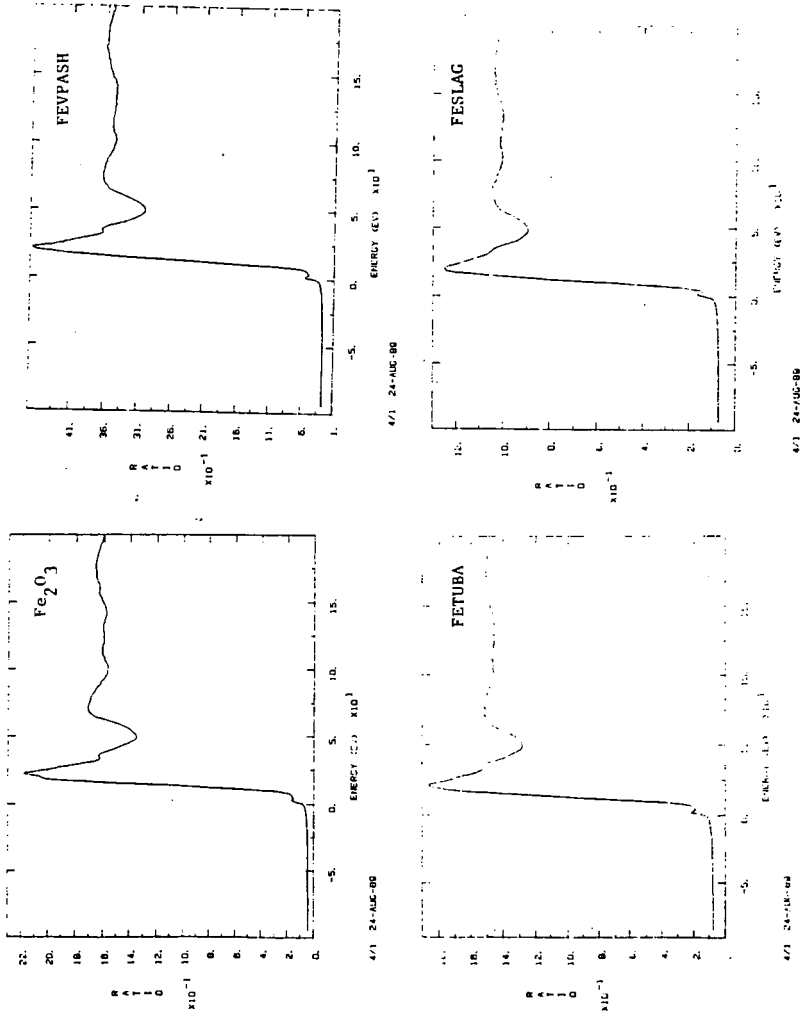
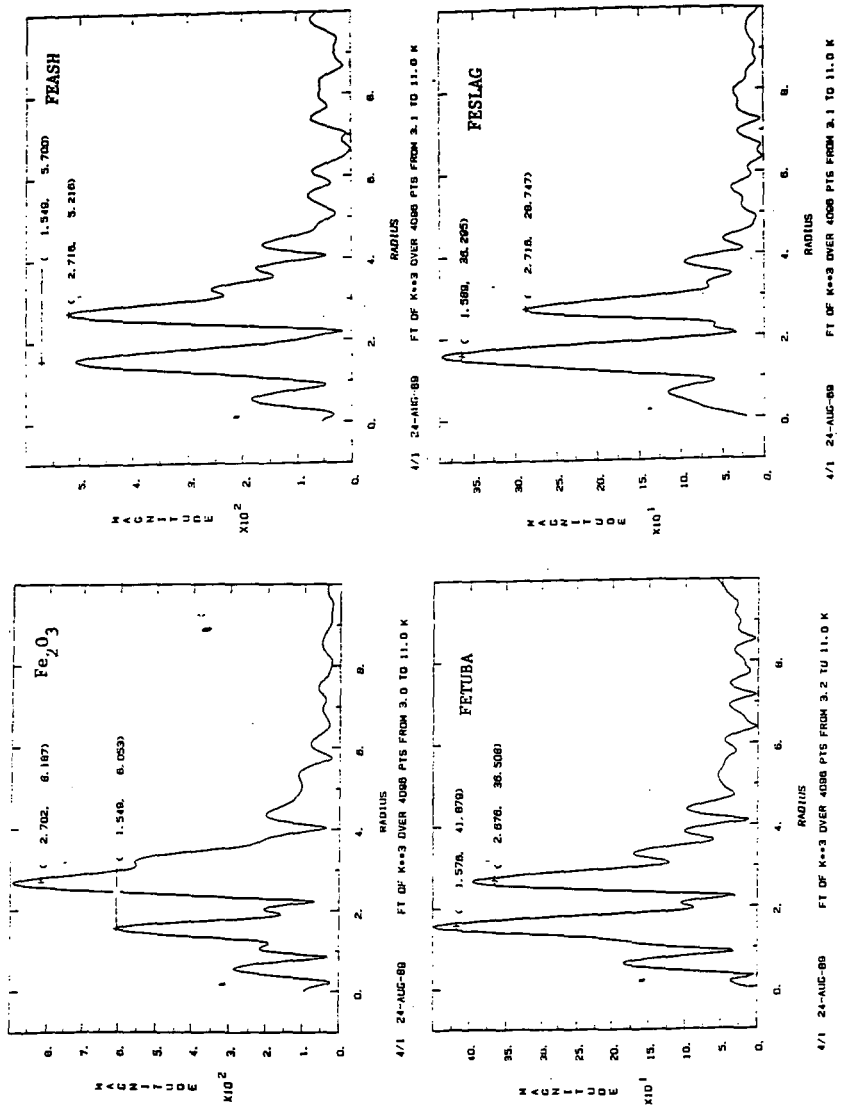


FIGURE 1. X-RAY ABSORPTION NEAR EDGE SPECTRA (IRON K EDGE)



4/1 24-AUG-88 FT OF K $\alpha$ 3 OVER 4000 PIS FROM 3.0 TO 11.0 K  
 4/1 24-AUG-88 FT OF K $\alpha$ 3 OVER 4000 PIS FROM 3.1 TO 11.0 K  
 4/1 24-AUG-88 FT OF K $\alpha$ 3 OVER 4000 PIS FROM 3.2 TO 11.0 K  
 4/1 24-AUG-88 FT OF K $\alpha$ 3 OVER 4000 PIS FROM 3.1 TO 11.0 K

FIGURE 2. Fe K-EDGE PSEUDO RADIAL DISTRIBUTION FUNCTIONS

## RESERVATIONS CONCERNING THE USE OF "MODEL COMPOUNDS" FOR COALS

John Larsen  
Department of Chemistry  
Lehigh University  
Bethlehem, PA 18015

Keywords: Model compounds, structure, reactivity, macromolecular

### INTRODUCTION

A major goal in coal chemistry is understanding the chemical reactions which occur in coals, especially those reactions which occur during coal conversion. One frequently used approach is to study the reaction of compounds which are thought to contain specific functional groups which occur in coals and assume these functional groups will react identically in the coal and in the model system. This paper is an exploration of the "model compound" approach and an attempt to develop criteria for judging the relevance of "model compound" studies to more complex coal systems.

To provide correct insights into the chemistry which occurs during a reaction of a coal, three major criteria must be met: 1) The functional group being studied must exist in coals and its reactivity range in coals due to different substituent effects must be understood and explicitly considered. 2) Knowledge of the reaction environment in the coal must be understood at a level which allows reactivity to be corrected for differences in environment. This includes correcting reactions for "solvent effects". 3) The actual reaction occurring in the coal must be identified and understood. If all these criteria are met, the use of "model compounds" can be a very powerful means for exploring coal reactivity. If even one of the criteria is not met, then the "model compound" study may not provide insight into the chemistry occurring in the coal.

It is my belief that our knowledge of coal structure is sufficiently incomplete to make the routine utilization of model compounds unwise. A wise approach is to identify a reaction which is occurring in coals and then to develop a thorough understanding of that reaction and how it will be altered when it occurs in a coal's macromolecular system. This will involve work with pure compounds, some of which may be, but do not need to be, directly representative of coal structures. Often, the greatest insight into reactions comes from working at the extremes of reactivity. It is much better to understand the reaction thoroughly than it is to carry out an incompletely understood reaction on molecules which are believed to be representative of structures which occur in coals. Once the reaction is understood, attempts can be made to extrapolate this chemistry into the complex macromolecular coal system. In doing this, it is incumbent upon us to explicitly recognize the uncertainties in that extrapolation which derive from our uncertainties about the structure of coals. The work should come full circle. It will start with a study of real coals to identify an important reaction. This stage should be thorough enough to provide certainty as to the identity of that reaction. Then the laboratory or the library is used to gain a mastery of that particular reaction. With a thorough understanding of the reaction in hand, one then moves back to predictions about the

behaviors of coals by considering the effects of the coal medium and structure on the understood reaction, completing the circle.

I will consider briefly our state of knowledge in the three areas I regard as crucial: coal structure, coal as a reaction environment, and our knowledge of the reactions which are actually occurring in coals. My conclusion is that our knowledge in all three areas is sufficiently uncertain to make extrapolations from routine "model compound studies" to coals quite unreliable, and the circular experimental pathway described above is strongly recommended.

Our knowledge of the functional groups which are present in coals has increased enormously, but is still inadequate in some major areas. Consider first our knowledge of the composition of coals. Finseth has recently demonstrated that significant errors in the hydrogen content can derive from incomplete drying of coals under conditions currently in wide use for drying coals. Oxygen content is usually done by difference, a procedure which concentrates all of the errors here. A recent paper compared many different methods for oxygen analysis and showed<sup>2</sup> that they give divergent results in a non-systematic way. There remain significant problems in the routine determination of the composition of coals. It would be nice to have well checked, very accurate compositional data for all of the Argonne coals which explicitly include consideration of the analytical difficulties.

The oxygen functional group distribution has received much attention. Stock has done a magnificent job in determining the oxygen functional group distribution of Illinois No. 6 coal.<sup>3</sup> This was a major research undertaking, and I believe this is the only coal for which a complete and reasonably detailed oxygen functional group distribution has been published. Liotta has published some detailed information on oxygen functional group distribution in a Rawhide (Wyodak subbituminous) coal, and there are attempts to characterize oxygen using NMR spectroscopy without chemical derivatization.<sup>4,5</sup> This latter work provides no information about substitution patterns, which are important. Stock has provided some information on the number of aromatic rings which have two oxygen functionalities. This seems to be all that is available. This is an important issue because of the possibility of large substituent effects. Important simple questions remain unanswered. What is the distribution of the phenolic hydroxyls or ethers over the different polynuclear aromatic systems? A 9-phenanthryl ether often reacts very differently than does a phenyl ether. What is the size distribution of the alkyl chains in aralkyl ethers? To fully understand the behavior of a functional group, the range of coal structures in which it occurs must be known. NMR techniques to explore the environment of oxygen atoms using cross-polarization are under development.

The introduction of sophisticated NMR techniques has made possible the determination of the range of PNA structures in coals<sup>6</sup> and this has been done for all of the Argonne premium coals.<sup>7</sup> But, in spite of the advances in NMR, there are still major disagreements about the ring size distributions of the aromatics in coals.<sup>8</sup> Our knowledge of aliphatic structures is not as great. In fact, only recently have definitive structural assignments been made of a majority of the aliphatic carbons in a single coal.<sup>9</sup> Only recently have there been attempts to quantitatively explore the number of acidic carbon sites

in coals.<sup>10</sup> There are few, if any, functional groups whose population in several coals of varying rank is unquestioned.

Coals are horrendously complex reaction environments. As mined, they are glassy, macromolecular systems containing a complex pore structure.<sup>11</sup> Molecular diffusion through glassy materials is very slow and many organic reactions of coals, carried out at or near room temperature are mass transport limited.<sup>4,12</sup> Coals imbibe many solvents and swell in the process. With strongly swelling solvents such as pyridine, the glass-to-rubber transition is suppressed significantly below room temperature and the coals are in a rubbery state.<sup>13</sup> Diffusion rates in the rubbery state are enhanced by several orders of magnitude over those in the corresponding glass. The rubbery coal is still a macromolecular system which does not dissolve, so the kind of intimate mixing familiar in solution reactions does not occur. The reagent must gain access to the reaction site by diffusing through a rubbery solid. There will usually be significant mass transfer constraints on reactions of coals which involve reagents even if the coals are rubbery.

Even in reactions which do not involve an outside reagent but which are initiated within the coal, mass transport plays a role. If thermal bond homolysis occurs in a coal, the pair of radicals produced may be constrained to stay near each other by large cage effects. If the coal is still glassy, they will not be able to separate rapidly because of the absence of large scale molecular motion. If the coal is rubbery, cage effects will be much less, but the ultimate translational freedom of the radicals will be limited by their position in the coal macromolecular structure. They may not be able to diffuse to their most thermodynamically or kinetically favorable reaction partner, but may be forced by the constraints of the macromolecular system to react with a nearby group. To understand reactions in coals, the environment of the intermediates must be known, at least on a statistical basis. No information of this sort has been published. The very important work of Poutsma, Buchanan and co-workers has demonstrated another pathway for radical diffusion. They have recently shown that radicals can migrate across a plane of molecules bonded to a silica surface by sequential hydrogen abstraction reactions.<sup>14</sup> This is a crucial observation since it provides a mechanism for the rapid diffusion of a reactive center through the coal and justifies ignoring diffusional limitations for a range of radical reactions. Some mechanism of this sort must be involved in the artificial coalification experiments of Winans et al. which are catalyzed by clays, yet which occur throughout the mass of the sample, not just adjacent to the clay surface.<sup>15</sup> Whether the intermediates involved are radicals or ions has not been established.

One other aspect of the macromolecular nature of coal has important effects on reactivity. It is that coals are selective absorbents.<sup>16</sup> While extensive work has been done to model coal reactivity containing good hydrogen donors like tetralin, the composition of the reacting coal in any direct liquefaction process has never been defined. The coal will have been swollen by components from the recycle solvent. It has been documented extensively that coals are selective absorbents,<sup>16-18</sup> and that they do not have a large affinity for aliphatic materials. The reacting coal system will consist of coal and an unknown mixture of components selectively extracted from

the recycle oil, probably in about equal amounts. Modeling coal conversion processes using model compounds will be a fatuous activity until the reacting system has been adequately defined. The same constraints do not apply to pyrolysis reactions, but there cage effects and other mass transport issues become complex and difficult to handle.

The last issue to be discussed is the nature of the reactions which are occurring in coals. There is general agreement that radical reactions are involved in coal conversion. An early simplistic mechanism that the reaction proceeded totally by bond homolysis followed by "capping" of the radicals by hydrogen donors has largely been replaced by the realization that a variety of chain processes are occurring in addition to the simple homolytic bond cleavage.<sup>19,20</sup> The extent and role of these chain reactions is still an object of much discussion. The family of radical reactions which are occurring still has not been completely elucidated. The use of probe molecules should be a major help.<sup>21</sup>

Radical reactions may not be the only ones occurring. Brower has published impressive evidence based on volumes of activation and isotope effects that ionic and/or electrocyclic processes must be occurring during coal liquefaction.<sup>22</sup> I have yet to see a convincing explanation for or rationalization of Brower's data. Ross has recently become concerned with ionic reactions occurring at the coal-mineral matter interface.<sup>23</sup> Much chemistry is possible here as demonstrated by the Winans' coalification experiment. Its role in coal conversion, if any, has not yet been elucidated. Finally, there is the whole question of radical anion and radical cation chemistry.

In summary, there is abundant evidence for the existence of a variety of radical processes occurring during coal conversion. The snarl of competing and parallel reactions has not yet been unraveled. There exists evidence that the principle pathways may not be solely radical reactions, and this evidence has been largely ignored. It seems clear that one must deal with complex radical chemistry when considering coal conversion and coal pyrolysis. Whether radical reactions are the only pathways which must be considered is not yet clear.

Coal is perhaps the most complex organic material whose structure and reactivity has been systematically studied. It is a largely insoluble, black, amorphous, inhomogeneous system containing a wide variety of structural groups and a respectable population of free radicals, and it is not surprising that the progress has been slow and difficult. I believe that achieving the most rapid progress possible requires explicit recognition and acceptance of the enormous complexity of the material. There have been many model compound studies published in which many of the structural complexities are ignored. The use of simplified models and procedures imposes the duty to identify the simplifying assumptions and their potential impact on any conclusions reached.

#### ACKNOWLEDGEMENT

Grateful acknowledgement is made of the financial support of our efforts in coal chemistry received from the U.S. Department of Energy, the Exxon Education Foundation, and Exxon Research and Engineering Co.

#### REFERENCES

- (1) Finseth, D. Am. Chem. Soc. Div. Fuel Chem. Prepr. **1987**, 32(4), 260-263.
- (2) Ehmman, W. D.; Koppenaar, D.; Hamrin, C. E. Jr.; Jones, W. C.; Prasad, M. N.; Tian, W.-Z. Fuel **1986**, 65, 1563-1570.
- (3) Stock, L. M.; Willis, R. S. J. Org. Chem. **1985**, 50, 3566-3573.
- (4) Liotta, R.; Brons, G. J. Am. Chem. Soc. **1981**, 103, 1735-1742 and previous papers in this series.
- (5) Dereppe, J.-M.; Moreaux, C.; Landais, P.; Monthieux, M. Fuel **1987**, 66, 594-599 and references therein.
- (6) Hagaman, E. W. Energy Fuel **1988**, 2, 861-862.
- (7) Solum, M. S.; Pugmire, R. J.; Grant, D. M. Energy Fuels **1989**, 3, 187-193.
- (8) Winans, R. E.; Hayatsu, R.; McBeth, R. L. Am. Chem. Soc. Div. Fuel Chem. Prepr. **1988**, 33(1), 407-414.
- (9) Stock, L. M.; Wang, S.-H. Energy Fuels **1988**, 3, 533-535.
- (10) Hagaman, E. W.; Chambers, R. R. Jr.; Woody, M. C. Energy Fuels **1987**, 1, 352-360.
- (11) Coal Structure, Meyers, R. A. Ed., Academic Press; New York: **1982**.
- (12) Larsen, J. W.; Green, T.K.; Choudhury, P.; Kummerle, E. W. Adv. in Chem. Ser. **1981**, 192, 277-291.
- (13) Brenner, D. Fuel **1985**, 64, 167-173.
- (14) Buchanan, A. C. III; Britt, P. F.; Biggs, C. A. Proc. Intl. Conf. Sci. **1989**, 1, 185-188.
- (15) Hyatsu, R.; McBeth, R. L.; Scott, R. G.; Botto, R. E.; Winans, R. E. Org. Geochem. **1983**, 6, 463-471.
- (16) Whitehurst, D. D.; Mitchell, T. O.; Farcasiu, M.; Coal Liquefaction, Academic Press; New York: **1980**, p. 92.
- (17) Hombach, H.-P. Fuel, **1980**, 59, 465-470.
- (18) Green, T. K.; Larsen, J. W.; Fuel, **1984**, 63, 1538-1543.
- (19) Curran, G. P.; Struck, R. T.; Gorin, E. I&EC Proc. Des. Develop. **1967**, 6, 166-173.
- (20) McMillen, D. F.; Malhotra, R.; Nigenda, S. E. Fuel, **1989**, 68, 380-386.
- (21) Bockrath, B. C.; Schroeder, K. T.; Smith, M. R. Energy Fuels **1989**, 3, 268-272.
- (22) Brower, K. R.; Paja, J. J. Org. Chem. **1984**, 49, 3970-3973.
- (23) Ras, D. R., personal communication.

## A SEARCH FOR THE RADICAL HYDROGEN TRANSFER PATHWAY IN COAL HYDROLIQUEFACTION.\*

Tom Autrey and James A. Franz  
Pacific Northwest Laboratory\*\*

### INTRODUCTION

It is generally accepted that the formation of petroleum liquids produced in the thermal liquefaction of coal can not be completely explained by simple homolytic cleavage of strong linkages in coal structures. Model compound studies have been employed to elucidate the mechanisms of scission of strong bonds in coal structures and have provided useful information for increasing the efficiency of the coal liquefaction processes (1).

Radical Hydrogen Transfer (RHT), the transfer of a hydrogen atom from a solvent-derived cyclohexadienyl substituted radical to the ipso position of an aryl-alkyl linkage, has been proposed as an important pathway for the cleavage of strong bonds in coal structures during coal liquefaction (2-4). Elegant numerical modeling studies of the scission of diarylmethane model compounds in the presence of a variety of solvent molecules demonstrated that an alternative mechanism for the scission of the strong bonds in these model compounds may be operative that involves cyclohexadienyl-derived solvent molecules rather than free hydrogen atoms. These studies predicted an activation barrier of 18 to 22 kcal/mol for an endothermic transfer of a hydrogen atom from a cyclohexadienyl solvent molecule to the ipso position of a diarylmethane model compound (5-7). Furthermore, these studies have been utilized to predict the efficiencies of hydrogen donor solvents in the liquefaction of coal samples (8,9). The evidence, however, does not preclude other mechanisms involving the cyclohexadienyl solvent molecules. Other possible mechanisms include an addition-transfer-elimination reaction (10) or other, more traditional radical mechanisms that do not require an exotic reaction pathway involving a hydrogen atom carrier donating a hydrogen atom to a closed shell species.

### EXPERIMENTAL

The model compound, 3,6-dihydro-3-methoxycarbonyl bibenzyl, 2, was prepared by the following reaction sequence. *m*-bromobenzaldehyde was added to an ether solution of benzyl grignard at room temperature to yield the expected alcohol. The alcohol was converted to the chloride (SOCl<sub>2</sub>) and reduced with LiAlH<sub>4</sub> to give *m*-bromobibenzyl. A grignard reagent from *m*-bromobibenzyl was quenched with CO<sub>2</sub>. Following acidic work-up esterification in methanol gave the methyl ester. Birch reduction of the ester yielded our model compound, 2.

Decane solutions of the ester, 2, (10<sup>-3</sup> M to 10<sup>-4</sup> M) containing an internal standard for GC product analysis were prepared in quartz tubes. The

\* This work was supported by the Office of Basic Energy Sciences, U. S. Department of Energy.

\*\* Pacific Northwest Laboratory is operated for the U. S. Department of Energy by Battelle Memorial Institute under contract OE-AC06-76RLO 1830.

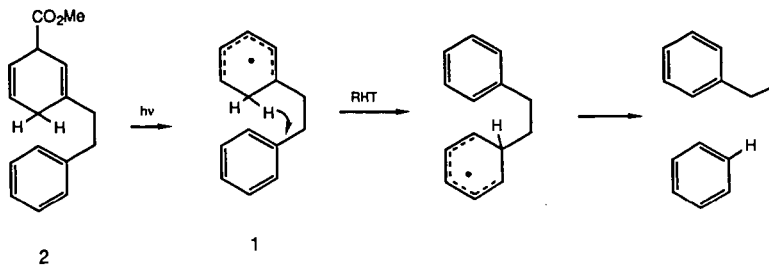
samples were degassed, using three freeze-thaw cycles, and sealed under vacuum. The sealed tubes were irradiated with a high-pressure, 1000-W Hg lamp through the quartz window of a hot air bath, and the temperature was monitored using a thermocouple. Photolysis times ranged from 10 to 15 minutes to yield about 30% decomposition of the starting material. Control experiments showed that the ester was thermally stable under the reaction conditions. Products were analyzed on a HP 5890A GC using on-column injection techniques and were identified by the retention times and GC/mass spectra of authentic compounds.

## RESULTS AND DISCUSSION

Our approach to this problem was to design and prepare a new model compound that would provide an unambiguous answer to our question, "What role does Radical Hydrogen Transfer play in the cleavage of strong bonds in coal liquefaction?" We chose a model compound that would provide us with a cyclohexadienyl radical hydrogen donor and an alkyl-phenyl hydrogen acceptor within the same molecule. We anticipated several advantages to this approach in the preparation of our model compound 3,6-dihydro-3-methoxycarbonyl bibenzyl, **2**:

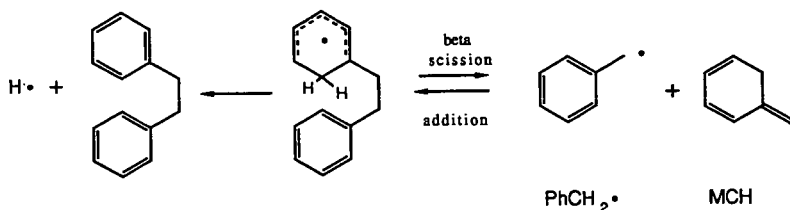
- 1) The cyclohexadienyl transferring agent could conveniently be prepared from a Norrish Type I photo-cleavage of the methyl ester, **1**, at any desirable temperature and at very low rates of initiation favoring unimolecular RHT or scission reactions over bimolecular termination;
- 2) A thermal-neutral hydrogen transfer from a cyclohexadienyl to a phenyl aromatic would provide a lower activation barrier than the endothermic barrier from the numerical modeling studies;
- 3) An intramolecular hydrogen transfer would increase the Arrhenius factor ( $\log A$ ) from 8.5 (bimolecular RHT) to 10 to 11 (intramolecular RHT) thereby suppressing competing side reactions;
- 4) Intramolecular RHT of **1** would proceed through a transition structure of nearly optimal regio- and stereo-chemical orientation, a 1,5 hydrogen migration (11) to yield benzene and phenylethyl radical products as shown in Scheme I;

Scheme I



- 5) A competing  $\beta$ -scission reaction of the cyclohexadienyl radical 1 to yield benzyl radical and methylenecyclohexadiene (MCH) products would provide an internal "clock" to quantify the activation barrier for RHT in this model system as shown in Scheme II;

Scheme II



Irradiation of a dodecane solution containing the methyl ester, 2, ( $2.4 \times 10^{-4}$  M) heated to 250 °C in a quartz reactor vessel led to the decomposition of the model compound and the appearance of two cleavage products, toluene (8%) and bibenzyl (24%), yields are based on conversion of starting material. Control experiments showed that the methyl ester was thermally stable under the reaction conditions. Benzene, the RHT product, was not detected.

Irradiation of a concentrated solution of 2 ( $1.6 \times 10^{-3}$  M) under the above reaction conditions gave the same products, toluene (3%) and bibenzyl (18%) but no benzene. The decrease in yield of toluene was expected because higher concentrations of benzyl radical lead to an increased rate of termination.

These results require that RHT from the cyclohexadienyl radical to the appended phenyl ring not compete with  $\beta$ -scission of the cyclohexadienyl radical in this model compound,  $E_a(\text{RHT}) > E_a(\beta\text{-scission})$ . Although we did not observe RHT products in this model system, a lower limit for the activation barrier of a RHT pathway for this system can be determined. This lower limit can be obtained from a calculation of activation barrier for the competing  $\beta$ -scission reaction (Scheme II) determined by Equation [1].

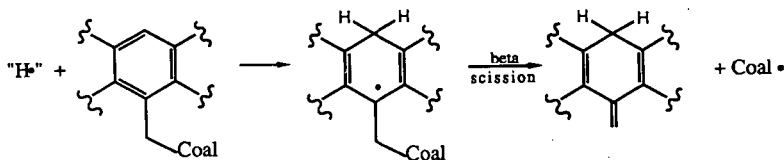
$$E_a = \Delta H_f^\circ(\text{MCH}) + \Delta H_f^\circ(\text{PhCH}_2\cdot) + E_a(\text{addition}) - \Delta H_f^\circ(1) \quad [1]$$

Only one approximation is necessary in our calculation: The barrier for addition of benzyl radical to methylenecyclohexadiene (MCH), which is the reverse reaction of  $\beta$ -scission. The addition of benzyl radical to styrene was determined to have a barrier of 7 kcal/mol (12). We assume that the barrier for the more exothermic reaction, addition of benzyl radical to MCH, will be no less than 4 kcal/mol. The thermochemical data for the products of the  $\beta$ -scission reaction

were determined previously. We used 48 kcal/mol as the  $\Delta H_f^\circ$  of benzyl radical (13), and 35 kcal/mol as the  $\Delta H_f^\circ$  of MCH (14) and we calculated the  $\Delta H_f^\circ$  of radical 1 to be 60.6 kcal/mol (15). The solution to Equation [1] yields a barrier of  $28 \pm 3$  kcal/mol for  $\beta$ -scission of cyclohexadienyl radical 1 to yield MCH and benzyl radical, just slightly lower than the barrier we calculate for scission of hydrogen atom from a cyclohexadienyl radical ( $E_a = 30$  kcal/mol).

It is important to note that this novel  $\beta$ -scission reaction can be responsible for the cleavage of "strong bonds" in coal structures at relatively low temperatures if the appropriate hydrogen atom donors are available. Our new finding suggests that addition of hydrogen atoms to non-ipso ring positions should promote bond cleavage by this  $\beta$ -scission pathway as shown in Scheme III. In this

Scheme III



work  $\beta$ -scission just barely competes with loss of hydrogen ( $E_a = 30$  kcal/mol). However, with the addition of hydrogen atoms to larger ring systems the  $\beta$ -scission reaction becomes more important because the barrier for hydrogen loss increases with increasing ring size. When the alkyl linkages are longer than two carbon units the barrier of scission increases, obviously the stability of the radicals produced is a driving force, but  $\beta$ -scission may still compete with loss of hydrogen in larger ring systems. The barrier for  $\beta$ -scission of diarylmethanes is prohibitively high, due to the formation of aryl radicals, and therefore would not have been observed in the numerical model studies.

#### CONCLUSION

Our examination of the RHT process yields an important result. Our model compound allowed us to "isolate" the RHT process from any competing intermolecular cleavage reaction involving cyclohexadienyl solvent molecules. Our 6-(2-phenylethyl)-cyclohexa-1,3-dien-6-yl radical is consumed by a  $\beta$ -scission pathway, with an activation barrier we calculate to be 28 kcal/mol. No RHT products are observed in our model system. This requires the  $E_a$  for RHT to be  $> 28$  kcal/mol, which is substantially higher than the value obtained by the numerical modeling studies ( $E_a$  16 to 22 kcal/mol).

There is convincing evidence that donor solvent structures play an active role, perhaps a predominant role in the cleavage of strong bonds (7-10). In the present work we have conveniently suppressed all side reactions from our

experiments in order to selectively examine the RHT contribution. We do not imply that a RHT pathway does not occur to some extent in the liquefaction of coal, we expect it to have a lower activation barrier than the well-documented Molecular Assisted Homolysis (MAH) reaction (17,18). However, unless significant tunneling of the hydrogen atom through the high barrier (>28 kcal/mol) for RHT occurs, a low activation process responsible for the cleavage of strong bonds in coal structures must occur by an alternative mechanism. The addition-transfer-elimination mechanism (10), a concerted-transfer with elimination pathway (19), and a simple addition-abstraction-elimination reaction pathway are presently being investigated by this group.

#### REFERENCES

- 1) M. L. Poutsma, A Review of the Thermal Studies of Model Compounds Relevant to Processing Coal. 1987 NTIS Report No. DE88003690/GAR
- 2) D. F. McMillen, W. C. Ogier, S. J. Chang, R. H. Fleming and R. Malhotra, Proceedings of the 1983 International Conference on Coal Science, Pittsburg, Pennsylvania, 15-19 August, 1983, p. 199.
- 3) R. Billmers, L. L. Griffith and S. E. Stein, J. Phys.Chem. 1986, 90, 517.
- 4) J. A. Franz, Gordon Research Conference on Free Radical Reactions, June 1981.
- 5) D. F. McMillen, R. Malhotra, S.-J. Chang, and S. E. Nigenda, Am. Chem. Soc., Div. Fuel Chem. Preprints, 1985, 30(4), 297.
- 6) D. F. McMillen and R. Malhotra, Proceedings of the 1987 International Conference on Coal Science, Maastricht, The Netherlands, 26-30 October, 1987.
- 7) D. F. McMillen, R. Malhotra, S.-J. Chang, W. C. Ogier, E. Nigenda and R. H. Fleming, Fuel, 1987, 66, 1611.
- 8) D. F. McMillen, R. Malhotra, G. P. Hum and S.-J. Chang, Energy and Fuels, 1987, 1(2), 193.
- 9) R. Malhotra and D.F. McMillen, Am. Chem. Soc., Div. Fuel Chem. Preprints, 1988, 33(3), 319.
- 10) R. Billmers, R. L. Brown and S. E. Stein, International J. Chem. Kinetics, 1989, 21, 375.
- 11) 1,5 Hydrogen atom shifts are the most common. R. K. Freindlina and A. B. Terent'ev, Acc. Chem. Res. 1977, 10, 9.
- 12) M. L. Poutsma and C. W. Dyer, J. Org. Chem. 1982, 47, 4903.
- 13) M. Rossi and D. M. Golden, J. Am. Chem. Soc. 1979, 101, 1230.
- 14) J. E. Bartmess, J. Am. Chem. Soc. 1982, 104, 335.

- 15) S. W. Benson in Thermochemical Kinetics, 1976, Wiley-interscience. Group additivities were used to calculate the  $\Delta H_f^\circ$  of the parent cyclohexadienyl compound and a BDE of 73 kcal/mol was used for the ipso hydrogen.
- 16) D. F. McMillen, W. C. Ogier, and D. S. Ross, J. Org. Chem. 1981, 46, 3322.
- 17) J. A. Franz, D. M. Camaioni, R. R. Beishline and D. K. Dalling, J. Org. Chem. 1984, 49, 3563.
- 18) W. D. Graham, J. G. Green and W. A. Pryor, J. Org. Chem. 1979, 44, 907.
- 19) L. M. Tolbert and R. K. Khanna, J. Am. Chem. Soc. 1987, 109, 3477.

#### ACKNOWLEDGMENT

We thank D. M. Camaioni and C. M. Pollock of the Physical Organic Chemistry Group for sharing the results of their calculations on the concerted transfer mechanism and informing us of Reference (19). This work was supported by the Office of Basic Energy Sciences, U. S. Department of Energy, under contract DE-AC06-76RLO 1830.

KEYWORDS (Radical Hydrogen Transfer, Novel  $\beta$ -scission of Bibenzyl)

## THERMOLYTIC CLEAVAGE OF SELECTED ETHER LINKAGES AT MILD TEMPERATURES

Birbal Chawla<sup>1\*</sup>, Burtron H. Davis<sup>1</sup>, Buchang Shi<sup>2</sup>, and  
Robert D. Guthrie<sup>2</sup>

<sup>1</sup>Center for Applied Energy Research  
3572 Iron Works Pike  
Lexington, KY 40511

<sup>2</sup>Department of Chemistry  
University of Kentucky  
Lexington, KY 40506

### INTRODUCTION

Most discussions of coal structure describe the substance as constituted of aromatic, hydroaromatic and heterocyclic aromatic clusters joined by short aliphatic and ether linkages. Various functional groups including phenolic hydroxyl groups and carboxylic acid groups are also present. Because coals are solids with no recognizable repeating units and generally have limited solubility in all solvents, the enterprise of understanding their structures and relating this understanding to practical purposes, necessarily involves some chemical or physical structure disruption with potential loss of information. Most frequently this has involved thermolysis with hydrogen-donor species present. Recently there has been an increased interest in chemical processing which can be carried out under relatively mild conditions (1) which might be hoped to preserve more of the structural features of the initial material.

Analysis of the materials produced by the processing of coal has tended to focus on carbon-carbon bond breaking. Ether linkages, although believed to be present, have not been considered in detail for their potential role in the thermal or chemical reactions of coal under relatively mild conditions. This is surprising in view of the fact that compounds which model the types of ether moieties which might be present in coals are known to undergo pyrolytic scission at temperatures comparable to those of coal liquefaction (2,3). Moreover, benzyl phenyl ether has been shown to promote hydrogen transfer between tetralin and diphenylmethane under thermolysis conditions (4) suggesting an indirect role for ether structural units in facilitating thermolytic liquefaction. A number of radical chain processes have been suggested

---

\*Present Address: Mobil Research and Development Corporation, Paulsboro  
Research Laboratory, Paulsboro, NJ 08066

as explanations for carbon-carbon bond breaking (5-7), and these would require an initiating radical such as an oxygen-center radical produced by ether scission.

Most of the reported studies describing the thermolysis of coal model compounds, ethers in particular, have been performed at much higher temperatures than used in coal liquefaction processes. Obviously, conclusions derived from thermolysis at the higher temperatures cannot be applied directly toward understanding of coal dissolution and/or thermolysis processes. Therefore, we initiated studies on the chemistry of thermolysis of four arylmethyl aryl ethers which undergo thermolysis to a significant extent under relatively mild reaction conditions.

## EXPERIMENTAL

Thermolysis experiments were performed in evacuated glass ampoules at reaction temperatures of 250°C to 350°C. In a typical thermolysis experiment, about 50 to 150 mg of the material was sealed in an evacuated glass ampoule (0.5 cm x 10 cm). The sealed ampoule was wrapped with steel wool and then inserted in a tubing bomb reactor of about 10-15 ml capacity. The reactor was then immersed in a heated sand bath for the desired reaction time. Typically, it required less than two minutes to reach the desired reaction temperature. At the end of the experiment, the reactor was immersed in a cold sand bath. Once the reactor had come back to ambient temperature, the sealed tube was removed from the reactor and was cut open to recover its contents. For comparison purposes, some of the thermolysis experiments were also conducted by charging the microautoclave reactor directly with 50 to 150 mg of the material. The products were recovered from the glass ampoule or from the reactor using tetrahydrofuran (THF). The THF solutions containing the reaction products were analyzed by GC and GC-MS equipped with SUPERCAP "High Temperature", Al clad fused silica bonded methyl silicone column (15 m x 0.25 mm id, 0.1  $\mu$ m film).

Four ethers, namely,  $\alpha$ -naphthylmethyl phenyl ether ( $\alpha$ -NMPHE),  $\alpha$ -benzyl naphthyl ether ( $\alpha$ -BNE),  $\beta$ -naphthylmethyl phenyl ether ( $\beta$ -NMPHE) and  $\beta$ -benzyl naphthyl ether ( $\beta$ -BNE) were prepared by procedures reported in the literature (8,9).

## RESULTS AND DISCUSSION

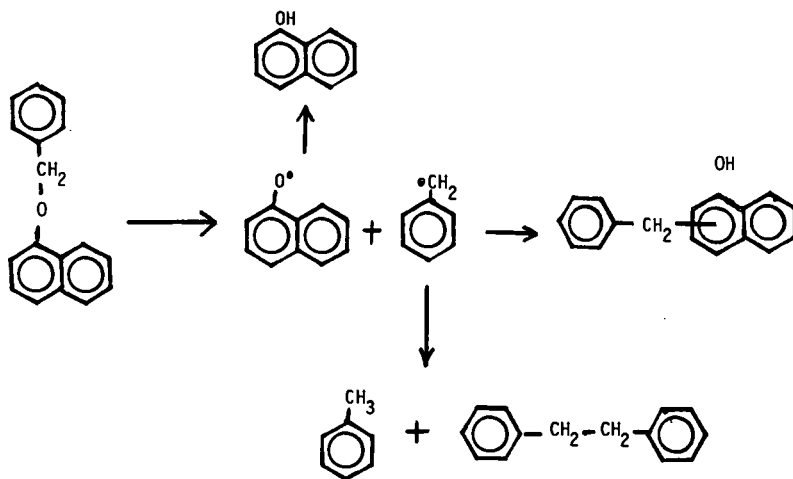
The results of thermolysis of four ethers ( $\alpha$ -NMPHE,  $\alpha$ -BNE,  $\beta$ -NMPHE,  $\beta$ -BNE) conducted at mild temperatures of 225°C to 350°C with a 30 minute reaction time are given in Table 1 and Figures I and II. Results reported here were calculated based upon the amount of ether left unreacted or decomposed. In order to provide insurance that no appreciable amount of non-volatile product was present, a known amount of triphenylene was added, as an internal standard, during the work up procedure.

As shown by the data in Table 1 and Figures I and II, all the four ethers underwent thermolysis to a significant extent of more than 80% at 325°C or below.

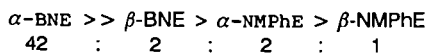
The major products in each case were ArOH, Ar'CH<sub>3</sub>, and isomers of the starting ethers which almost certainly have the structures: Ar'CH<sub>2</sub>ArOH. Relatively minor amounts of Ar'CH<sub>3</sub>CH<sub>2</sub>CH<sub>2</sub>Ar', Ar'CH=CHAR', Ar'CH<sub>2</sub>Ar, and a "dehydrocompound" (parent ion = 232) were also observed. Higher molecular weight materials were found in trace amounts. Isomer yields in sealed tube runs were 30 to 40%, ArOH yields were 20 to 30% and Ar'CH<sub>3</sub> yields were 10 to 30% of GC-observable products.

Formation of observed products could be understood with the help of a typical reaction scheme given below:

### THERMOLYSIS OF ALPHA-NAPHTHYL BENZYL ETHER



The relative rates of thermolysis of the four ethers were calculated using the experimental data and were found to be:

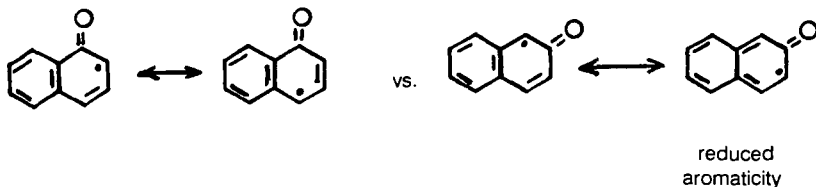


Temp. °C      Rate Constant in s<sup>-1</sup> x 10<sup>4</sup> Based on Ether Remaining

	<u><math>\alpha</math>-BNE</u>	<u><math>\beta</math>-BNE</u>	<u><math>\alpha</math>-NMPHE</u>	<u><math>\beta</math>-NMPHE</u>
325	---	17	17	9.4
300	---	2.9	2.3	1.2
285	4.1	0.62	---	0.17
275	7.1	0.34	0.3	---
365	2.6	0.1	---	---

The main conclusion is that the ethers all undergo thermolysis at relatively mild temperatures, presumably by homolysis of the CH<sub>2</sub>-O bond followed by recombination of the resultant radicals to give substituted phenols or naphthols or they abstract hydrogen to give ArOH and Ar'CH<sub>3</sub>.

An explanation of the relative rates can be found in the relative stabilities of the various radical pairs. Apparently,  $\alpha$ -NpCH<sub>2</sub>• and  $\beta$ -NpCH<sub>2</sub>• differ only slightly in stability whereas  $\alpha$ -NpO• is appreciably more stable than  $\beta$ -NpO•. This can be rationalized by assuming that resonance delocalization into the naphthalene ring is much more important in stabilizing NpO• than NpCH<sub>2</sub>•. This makes sense because of the instability of oxygen radicals and the strengthening of the C-O bond which results from increasing its C=O character. This analysis also explains why  $\alpha$ -NpOCH<sub>2</sub>Ph cleaves so much faster than  $\beta$ -NpOCH<sub>2</sub>Ph as the  $\alpha$ -naphthoxy radical has a contribution of an extra resonance structure:



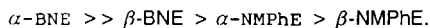
That  $\alpha$ -NpOCH<sub>2</sub>Ph and  $\beta$ -NpOCH<sub>2</sub>Ph should cleave at similar rates is not obvious but the increased stability of  $\alpha$ -NpCH<sub>2</sub>• relative to PhCH<sub>2</sub>• is accidentally equal to the advantage of  $\beta$ -NpO• over PhO•.

A significant difference in product distribution in the thermolysis of  $\alpha$ -NMPHE was observed when the reaction vessel was changed from a small glass ampoule (50-150 mg of ether in a 0.5 x 10 cm pyrex ampoule) to a stainless steel pipe reactor (0.5 - 1 g of ether in a 10-15 ml reactor). Relatively larger values of isomers/NpCH<sub>3</sub> + PhOH were observed in the glass vessel. In a previous thermolysis of this ether by Badr and El-Sherief (8) in a sealed glass tube (40 g of ether at 260°C for 7 days), they obtained about the same yield of isomers, but much

more  $\text{NpCHCH}_2\text{Np}$  ( $\sim 50\%$ ). The reasons for these different product distributions are unknown at the present time.

## SUMMARY

Thermolysis of four ethers of general structure  $\text{Ar}'\text{CH}_2\text{OAr}$ , namely,  $\alpha$ -naphthylmethyl phenyl ether ( $\alpha$ -NMPHE),  $\alpha$ -benzyl naphthyl ether ( $\alpha$ -BNE),  $\beta$ -naphthylmethyl phenyl ether ( $\beta$ -NMPHE) and  $\beta$ -benzyl naphthyl ether ( $\beta$ -BNE) at mild temperatures of 225°C to 350°C with a 30 minute reaction time was investigated. It was observed that all of the four ethers underwent significant thermolysis to the extent of more than 80% at 325°C or below. The major products in each case were  $\text{ArOH}$ ,  $\text{Ar}'\text{CH}_3$ , and isomers of the starting ethers. Relatively minor amounts of  $\text{Ar}'\text{CH}_2\text{CH}_2\text{Ar}'$ ,  $\text{Ar}'\text{CH}=\text{CHAr}'$ ,  $\text{Ar}'\text{CH}_2\text{Ar}$  and an unknown compound (parent ion = 232) were also observed. Higher molecular weight materials were found in trace amounts. The relative rates of thermolysis were:



## ACKNOWLEDGMENT

This research was supported by funds from the U.S. DOE as part of the Consortium for Fossil Fuel Liquefaction Science (CFMLS). Robert D. Guthrie thanks the Research Corporation for a Research Opportunity Award which helped to support the research described above.

## REFERENCES

1. (a) Chawla, B.; Davis, B. *Prepr. Pap., Am. Chem. Soc., Div. Fuel Chem.*, **33**, 440, (1988); (b) Keogh, R. A.; Chawla, B.; Tsai, K. J.; Davis, B. H. *ibid.*, 333; (c) Chawla, B.; Keogh, R.; Davis, B. H. *ibid.*, **32**, 324, (1987); (d) Chawla, B.; Davis, B. H. *Fuel Sci. and Tech. Int.*, **7**, 1, (1988); (e) Chawla, B.; Davis, B. H. *Fuel Proc. Tech.*, accepted, (1989); (f) Chawla, B.; Keogh, R.; Davis, B. *Energy & Fuels*, in press, (1989); (g) Keogh, R.; Poe, S. H.; Chawla, B., in "Coal Science and Technology", Vol. 11, J. A. Moulijn, K. A. Nater, H. A. G. Chermin, eds., Elsevier, New York, 1987, p. 269; (h) Keogh, R.; Klapheke, J.; Poe, S.; Hardy, R.; Taghizadeh, K.; Medina, R.; Taulbee, D.; Chawla, B.; Tsai, K.; Pollock, D.; Hower, J.; Davis, B. Final Report, Contract No. DE-FC22-86PC90017.
2. Chawla, B.; Davis, B. unpublished results.
3. Larsen, J. W.; Keummerle, E. W. *Fuel*, **55**, 162, (1976).
4. Sharma, D. K.; Mirza, Z. B. *Fuel*, **63**, 1329, (1984).
5. Reggel, L.; Raymond, R.; Friedman, S.; Friedel, R. A.; Wender, I. *Fuel*, **37**, 126, (1958).

6. Stock, L. M.; Malya, N.; Willis, R. S. Proc. Int. Conf. Coal Science, 722, 1985.
7. Sternberg, H. W.; Dolle Donne, C. V.; Pentagees, P.; Moroni, E. C.; Markby, R. E. Fuel, 50, 432, (1971).
8. Badr, M. Z. A.; El-Sherief, H. A. H. Indian Journal of Chemistry, 12, 1067, (1974).
9. Maslak, P.; Guthrie, R. D. J. Am. Chem. Soc., 108, 2637-2640, (1986).

Figure 1. Temperature dependence of the extent of conversion of naphthyl methyl phenyl ether ( $\alpha$ ,  $\circ$ ;  $\beta$ ,  $\bullet$ ).

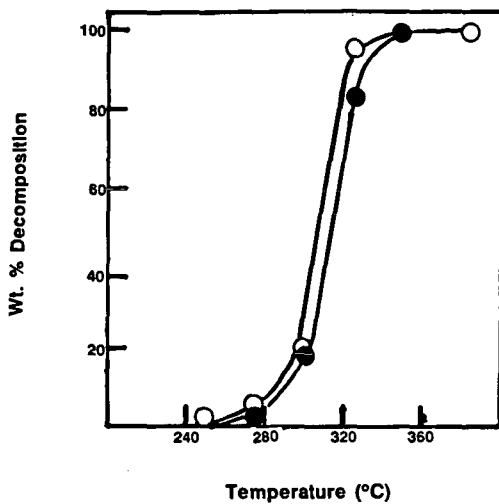
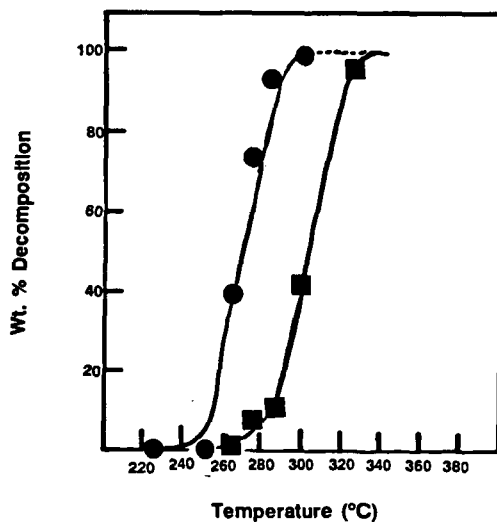


Figure 2. Temperature dependence of the extent of conversion of benzyl naphthyl ether ( $\alpha$ ,  $\bullet$ ;  $\beta$ ,  $\blacksquare$ ).



## Pyrolysis of Polycyclic $\alpha,\omega$ -Diarylpropanes Pathways, Kinetics, and Mechanisms

C. Michael Smith and Phillip E. Savage  
Department of Chemical Engineering  
The University of Michigan  
Ann Arbor, MI 48109-2136

Division of Fuel Chemistry  
Symposium on Model Compounds in Coal Liquefaction  
American Chemical Society  
Boston, MA Meeting  
April 1990

### INTRODUCTION

$\alpha,\omega$ -Diphenylalkanes have been commonly used as chemical models of the scissile aliphatic linkages between aromatic moieties in coal (e.g., Vernon, 1980; Poutsma and Dyer, 1982; Gilbert and Gajewski, 1982; Sweeting and Wilshire, 1962; Miller and Stein, 1981). In coal, of course, the terminal aromatic moieties are generally neither single ringed nor identical, thus unsymmetrical polycyclic  $\alpha,\omega$ -diarylalkanes might better mimic these moieties. Studies of these apparently relevant model compounds are few, however. The most probable reason for this gap in the literature stems from the reasoning that the reaction pathways, kinetics, and mechanisms of polycyclic  $\alpha,\omega$ -diarylalkanes can be extrapolated from those of single ring  $\alpha,\omega$ -diphenylalkanes. Indeed, the limited previous studies (e.g., Vernon, 1980; Sato, 1979; Javanmardian et al., 1988; Depp et al., 1956) with polycyclic  $\alpha,\omega$ -diarylalkanes suggest that this premise is reasonable. For example, Javanmardian et al. (1988) reported that the pyrolysis pathway for 2-(3-phenylpropyl)-naphthalene (PPN) led to toluene plus 2-vinylnaphthalene and 2-methylnaphthalene plus styrene; products analogous to those formed during 1,3-diphenylpropane pyrolysis. They further observed approximately equal molar yields of 1-methylnaphthalene and toluene from PPN pyrolysis suggesting that the presence of the naphthyl moiety in a 1,3-diarylalkane had little effect on the selectivity. It did, however, increase the rate of pyrolysis in comparison to that observed for 1,3-diphenylpropane.

In the present work, we further probe the pyrolysis pathways and kinetics of polycyclic  $\alpha,\omega$ -diarylalkanes. In particular, we present results of pyrolysis studies of two  $\alpha,\omega$ -diarylpropanes: 2-(3-phenylpropyl)-naphthalene (PPN) and 1,3-bis-(1-pyrene)propane (BPP). This work was motivated by our recent findings that the pyrolysis pathways for *n*-alkyl-substituted pyrenes are markedly different than the pathways for *n*-alkyl-substituted benzenes (Savage et al., 1989; Smith and Savage, 1989). The key differences were the presence of apparent autocatalytic kinetics and the cleavage of the strong aryl-alkyl C-C bond as the pathway to the major products.

### EXPERIMENTAL

The pyrolysis of PPN (API Standard Reference Materials) and BPP (Molecular Probes) both neat and in benzene were conducted in constant-volume, 316 stainless steel batch reactors. These reactors were made from one 1/4 in. Swagelok port connector and two 1/4 in. Swagelok end caps and had a volume of  $0.59 \pm 0.05$  ml. For the PPN neat pyrolyses, the batch reactors were loaded with approximately 40 mg of a previously prepared stock solution of PPN and biphenyl (an internal standard), and for BPP neat pyrolyses the batch reactors were loaded with an average of 2.3 mg of BPP and 9.3 mg of biphenyl. For the pyrolyses in benzene, the batch reactors were loaded with approximately 350 mg of a previously prepared stock solution comprising the model compound, biphenyl, and benzene as the inert diluent. All quantities were carefully weighed with an analytical balance. For the pyrolyses in benzene, the reactant concentration was calculated as the number of moles of reactant added to the reactor divided by the reactor volume. After being purged with argon, the reactors were placed in an isothermal fluidized sand bath at the desired temperature (e.g., 400°C). Upon reaching the desired holding time, the reactors were removed from the sand bath and rapidly cooled in an ambient temperature water bath. The reactors were opened, and products were recovered by benzene extraction for BPP and acetone extraction for PPN. Products were identified using GC (HP 5890) and GC-MS (HP 5890 Series 11 - HP 5970 MSD) and quantified by GC using biphenyl as an internal standard. GC response factors for the reaction products were experimentally determined from standard solutions that contained the reaction products and biphenyl in varying amounts. Plotting the ratio of the mass of a particular compound to the mass of biphenyl in the solution as a function of the ratio of

their integrated GC areas resulted in a straight line and gave the response factor as the slope. The average error for these response factors was 3% (Noggle, 1985).

## PPN PYROLYSIS

### Experimental Results

Table 1 displays the molar yields of the major products from the neat pyrolysis of PPN at 365 and 400°C and the pyrolysis of PPN in benzene at 375, 400, and 450 °C. The principal products at low PPN conversions were toluene, 2-vinylnaphthalene, 2-methylnaphthalene and styrene, but at high PPN conversions, 2-ethylnaphthalene and ethylbenzene were also present in high yields. The presence of these products and their temporal variations are consistent with the reaction pathway previously determined by Javanmardian et al. (1988). There is, however, a discrepancy with the previous work. Our present work showed that the yields of toluene were higher than the yields of 2-methylnaphthalene, whereas, in the earlier work the yields of toluene and 2-methylnaphthalene were essentially equal. We suspect that the reason for this discrepancy stems from our taking a more careful approach in determining GC response factors for the observed reaction products. Javanmardian et al. (1988) used a single point calibration for the response factors whereas the present analysis used linear regression of at least five points.

The minor products from PPN pyrolysis included 1,3-diphenylpropane and 2-*iso*-propylnaphthalene, which were previously observed by Javanmardian et al. (1988), and naphthalene. The neat pyrolysis also led to the production of acetone-insoluble char. The amounts of this dark solid material increased with temperature and batch holding time. We expect that the formation of this char satisfies the global material balance.

Javanmardian et al. (1988) found that the neat pyrolysis of PPN correlated well with pseudo-first order kinetics. Thus, we calculated pseudo-first-order rate constants from our data and plotted them along with those of Javanmardian et al. (1988) on the Arrhenius plot given as Figure 1. Clearly, the present kinetics results for PPN neat pyrolysis are consistent with the previous work. The Arrhenius parameters determined by Figure 1 are  $\log_{10} A = 9.6 \text{ sec}^{-1}$  and  $E^* = 38.5 \text{ kcal mol}^{-1}$  for the neat pyrolysis and  $\log_{10} A = 7.7 \text{ sec}^{-1}$  and  $E^* = 35.2 \text{ kcal mol}^{-1}$  for the pyrolyses in benzene.

### Reaction Mechanism

Our results from PPN pyrolysis and previous pyrolyses of its single ring analogue (Poutsma and Dyer, 1982; Gilbert and Gajewski, 1982) led us to propose the free-radical reaction mechanism in Figure 2 to describe PPN pyrolysis. The 18 step mechanism comprises initiation, propagation, and termination steps. Initiation entails the unimolecular dissociation of the weak C-C bonds in the reactant, and we included two possible initiation steps for PPN. The first route corresponds to the formation of benzyl and 2-ethylnaphthyl radicals (denoted  $\beta_1$  and  $\beta_1'$  in Figure 2), and the second route leads to ethylbenzyl and 2-methylnaphthyl radicals (denoted  $\beta_2$  and  $\beta_2'$  in Figure 2). Propagation occurs through abstraction of  $\alpha$  hydrogens in PPN by  $\beta$  radicals and subsequent  $\beta$ -scission of the resulting radical,  $\mu$ , to form a stable product Q and regenerate a  $\beta$  radical. Termination of the chain reaction can occur through all possible radical recombination steps.

### Kinetics Development

The steady state and long chain approximations can be used to derive an analytical rate expression for the mechanism of Figure 2. The rate of reaction for PPN (denoted as R in Figure 2) is given by Equation 1.

$$-r_R = (k_{11} + k_{12})\beta_1 R + (k_{21} + k_{22})\beta_2 R \quad (1)$$

Expressions for  $\beta_1$  and  $\beta_2$  as functions of the rate constants and the reactant concentration can be obtained by writing the long chain rate expressions for  $\beta_1$ ,  $\beta_2$ ,  $\mu_1$ , and the total radical population ( $R\cdot$ ). Equations 2-5 display these expressions.

$$r_{\beta_1} = k_{\mu_1} \mu_1 \cdot (k_{11} + k_{12})\beta_1 R = 0 \quad (2)$$

$$r_{\beta_2} = k_{\mu_2} \mu_2 \cdot (k_{21} + k_{22}) \beta_2 R = 0 \quad (3)$$

$$r_{\mu_1} = k_{11} \beta_1 R + k_{21} \beta_2 R - k_{\mu_1} \mu_1 = 0 \quad (4)$$

$$r_{R_0} = 2(\alpha_1 + \alpha_2) R \cdot 2\omega_T (\mu_1 + \mu_2 + \beta_1 + \beta_2)^2 = 0 \quad (5)$$

Simultaneous solution of Equations 2-5 provides the required expressions for  $\beta_1$  and  $\beta_2$ . These can then be substituted into Equation 1 to derive Equation 6 as the rate law for PPN disappearance.

$$-r_R = \frac{\sqrt{\frac{\alpha_1 + \alpha_2}{\omega_i}} \left[ \left( \frac{k_{12}}{k_{21}} \right) (k_{21} + k_{22}) + (k_{11} + k_{12}) \right] R^{3/2}}{\left[ \frac{(k_{11} + k_{12})}{k_{\mu_1}} + \left( \frac{k_{12}}{k_{21}} \right) \frac{(k_{21} + k_{22})}{k_{\mu_2}} \right] R + \left[ 1 + \left( \frac{k_{12}}{k_{21}} \right) \right]} \quad (6)$$

Defining the parameters  $\zeta$  and  $\xi$  as

$$\zeta = \frac{\left[ \frac{(k_{11} + k_{12})}{k_{\mu_1}} + \left( \frac{k_{12}}{k_{21}} \right) \frac{(k_{21} + k_{22})}{k_{\mu_2}} \right]}{\sqrt{\frac{\alpha_1 + \alpha_2}{\omega_i}} \left[ \left( \frac{k_{12}}{k_{21}} \right) (k_{21} + k_{22}) + (k_{11} + k_{12}) \right]} \quad (7)$$

$$\xi = \frac{\left[ 1 + \left( \frac{k_{12}}{k_{21}} \right) \right]}{\sqrt{\frac{\alpha_1 + \alpha_2}{\omega_i}} \left[ \left( \frac{k_{12}}{k_{21}} \right) (k_{21} + k_{22}) + (k_{11} + k_{12}) \right]} \quad (8)$$

permits the rate law (Equation 6) to be written in more compact form.

$$-r_R = \frac{R^{3/2}}{\zeta R + \xi} \quad (9)$$

Substituting this rate law into the constant volume batch reactor design equation, writing the reactant concentration as a function of conversion (i.e.,  $R = R_0(1-X)$ ), integrating, and rearranging, results in a simple expression for the batch holding time ( $t$ ) as a function of conversion ( $X$ ) and the initial PPN concentration ( $R_0$ ).

$$t = \frac{2\xi}{\sqrt{R_0}} \left[ \frac{1}{\sqrt{1-X}} - 1 \right] - 2\zeta \sqrt{R_0} \left[ \sqrt{1-X} - 1 \right] \quad (10)$$

The mechanism of Figure 2 also permits derivation of an analytical expression for the product selectivity. The instantaneous selectivity ( $S$ ) of PPN to toluene relative to 2-methynaphthalene is given as the ratio of the reaction rates.

$$S = \frac{r_{\text{TOL}}}{r_{2\text{-MN}}} = \frac{(k_{11} + k_{12}) \beta_1}{(k_{21} + k_{22}) \beta_2} \quad (11)$$

Substituting the relationship between  $\beta_1$  and  $\beta_2$  that results from the solution of Equations 2-5 into Equation 11 leads to Equation 12 for the instantaneous selectivity.

$$S = \frac{r_{\text{TOL}}}{r_{2\text{-MN}}} = \frac{\left(1 + \left(\frac{k_{11}}{k_{12}}\right)\right)}{\left(1 + \left(\frac{k_{22}}{k_{21}}\right)\right)} \quad (12)$$

#### Rate Constant Estimation

Employing Equations 10 and 12 to model the kinetics and selectivity of PPN pyrolysis requires values for each of the rate constants in the reaction mechanism shown in Figure 2. In the following paragraphs we describe our rate constant estimation procedures. Note that the values we used for the rate constants were semi-quantitative. More accurate estimates could be made using thermochemical kinetics.

Rate constants for initiation via homolytic dissociation of C-C bonds typically have pre-exponential factors in the range of  $10^{16 \pm 1} \text{ s}^{-1}$  (Benson, 1976). Thus, we selected a value of  $A = 10^{16} \text{ s}^{-1}$  for both of the initiation rate constants  $\alpha_1$  and  $\alpha_2$ . We used  $69 \text{ kcal mol}^{-1}$  as the activation energy for  $\alpha_1$  (which produces a benzyl and 2-ethylnaphthyl radical). This value is in good accord with the calculated bond dissociation energy (BDE) of  $68.81 \text{ kcal mol}^{-1}$  for the identical bond in 1,3 diphenylpropane (King and Stock, 1984). The rate of initiation via step  $\alpha_2$  will be faster than via step  $\alpha_1$  because the additional resonance stabilization energy associated with the naphthyl moiety reduces the BDE of the benzylic C-C bond. Thus, the activation energy for this step was taken to be  $E^* = 69 - \Delta\text{RSE}$ , where  $\Delta\text{RSE}$  is the difference in the resonance stabilization energies between a 2-methylnaphthyl radical and a benzyl radical. We used Sato's calculated value of  $0.41 \text{ kcal mol}^{-1}$  for the  $\Delta\text{RSE}$ .

Hydrogen abstraction rate constants were estimated by first assuming that the pre-exponential factors for  $k_{11}$ ,  $k_{12}$ ,  $k_{21}$ , and  $k_{22}$  were all equal to  $A = 10^8 \text{ l mol}^{-1} \text{ s}^{-1}$  and that the activation energy for  $k_{12}$  was  $14.2 \text{ kcal mol}^{-1}$ . These Arrhenius parameters for  $k_{12}$  are identical to those estimated by Poutsma and Dyer (1982) for abstraction of a secondary benzylic hydrogen by a primary benzyl radical. The activation energy for  $k_{21}$  was also taken as  $14.2 \text{ kcal mol}^{-1}$  because the reduction in rate for this step relative to  $k_{12}$  due to the increased stability of the abstracting radical (i.e., 2-methylnaphthyl vs. benzyl) should be roughly offset by the increase in rate due to the lower C-H bond strength of the  $\beta$ -position being attacked. Finally the activation energies for  $k_{11}$  and  $k_{22}$  were estimated from the activation energies for  $k_{21}$  and  $k_{12}$  by assuming that half of the  $\Delta\text{RSE}$  associated with the two different hydrogens being abstracted radicals would appear as the activation energy difference. This is essentially the same as employing the Evans-Polanyi relation with  $\alpha=0.5$ , a value commonly used (Stein, 1985; Poutsma and Dyer, 1982) for hydrogen abstraction reactions.

Poutsma and Dyer (1982) estimated the Arrhenius parameters for  $\beta$ -scission of an  $\alpha$ -radical in 1,3-diphenylpropane to be  $A = 10^{14.8} \text{ s}^{-1}$  and  $E^* = 28.3 \text{ kcal mol}^{-1}$ . For PPN pyrolysis, we expect  $k_{\mu 1}$  to be lower than the  $\beta$ -scission rate constant for 1,3-diphenylpropane pyrolysis because the  $\mu_1$  radical should be more stable than the corresponding 1,3-diphenylpropane-derived radical. On the other hand, we expect  $k_{\mu 2}$  to be higher because the additional RSE due to the presence of the naphthyl moiety in PPN results in the  $\beta$ -scission of a weaker C-C bond. We quantified the foregoing qualitative arguments by taking  $10^{14.8} \text{ s}^{-1}$  as the pre-exponential factor for the  $\beta$ -scission steps and using  $28.2 \text{ kcal mol}^{-1}$  as the activation energy for  $k_{\mu 1}$  and  $28.4 \text{ kcal mol}^{-1}$  as  $E^*$  for  $k_{\mu 2}$ .

Termination rate constants for radical recombination generally have zero activation energy and pre-exponential factors of  $A = 10^{9.0 \pm 1} \text{ l mol}^{-1} \text{ s}^{-1}$  (Benson, 1976). For our termination rate constant,  $\omega_T$ , we used  $A = 10^{8.5}$  and  $E^* = 0.0 \text{ kcal mol}^{-1}$ .

### Modeling Results

We used the semi-quantitative rate constant estimates described above as parameters in Equations 10 and 12 to calculate the kinetics and selectivity for PPN pyrolysis under the conditions at which we had performed experiments. Figure 3 compares the calculated and experimentally determined temporal variation of the PPN molar yield for the pyrolyses in benzene. Clearly, the kinetics predicted from the reaction model are in good agreement with the experimental data. Figure 4 provides the calculated and experimentally determined instantaneous selectivity of PPN to toluene relative to 2-methylnaphthalene. The data points were calculated as the mean values for all batch holding times at a given temperature. Once again, we find satisfactory agreement between the results of the reaction model and the experiments.

## BPP PYROLYSIS

### Experimental Results

Table 2 provides the molar yields of the major products from the pyrolysis of BPP neat at 365°C and in benzene at 400°C. The major products from pyrolysis in benzene at short batch holding times (e.g., 10 min), were 1-methylpyrene and 1-vinylpyrene. At long times, however, the yield of 1-vinylpyrene decreased while the yield of 1-ethylpyrene increased. Additionally, pyrene became a major product at the longer holding times. Figure 5, which presents the temporal variations of the product yields for BPP pyrolyses in benzene, displays these trends more clearly.

The neat pyrolysis of BPP led to 1-methylpyrene, 1-ethylpyrene, and pyrene as principal products. No vinylpyrene was detected, but trace amounts of 1-propylpyrene and 1-allylpyrene were observed along with visible amounts of benzene-insoluble char. At a batch holding time of 90 minutes the respective molar yields for 1-methylpyrene, 1-ethylpyrene, and pyrene were 62%, 40% and 23% respectively.

### Reaction Pathway

The initial products formed from BPP pyrolysis were 1-methylpyrene and 1-vinylpyrene. These are analogous to toluene and styrene, the primary products of 1,3-diphenylpropane pyrolysis. The coincidence of initial products indicates that the pathway for BPP pyrolysis at short times is identical to the pyrolysis pathway for its single ring analogue, 1,3-diphenylpropane. At longer times and higher concentrations, however, the pyrolysis of BPP led to the formation of appreciable yields ( $\geq 30\%$ ) of pyrene. Similarly high yields of benzene have never been observed from 1,3-diphenylpropane pyrolysis. The pathways responsible for pyrene formation can be inferred from the temporal variations of the product yields illustrated in Figure 5. The molar yields of methylpyrene and ethylpyrene both decreased at the longer holding times where the molar yield of pyrene increased. Thus, it appears that ethylpyrene and methylpyrene underwent secondary reactions that resulted in the loss of their alkyl substituents at the aromatic ring. Such a pathway is entirely consistent with our recent studies of 1-dodecylpyrene pyrolysis (Savage et al., 1989; Smith and Savage 1989) where aryl-alkyl C-C bond cleavage was an important reaction pathway. The amount of pyrene formed, however, may be too high to be the sole result of secondary decomposition reactions of methyl- and ethylpyrene. This suggests that BPP itself may have undergone primary reaction to form pyrene. The precise mechanism for these pathways involving cleavage of strong aryl-alkyl C-C bonds is currently unknown, although the literature does provide some possibilities (e.g., Vernon, 1980; McMillen et al., 1987). Indeed, our earlier work with 1-dodecylpyrene pyrolysis (Smith and Savage, 1989) suggests that radical hydrogen transfer may be responsible for the cleavage of the strong aryl-alkyl C-C bonds during alkyl-pyrene pyrolysis. Figure 6 summarizes the foregoing discussion by displaying the postulated pyrolysis pathways for BPP. Note that the presence of pathways involving aryl-alkyl bond cleavage is a completely new feature of  $\alpha,\omega$ -diarylpropane pyrolysis.

## CONCLUSIONS

1. The pyrolysis pathways for  $\alpha,\omega$ -diarylalkanes and hence the corresponding moieties in coal have not been completely elucidated. BPP, a polycyclic diarylalkanes, followed a pyrolysis pathway where strong aryl-alkyl C-C bonds were cleaved. This appearance of this new pathway clearly

indicates that the complete pyrolytic behavior of  $\alpha,\omega$ -diarylpropanes can not always be inferred from 1,3-diphenylpropane.

- For the pyrolysis of PPN, aryl-alkyl cleavage was not a major pathway. The pathways and mechanisms for PPN pyrolysis can be inferred from knowledge of 1,3 diphenylpropane pyrolysis. Furthermore, the reaction kinetics and product selectivities can be accurately calculated for by the accounting for the relevant resonance stabilization energy differences.

#### NOTATION

A	pre-exponential factor, (l/s, l/mol-s)
E <sup>‡</sup>	activation energy, (kcal/mol)
k <sub>βi</sub>	β-scission rate constant, (l/s)
k <sub>ij</sub>	hydrogen abstraction rate constant, (l/mol-s)
Q	reaction product in Figure 2
r	reaction rate, (mol/l-s)
R	reactant in Figure 2 or reactant concentration, (mol/l)
R <sub>0</sub>	initial reactant concentration, (mol/l)
t	batch holding time, (s)
X	reactant conversion
α <sub>i</sub>	initiation rate constant, (l/s)
β <sub>i</sub>	radical reacting in bimolecular propagation step
β <sub>iH</sub>	stable product in Figure 2, (mol/l)
μ <sub>i</sub>	radical reacting in unimolecular propagation step
ζ <sub>i</sub> , ξ <sub>i</sub>	parameters in equation 10
ω <sub>T</sub>	termination rate constant, (l/mol-s)

#### LITERATURE CITED

- Benson, S. W. *Thermochemical Kinetics* John Wiley and Sons, New York, 1976.
- Depp, E. A., Stevens, C. M., Neuworth, M. B. Pyrolysis of Bituminous Coal Models *Fuel*, 1956, 35, 437.
- Gilbert, K.E., Gajewski, J. J. Coal Liquefaction Model Studies: Free Radical Chain Decomposition of Diphenylpropane, Dibenzyl Ether, and Phenyl Ether via β-Scission Reactions. *J. Org. Chem.*, 1982, 47, 4899.
- Javanmardian, M., Smith, P.J., Savage, P. E. Pyrolysis of Compounds Containing Polycyclic Aromatic Moieties. *Prepr.-Am. Chem. Soc., Div. Fuel. Chem.* 1988,33,242.
- King, H., Stock, L.M. Aspects of the Chemistry of Donor Solvent Coal Dissolution *Fuel*, 1984, 63, 810.
- McMillen, D. F., Malhorta, R., Chang, S.J., Olgier, W.C., Nigenda, E, Fleming, R. H. Mechanisms of Hydrogen Transfer and Bond Scission of Strongly Bonded Coal Structures in Donor-Solvent Systems. *Fuel*, 1987, 66, 1611.
- Miller, R. E., Stein, S. E. Liquid-Phase Pyrolysis of 1,2 Diphenylethane, *J. Phys. Chem.*, 1982, 580.
- Noggle, J. H. *Physical Chemistry* Little, Brown, and Company, Boston 1985.

- Poutsma, M. L., Dyer, C. W. Thermolysis of Model Compounds for Coal. 3. Radical Chain Decomposition of 1,3-Diphenylpropane and 1,4-Diphenylbutane, *J. Org. Chem.*, 1982, 47, 4903.
- Sato, Y. Dissociation Energies of C-C Bonds in Bibenzyl and 1,2-di-1-Naphthylethane *Fuel*, 1979, 58, 318
- Savage, P.E., Jacobs, G.E., Javanmardian, M. Autocatalysis and Aryl-Alkyl Bond Cleavage in 1-Dodecylpyrene Pyrolysis *Ind. Eng. Chem. Res.*, 1989, 28, 645.
- Smith, C. M., Savage, P. E. Pyrolysis of Alkyl-Substituted Polycyclic Aromatic Compounds Paper 93d Presented at AIChE Annual Meeting, San Francisco, CA November, 1989.
- Stein, S. E. Free Radicals in Coal Conversion in Chemistry of Coal Conversion, Edited by Richard Scholsberg, 1985, 13.
- Sweeting, J. W., Wilshire, J. F. K. The pyrolysis of  $\omega\omega'$ -Diphenylalkanes *Aust. J. Chem.*, 1962, 15, 89.
- Vernon, L. W. Free Radical Chemistry of Coal Liquefaction: Role of Molecular Hydrogen *Fuel*, 1980, 59, 102.

#### ACKNOWLEDGEMENTS

This work was supported, in part, by the Shell Faculty Career Initiation Fund, an Energy Research Grant from the University of Michigan Office of the Vice President for Research, and the National Science Foundation (Grant No. CTS-8906859)

**Table 1: Summary of PPN Pyrolysis Data**  
**Molar Yields (%) of Products at Different Reaction Conditions**

Time	Temp. °C	Conditions	TOL	STY	EB	MN	EN	VN	PPN
40	365	Neat	17.4	4.9	1.5	14.4	2.3	2.2	53.2
40	365	Neat	18.0	4.6	1.6	15.0	2.5	2.2	52.8
46	365	Neat	19.0	4.4	2.1	16.9	3.3	2.0	46.4
76	365	Neat	30.1	3.2	4.9	24.9	6.8	1.5	26.7
99	365	Neat	39.0	0.8	3.1	29.8	10.1	1.1	19.2
158	365	Neat	49.0	1.0	16.3	35.9	17.5	0.5	8.0
11	400	Neat	17.1	8.9	1.4	16.5	2.7	4.5	49.9
17	400	Neat	29.3	9.4	4.7	28.0	7.7	3.3	22.9
31	400	Neat	49.1	3.2	13.2	37.3	15.2	1.2	6.6
47	400	Neat	52.5	1.3	18.1	40.3	18.7	0.0	5.9
105	400	Neat	61.0	0.0	23.3	41.9	19.7	0.0	0.0
151	400	Neat	61.5	0.0	24.3	41.9	19.7	0.0	0.0
10	375	0.12 M Benzene	0.7	0.7	0.0	0.6	0.0	1.0	98.7
30	375	0.12 M Benzene	1.8	1.5	0.0	1.5	0.0	2.2	97.5
60	375	0.12 M Benzene	3.4	2.6	0.0	2.9	0.3	3.8	93.9
95	375	0.12 M Benzene	6.5	4.9	0.4	5.6	1.1	6.8	84.5
150	375	0.12 M Benzene	10.0	7.3	0.7	9.2	1.7	9.4	76.1
240	375	0.12 M Benzene	24.5	11.9	3.6	23.3	7.1	11.7	42.3
20	400	0.12 M Benzene	4.4	3.4	0.0	3.6	0.4	4.8	88.3
30	400	0.12 M Benzene	11.9	8.1	1.3	10.0	2.7	9.6	71.1
45	400	0.12 M Benzene	13.0	9.1	1.1	11.2	2.0	11.3	68.5
60	400	0.12 M Benzene	17.5	11.8	1.6	15.2	2.9	14.2	58.4
60	400	0.12 M Benzene	24.6	11.8	4.9	21.1	8.7	11.7	41.3
90	400	0.12 M Benzene	22.2	13.1	2.6	19.8	4.8	14.4	47.7
150	400	0.12 M Benzene	35.6	9.3	8.4	32.5	12.6	8.2	17.1
153	400	0.12 M Benzene	32.8	9.9	7.4	29.7	11.3	9.1	23.3
10	450	0.12 M Benzene	9.1	6.9	0.7	7.9	1.2	9.7	77.0
15	450	0.12 M Benzene	20.8	12.6	2.6	19.2	4.1	16.5	46.6
30	450	0.12 M Benzene	32.6	9.5	8.7	30.3	12.5	9.9	12.9
45	450	0.12 M Benzene	34.7	9.3	10.6	31.4	16.0	8.9	6.7
60	450	0.12 M Benzene	34.9	0.7	15.8	31.1	18.8	0.6	1.2
90	450	0.12 M Benzene	35.2	0.6	15.0	31.1	18.5	0.5	0.7

**Table 2: Summary of BPP Pyrolysis Data**  
**Molar Yields (%) of Products at Different Reaction Conditions**

Time	Temp. °C	Conditions	Pyrene	Methylpyrene	Ethylpyrene	Vinylpyrene
10	365	Neat	5.5	34.1	23.9	
20	365	Neat	9.1	43.5	31.1	
40	365	Neat	16.7	58.1	40.9	
50	365	Neat	17.2	63.4	45.4	
90	365	Neat	23.0	61.7	39.6	
155	365	Neat	25.9	52.3	29.9	
10	400	0.005 in Benzene	0.8	3.7	2.3	5.9
20	400	0.005 in Benzene	1.4	10.4	8.2	7.0
30	400	0.005 in Benzene	2.0	15.7	12.0	7.1
45	400	0.005 in Benzene	1.6	15.9	11.4	7.1
60	400	0.005 in Benzene	4.0	35.5	31.0	7.6
120	400	0.005 in Benzene	7.7	51.2	48.5	3.5
180	400	0.005 in Benzene	11.6	56.2	54.3	1.2
240	400	0.005 in Benzene	16.0	62.9	58.3	0.0
411	400	0.005 in Benzene	23.9	60.8	53.4	0.0
816	400	0.005 in Benzene	36.0	42.1	34.2	0.0

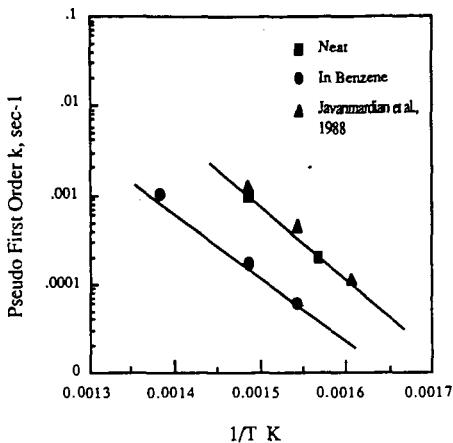


Figure 1: Arrhenius Plot for PPN Pyrolysis

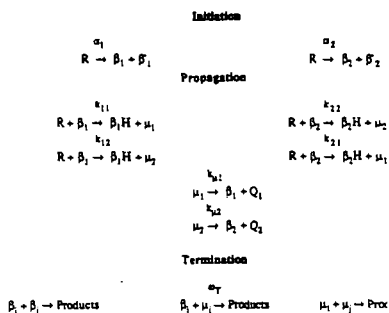


Figure 2: PPN Reaction Mechanism

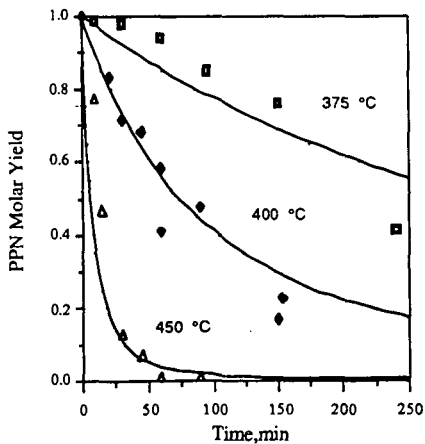


Figure 3: Modeling and Experimental Results for PPN Pyrolysis in Benzene 0.12M

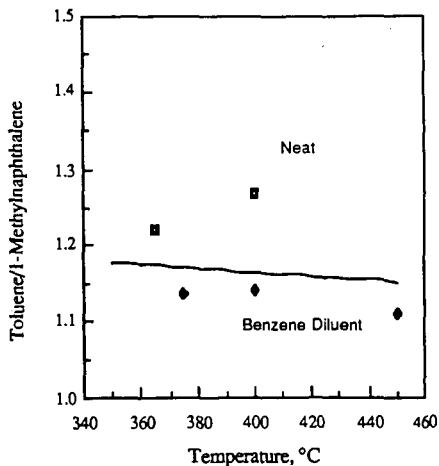


Figure 4: Model Predictions for PPN Pyrolysis Selectivity

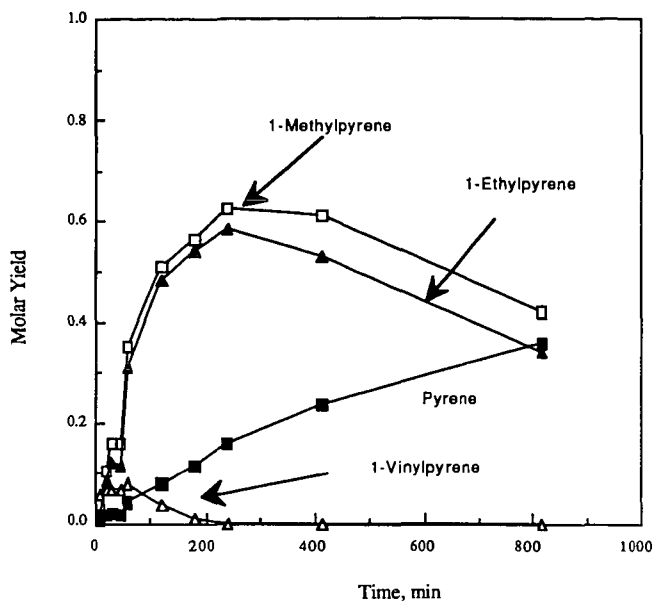


Figure 5: Molar Yields of Major Products for BPP Pyrolysis in Benzene (0.005 M, 400°C)

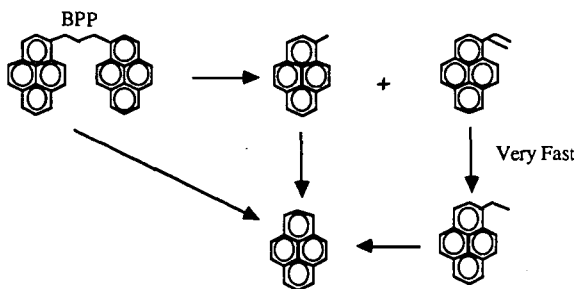


Figure 6: BPP Pyrolysis Pathway

MODELING COAL LIQUEFACTION: DECOMPOSITION OF  
4-(1-NAPHTHYLMETHYL)BIBENZYL CATALYZED BY CARBON BLACK\*

Malvina Farcasiu and Charlene Smith\*\*  
Pittsburgh Energy Technology Center  
U.S. Department of Energy  
P.O. Box 10940  
Pittsburgh, PA 15236

\*Reference in the paper to any specific commercial product, process, or service is to facilitate understanding and does not necessarily imply its endorsement or favoring by the United States Department of Energy.

\*\*Oak Ridge Associated Universities Appointee, Postgraduate Research Training Program.

Keywords: coal liquefaction, modeling, carbon black

ABSTRACT

The early stages of coal liquefaction involve cleavage of methylene and ethylene bridges connecting aromatic rings. We modeled this process by the reaction of 4-(1-naphthylmethyl)bibenzyl (I) in the presence of a hydrogen donor (9,10-dihydrophenanthrene). The reactions were conducted over a range of temperatures (320-430°C) and reaction times (30-90 min). We found that the bond between the methylene group and the naphthalene ring and the methylene to methylene bond of the bibenzyl moiety are broken with equal probability. Addition of carbon black (BP 2000) as catalyst (2-10%) increases significantly the conversion of I. For instance, at 419°C and 1h, 18% of I is converted without catalyst and 42% is converted in the presence of 2% of BP 2000. The increase in conversion is due to additional breaking of the bond between the naphthyl and the methylene groups. This particular carbon black is, therefore, a very active and selective catalyst for the cleavage of the naphthyl-to-methylene bond.

INTRODUCTION

Cleavage of covalent bonds is the essential reaction occurring during coal liquefaction. Thermal cleavage requires temperatures so high, that other, mostly undesirable reactions take place resulting in little if any selectivity in the cleavage process. However, specific bonds can be cleaved catalytically, at temperatures where thermal reactions are not important.

Because of the complexity of coal structure, it is not possible to investigate and optimize conditions for cleaving specific bonds, or to sort out desired processes from side-reactions. In order to obtain meaningful data relevant to coal liquefaction and to be able to develop proper catalysts for the process, the study of model compounds containing the critical structural elements of coal in simpler structures is necessary. The study of appropriate model compounds allows determinations of kinetic parameters (rates, activation energies, selectivities) that can be applicable to the cleavage of specific bonds in coal.

To be relevant to coal liquefaction under heterogeneous catalysis, a study of model compounds should satisfy a number of requirements concerning the structure of the model compound, and the type of data to be gathered. Some of these criteria are:

1. The model compound should be liquid or solid under the reaction conditions to mimic the conditions prevalent during coal liquefaction.

This usually means that the model compound should have a molecular weight of at least 300. A macromolecular structure could be desirable in some cases.

2. The model compound should contain several types of potentially reactive chemical bonds under the reaction conditions. The presence of different reactive structures in the same molecule permits the study of competitive kinetics in the presence of intramolecular interactions. Many of the reactions taking place during coal liquefaction are influenced by other chemical structures present in the same molecule. Because competitive reactions certainly occur in coal processing, study of model compounds with only one type of bond that cleaves affords only limited information.
3. The products of reactions should be unambiguously identified and their rate of formation determined. Determination of rates (both absolute and relative) and of activation energies of different reactions is essential for the study of the mechanisms of reactions. Relative reaction rates and activation energies for cleavage of specific bonds is necessary information that cannot be obtained directly from the study of very complex systems such as coal. In the latter case only an overall conversion of a complex starting material to a complex product mixture can be determined. An attempt at calculating an activation energy for such a transformation gives a number with no physico-chemical meaning. In these cases the use of appropriate model compounds is highly desirable.

In the current study, we examined the cleavage of methylene and ethylene bonds linking aromatic fragments. These particular reactions are considered important for the chemistry of coal liquefaction (1). The model compound investigated, 4-(1-naphthylmethyl)biphenyl (I), contains a methylene and ethylene linkage in the same molecule. Thermal as well as catalytic cleavage of the bonds were studied. A novel catalyst was employed (carbon black, Cabot Corporation Black Pearls 2000) for the catalytic reactions. This material has been used as support for metal-based catalysts (2), but has never been reported to be a catalyst itself.

#### EXPERIMENTAL SECTION

Materials and Analytical Procedures. 9,10-Dihydrophenanthrene was obtained from Aldrich Chemical Co., Black Pearls 2000 carbon black was obtained from Cabot Corporation. Elemental analysis of the carbon black, performed by Huffmann Laboratories, Golden, CO, gave % C, 95.4; O, 1.4; S, 1.8; Ash, 1.3. Surface area (BET) quoted by Cabot is 1475 m<sup>2</sup>/g. 4-(1-naphthylmethyl)biphenyl (I) was prepared in the laboratory of Prof. Paul Dowd at the University of Pittsburgh. The compound was completely characterized by IR, UV, <sup>1</sup>H NMR, <sup>13</sup>C NMR, elemental analysis and high and low resolution mass spectroscopy. The purity of the product was better than 99%. The above substances were used as received. Dichloromethane was stored over 4 Å molecular sieves.

Glass reaction tubes were made from Pyrex tubing, 5 x 7 mm (i.d. x o.d.). Sealed sample tubes were approximately 75 mm in length.

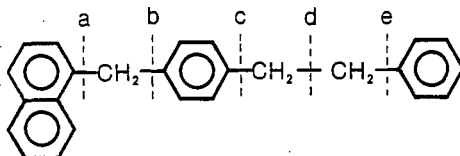
Gas chromatographic analyses were carried out on a Hewlett Packard Model 5730A gas chromatograph equipped with an SE-30 60 m column. Gas chromatography/mass spectra (GC/MS) were obtained on a Hewlett Packard GC/MS Model 5985 instrument operated using 70 eV electron impact voltage and equipped with a 30 m SE-52 column.

Identification of reaction products was accomplished by GC/MS analysis and, when possible, by GC comparison with authentic chemical samples. Reported products yields and overall conversion of I are based on GC measurements. The most volatile material, toluene, could not be determined accurately, but the quantity was always found to be close to that of naphthyl tolyl methane. The amount of toluene reported was set to equal the amount of naphthyl tolyl methane found.

**General Experimental Procedure.** The reaction components (9,10-dihydro-phenanthrene, ca. 100 mg; I, ca. 25 mg and carbon black, 0, 2, 5, 10 wt % based on I) were weighed into an open-ended glass reaction tube. The tubes were flame sealed, taking no precautions to exclude air. Warm water was used to melt the hydrogen donor and effect mixing of the reactants. The samples were placed upright in a temperature equilibrated Lundberg muffle furnace and heated at the indicated temperatures for the given times. The samples were then removed from the oven, cooled to room temperature and diluted with ca. 0.5 mL of dichloromethane. The samples were filtered through a plug of MgSO<sub>4</sub> and glass wool. An additional 0.5 mL of dichloromethane was used to wash the filter and, in catalytic reactions, the carbon black catalyst. An aliquot of the resulting solution was analyzed by gas chromatography.

#### RESULTS AND DISCUSSION

To facilitate the discussion of the results we identify in the structural formula of 4-(1-naphthylmethyl)biphenyl (I) different bonds that can be potentially cleaved, by the letters a through e, and identify in Table 1 the compounds that are formed after cleavage.



The conversion of I was studied under a variety of reaction conditions. The majority of the reactions were performed in the presence of 9,10-dihydro-phenanthrene (9,10-DHP) as hydrogen donor. Several experiments however, were performed in the absence of the hydrogen donor.

The overall conversion of I to products is given in Tables 2 and 3 for the reactions performed in the presence of 9,10-DHP under thermal and catalytic conditions at various temperatures and reaction times. As shown in Table 2, the thermal reaction is insignificant even at 400°C, (ca 3% conversion), and becomes important only at higher temperatures (18% at 419°C). Under the same reaction conditions, but with the addition of 5% Black Pearls 2000 (BP 2000) catalyst, the conversion at 400°C is ca 34%, and at 419°C it is increased to 63%. Using the data in Table 3 we have found that the cleavage of bond a follows reasonably well, first order reaction kinetics under both thermal and catalytic conditions.

Aside from increasing the overall rate of reaction of I, we found that this carbon black is an extremely selective catalyst for bond cleavage. Table 4 gives the product distribution obtained from I under thermal and catalytic conditions at 419°C. In the absence of the catalyst, bonds a and d are cleaved to almost the same extent, with nearly equimolar quantities of 4-methylbiphenyl (MeBz<sub>2</sub>) and naphthyl tolyl methane (NTM) being produced. Bond b (1-methyl-

naphthalene and bibenzyl products) is cleaved only to a very limited extent. In the presence of the catalyst, however, a remarkable selectivity toward cleavage of bond a is observed as seen in the increased amount of MeBz<sub>2</sub> formed. In fact, cleavage of bond a is practically the only reaction promoted by this catalyst. This activity and selectivity were observed for all temperatures and catalyst concentrations studied.

Reaction rate constants and activation energies for thermal and catalytic reactions are given in Tables 5 and 6. The values for these parameters illustrate the dramatic effect of the added catalyst on the reaction of I in the presence of 9,10-DHP. One of the most important results is the large difference in the activation energies calculated for the thermal and catalytic reactions for the cleavage of bond a; E<sub>a</sub> is -60 kcal/mole for the thermal reaction (Table 5) and 17-25 kcal/mole for the catalytic reactions (Table 6). The variation of the activation energy with the quantity of catalyst (Table 6) is an indication that diffusion may play a role in the catalytic process (3).

When I is allowed to react in the absence of the hydrogen donor, the selectivity of the thermal reaction changes and cleavage of bond d is favored. The catalytic reaction, in the absence of 9,10-DHP, still shows the same remarkable selectivity toward bond a cleavage (Table 7). In the absence of hydrogen donor, however, compounds heavier than I are formed in all experiments, indicating that I is acting as a hydrogen source by dehydrogenation and condensation reactions. Besides these heavier compounds we also observed the formation of some methylidihydrophenanthrene, formed perhaps by cyclization of MeBz<sub>2</sub>.

In order to put into perspective our findings regarding the high activity and exceptional selectivity of the BP 2000 catalyst in reactions with 4-(1-naphthylmethyl)bibenzyl, I, it is worth discussing the following points.

When the reactions of I, both with and without 9,10-DHP, are performed in the presence of a graphite carbon (Alfa) or of Illinois No. 6 coal, there is no increase in conversion of I above the thermal level nor is there any enhanced bond cleavage selectivity. Whether the behavior of BP 2000 is due to its physical structure or some other property is currently under investigation.

The BP 2000 catalyst appears to be specific for the cleavage of bonds between saturated carbons and polycyclic aromatic structures. This is illustrated by the reaction of diphenylmethane with BP 2000, both with and without 9,10-DHP. Even at 420°C, 1h, the methylene linkage in this compound remains intact.

Cleavage of bonds between methyl groups and polycyclic aromatic radicals in the presence of hydrogen donors has been explored extensively by McMillen, et al. (4). They have rationalized this reaction as a "solvent mediated hydrogenolysis", involving a H-transfer by a free radical mechanism. In this mechanism, a dihydroaromatic forms an ArH<sub>2</sub>· free radical in a rate-determining step. The ArH<sub>2</sub>· free radical then transfers a H-atom to the ipso position of the substituted polycyclic compound. The cyclohexadienyl-type free radical thus formed from the latter undergoes the aromatic carbon-methylene carbon bond scission. The above mechanism may be operating alongside other pathways, in the reaction of I in the presence of H-donors. Our findings for the reaction run in the presence of BP 2000, but in the absence of H-donor suggest however, that the radical-transfer sequence cannot be the prevailing mechanism for the cleavage of bond a in I under the catalytic conditions which we investigated.

Our work shows that it is possible to have high selectivity in breaking specific bonds under mild conditions if proper catalysts can be identified. Experiments are in progress toward the goal of understanding the mechanism of action of the BP 2000 catalyst. We are also investigating its use as a catalyst

for cleavage reactions in diquinolyl ethane and dehydroxylation reactions of some phenols.

#### CONCLUSIONS

Our study of the decomposition 4-(1-naphthylmethyl)bibenzyl as a model for reactivity of methylene and ethylene linkages during coal liquefaction showed that, in the presence of a hydrogen donor, the bond connecting 2 benzylic carbons and the bond between naphthyl and methylene units in naphthylphenyl methane, are broken with the same probability in a thermal reaction. We discovered that a high surface area carbon black (Cabot Corp., Black Pearls 2000) is a very active and selective catalyst for the cleavage of the naphthyl-methylene bond.

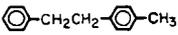
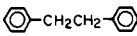
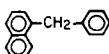
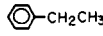
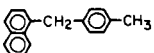
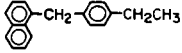
#### ACKNOWLEDGEMENTS

We would like to thank Prof. Paul Dowd and his group at the University of Pittsburgh for the synthesis and characterization of compound I, Louise Douglas for GC/MS work, and Prof. Dan Farcasiu for helpful discussions. This work was supported in part by an appointment to the Postgraduate Research Training Program under Contract No. DE-AC05-76OR00033 between the U.S. Department of Energy and Oak Ridge Associated Universities.

#### REFERENCES

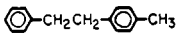
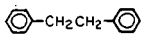
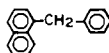
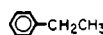
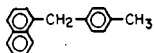
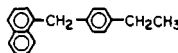
1. Whitehurst, D.D.; Mitchell, T.O.; Farcasiu, M. "Coal Liquefaction The Chemistry and Technology of Thermal Processes" Academic Press: NY, 1980.
2. Kaminsky, M.; Yoon, K.J.; Geoffroy, G.L.; Vannice, M.A. *J. Catal.* 1985, 91, 338. Venter, J.J.; Vannice, M.A. *J. Amer. Chem. Soc.* 1989, 111, 2377.
3. Satterfield, C.N. "Mass Transfer in Heterogeneous Catalysis" MIT Press: Cambridge, MA, 1970.
4. McMillen, D.F.; Malhotra, R.; Chang, S.-J.; Ogier, S.; Nigenda, S.E.; Fleming, R.H. *Fuel*, 1987, 66, 1611. McMillen, D.F.; Malhotra, R.; Hum, G.P.; Chang, S.-J. *Energy & Fuels*, 1987, 1, 193.

**TABLE 1.**  
**IDENTIFICATION OF PRODUCTS RESULTING**  
**FROM BOND CLEAVAGE OF**  
**4-(1-NAPHTHYLMETHYL)BIBENZYL, I.**

<u>Bond Cleaved</u>	<u>Observed Products</u>	<u>Name</u>	<u>Symbol</u>
a		Naphthalene	N
		Tetralin <sup>1</sup>	Te
		4-Methylbibenzyl	MeBz <sub>2</sub>
		3-Methyl-9, 10-dihydrophenanthrene <sup>2</sup>	Me-9,10-DHP <sup>2</sup>
b		1-Methylnaphthalene	MeN
		Bibenzyl	Bz <sub>2</sub>
c		1-(Naphthyl)phenyl methane	NPM
		Ethyl benzene	EtB
d		1-(Naphthyl)-4-tolyl methane	NTM
		Toluene	To
		p-Xylene <sup>3</sup>	pX
e		1-(Naphthyl)-4-(ethyl phenyl) methane	NEPM
		Benzene	B

- 1 From hydrogenation of N
- 2 From cyclization of MeBz<sub>2</sub>
- 3 From further fragmentation of NTM

**TABLE 1.**  
**IDENTIFICATION OF PRODUCTS RESULTING**  
**FROM BOND CLEAVAGE OF**  
**4-(1-NAPHTHYLMETHYL)BIBENZYL, I.**

<u>Bond Cleaved</u>	<u>Observed Products</u>	<u>Name</u>	<u>Symbol</u>
a		Naphthalene Tetralin <sup>1</sup>	N Te
		4-Methylbibenzyl	MeBz <sub>2</sub>
		3-Methyl-9, 10- dihydrophenanthrene <sup>2</sup>	Me-9,10-DHP <sup>2</sup>
b		1-Methylnaphthalene	MeN
		Bibenzyl	Bz <sub>2</sub>
c		1-(Naphthyl)phenyl methane	NPM
		Ethyl benzene	EtB
d		1-(Naphthyl)-4- tolyl methane	NTM
		Toluene	To
		p-Xylene <sup>3</sup>	pX
e		1-(Naphthyl)-4- (ethyl phenyl) methane	NEPM
		Benzene	B

- 1 From hydrogenation of N
- 2 From cyclization of MeBz<sub>2</sub>
- 3 From further fragmentation of NTM

Table 2. Influence of Temperature on Overall Conversion of I to Products at x% Carbon Black BP 2000 Catalyst.<sup>1</sup>

Temperature °C	Conversion at x% Catalyst			
	0	2	5	10
320	0	0.8	---	3.9
360	0	4.6	15	23
375	0	9.1	16.2	27.0
400	3.0	17.6	33.6	43.6
408	7.3	---	49.8	---
419	17.8	42.7	63.0	77.0
429	28.7	53.8	78.9	87.2

<sup>1</sup>Reaction conditions: 1h; wt ratio I:9,10-DPH 1:4; catalyst wt based on I.

Table 3. Influence of Reaction Time on Overall Conversion of I to Products at 421°C and x% Carbon Black BP 2000 Catalyst.<sup>1</sup>

Reaction Time Minutes	Conversion at x% Catalyst		
	0	5	10
30	7.1	39.1	58
60	17.8	63	77
90	24.5	67	86.6

<sup>1</sup>Reaction conditions: 1h; wt ratio I:9,10 DPH 1:4; catalyst wt based on I.

Table 4. Moles of Compounds<sup>1</sup> Formed/100 Moles I Consumed at x% Carbon Black BP 2000 Catalyst.<sup>2</sup>

Compound	Moles Compound Formed at x% Catalyst			
	0	2	5	10
To	52.1	10.1	4.9	2.5
pX	3.8	5.7	6.0	4.7
Te	14.1	21.3	24.8	25.8
N	22.4	64.4	68.4	64.6
MeN	3.6	4.3	4.3	3.9
Bz <sub>2</sub>	4.4	5.1	5.4	5.9
MeBz <sub>2</sub>	40.2	77.8	82.0	88.6
NTM	52.1	10.1	4.9	2.5

<sup>1</sup>Refer to Table 1 for compound identification.

<sup>2</sup>Reaction conditions: 419°C; 1h; wt. ratio I:9,10-DPH 1:4; catalyst wt based on I.

Table 5. Reaction Rate Constants (k) and Activation Energies (E<sub>a</sub>) for Thermal Reactions of Bonds a and d of I.<sup>1</sup>

Temperature °C	k <sub>a</sub> × 10 <sup>-4</sup> (min <sup>-1</sup> )	k <sub>d</sub> × 10 <sup>-4</sup> (min <sup>-1</sup> )
400	~ 2.4	~ 2.7
408	5.2	6.1
419	12.5	16.3
429	18.3	26.7
E <sub>a</sub> bond a (kcal/mol) ~ 60		E <sub>a</sub> bond d (kcal/mol) ~ 70

<sup>1</sup>Reaction conditions: 1h; wt. ratio I:9,10-DPH 1:4.

Table 6. Reaction Rate Constants (k) and Activation Energies (Ea) for Catalytic Reaction of Bond a of I at x% Carbon Black BP 2000 Catalyst.<sup>1</sup>

Temperature °C	k x 10 <sup>-4</sup> (min <sup>-1</sup> ) at x% Catalyst <sup>2</sup>		
	2	5	10
360	7.9	27.1	43.6
400	26.3	60.9	86.8
408	----	92.2	----
419	47.7	100.2	149.4
429	48.2	116.2	146.6
Ea at x% catalyst (kcal/mol)	-25	-19	-17

<sup>1</sup>Reaction conditions: 1h; wt. ratio I:9,10-DPH 1:4; catalyst wt based on I.

<sup>2</sup>Reported for catalytic contribution only. Thermal background has been subtracted.

Table 7. Moles of Compounds<sup>1</sup> Formed/100 MoI I Consumed in the Absence of 9,10-DPH Under Thermal and Catalytic Conditions.<sup>2</sup>

Compound	Moles Compound Formed at x% Catalyst <sup>3</sup>	
	0 (7.5)	5 (25.3)
To	70.6	35.4
pX	0	4.3
N	4.8	52.4
MeN	3.7	7.2
Bz <sub>2</sub>	3.4	5.2
MeBz <sub>2</sub>	19.3	49.6
NPM	17.4	8.5
NTM	70.6	35.4

<sup>1</sup>See Table 1 for compound identification.

<sup>2</sup>Reaction conditions: 408°C; 1h; catalyst wt based on I.

<sup>3</sup>Overall conversion of I at x% catalyst given in parentheses.

## HYDROCRACKING WITH NEW SOLID ACID CATALYSTS: MODEL COMPOUNDS STUDIES.

Ramesh K. Sharma, John W. Diehl, and Edwin S. Olson

Energy and Environmental Research Center  
University of North Dakota  
Grand Forks, ND 58202

Two new solid acid catalysts have been prepared by supporting zinc chloride on silica gel and acid-exchanged montmorillonite. The acid properties of these catalysts were determined by Hammett indicator method which showed that highly Bronsted acidic sites were present. SEM/EDS studies indicated a uniform distribution of silicon, zinc, and chlorine in the silica gel-zinc chloride catalyst. The activities of these catalysts in the hydrocracking of bibenzyl, polybenzyl, alkylbenzenes, and other heteroatom substituted aromatics were investigated. Products from these reactions were analyzed by GC/FTIR/MS/AED and are consistent with an ionic or acid-catalyzed mechanism. High conversions to benzene and other small molecular weight products depend not only on the presence of strong acid sites but also on the ability of the catalyst to promote hydrogenation of complexed cationic intermediates, rather than condensation to oligomeric or polymeric (retrograde) materials. Our results with model compounds account for the effectiveness of these solid acid catalysts for conversion of coals to lower molecular weight materials.

Key words: Depolymerization, solid acid catalyst, hydrocracking

### INTRODUCTION

New concepts are required in designing catalysts for coal liquefaction to produce distillate fuels with a low content of heteroatoms such as sulfur, oxygen, and nitrogen. In a two stage process, heteroatoms are removed by catalytic hydrotreatment of high molecular weight coal liquids produced in a preliminary low-severity process. The preparation and use of strong acid-catalysts and superacids are active areas of research for isomerization, cracking, hydrocracking, alkylation, acylation, methanol to gasoline, etc. (1). Because of the reported advantages of the solid acid catalysts (2), recent research has focused on the preparation and characterization (2-6) of stronger acid catalysts.

Although molten zinc chloride effectively depolymerizes coals (7,8), significant hydrodesulfurization of aryl sulfur compounds is not effected with this reagent (9). Other disadvantages of zinc chloride are its difficulty of recovery and corrosive nature. In a recent paper we reported a solid catalyst prepared by supporting zinc chloride on silica gel to be effective in hydrodesulfurization of diphenyl sulfide and dibenzothiophene(10). In this paper we report the preparation and characterization of solid acid catalyst prepared by supporting zinc chloride on acid-exchanged montmorillonite. The catalytic hydrotreatment of bibenzyl, polybenzyl, cumene, 1-phenyldecane, and n-hexadecane with silica gel and acid-exchanged montmorillonite supported zinc chloride, and acid-exchanged montmorillonite catalysts is being reported here.

### EXPERIMENTAL

#### Reagents

Bibenzyl, cumene, 1-phenyldecane, n-hexadecane and zinc chloride were obtained from

Aldrich. Montmorillonite was obtained from Clay Spur, Wyoming and purified as reported (11).

#### Preparation of Polybenzyl:

Dichloromethane (200 ml) was placed in a three necked round bottomed flask (500 ml) fitted with three septa, one for the nitrogen inlet syringe needle, a second for the nitrogen outlet syringe needle (oil bubbler), and third for injecting the reactants. The flask was flushed with dry nitrogen, and 40 ml of stannic chloride was injected into the flask. Freshly distilled benzyl chloride (40 ml) was added to the flask with occasional stirring. After the addition was over, the reaction mixture was allowed to age at room temperature for four hours. At this stage the reaction mixture was quenched by slowly (dropwise) adding ice-cold methanol. When the reaction subsided, 200 ml more of ice-cold methanol was added. A yellow viscous solid was formed. The cloudy supernatant liquid was poured off, and the precipitate was washed several times with ice-cold methanol, dilute NaOH, deionized water, and methanol. The resulting solid was dissolved in a minimum amount of dichloromethane and freeze dried. The dried polymer was redissolved in a minimum amount of tetrahydrofuran by adding a large volume of methanol. The precipitate was filtered, washed with methanol and dried in vacuo.

#### Preparation of Catalysts:

Preparation of acid-exchanged clay (AM): Sodium-exchanged clay (5.0 g) was suspended in 200 ml of 0.1N HCl and stirred for three hours. The acid washed clay was separated by centrifugation, and washed with deionized water until free of chloride ions. The resulting clay was air dried. Final drying was accomplished by heating the clay at 250°C until constant weight was achieved.

Silica gel and acid-exchanged montmorillonite supported zinc chloride catalysts were prepared as described earlier (10). Total acidity and pKa's of the catalysts were determined by n-butylamine titrations using Hammett indicators (12).

#### Analytical procedures; Instrumentation:

Carbon, hydrogen, and nitrogen analyses were performed on Control Equipment Corporation Model 240XA Elemental Analyzer. The method of Vogel (13) was used for chlorine analysis. Proton and <sup>13</sup>C NMR spectra were obtained in d<sub>2</sub>-dichloromethane with TMS as standard on a Varian XL200 NMR spectrometer. Infrared spectra were recorded in KBr on either a Perkin Elmer Model 283 spectrophotometer or a Nicolet 205XB FTIR spectrometer equipped with a mercury cadmium telluride (MCTA) detector, and a Nicolet 1280 computer with a fast Fourier transform coprocessor.

Weight averaged molecular weight determination was performed in THF by gel phase chromatography (GPC, Waters Associates Liquid Chromatograph Model M6000) on a triple column (microstrogel) system calibrated with polystyrene and aromatic standards in the molecular weight range 34,500 to 202 and with UV detection.

Quantitative GC/FID analyses were performed with a Hewlett Packard 5880A gas chromatograph equipped with J&W 60 m x 0.25 mm (i.d.), 1.0 micron DB-1701 capillary column. n-Octadecane was the internal standard. Isotope dilution GC/MS was performed on a Finnigan 800 ITD ion trap detector with an HP 5890A gas chromatograph and a J&W 30 m x 0.32 mm (i.d.), 1.0 micron film of DB-5. Phenol, naphthalene, and tetralin were determined with the per-deuterated analogs as the respective internal standards. A 15 m x 0.25 mm (i.d.), 0.25 micron DB-5 film capillary column was used for the analysis of high boiling components.

#### Hydrocracking reactions:

In a typical run, 1.0 g of substrate and 0.5 g of the desired catalyst were placed in a tubing bomb (12 ml microreactor). The microreactor was evacuated, pressurized with 1000 psig of hydrogen, and placed in a rocking autoclave heated to 350°C. The heating continued for three hours. At the end of the reaction period, the microreactor was cooled to room temperature, degassed, and opened. The desired amount of internal standard was added to the product slurry, the product slurry was transferred into a centrifugation tube by washing with methylene chloride, and the solid catalyst was removed by centrifugation. The liquid sample was analyzed by gas chromatography/flame ionization detection (quantitative) and gas chromatography/Fourier transform infrared spectroscopy/mass spectrometry/atomic emission spectroscopy (14).

For the reaction of polybenzyl, the microreactor was attached to a series of three pre-weighed traps that were cooled in air, dry ice-acetone, and liquid nitrogen. The microreactor was slowly heated (3°C/min) to 250°C and held at this temperature until distillation stopped. The distillate was weighed, and dissolved in 10 ml methylene chloride. This solution was mixed with appropriate internal standards and analyzed by GC/FID, isotope dilution GC/MS, and GC/FTIR/MS/AED. The undistilled product was extracted with THF and separated into THF-soluble and insoluble fractions. Both these fractions were vacuum dried, weighed, and analyzed by FTIR, elemental analysis, and m.w. determinations.

#### Results and Discussion:

Elemental analysis of zinc chloride supported on silica gel (SZC) and acid-exchanged montmorillonite (AMZC) suggests a high loading of zinc chloride on the support surface. Most of the chlorine is present as zinc chloride (Ca. 98%), and only a small amount of chlorine (<3%) is present as M-O-Zn-Cl. SEM/EDS studies indicated a uniform distribution of silicon, zinc, and chlorine in the silica gel-supported zinc chloride catalyst (10). In this paper we prepared another catalyst by supporting zinc chloride on acid-exchanged montmorillonite. The pKa's and total acidity of silica gel-zinc chloride, acid-exchanged montmorillonite-zinc chloride, and acid-exchanged montmorillonite were determined by n-butyl amine titrations using Hammett indicators, and results are presented in (Tables 1 and 2).

TABLE 1  
ACID STRENGTH ON CATALYST SURFACE

Catalyst	pKa						
	-5.6	-8.2	-11.30	-11.99	-12.70	-13.75	-14.56
SZC	+	+	+	+	-	-	-
AM	+	-	-	-	-	-	-
AMZC-B	+	-	-	-	-	-	-

- + Color of the conjugate acid of a basic indicator appeared on the surface.
- The above color did not change.

TABLE 2  
TOTAL ACIDITY BY AMINE TITRATION

Indicator	pKa	Amount of Acid (mmole/g)		
		SZC	AM	AMZC-B
m-Nitrotoluene	-11.99	0.71		
p-Nitrotoluene	-11.30	0.97		
Benzalacetophenone	-5.6	1.96	1.28	1.55

The total number of moles adsorbed using amine titration was based on the benzalacetophenone as an indicator (all acid sites with strength up to  $pK_a = -5.6$  were determined). Due to the brown color of acid-exchanged montmorillonite-zinc chloride catalyst, the detection of color change was difficult. Therefore, this catalyst was mixed with silica gel-zinc chloride with a known acidity prior to titration with n-butyl amine. These titrations indicate that silica gel-zinc chloride catalyst has the greatest number of acid sites, and acid-exchanged montmorillonite the fewest. Comparison of the total amount of acidity for silica gel-zinc chloride catalyst using benzalacetophenone ( $pK_a = -5.6$ ), p-nitrotoluene ( $pK_a = -11.3$ ), and m-nitrotoluene ( $pK_a = 11.99$ ) indicated a decrease in the total acidity as the  $pK_a$  of the of the indicator changed from -5.6 to -11.3.

The acid strength for the three catalysts, as determined by the amine titration, is provided in Table 1. For the silica gel zinc chloride the acid strength  $H_0$  lies between -5.6 and -12.7 ( $-5.6 < pK_a < -12.7$ ). Acid-exchanged montmorillonite, and acid-exchanged montmorillonite-zinc chloride have acid strength  $H_0 \leq 5.6$ . Comparing the results of the acidity measurements of the three catalysts it appears that silica gel-zinc chloride is most acidic among the catalysts investigated.

#### Catalytic hydrocracking of model compounds:

In order to understand the nature and extent of catalytic activity of supported zinc chloride, reactions of bibenzyl, cumene, 1-phenyldecane, and n-hexadecane were investigated. All reactions were carried out with or without solvent in the presence of 1000 psig molecular hydrogen at 350°C for three hours. The catalyst-to-substrate ratio was 0.5. Percent conversion, which is a measure of the aryl-carbon bond cleavage, was calculated on the basis of the starting material reacted. The results are given in Table 3 as product yields (mmoles) and percentage conversion of the substrate to the products.

TABLE 3  
 CATALYTIC HYDROCRACKING OF MODEL COMPOUNDS  
 (1000 psig H<sub>2</sub> pressure, 350°C, 3 hrs, catalyst wt/substrate wt = 0.5)

Catalyst (g)	Substrate (mmoles)	Solvent (mmoles)	Conv. (%)	Major Product (mmoles)
none	BB (5.49)	none	1	toluene (trace)
SZC (0.50)	BB (5.49)	none	85	benzene (3.35) ethylbenzene (3.26)
*SZC (0.50)	BB (5.49)	none	70	benzene (3.14) ethylbenzene (3.03)
SZC (0.50)	BB (5.49)	p-Cresol (18.52)	37	phenol (2.27)
SZC (0.50)	p-Cresol (9.44)	none	80	phenol (2.04)
AM (0.50)	BB (5.49)	none	75	benzene (4.89)
AMZC (0.50)	BB (5.49)	none	66	benzene (3.96)
SZC (0.50)	Cumene (8.33)	none	99	benzene (1.84)
SZC (0.50)	1-Phenyldecane (4.59)	none	40	benzene (0.65) C <sub>1</sub> -C <sub>6</sub> benzenes
SZC (0.50)	n-Hexadecane (4.42)	none	20	C <sub>3</sub> -C <sub>6</sub> alkanes

• = aged catalyst  
 BB = bibenzyl

A blank reaction of bibenzyl (without catalyst) gave almost complete recovery of the starting material, and only a trace amount of toluene was detected. No benzene or ethylbenzene were observed in the products. However, when bibenzyl was reacted with zinc chloride supported on silica gel, 85.5% of bibenzyl was converted into smaller molecules. The major products from this reaction were benzene, toluene, and ethylbenzene. Small amounts of propylbenzene, butylbenzene, tetralin, benzylethylbenzene, benzylpropylbenzene, etc. were also formed. No chlorine from the catalyst was found to be incorporated into the organic products. The catalyst was recovered in almost quantitative amounts, and the chlorine contents were the same as in the starting catalyst. The amount of coke or polymeric material in the recovered catalyst that could have been formed due to acid-catalyzed retrograde condensation reaction was negligible, and no corrosive melt was formed. In a reaction with aged catalyst, lower conversion (70%) of bibenzyl was observed. Aging, or perhaps

exposure of the catalyst to atmospheric conditions may have changed the nature of the acidity of the catalyst (10).

Although this catalyst gave high conversion in the absence of solvent, a suitable solvent may be necessary for this catalyst to be useful for the coal liquefaction. Reaction of bibenzyl in p-cresol (solvent) was investigated. In contrast to the neat reaction, the conversion was low (37%) in this solvent. In addition, only 39% p-cresol was recovered at the end of the reaction. Bibenzyl gave the same major and minor products as in the reaction without solvent, but in much smaller amounts than expected. Bibenzyl substituted cresol, tetralin, naphthalene, anthracene, naphthol, and mono, and dimethylbibenzyl were some of the products. In order to understand the role of the solvent in the cleavage reactions, p-cresol was reacted with this catalyst and hydrogen under the same reaction conditions as those used for bibenzyl. Reaction of the solvent alone resulted in 80.4% conversion of cresol to other products. Only 27% of the expected phenol was formed. Dimethylphenols and phenoxyphenol were some of the other products of this reaction. The high reactivity of cresol eliminates it from consideration as a solvent. Under strongly acidic conditions, it apparently condenses extensively to high molecular weight products. Solutes also would become involved in these condensations.

In order to further demonstrate that the Bronsted and/or Lewis acidity was responsible for the reductive cleavages of aryl-methylene bonds, reactions of bibenzyl were also carried out with acid-exchanged montmorillonite and acid-exchanged montmorillonite supported zinc chloride. These reactions gave 75 and 66% conversions for acid-exchanged montmorillonite and acid-exchanged montmorillonite supported zinc chloride, respectively. A majority of the product was benzene, and small amounts of toluene, o-xylene, and ethylbenzene were also formed. In addition, almost 40% of the product was polymeric material, mainly polybenzyls. The origin of this polymeric material may have been acid-catalyzed polymerization of the benzyl species formed during initial stages of the reaction. Because of formation of the condensation products from the hydrotreating of bibenzyl with these catalysts, their effectiveness in hydrotreating coal liquids might be questioned. With regard to avoiding extensive condensation reactions, the zinc chloride supported on silica gel is most effective. Nevertheless, the zinc chloride supported on acid-exchanged montmorillonite gave respectable conversions in the hydrotreating of low severity liquefaction products from Wyodak subbituminous coal (15).

Although the conversions were high, the product yields are suggestive of the fact that only one aryl-methylene bond is cleaved under the reaction conditions employed. In order to further understand the mechanism of this reaction, iso-propylbenzene (cumene) was reacted with zinc chloride supported silica gel. This reaction gave almost complete conversion of the iso-propylbenzene, and benzene was the major product. The reaction of 1-phenyldecane with this catalyst gave 40.3% conversion. A large number of products were formed from this reaction. Major products were benzene, toluene, ethylbenzene, propylbenzene, butylbenzene, pentylbenzene and hexylbenzene, indane, etc.

Examination of the products obtained from the reaction of n-hexadecane with zinc chloride supported silica gel indicated 20% cracking to smaller molecules. Major products of this reaction being propane, butane, pentane, and hexane etc. The low conversion suggests that this catalyst may be useful for cleaving bonds attached to aromatic rings in coal macromolecules without unwanted cracking of alkanes to gases. No cracking of alkanes was observed when they were used as solvents for the model compound reactions.

In silica gel supported zinc chloride catalyst, highly acidic Bronsted sites are available due to the silica hydroxyls associated with zinc chloride. Protonation of the ipso position of the ring will give the arenium ion intermediate, which can

undergo aryl-methylene bond cleavage. The presence of benzylethylbenzene, benzylpropylbenzene, etc. in the hydrotreating products is indicative of carbonium ion intermediates in the reaction of bibenzyl. Formation of a "surfacebound" carbonium ion is hypothesized to explain the lack of extensive condensation that might occur if free carbonium ions were formed. Since the reaction rate is much higher with secondary alkyl groups (cumene reaction), it is clear that the reaction proceeds rapidly whenever the cationic leaving group can be stabilized by  $\alpha$ - or  $\beta$ -phenyl groups or alkyl groups, and more slowly or with extensive rearrangement when the leaving group is primary (1-phenyldecane reaction). It is clear that the acid catalyst is effective in cleaving aryl-methylene bonds at relatively lower temperature and without chlorine substitution or extensive condensation of carbonium ion intermediates.

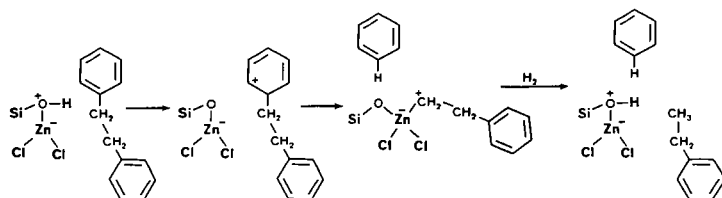


Figure 1. ACID-CATALYZED MECHANISM

Research is in progress to characterize the spent catalyst and to test the catalytic activity of the spent catalysts at higher temperatures.

Catalytic hydrocracking of model polymer:

Model coal polymers with well defined structures, thermally more stable than polystyrene or polybenzyl ethers, are needed for testing of hydrotreating reactions in order to understand the coal liquefaction. The synthesis of a model coal polymer, which meets the criteria of being highly branched, highly soluble, and thermally stable, has been accomplished. It was not clear from the literature that this is a bulky (branched) polymer; however, the thermal stability is good because of the methylene bridges between the benzene rings.

The infrared of the polymer showed a weak absorption in the 800-850  $\text{cm}^{-1}$  range, corresponding to two adjacent hydrogens on an aromatic ring. This indicates that the para substituted benzene components of the polymer structure are relatively minor, probably less than 10%. Because of the intense absorption at 740 to 760  $\text{cm}^{-1}$ , corresponding to monosubstituted benzenes, the structure must be highly branched containing many (90%) benzyl groups attached to the backbone system. A weak absorption at 900  $\text{cm}^{-1}$ , corresponding to single hydrogens on an aromatic ring, was also present in the spectrum. This absorption is usually weak, thus there are still some unsubstituted aromatic positions in the backbone system. The highly branched structure explains the high solubility of the polymer in organic solvents. NMR evidence shows that there are anthracene groups, but no chloromethyl groups.

The anthracene is undoubtedly formed by oxidation of dihydroanthracene by the stannic chloride. Although the formation of dihydroanthracene terminates the chain in terms of obliterating the electrophilic chloroethyl groups, the reaction of additional benzyl groups on the polymer can occur at any point. Thus, the

anthracene may not necessarily be on the end of the chain. Calculation of a molecular weight, based on the 1 to 23 ratio of anthracene to benzyl, gives a value of 2250 per anthracene unit. The weight average molecular weight was found from the GPC data to be 1300 daltons. The presence of anthracene units in the polymer will, however, delay the elution of the polymer substantially and cause a severe error in the GPC determination, which is based on the calibration with polystyrene.

The hydrotreating of polybenzyl (C, 92.96; H, 6.98; H/C ratio, 0.9) with zinc chloride supported on silica gel and 1000 psig hydrogen at 350°C for 3 hours gave 61% distillate. The distillate was found to consist of 95% benzene, toluene, oxylene in approximately equimolar amounts. Small amounts of cyclohexane methylcyclohexane, C<sub>3</sub> and C<sub>4</sub> benzenes, naphthalene, indane, tetralin, methylnaphthalenes, and anthracenes were also present in the distillate.

Mass balance and infrared analysis of the THF-soluble fraction indicated a small amount of polymeric material (6.9%) present. THF-solubles (Vacuum bottoms, C, 89.5; H, 6.21; H/C ratio, 0.83) were 32.9% of the starting polymer. Detailed characterization of the THF-soluble fraction is in progress.

This experiment demonstrates that the silica gel-zinc chloride catalyst is effective in depolymerization of highly branched alkylbenzene polymers without extensive condensation to insoluble chars.

#### ACKNOWLEDGEMENT

This research was supported by Contract No. DOE-FC2186-MC10637 from the U.S. Department of Energy. References herein to any specific commercial product by trade name or manufacturer does not necessarily constitute or imply its endorsement, recommendation, or favoring by the United States Government or any agency thereof. The assistance of Jonathan Kautz is greatly appreciated.

#### REFERENCES

1. K. Tanabe, In *Heterogeneous Catalysis; Catalysis by Novel Solid Strong Acids and Superacids*; B.L. Shapiro, Ed., Texas A&M University Press, College Station, TX (1984) 71-94.
2. J.C. Vedrine, A. Auroux, V. Bolix, P. Dejaifve, C. Naccache, P. Wierzchowski, E.G. Derovane, J.B. Nagy, J. Gilson, J.H.C. Van Hooff, J.P. Van Den Berg, and J.J. Wolthozen, *Catalysis*, 59 1979 48-162.
3. H. Pines, *The Chemistry of Catalytic Hydrocarbon Conversion*, Academic Press, New York/London, (1981) 100-122.
4. G.A. Olah, G.K. Surya Prakash, and J. Sommer, *J. Superacids*. Wiley, New York, (1985) 53.
5. R.S. Drago, E.E. Getty, US Patent 4 719 190, January 12, 1988.
6. R.S. Drago and E.E. Getty, *J. Am. Chem. Soc.* 110 1988 3311-3312.
7. D.P. Mobley and A.T. Bell, *Fuel*, 59 1980 507-510
8. C.W. Zielke, R.T. Struck, J.M. Evans, C.P. Costanza and E. Gorin, *Ind. Eng. Chem. Proc. Des. Dev.*, 5 1966 158-164.
9. R.T. Struck and C.W. Zielke, *Fuel*, 60 1981 795-800.

10. R.K. Sharma, J.W. Diehl, and E. S. Olson, 3rd Int. Conf. on Proc. and Utilz. of High Sulfur Coals, Ames, Iowa, Nov. 14-16, 1989.
11. T.J. Pinnavaia, Science, 220 1983 365-371 and references therein.
12. K. Tanabe, Solid Acids and Bases, their catalytic properties, Academic Press, New York/London, (1970) 528.
13. A. Vogel, Textbook of Quantitative Inorganic Analysis, 4th edn., Longman Sci. and Tech. Group, Essex, Eng., (1978) 434.
14. E.S. Olson, and J.W. Diehl, Anal. Chem., 1987 443-448
15. E.S. Olson, J.W. Diehl, and R.K. Sharma, ACS Div. of Fuel Chem., Boston, MA, April, 1990 (communicated).

## USE OF MODEL COMPOUNDS IN COAL STRUCTURE AND REACTIVITY STUDIES

Randall E. Winans, Ryoichi Hayatsu, Thomas G. Squires†,  
Kathleen A. Carrado, and Robert E. Botto

Chemistry Division, Argonne National Laboratory, Argonne, IL 60439, and  
†Associated Western Universities, Inc., Salt Lake City, UT 84124

### INTRODUCTION

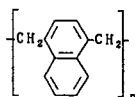
The interpretation of data from chemical and thermal reactions of coals is often facilitated and can be strengthened by investigating analogous reactions in appropriate model systems. While coal models have ranged from small molecules to polymers to synthetically coalified biomolecules and biomacromolecules, it appears that there are dangers in extrapolating the behavior of small, soluble molecules to that of solid coal. We have found that polymers and synthetic coals are much more appropriate models for coal behavior. In the present report, pyrolysis data from the latter models and coals will be compared and contrasted.

### EXPERIMENTAL

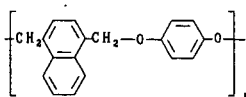
The compositions of the Argonne Premium coals and polymers used in this study are given in Table I. The preparations of the coal samples<sup>1</sup> and of the two polymers<sup>2</sup> have been described.

TABLE I. Elemental Analyses for the Argonne Premium Coal Samples.

Sample	Name	%C(maf)	Per 100 Carbons			
			H	N	S	O
8	Beulah-Zap Lignite	72.9	80	1.4	0.4	20.9
2	Wyodak-Anderson SubB	75.0	86	1.3	0.2	18.0
3	Illinois Herrin hvCB	77.7	77	1.5	1.2	13.0
6	Blind Canyon hvBB	80.7	86	1.7	0.2	10.8
7	Lewiston-Stockton hvAB	82.6	76	1.6	0.3	8.9
4	Pittsburgh hvAB	83.2	77	1.7	0.4	8.0
1	Upper Freeport mvB	85.5	66	1.5	0.3	6.6
5	Pocahontas lvB	91.0	59	1.3	0.2	2.0
	Polymer I	92.6	87	-	-	-
	Polymer II	79.6	84	-	-	11.0



I



II

Scheme 1.

GCMS and PYMS data were obtained on a Kratos MS-25 mass spectrometer. A 60 m x 0.25 mm DB-1701 fused silica column was used in GCMS analysis. The details of the PyMS experiment have been reported.<sup>3</sup> The samples were all heated at 50°/min or at 75°/min on a platinum screen and the instrument was operated in the precise mass measurement mode.

For the very high resolution experiments, the samples were inserted into an all glass heated inlet system (300° C) and leaked into the source of a Kratos MS-50 ultra high resolution mass spectrometer.<sup>4</sup> A dynamic resolution of 80,000 was obtained for the low voltage (11 eV) electron impact LVHRMS experiment with a scan rate of 1000 seconds/decade. The 70 eV EI spectra were obtained with 50,000 dynamic resolution with a scan rate of 100 seconds/decade. Both spectrometers were operated with a Kratos DS 90 data system. Data was transferred to a Micro Vax II for final analysis. The data are sorted by both heteroatom content and by hydrogen deficiency (HD). The term HD corresponds to number of rings plus number of unsaturations ( $HD = -2Z$ ).

#### Synthetic Polymer Models

In the present investigation, we have examined the PyMS behavior of two synthetic polymers containing linkages presumed to exist in coals, an ethylene-linked naphthalene (I) and a hydroquinone-linked naphthalene (II). Our initial studies on the PyMS, oxidation, and liquefaction behavior of these polymers have been reported.<sup>2</sup> Solomon and coworkers have examined the pyrolysis products of similar polymers using FIMS.<sup>5</sup> The PyMS techniques used in the present study have the distinct advantage of detecting and analyzing the pyrolysis products in the time-resolved mode, i.e. as soon as they are released to the vapor phase. From Figure 1, it is clear that polymer I is much less reactive than II. The pyrograms of I look much like those produced in the PyMS of inertinite macerals, with no major peak until the temperature reaches approximately 540°C. In contrast, the major devolatilization of polymer II occurs at a much lower temperature (310°C).

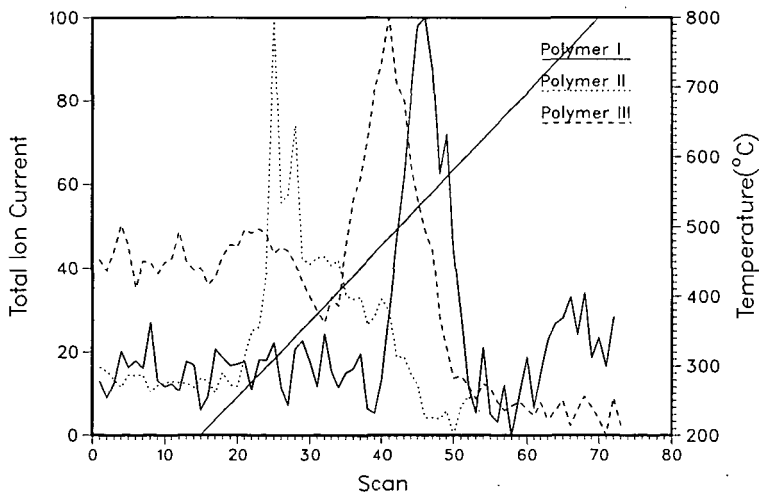
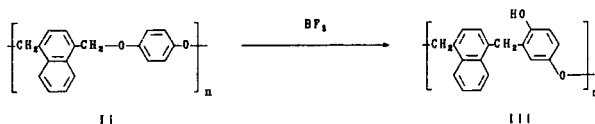
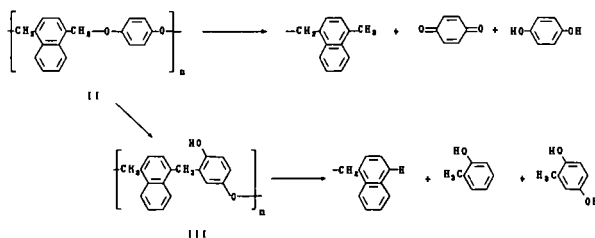


Figure 1. Total ion current pyrograms of the synthetic polymers heated beginning with scan 15 at 75° C/min from 200° to 800° in high resolution mode.

We have previously reported that attempts to unlink polymer II under mild acid conditions afforded only trace amounts of solubilized oligomeric product and almost quantitative rearrangement to a methylene linked polymer (III) as shown in Scheme 2.<sup>5</sup> Both chemically and pyrolytically, the rearranged polymer, III, is much less reactive than the original oxymethylene-linked polymer, II. Pyrolysis of the rearranged polymer (III) affords a major devolatilization peak at 480°C, 170°C higher than that of the original (Figure 1).



In addition, we have found the following convincing evidence that pyrolysis of the unrearranged oxymethylene-linked polymer II involves, as one of the reaction pathways, an analogous rearrangement to a methylene-linked polymer. In the PyMS of polymer II, a fragment with  $M/Z=108$  can be due to quinone, a cresol, or a hydrocarbon. High resolution mass spectrometry makes it possible to differentiate among these species; and the results of using this technique in our PyMS experiments with polymer II are shown in Figure 2. At temperatures below 300°C, quinone but no cresols is detected while above 350°C, the reverse is observed. A very simple and reasonable explanation of these results is shown in Scheme 3.



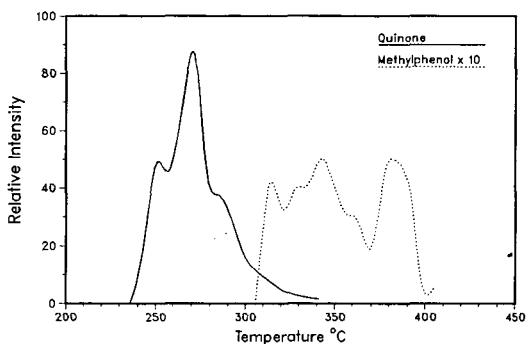


Figure 2. Selected ion chromatogram for quinone and methylphenol fragments from PyMS of Polymer II.

The time resolved high resolution MS data makes it possible to differentiate between these two different pyrolysis products even though they have the same nominal mass.

In light of these results from the model polymer, the data from PyMS of some of the Argonne Premium Coal Samples were examined for alkylated phenols and quinones. For the subbituminous coal (APCS #2) peaks which could be assigned quinone structures were observed at the lower temperatures. In Figure 3, the evolution of selected peaks are shown as a function of temperature. There is no evidence for quinones at the higher temperatures while alkylphenols are still observed. Higher rank coals such as the Illinois No. 6 (APCS #3) yielded only trace amounts of peaks corresponding to quinones while none were observed for coals with greater than 80% carbon, however, alkylphenols are observed.

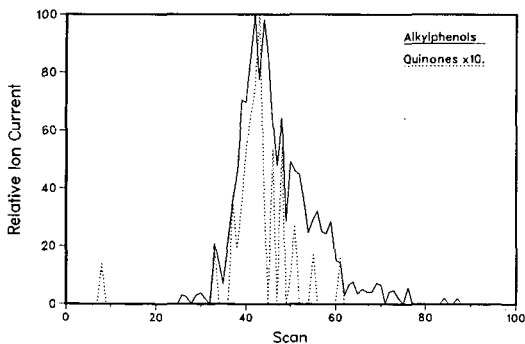
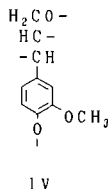


Figure 3. Selected ion pyrograms for the subbituminous coal (APCS #2).

### Synthetic Coal Models

Lignins are thought to be the major precursors of vitrinite macerals. Synthetic vitrinites have been prepared heating the lignin with promotion by clays.<sup>7</sup> Softwood lignins are made up mostly from the coniferyl alcohol monomers (IV). Some of the initial reactions are the loss of methyl and methoxyl with realkylation of the benzene ring. Also, studies of sediments confirm that these types of transformations occur.<sup>8</sup>



Model compounds of the softwood lignin structure were reacted under simulated coalification conditions in order to elucidate the clay-organic reactions responsible for bond cleavage and rearrangement processes in these systems. Of specific interest was the reactivity of anisole (phenyl methyl ether) groups in these model compounds, which include *m*-methyl anisole (mMA), guaiacol, 4-hydroxy-3-methoxy toluene and 4-phenoxy-3-methoxy toluene. Pillared clays (PILCs) were chosen as the catalysts because they are an order of magnitude more active than untreated clays under these specific conditions. PILCs are smectite clays with permanent intracrystalline porosity made by metal oxide molecular props, usually alumina, that hold the clay layers apart.

The predominant reaction observed is O-methyl bond cleavage of anisoles to lead to phenolic functionality. Transalkylation and dealkylation reactions are also observed by GCMS and solid-state <sup>13</sup>C NMR techniques. In addition, isotopically labeled <sup>13</sup>C anisoles were synthesized and reacted with clays. Mass spectra of volatile products reveal the presence of <sup>13</sup>CH<sub>3</sub>OH and large amounts of (<sup>13</sup>CH<sub>2</sub>)<sub>2</sub>O due to further dehydration of methanol over the clay surface.

Table 2 gives the distribution of solvent-extractable products obtained from mMA catalysis as determined by GCMS. The amount of mMA decreases as it is reacted to *m*-cresol and alkylated cresols (major products), and alkylated anisoles (minor products). The amount of dialkylated products begins to decline after a certain amount of reaction time, as they are further cracked to simpler products.

TABLE 2. Distribution (mole %) of soluble products obtained from the reaction of *m*-methyl anisole with pillared bentonite clay at 150° C.

Product	Time (hours)			
	0	22	49	72
mMA	100	69.2	9.4	4.9
Me-mMA	0	3.3	9.8	10.1
Me <sub>2</sub> -mMA	0	0	1.8	1.0
<i>m</i> -cresol	0	27.7	33.2	34.8
Me-cresol	0	0	24.5	41.4
Me <sub>2</sub> -cresol	0	0	21.3	7.8

mMA = *m*-methyl anisole

Me = methyl

These results give an indication of the types of reactions that occur under simulated coalification conditions. These necessarily involve heterogeneous interactions with a solid acid catalyst and reactions that are typically catalyzed by protons.

From the model studies one would predict that the number of benzene rings with two oxygen substituents would decrease with increasing rank. Also, the overall phenolic content should decrease with rank. PyHRMS data have been obtained for the eight Premium Coal Samples. An estimate of yields of phenols from the high vacuum pyrolysis is shown in Figure 4. The trends observed are as expected except for the Utah Blind Canyon Coal (APCS #6). This coal is rich in liptinites which would mean that the products would be dominated by the high yield hydrocarbons from the liptinites. Overall, the species with two oxygens decrease rapidly after about 78% carbon content. The Illinois No. 6 coal may be a little unusual since it has a fairly high oxygen content for a high volatile bituminous coal. There appears to be a significant amount of lignin character left in the lignite. This conclusion is supported by oxidative degradation data and by characterization of extracts from lignite.

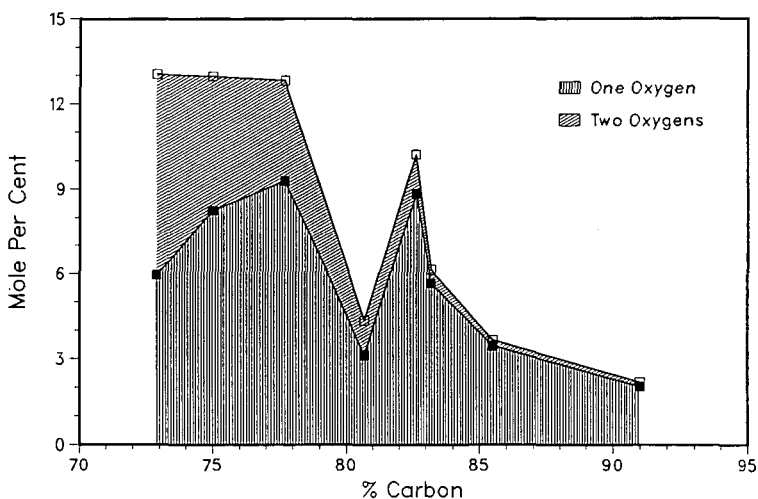


Figure 4. Phenols from PyHRMS of the Premium Coals presented as a stacked plot.

## CONCLUSIONS

It would be very difficult to say anything about chemical structures in coals without results from model systems. Many times the systems were not studied as a model for coals, but the results can still be used to interpret the coal data when similar methods are used. Macromolecular models can be quite realistic and some of the examples described in this paper show how they can be used to better understand the coal results. However, one must be careful that the model results are not over-interpreted much like the problem that has occurred with drawing or modeling of "average structures."

## ACKNOWLEDGMENTS

This work was performed under the auspices of the Office of Basic Energy Sciences, Division of Chemical Sciences, U.S. Department of Energy, under contract number W-31-109-ENG-38.

## REFERENCES

1. Vorres, K.S.; Janikowski, S.K. *Preprints, Div. Fuel Chem., ACS 1987, 32(1)*, 492.
2. Squires, T.G.; Smith, B.F.; Winans, R.E.; Scott, R.G.; Hayatsu, R. *Proceedings International Conference on Coal Science 1983*, p. 292.
3. Winans, R.E.; Hayatsu, R.; Scott, R.G.; McBeth, R.L. In *Chemistry and Characterization of Coal Macerals*; Winans, R.E.; Crelling, J.C., Eds.; ACS Symposium Series No. 252, ACS:Washington, D.C. 1984; p. 137.
4. Winans, R.E.; McBeth, R.L.; Neill, P.H. *Preprints, Div. Fuel Chem., ACS 1988, 33(3)*, 85.
5. Squire, K.R.; Solomon, P.R.; Caranzelo, R.M.; DiTaranto, M.B. *Fuel 1986, 65*, 833.
6. Smith, B.F.; Venier, C.G.; Squires, T.G. *Preprints, Div. Fuel Chem., ACS 1984, 29(5)*, 15.
7. Hayatsu, R.; McBeth, R.L.; Scott, R.G.; Botto, R.E.; Winans, R.E. *Org. Geochem. 1984, 6*, 463.
8. Hatcher, P.G.; Lerch, H.E. *Preprints, Div. Fuel Chem., ACS 1989, 34(3)*, 617.

# SYNTHESIS AND CONVERSION STUDIES OF POLYMERIC MODELS FOR LOW-RANK COALS

Donald E. McMillen and Ripudaman Malhotra

Chemical Kinetics Department, Chemistry Laboratory  
SRI International, Menlo Park California, 94025-3493

and Michael A. Serio

Advanced Fuel Research  
East Hartford, Connecticut 06108

**KEYWORDS:** Coal Models, Poly(eugenol), FIMS, Liquefaction, Pyrolysis

## INTRODUCTION

Efforts to understand the key chemical reactions responsible for coal conversion have been severely hindered over the years by the necessity of having to infer a complex sequence of chemical reactions for a substrate, coal, whose critical linkages are basically unknown. To aid in the effort, many workers have studied the reactions of coal "models" under various conversion conditions. However, this already imperfect solution has itself been limited by the inappropriateness of many of the models, and by the widespread misconception that the spontaneous thermal scission of inherently weak linkages in the coal structures is solely responsible for the fragmentation of the coal matrix. In fact, the combination of these two factors has compounded the situation: the perception of control by homolysis of weak linkages has led to a disproportionate focus on weakly bonded models such as bibenzyl, benzylphenyl ether, and related structures. This paper reports the initial results of an effort to use model structures that (1) have inter-cluster linkages that are perhaps more representative of those in coals, and (2) are incorporated into polymeric networks in order that mass transport and other effects that can be important in heterogeneous systems might be more appropriately mimicked.

The basic linkage chosen for the present study is the oxy-ethylene linkage of phenyl phenethyl ether. Although phenyl phenethyl ether and related structures have been previously studied as coal models (1-4), they have not received the attention commensurate with their recognized abundance in lignins. No studies, to our knowledge, have been reported for specially synthesized and characterized polymers containing this linkage. As it happens, the weakest bond in phenyl phenethyl ether, the phenoxy-carbon bond, is about equal in strength to the central bond in bibenzyl (5,6). At  $\sim 61$  kcal/mol, the bibenzyl bond undergoes homolysis at  $400^\circ\text{C}$  with a half life of  $\sim 25$  hours, but as has been well-demonstrated in studies of several three-atom-linked di-aryls (1-4), homolysis typically serves only as the initiation process for their decomposition. In the case of phenyl phenethyl ether itself, the very facile  $\beta$ -scission of the benzylic radical formed by H-abstraction results in an observed half-life (at  $400^\circ\text{C}$ ) that is at least 10 times shorter than that for the homolysis (2). Clearly, either coals do not have very many such linkages, or some other factor (viz., retrograde reaction) counteracts the demonstrated reactivity of the  $-\text{O}-\text{C}-\text{C}-$  linkage. Interestingly, low-rank coals have for a long time been known to be more reactive than bituminous coals, but they give lower liquefaction conversions. Therefore, it seems likely that a crosslinked or intertwined polymeric network, or the presence of additional functional groups (i.e.,  $-\text{OH}$ ,  $-\text{OMe}$ , or  $-\text{COOH}$ ) result in a proclivity for retrograde reactions that makes coals with very labile linkages unusually hard to convert. To better understand those retrograde processes and the approaches that might be used to limit them, we have embarked on a program to synthesize, characterize, and study the conversion of the polymeric, three-atom-bridged models described below.



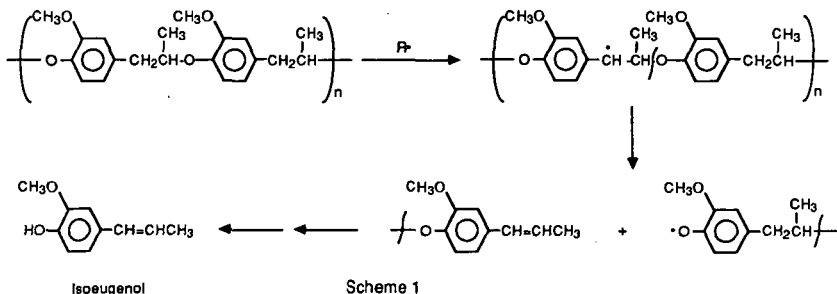
The  $\alpha,\alpha'$ -dibromo-*p*-xylene (V) was treated with the monoanion of dithiane (VI) in THF at  $-50^\circ$  to  $-30^\circ\text{C}$ . The product (VII) was characterized by TLC and NMR and found to be consistent with the anticipated structure. The dianion from VII was treated with the dibromide (V) at low temperatures for 3 hours and thereafter at room temperature for 15 hours. The THF-soluble fraction showed a polymer of MW  $\sim 2500$ . Desulfurization of the THF-soluble portion was effected using Raney Ni and the product was exhaustively extracted to yield a polymer of MW  $\sim 1500$ . Elemental analysis gave C = 83.86% and H = 8.7%, indicating an H/C ratio of 1.24 (as compared with an expected ratio of 1.11).

### Polymer Characterization by Pyrolysis-FIMS

As with the elemental and NMR analyses, the Py-FIMS characterization of the poly(eugenol) and the poly(4-allylphenol) is appropriately described as consistent with, but not conclusive evidence of, the desired structures. Since the FIMS characterization of a material that is not volatile under high-vacuum conditions involves programmed-temperature heating to pyrolytically generated volatiles that are then mass spectrometrically analyzed, it constitutes a thermal conversion experiment that bears relevance to coal liquefaction or pyrolysis. Therefore the Py-FIMS results will be discussed in some detail.

The Py-FIMS spectra of the poly(eugenol) and the poly(4-allylphenol) are shown in Figures 1 and 2. The spectra are relatively simple and are dominated by  $C_1$ - to  $C_3$ -phenols or dihydroxybenzenes (catechols), and, in the case of the poly(eugenol), by an ion corresponding to the monomer ( $m/z$  164). These products are all to be expected from the desired polymer structure. However, the relative amounts of the various fragments are quite unexpected, indicating either that the decomposition sequence is not as anticipated, or the polymer structure is not exactly as desired, or both.

In both cases, the sequence of oligomeric groupings commonly seen in Py-FIMS of linear polymers (7) is essentially absent. The poly(eugenol) (Figure 1) has a large peak at  $m/z$  164, representing the monomer, but very little intensity in the vicinity of the dimer ( $m/z$  328), and none in the vicinity of the trimer ( $m/z$  492). The spectrum of the poly(4-allylphenol) is even more pronounced in this regard: there is only moderate intensity at the monomer ( $m/z$  134) and essentially none at the dimer and trimer masses (268, 402). The ten-fold decline in intensity of the dimer relative to the monomer, and the total absence of any ion intensity corresponding to the trimer is highly unexpected for a linear polymer that cannot unzip and is thus limited to scission by random attack on its linkages. The principal expected bond scission pathways shown below for the case of the eugenol polymer should occur randomly along the polymer chain and would result in a whole sequence of oligomers, as has been reported in the pyrolysis of other linear polymers.(7)



Along with the absence of higher oligomers, Figures 1 and 2 also show that each polymer yields substantial amounts of several alkylated dihydroxybenzenes and phenols, respectively. In the case of poly(eugenol), the  $C_1$ - and  $C_2$ - dihydroxybenzenes are of comparable abundance to the monomer itself. In the case of the poly(4-allylphenol),  $C_1$ - and  $C_2$ - phenols are about ten times as abundant as the monomer. In both cases, the sum of  $C_1$ -,  $C_2$ - and  $C_3$ - phenols is substantially greater than the intensities of the monomers themselves.

Examination of the temperature dependence for evolution of the major peaks in Figures 1 and 2 suggests there are separate production routes for the monomers and the more highly fragmented phenolics, at least in the case of the poly(eugenol). Figures 3 and 4 show the abundance of the individual peaks as a function of temperature for the two polymers. In the case of poly(4-allylphenol) (Figure 3), the monomer and the C<sub>1</sub>-phenol evolve at similar temperatures. On the other hand, in the case of poly(eugenol) (Figure 4), there is substantial evolution of the monomer (164) well below 300°C, while the methyl catechol (124) does not peak until about 400°C.

Preferred evolution of the monomers at lower temperatures is consistent with the expectation (1-3,8) that depolymerization results from H-abstraction--β-scission chain processes, as depicted above in Scheme 1. The C<sub>1</sub>- to C<sub>3</sub>-phenols and catechols, on the other hand, do not have easily identifiable chain routes, and would be expected to be rapidly evolved only at higher temperatures. Monomer evolution is expected to be more facile for poly(eugenol) because the methoxy group decreases the strength of the phenoxy-carbon bond in the -O-C-C- linkage by about 4 kcal/mol (9, 10). All other things being equal, this decrease in bond strength would be expected to decrease by about 150°C the temperature at which an equivalent decomposition rate is observed. As Figures 3 and 4 show, the peak of monomer evolution in poly(eugenol) is at least 150°C lower than for poly(4-allylphenol). This result may have bearing on the as-yet unresolved question (8) of whether phenyl phenethyl ether-type structures are a class for which concerted decomposition in a retro-ene process is competitive with the free radical chain process shown above (Scheme 1).

The mode of formation of the C<sub>1</sub>- to C<sub>3</sub>-catechols and phenols is even more puzzling than the oligomer distribution. Possible routes to the C<sub>1</sub>- to C<sub>3</sub>-catechols could involve initial methylphenoxy cleavage, as the homolysis of the ca. 61 kcal/mol methyl-O bonds becomes rapid in the vicinity of 400°C. However, this suggestion is not consistent the fact that the yield of C<sub>1</sub>- and C<sub>2</sub>-phenolics, is actually greater for the poly(4-allylphenol), which has no methoxy group, nor with the fact that the evolution of methylphenolics reaches its maximum at about the same temperature for both the poly(eugenol) and the poly(4-allylphenol).

#### Liquefaction of -O-C-C- Polymers

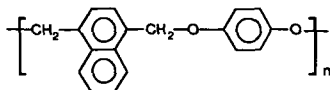
The batch microautoclave liquefaction results for poly(eugenol) and poly(p-allylphenol), and for comparison, the results for a weakly linked (-O-C-) polymer and a sample of the Argonne Zap Lignite are shown below.

PRODUCT YIELDS<sup>a</sup> IN THE LIQUEFACTION OF MODEL POLYMERS

Sample	Hexane-Solubles	Toluene-Solubles	Pyridine-Solubles	Toluene-Insolubles	Pyridine-Insolubles	Gas
Poly(eugenol)	27	66	93	27	0	8
Poly(4-allylphenol)	1	52	96	44	0	5
Polymer VIII	85	96	100	4	0	3
Zap Lignite	14	28	46	62	50	5

<sup>a</sup> The liquefaction tests were performed in a microautoclave reactor, using 9,10-dihydrophenanthrene as the solvent. The reactor was purged and sealed under N<sub>2</sub>, and then immersed in a sand bath at 400°C for 30 minutes.

<sup>b</sup> Polymer VIII is a linear polymer having the structure:



The hexane- and toluene-soluble conversions of the two -O-C-C- linked polymers are in the same order as the Py-FIMS volatilities (53 and 28%, respectively for the poly(eugenol) and the poly(4-allylphenol). They are substantially harder to convert than the weakly bonded Polymer VIII, but, in the case of the poly(eugenol), easier to convert than low-rank coal. The similarities and differences will be further considered in the Discussion Section.

## DISCUSSION

The fact that the pyrolysis products are dominated by lower oligomers and smaller fragments does not, by itself, indicate whether the crosslinks were pre-existing or were generated in the course of the thermal treatment. This question is of course central to both the characterization of the original polymers, and also to an understanding of their behavior under liquefaction and other conversion conditions. Comparison of the conversion of the two -O-C-C- linked polymers with the "conversion" of other three-atom-linked models, including phenyl phenethyl ether itself, shows the apparent rate of polymer conversion to be somewhat slower than expected. Gilbert and Gajewski report (2) apparent rate parameters for phenyl phenethyl ether decomposition that correspond to a half-life at 400°C of about two hours. Considering that the linkages are somewhat weaker in both poly(4-allylphenol) and poly(eugenol) (5,9), and that many fewer than half the linkages need to be broken to make either of these polymers, if linear, fully soluble in toluene certainly supports the other indications of significant crosslinking at some stage. We are presently preparing additional batches of the poly(4-allylphenol) with phenol added during the synthesis to purposely terminate the growing polymer chains at a molecular weight level well below one million.

In general, the behavior of these two polymers is similar to the behavior of other polymeric models that are either crosslinked to begin with or are easily crosslinked during conversion and to the behavior of low-rank coals themselves, as previously discussed by Solomon and coworkers (7, 11-13). A high degree of crosslinking results in cleavage to free, and hence volatile, fragments of mainly small units, rather than large segments of a linear polymer chain. In addition, the high yields of the dihydroxybenzenes and the cresols are specifically quite similar to products generated during the pyrolysis (or liquefaction) of lignites and subbituminous coals (11-13).

Specifically, the poly(eugenol): (1) has a linkage known to be highly reactive; (2) begins to produce some monomer at temperatures lower than 200°C; (3) is nevertheless rather hard to fully convert to soluble or volatile products; and (4) has as its most abundant pyrolysis products those same alkylated catechols that tend to dominate the pyrolysis products of lignites and subbituminous coals. In other words, it bears a rather curious similarity to low-rank coals, given the limited range of structures in the original polymer. Thus it appears that these polymeric models containing -O-C-C- linkages may represent appropriate structures for use in determining the chemical details (and therefore what controls) the facile retrograde reactions of low-rank coals.

## ACKNOWLEDGEMENTS

The authors wish to acknowledge the support of the U.S. Department of Energy under Contract No. DE-AC22-88PC88814.

## REFERENCES

1. Poutsma, M. L.; Dyer, C. W., *J. Org. Chem.*, **1982**, *47*, 4903.
2. Gilbert, K. E.; Gajewski, J. J., *J. Org. Chem.*, **1982**, *47*, 4899.
3. Gilbert, K. E., *J. Org. Chem.*, **1984**, *49*, 6.

4. Klein, M. T.; Virk, P. S., *Ind. Eng. Chem., Fundam.*, **1983**, *22*, 35.
5. McMillen, D. F.; Golden, D. M. "Hydrocarbon Bond Dissociation Energies," *Annu. Rev. Phys. Chem.*, **1982**, *33*, 497.
6. Pedley, J. B.; Naylor, R. D.; Kirby, S. P., *Thermochemical Data of Organic Compounds*, 2nd Ed., Chapman and Hall, New York, 1986.
7. Squire, K. C.; Solomon, P. R.; Carangelo, R. M.; DiTaranto, M. B., *Fuel*, **1986**, *65*, 833.
8. Poutma, M. L., "A Review of Thermolysis Studies of Model Compounds Relevant to Processing of Coal," Report ORNL.TM-10637, Oak Ridge National Laboratory, 1987.
9. Suryan, M. M.; Kafafi, S. A.; Stein, S. E., *J. Am. Chem. Soc.*, **1989**, *111*, 1423.
10. Benson, S.W., *Thermochemical Kinetics*, 2nd ed., John Wiley and Sons, Inc., New York, 1976.
11. Serio, M. A.; Solomon, P.R.; Carangelo, R. M., *Am. Chem. Soc. Div. Fuel Chem. Preprints*, **1988**, *33(2)*, 295.
12. Deshpande, G. V.; Serio, M. A.; Solomon, P.R., *Am. Chem. Soc. Div. Fuel Chem. Preprints*, **1988**, *33(2)*, 310.
13. Solomon, P. R.; Serio, M. A.; Deshpande, G. V.; Kroo, E., "Crosslinking Reactions during Coal Conversion" accepted for publication in *Energy & Fuels*, **1990**.

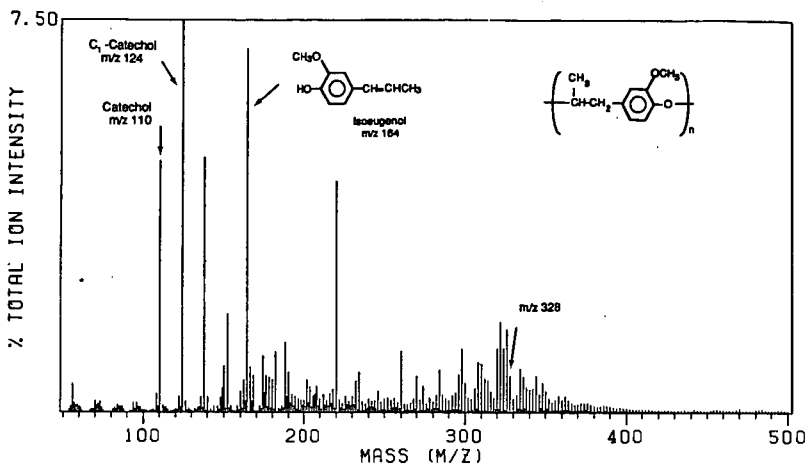


Figure 1. Pyrolysis-FI mass spectrum of poly(eugenol).

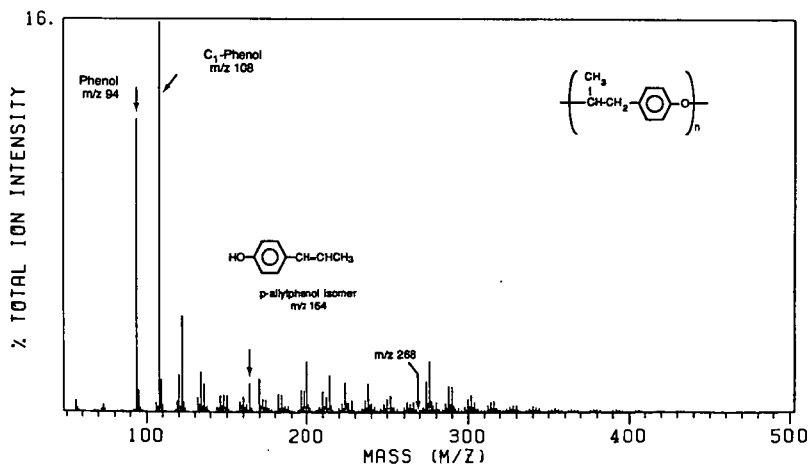


Figure 2. Pyrolysis-FI mass spectrum of poly(p-allylphenol).

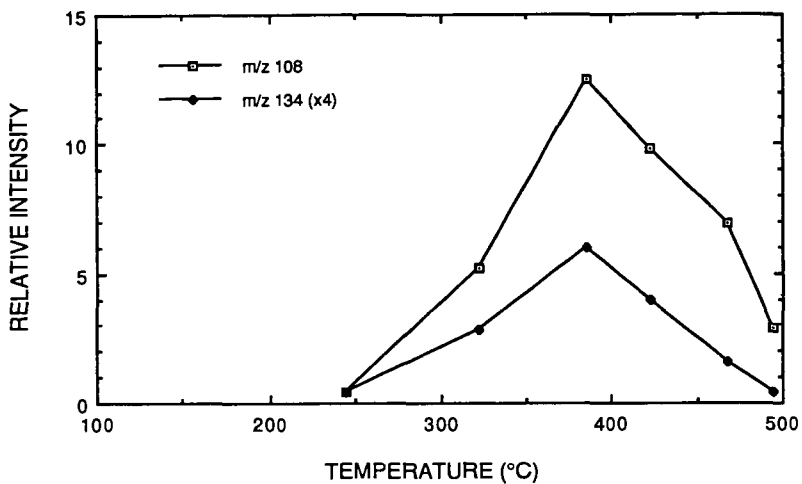


Figure 3. Thermal evolution of cresol and monomer from poly(4-allylphenol).

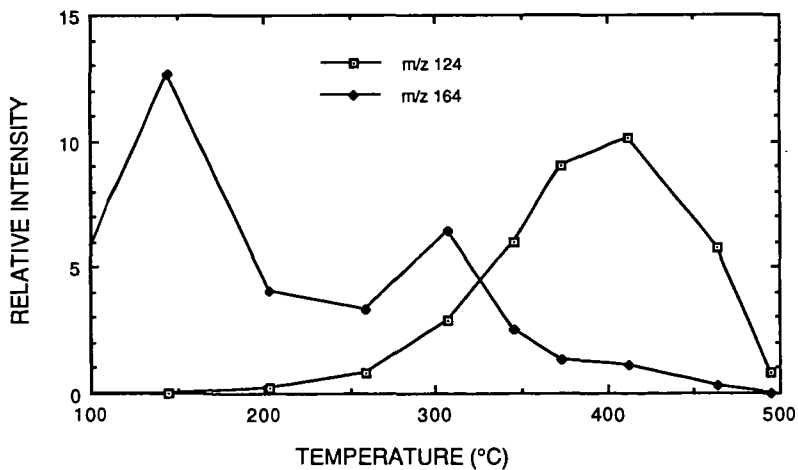


Figure 4. Thermal evolution of methyl dihydroxybenzene and monomer from poly(eugenol).

## HYDROQUINONE COPOLYMERS: MODELS FOR RETROGRADE REACTIONS IN LIQUEFACTION PROCESSING

E. S. Olson, R. K. Sharma, L. J. Radonovich, Jr., M. J. Heintz, and J. W. Diehl  
University of North Dakota, Energy and Environmental Research Center  
Grand Forks, North Dakota 58202

The identification of structures responsible for retrograde reactions is a high priority research objective in coal liquefaction. Interest has focused on the cleavage of benzyl aryl ethers and subsequent polymerization of the fragments. In our work, the reactions of the polyethers prepared by reaction of bis(bromomethyl)naphthalene with hydroquinone were investigated in a tetralin system. Analysis of the products from the copolymers demonstrated that almost all of the naphthyl moieties were converted to dimethylnaphthalene, whereas the hydroquinone groups were converted to very high molecular weight macromolecules. Light-scattering studies showed that the product has a very high depolarization ratio, a property also demonstrated by coal macromolecules obtained by mild liquefaction and extraction but not by synthetic polymers, including polyphenylene oxides. Similar macromolecules were obtained in thermal reactions of benzyloxyphenol and dihydroxybenzenes in tetralin.

Key words: benzyl aryl ether cleavage, retrogressive reactions, dihydroxybenzene polymers

### INTRODUCTION

Formation of char during coal liquefaction is deleterious to the process because of deposition on the catalyst as well as in the apparatus. Phenolic groups have been implicated in the retrogressive reactions that result in char formation in SRC materials (1,2); however, the nature of the condensation reaction that the phenolic substances undergo has never been precisely defined. The addition of hydrogen donors, such as tetralin, to SRC fractions with high phenolic content inhibited char formation (2). It is important to note in these studies that derivatization of the phenolic groups in the SRC with acetic anhydride resulted in higher char yields when the acetylated products were heated. The explanation for this was that the thermally labile esters readily decomposed forming phenoxy and acetyl radicals, which then abstracted hydrogen from other coal groups. Dimerization and addition reactions of the resulting radicals would result in char formation.

The thermal reactions of benzyl phenyl ether have been investigated as a model for the cleavage of the oxymethylene bridge in coal. The data from these modeling experiments is consistent with a mechanism involving homolytic cleavage of the C-O bond, forming phenoxy and benzyl radical intermediates. In a good hydrogen donor solvent such as tetrahydroquinoline, the radicals are capped and toluene and phenol are formed (3). However, when hydrogen donor solvent was not present or even in the presence of some tetralin, addition or condensation products were obtained (4).

The presence of dihydroxyarenes in coal structures and the well-known tendency of dihydroxybenzene to condense to polymers under oxidative conditions (5) suggests that retrogressive reactions of compounds containing dihydroxy or dioxy groups should be investigated under conditions typical of coal liquefaction. The initial model chosen for this investigation was the insoluble copolymer, poly(2,6-dimethylnaphthaleno-1,2-dioxybenzene). The 1,4-substituted analog was previously used in modeling coal pyrolysis and swelling studies (6,7,8). Reactions of the

copolymer and related monomers were carried out in tetralin so that we could determine whether retrogressive reactions could occur even when hydrogen donor solvent molecules are readily available.

#### EXPERIMENTAL

The procedure of Squires et al. (6) was used for preparation of poly(2,6-dimethylnaphthaleno-1,4-dioxybenzene). 1,2,3,4-Tetrahydronaphthalene (tetralin), hydroquinone, catechol, and 4-benzyloxyphenol were obtained from Aldrich.

The reactions were carried out in a 75-ml stainless steel reactor. The reaction vessel was charged with 2.00 g of model compound or polymer and 16 g of tetralin, evacuated, sealed, and heated in a fluidized sand bath at 420°C for 6 min with shaking. The tube was removed from the sand bath, cooled, slowly depressurized and opened. The product slurry was transferred into a centrifugation bottle by washing with hexane, and the solid product was removed by centrifugation. The hexane-soluble product was analyzed by GC/FTIR/MS.

The hexane-insoluble product was separated into tetrahydrofuran (THF)-soluble and insoluble fractions by extraction of the solid into that solvent. The THF-soluble product was sublimed at 110°C/1.2 torr for two hrs. The sublimate was analyzed by GC/FTIR/MS. The residue left after sublimation was analyzed by FTIR and <sup>13</sup>C NMR in THF-d<sub>6</sub>. Molecular weight determinations were performed by GPC and low-angle laser light scattering photometry. The THF-insoluble fraction was analyzed by FTIR.

#### RESULTS AND DISCUSSION

The thermal reaction of the mixture of poly(2,6-dimethylnaphthaleno-1,4-dioxybenzene) in tetralin at 420°C for 6 min resulted in extensive degradation of the copolymer. The product distribution was 6.5% THF-insoluble material, 28% hexane-insoluble, THF-soluble fraction, and 63% hexane-soluble fraction. The hexane-soluble fraction consisted mostly of dimethylnaphthalene and a small amount of solvent-derived dimers. Since the weight % composition of dimethylnaphthalene units in the copolymer is 60%, the formation of dimethylnaphthalene was nearly stoichiometric.

The THF-soluble fraction was sublimed under vacuum (110°C, 1.2 torr) to remove low molecular weight material. A small amount of hydroquinone was isolated as the sublimate. The majority of the fraction did not volatilize. The residue from vacuum sublimation was redissolved in THF, and the molecular weight was determined by low-angle laser light scattering photometry with Cabbanes factor corrections (9). Depolarization ratios were large for the set of solutions, resulting in Cabbanes factors as large as 3.61 for a 0.13 mg/ml solution. These high depolarization ratios are comparable with those obtained for coal macromolecules, which also scatter light anisotropically. Most synthetic polymers, including poly(phenylene oxide), have low depolarization ratios. The reciprocal Rayleigh plot of the Cabbanes-corrected scattering factors was nearly linear ( $r^2 = .97$ ) with a positive slope ( $A_2 = .0063$ ). The weight average molecular weight ( $M_w$ ) was 1.92 million Da.

The high yield of dimethylnaphthalene indicates that the predominant pathway involves cleavage of the C-O (benzyl ether type) bonds. The resulting naphthylmethylene radicals are presumably rapidly capped by the hydrogen donor solvent. The fate of the oxy radical in this reaction is different than that of the phenoxy radical produced in the benzyl phenyl ether reaction. Only a portion of the oxy radicals produced from cleavage of the ether groups in the copolymer were converted to hydroquinone, while the majority were condensed to a high molecular weight material.

To further elucidate the difference between the mono and dioxybenzene systems, the thermal reaction of 4-benzyloxyphenol was carried out in tetralin under the same conditions. This model compound represents a single unit of the copolymer and was expected to give toluene from the benzyl radical as well as the reaction products from the oxyphenol radical. This reaction produced the expected toluene, the THF-insoluble fraction, and the hexane-insoluble, THF-soluble fraction. However, the amount of the THF-soluble fraction was smaller (14%) than that obtained from the copolymer. Sublimation of this fraction gave a small amount of hydroquinone. The molecular weight of the sublimation residue was 3.14 million Da. Depolarization ratios were similar to those observed for the product from the thermal reaction of the model polymer, resulting in Cabannes factors of 4.77 for the 0.12 mg/ml solution. The reaction of 4-benzyloxyphenol in tetralin has been reported previously (10), but no details concerning the product were given. The thermal reaction of methoxyphenols in tetralin were studied by Bredenbergh and Ceylon (11). The yields of hydroquinone from 4-methoxyphenol were quite small, but the fate of the oxy radicals generated from this ether were not elucidated, since polymeric materials were not investigated. Similar poor recoveries of products from tetralin reactions of hydroquinone and 4-methoxyphenol were mentioned by Kamiya et al. (12).

The thermal reactions of dihydroxybenzenes in tetralin were reinvestigated to determine the nature of the products and their similarity to those from the ether reactions. The reaction of hydroquinone in tetralin at 420°C was carried out, and a hexane insoluble, THF soluble fraction containing the anisotropic polymeric product ( $M_w = 0.95$  million Da) was obtained. Thus the cleavage of the phenolic O-H bond may give an oxyphenol radical which may be the same species as that produced in the ether C-O cleavage discussed above.

Catechol was also heated in tetralin at 420°C. Again, a polymeric product ( $M_w = 1.97$  million) was obtained. The polymer from the catechol was also anisotropic, giving a Cabannes factor of 3.63 for the 0.14 mg/ml solution.

Infrared spectra of the THF-soluble polymers exhibit large broad hydroxyl stretching absorptions similar to coals. Bands characteristic of both phenols and aryl ethers occur at about 1200 and 1260  $\text{cm}^{-1}$ , respectively. A small band corresponding to conjugated carbonyl is present at 1700  $\text{cm}^{-1}$ . In addition to the aromatic C-H stretching bands, aliphatic bands are also present, probably from incorporation of tetralin into the polymer. Cronauer has previously discussed the tendency of radicals to incorporate tetralin (13). Further characterization of the polymeric materials is in progress.

Schlosberg et al. (4) have described a number of potential reactions of the benzyl and phenoxy radicals that result from homolytic cleavage of benzyl phenyl ethers. Most of these will also apply to oxy radicals produced in the cleavage in the dioxy systems. Until detailed information on the structures in the polymers is available, we obviously can not write detailed mechanisms for the polymer formation. We can, however, state the following generalizations:

- (1) The oxy radicals are more involved in the polymer formation than the naphthylmethylene or benzyl radicals produced in the homolytic C-O cleavage reactions of ethers of dihydroxybenzenes. This is shown by the recovery of most of the dimethylnaphthalene units as dimethylnaphthalene and benzyl as toluene. This contrasts with the reactivities of phenoxy versus benzyl radicals, which were approximately equal in the presence of hydrogen donor solvents (4).
- (2) The thermal reactions of dihydroxybenzenes and their ethers in tetralin result in polymeric products in contrast with the reactions of phenyl ethers that give additional by-products composed of mainly two or three rings (4,14).

The oxygen functional groups in coals undoubtedly play an important role in coal liquefaction. Although benzyl phenyl ether linkages are cleaved under relatively mild liquefaction conditions, we see from this study that some of the radicals resulting from this scission may readily condense into highly anisotropic macromolecules, even in the presence of hydrogen donor solvents.

#### REFERENCES

1. Whitehurst, D.D.; Mitchell, T.O.; Farcasiu, M. Coal Liquefaction, Academic Press, New York 1980, pp 207-273.
2. Walker, P.L.; Spackman, W.; Given, P.H.; Davis, A.; Jenkins, R.G.; Painter, P.C. "Characterization of Mineral Matter in Coals and Coal Liquefaction Residues," EPRI Project 366-1, AF-832, December 1978.
3. Brucker, R; Kolling, G. Brennstoff-Chemie 1965, 46, 41.
4. Schlosberg, R.H.; Davis, W.H.; Ashe, T.R. Fuel 1981, 60, 210-204.
5. Mather, S.P.; Schnitzer, M. Soil Sci.Soc. Am. J. 1978, 42, 591-596.
6. Squires, T.G.; Smith, B.F.; Winans, R. E.; Scott, R.G.; Hayatsu, R. Proc. Intern. Conf. Coal Sci., 1983, 292-295.
7. Solomon, P.R. "Synthesis and Study of Polymer Models Representative of Coal Structure," Final Report to Gas Res. Inst. for Feb. 1982 to Mar. 1983.
8. Barr-Howell, B. O.; Peppas, N.A.; Squires, T.G.; J. Appl. Polym. Sci. 1986, 31, 39-53.
9. Olson, E.S.; Diehl, J.W. First Pacific Polymer Conference, Preprints. Maui, HI, Dec. 1989.
10. Carson, D.W.; Ignasiak, B.S. Fuel, 1980, 59, 757-761.
11. Bredenberg, J.B.; Ceylon, R. Fuel 1983, 62, 342-344.
12. Kamiya, Y.; Yao, T.; Oikawa, S. ACS Division of Fuel Chem., Preprints, 1979, 23 (4), 116-124.
13. Cronauer, D.C.; Jewell, D.M.; Shah, Y.T.; Modl, R..J.; Seshadri, K.S. Ind. Eng. Chem. Fundam. 1979, 18, 368-376.
14. Sato, Y.; Yamakawa, T. Ind. Eng. Chem. Fundam. 1985, 24, 12-15.

#### ACKNOWLEDGMENTS

This research was supported by Contract No. DOE-FC21-86MC10637 from the U.S. Department of Energy. References herein to any specific commercial product by trade name or manufacturer does not necessarily constitute or imply its endorsement, recommendation, or favoring by the United States Government or any agency thereof.

## REACTIONS OF MODEL COMPOUNDS WITH SUPERCRITICAL WATER

C. C. Tsao and T. J. Houser  
Chemistry Department  
Western Michigan University  
Kalamazoo, MI 49008

Keywords: supercritical water, model compounds, coal extraction

### INTRODUCTION

The possible use of supercritical fluid extraction (SFE) of coal to obtain cleaner, more versatile fluid products is of significant interest. Some fluids have the opportunity to participate as reactants at process conditions, which may yield extracts of very different compositions than those obtained from other treatments and which will be dependent on the fluid used. Thermodynamic consideration of SFE leads to the prediction that the enhanced solubility (volatility) of the solute may be several orders of magnitude(1-3). Thus, this method combines many of the advantages of distillation with those of extraction. However, despite the interest in SFE, only a few studies have reported the basic chemistry that may be taking place during coal extraction at these conditions(4-8).

The current program is concerned with nitrogen removal from, and the rupture of carbon-carbon bonds between, aromatic rings in model compounds thought to be representative of structures found in fossil fuels. Because of the difficulty of removing heterocyclic nitrogen, experiments were initiated by extensively examining the reactivities of quinoline and isoquinoline, as well as brief examinations of the reactivities of other compounds(4). The selection of water as the fluid was based on its physical and chemical properties(9) and on the observation that a few studies of SFE of coal using water as the fluid have given encouraging results(10,11). Zinc chloride was chosen as a catalyst because of its reported catalytic activity for hydrocracking aromatic structures(12). This paper discusses the results of a study of the reactions of supercritical water (SW) with organic compounds that were found, or postulated, to be intermediates in the reaction of isoquinoline with SW. Since the isoquinoline reaction produced significant yields of ethyl benzene and o-xylene(4) it was assumed that benzylamine (BA) would be representative of the intermediate structure formed after the initial bond rupture in the heterocycle. It was found that benzaldehyde, benzylidenebenzylamine (BBA) and benzyl alcohol were intermediates in the BA-SW reaction(5), thus these are the primary subjects of the current study.

### EXPERIMENTAL

The experiments were carried out in a small (47 cm<sup>3</sup>) stainless steel, batch reactor, which was not equipped for the collection of gaseous products for analysis. The reactor was loaded with about 2.00 g of an organic compound. Water (10 ml) was added for the SW experiments to produce the desired pressure at reaction temperature, catalysts were added as needed, then the reactor was purged with argon and bolted

closed using a copper gasket. The reactor was placed in a fluidized sand bath furnace for the required reaction time, about 15 minutes was required to reach 375°C. Following reaction, the vessel was air cooled, opened, the reaction mixture removed and the water and organic layers separated. Portions of methylene chloride solvent were used to rinse the reactor and extract the water layer. These portions were combined with the organic layer and additional solvent added to a standard volume for quantitative determinations made gas chromatographically using peak area calibrations from known solutions. The components for these solutions were identified mass spectrometrically.

There were certain limitations on the g.c.-m.s. determinations: Some components could not be separated completely and these are reported as a total yield of mixture using an average calibration factor. Some products are reported as an isomer of a probable structure as deduced from the molecular weight and m.s. fragmentation pattern. Finally, many of the higher molecular weight minor products could be measured only with a low degree of precision by g.c. and calibration factors were estimated.

#### RESULTS AND DISCUSSION

The previous study of the isoquinoline - SW reaction(4) has indicated that following the rupture of the CN bond in the 1-2 or 2-3 position, the nitrogen portion would undergo hydrolysis and decarboxylation while the carbon end was either capped directly, or shortened and capped, by hydrogen thus producing toluene, ethylbenzene or o-xylene, the major volatile products. To help substantiate this proposed sequence of reactions, the benzylamine - SW reaction was studied(5). Since benzaldehyde, benzyl alcohol and benzyldenebenzylamine ( $C_6H_5CH_2N=CHC_6H_5$ ) were observed as intermediates in the BA - SW reaction it was necessary to determine how they contributed to the formation of the final products.

The data reported in Tables 1-4 are a small portion, but representative, of the results obtained. Ammonia was added in some experiments since it would be present in the denitrogenation of amines.

##### Benzyl Alcohol

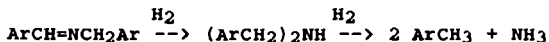
Table 1 shows that SW by itself had relatively little influence on the on the pyrolysis reaction, both giving low yields of volatile products and significant amounts of black char/tar. The added ammonia suppressed the char/tar formation, producing clear yellow solutions and significantly higher yields of volatile products. It is believed that the most important observations are: (a) that for all experiments toluene is formed in the highest yield and (b) the presence of SW does promote the formation of benzaldehyde which, as will be shown later, would lead to higher benzene yields. The second observation is consistent with other data that have shown SW capable of removing hydrogen from tetralin(4) and benzylamine (to be discussed later).

##### Benzyldenebenzylamine (BBA)

In this and the following sections, Ar will be used for the phenyl group ( $C_6H_5$ ). The formation of BBA in the BA - SW reaction was most probably from the standard imine preparation



since benzaldehyde was also found in this reaction. The data in Table 2 show that BBA - SW reaction produces benzene and toluene in comparable yields. However, since some benzaldehyde is also produced the above reaction must be somewhat reversible. It appears that benzene and other products formed from phenyl radicals have benzaldehyde as their precursor, the evidence for which will be given later. An important point to note is that the addition of a hydrogen donor, dihydroanthracene (DHA), promotes the formation of toluene at the expense of benzene and other species which form from benzaldehyde. The following reaction sequence is a possible explanation:



Thus, it appears that rupture of the single CN bond leads to toluene while the C=N segment can be hydrolysed by the reverse of the imine formation reaction.

#### Benzoic Acid

It has been assumed that benzene is formed from the decarboxylation of benzoic acid although it had not been observed as an intermediate in the reactions studied earlier. The data in Table 3 show that benzoic acid does react about as expected. However, while SW appears to slow the reaction compared to pyrolysis, ammonia acts as a catalyst to produce an almost quantitative yield of benzene.

#### Benzaldehyde

Again it would appear that SW has relatively little effect on the pyrolysis of benzaldehyde. The data in Table 4 show that the extents of reaction and product distributions are very similar (except the benzyl alcohol yields are increased somewhat with SW) for the reactions with and without water. However, with the addition of ammonia the reaction rates are increased as well as the toluene yields. The most important observation is that the major product is benzene indicating an oxidation/decarboxylation sequence is predominant. Clearly the presence of a source of hydrogen (DHA) promotes the benzyl alcohol sequence to form toluene at the expense of benzene. To a lesser degree ammonia has a similar effect but the mechanism by which this occurs would be very speculative.

The conclusion that can be drawn is that benzene and other products formed from phenyl radicals are produced through the oxidation of benzaldehyde. However, in that process since hydrogen is produced it is possible to reduce some unreacted benzaldehyde to the alcohol from which toluene and products formed from benzyl radicals are obtained, with some reversibility in the oxidation/reduction part of the sequence.

Another possibility is that the Cannizzaro disproportionation is taking place which is base catalyzed. However, this would be expected to lead to equal yields of benzoic acid and benzyl alcohol or their respective subsequent products. Since the products resulting from benzoic acid are predominant it appears that SW may alter the mechanism to favor this product, possible through hydrogen removal from a benzaldehyde-water adduct.

### Mechanism Considerations

The formation of biphenyl and 168 isomers (methyl biphenyls) as well as benzene demonstrate that phenyl radicals exist as intermediates. The formation of bibenzyl and other 182 isomers (benzyl toluenes) and the 168 isomers as well as toluene demonstrate the presence of benzyl radicals. The previous results with bibenzyl and SW(5) show conclusively that once benzyl radicals form, they abstract hydrogen or combine with other radicals resulting in very little (if any) oxidation/decarboxylation to benzene. These results from bibenzyl in addition to those obtained from BA, BBA and BBA plus DHA lead to the following conclusions: (a) The CN bond in the reactant is necessary for the hydrolysis/oxidation sequence to be initiated. (b) If a CN single bond exists in an aromatic side chain it may rupture to form a radical that is capped by hydrogen producing an alkylated aromatic, or hydrogen can be removed to form a CN multiple bond. (c) Once formed, the CN multiple bond can undergo the oxidation/decarboxylation process. (d) These reactions are somewhat reversible. (e) Ammonia catalyzes the hydrolysis/oxidation and decarboxylation processes. (f) Finally, it must be concluded that SW can facilitate the removal or transfer of hydrogen from many reactants and intermediates as evidenced by the results of tetralin in SW(4), benzaldehyde sequence of reactions from the BA-SW reaction(5), benzamide and from benzaldehyde-SW with added ammonia (Table 4) and for many of the hydrolytic/oxidation sequences leading to the observed products to be possible.

### REFERENCES

1. N. Gangoli and G. Thodos, Ind. Eng. Chem., Prod. Res. Dev., 16, 208, (1977).
2. D.F. Williams, Chem. Eng. Science, 36, 1769, (1981).
3. J.C. Whitehead and D.F. Williams, J. Inst. Fuel, 182, (1975).
4. T.J. Houser, D.M. Tiffany, Z. Li, M.E. McCarville and M.E. Houghton, Fuel, 65, 827, (1986).
5. T.J. Houser, C.C. Tsao, J.E. Dyla, M.K. VanAtten and M.E. McCarville, Fuel, 68, 323, (1989).
6. M.A. Abraham and M.T. Klein, Ind. Eng. Chem. Prod. Res. Dev., 24, 300, (1985).
7. S.H. Townsend and M.T. Klein, Fuel, 64, 635, (1985).
8. J.R. Lawson and M.T. Klein, Ind. Eng. Chem. Fund., 24, 203, (1985).
9. E.U. Frank, Endeavour, 27, 55, (1968).
10. G.V. Deshpande, G.D. Holder, A.A. Bishop, J. Gopal and I. Wender, Fuel, 63, 956, (1984).
11. V.I. Stenberg, R.D. Hei, P.G. Sweeny and J. Nowak, Preprints, Div. Fuel Chem., Am. Chem. Soc., 29(5), 63, (1984).
12. S.S. Salim and A.T. Bell, Fuel, 63, 469, (1984).

**Table 1** Benzyl Alcohol - SW Reaction\*

Water Pressure (psi)	0	3870	3870	3870
Added NH <sub>3</sub> (Molar)	0	0	2M	6M
Volatile Products <sup>b</sup> (%Yield)				
Benzene	2.8	2.6	19	21
Toluene	24	20	42	44
Benzaldehyde	0	6.0	9.5	5.5
Biphenyl	0.1	0	2.3	2.6
168 Isomers	3	3	4	5
182 Isomers	8	11	2	2
DHF/Stilbene	0	0	1.6	1.4
Benzylidenebenzylamine	-	-	1.2	1.6
Above 190	8	-	1	3

a. All experiments were at 400C for 3 hrs, all extents of reaction were about 100% and the two experiments without ammonia gave black tarry products, the others gave clear yellow solutions.

b. The numbers represent molecular weights of mixtures, DHF is dihydrophenanthrene.

**Table 2** Benzylidenebenzylamine - SW Reaction\*

Time (h)	1	3	6	9	3	3
Additive	0	0	0	0	6M NH <sub>3</sub>	2g DHA
Volatile Products <sup>b</sup> (%Yield)						
Benzene	22	29	35	34	28	11
Toluene	24	26	28	29	29	54
Benzaldehyde	22	11.0	3.4	2.0	3.1	0
Benzyl alcohol	2.8	2.4	0.2	0.1	0.4	0
Benzamide	0.6	0.4	0	0	0.5	0
Biphenyl	4.1	6.4	7.3	7.2	4.2	0.4
168 Isomers	4	6	7	7	5	-
Fluorene	0.1	0.4	0.6	0.8	0.4	-
Bibenzyl	2.7	2.6	2.0	1.9	3.4	-
Benzophenone	1.3	1.9	1.0	0.8	1.2	-
182-196 Mixture	4	4	2	2	2	-
Above 200	6	6	8	8	15	-

a. All experiments were at 400C and about 3870 psi water pressure. The extents of reaction were all above 95%. All solutions were clear.

b. The numbers represent molecular weights of product mixtures.

**Table 3** Benzoic Acid - SW Reaction\*

Time (h)	3	4	4
Water Pressure (psi)	0	3870	3870
Added NH <sub>3</sub>	0	0	2 M
% Reaction	95	58	100
Volatile Products(%Yield)			
Benzene	80	79	92
Phenol	1.5	0.4	0.1
Biphenyl	3.1	0.4	0.2

\* All experiments were at 400C<sub>446</sub>

**Table 4 Benzaldehyde - SW Reaction<sup>a</sup>**

	1 <sup>b</sup>	6 <sup>b</sup>	1	3	6	1	3	6	1	3	6	3	9	1
Time (h)	0	0	0	0	0	2M	2M	2M	2M	2M	2M	2M	2M	6M
NH <sub>3</sub> (M)	0	0	0	0	0	0	0	0	0	0	0	0	2	0
DHA (g)	0	0	0	0	0	0	0	0	0	0	0	0	2	0
% Reaction	29	76	25	53	71	73	85	93	89	99	99	89	99	94
Volatile Products <sup>c</sup> (% Yield)														
Benzene	70	54	36	49	50	32	41	44	16	18	28	16	18	28
Toluene	6.7	7.3	5.9	8.3	6.4	11	17	21	39	38	12	21	39	12
Benzyl Alcohol	1.7	0	6.8	1.2	0.9	2.1	2.8	2.5	-	-	3.4	2.8	2.5	3.4
Benzoic Acid	10	6.9	14	7.5	4.7	0	0	0	-	-	0	0	0	0
Benzamide	-	-	-	-	-	1.2	1.0	0.7	-	-	2.6	1.0	0.7	2.6
Biphenyl	11	14	3.4	6.1	8.3	4.8	9.2	12	-	-	3.4	9.2	12	3.4
168 Isomers	6	9	2	3	4	2	4	6	-	-	3	4	6	3
166,180-196 Mixture	19	8	10	8	5	6	7	5	-	-	5	7	5	5
Benzylidenebenzylamine-	-	-	-	-	-	2.0	4.3	4.0	-	-	6.1	4.3	4.0	6.1
Above 200	1	3	<1	2	4	20	7	5	-	-	13	7	5	13

a. All experiments were at 400C.

b. These experiments were pyrolyses, the others had about 3870 psi water pressure.

c. The numbers represent molecular weights.

## Chain Transfer During Coal Liquefaction: A Model System Analysis

Concetta LaMarca, Cristian Libanati and Michael T. Klein \*  
Center for Catalytic Science and Technology, Department of Chemical Engineering  
University of Delaware, Newark, Delaware 19716

Donald C. Cronauer  
Amoco Oil Company, Research and Development Department  
Naperville, IL 60566

### Introduction

Coal liquefaction is a complex set of chemical reactions involving coal and solvent that is usually summarized globally in terms of the reaction of solubility- or boiling point-defined product classes. This modelling approach is warranted because both identification and kinetics solution of the large number of elementary reactions governing coal liquefaction is formidable. Nevertheless, the number of elementary reaction families is far less than the actual number of governing elementary reactions, which permits a hybrid molecular/lumped analysis of coal liquefaction kinetics. This also allows some of the rigor of molecular chemistry to be brought to bear on the synthesis of novel coal liquefaction process concepts. The purpose of the present paper is to use a hybrid molecular/lumped analysis of coal liquefaction reaction families to suggest the possibility of optimal chain transfer solvents for the initial stages of coal fragmentation.

The liquefaction reaction families are organized in Figure 1. Bond homolysis, followed by radical capping, is a time-honored view of coal liquefaction that has recently been suggested [1] to constitute only a portion of the overall reaction set. Any coal- or solvent-derived radical can abstract hydrogen from a donor (within coal or from a solvent); these radicals can also induce cleavage of coal bonds through ipso substitution and radical-induced hydrogen transfer (RHT). Kinetically significant  $\beta$ -scission steps are also available to coal- and solvent-derived radicals. Radical recombination and radical addition to olefins, the reverse of bond homolysis and  $\beta$  scission, respectively, are also kinetically significant.

As regards coal liquefaction, steps 1-4 are desirable: they lead to molecular weight reduction. Steps 5 and 6 are undesirable, since they lead to molecular weight growth (these might be termed "primary" retrograde reactions). Increasing the rates of 1-4 relative to 5 and 6 during the initial stages of coal liquefaction would allow for better net fragmentation of the macrostructure. As developed below, this can amount to increasing the kinetic chain length during the initial stages of coal liquefaction.

The reaction families 1-6 collectively possess aspects of a kinetic chain process. Reaction 1 initiates, Reaction 2-4 (and 6) propagate, and Reaction 5 terminates a chain. The essential feature of the chain is its kinetic chain length, i.e., the rate of consumption of coal by steps 2-4 relative to that by step 1. At the condition of steady state, step 1 must be equal in rate to step 5, which is a primary retrograde reaction. As highlighted in Figure 1, a chain transfer solvent will catalyze the desirable kinetic cycle through hydrogen transfer steps, increasing the turnover of the propagation cycle by shuttling H atoms without net consumption of hydrogen;  $\mu_2$  is regenerated in the cycle. A chain transfer solvent will, by definition, have slow  $\beta$ -scission pathways available to  $\mu_2$ . Of course,  $\mu_2$  can terminate with itself or coal-derived radicals, and may also be less reactive than the original coal-derived radical,  $R$ , of Figure 1. Both of these factors would tend to lower the turnover or chain length, which motivates the need for quantitative kinetics analysis.

The classic Rice-Herzfeld (RH) formalism provides a convenient vehicle for the kinetics analysis of the foregoing chemistry. The reaction families of Figure 1 are organized according to the RH formalism in Figure 2, which includes unimolecular bond homolysis, bimolecular hydrogen transfer, unimolecular  $\beta$  scission and bimolecular termination steps for coal and coal-derived radicals. Additional bimolecular hydrogen transfer and recombination steps involve the chain transfer solvent. Note that the propagation cycle, i.e., the hydrogen transfer and  $\beta$ -scission steps, sum to include the RHT step, which is therefore implicitly included in this analysis.

In outline of the remainder of this communication, kinetics analysis of the scheme of Fig. 2 is aimed at resolving the attributes of solvents that will enhance turnover of the propagation cycle, i.e., the kinetic chain length. This analysis will also show, as suggested by McMillen [1], the existence of a solvent of optimal C-H bond strength. In particular, the solvent with the most easily donatable hydrogen is not the best liquefaction

\* Corresponding author.

solvent. We will show that the intrinsic chemistry that controls the catalytic effect of the chain transfer solvent is determined by the difference in reactivities of the coal- and solvent-derived radicals.

### Analysis

Kinetics analysis of the steps of Figure 2 is phrased in terms of the RH transformation of reactant ( $A_1 = \mu_1 H$ ) through free-radical intermediates  $\beta_1$  and  $\mu_1$  to products  $\beta_1 H$  and  $Q_1$ . Chain transfer occurs through the addition of  $A_2$  ( $\mu_2 H$ ), which can donate hydrogen to  $\beta_1$ , or to  $\mu_1$  in the case of slow  $\beta$  scission. The thus-derived  $\mu_2$  radical can abstract hydrogen from  $A_1$  or terminate with another radical. Individually,  $A_2$  is stable and, in particular,  $\mu_2$  does not have a kinetically significant  $\beta$ -scission path. This results in no net consumption of the catalyst  $A_2$ .

The long-chain rate of consumption of  $A_1$ ,

$$r_{A_1} = k_{11}A_1\beta_1 + k'_{21}A_1\mu_2 - k'_{12}A_2\mu_1 \quad (1)$$

can be written in terms of observable species' concentrations by invoking the pseudo-steady state approximation on radical concentrations. The  $\beta_1$  and  $\mu_1$  balances provide the concentrations  $\mu_1$  and  $\mu_2$  in terms of  $\beta_1$ . The equality of initiation and termination rates then provides the final information needed to express  $\beta_1$  (and, thus,  $\mu_1$  and  $\mu_2$ ) in terms of  $A_1$ ,  $A_2$  and the rate constants for elementary steps.

The thus-derived rate expression for the pyrolysis of  $A_1$  in the presence of a chain transfer solvent ( $A_2$ ) is:

$$r_{A_1}(A_1, A_2) = \left( \frac{\alpha_1 A_1}{k_t} \right)^{\frac{1}{2}} \frac{k_{11} A_1 (1 + \hat{k}' \theta' S_2)}{D^{\frac{1}{2}}} \quad (2)$$

where,

$$D = (1 + \hat{k}' S_2 (\gamma_3 + \gamma_5 \hat{k}' S_2) + M_1 (1 + \hat{k}' \theta' S_2) (\gamma_1 + \hat{k}' S_2 (\gamma_3 \phi' + \gamma_4 + 2\gamma_5 \phi' \hat{k}' S_2) + M_1^2 (1 + \hat{k}' S_2)^2 (\gamma_2 + \hat{k}' \phi' S_2 (\gamma_4 + \gamma_5 \hat{k}' \phi' S_2))) \quad (3)$$

In Eqs. 2 and 3,  $M_1 = k_{11}A_1/k_1$ ,  $\hat{k}' = k_{12}/k'_{21}$ ,  $\theta' = k'_{21}/k_{11}$ ,  $\phi' = k_{12}/k'_{12}$ ,  $S_2 = A_2/A_1$  and  $\gamma_i$  is a termination rate constant relative to that for  $\beta_1$  self-termination.

The influence of the chain transfer solvent  $A_2$  is emphasized by considering the enhancement  $E_1 = r_{A_1}(A_1, A_2)/r_{A_1}(A_1)$  of the rate of consumption of  $A_1$  caused by the addition of  $A_2$ . Recognizing  $r_{A_1}(A_1)$ , the rate in the absence of a chain transfer additive, to be:

$$r_{A_1}(A_1) = \left( \frac{\alpha_1 A_1}{k_t} \right)^{\frac{1}{2}} \frac{k_{11} A_1}{(1 + (\gamma_1) M_1 + (\gamma_2) M_1^2)^{\frac{1}{2}}} \quad (4)$$

$E_1$  reduces as:

$$E_1 = \frac{(1 + \hat{k}' \theta' S_2) (1 + (\gamma_1) M_1 + (\gamma_2) M_1^2)^{\frac{1}{2}}}{D^{\frac{1}{2}}} \quad (5)$$

The chain transfer solvent therefore effects rate enhancement through modified rates of chain propagation ( $\hat{k}'$ ,  $\theta'$ ,  $S_2$ ) and chain termination ( $\gamma_1$ ,  $\gamma_2, \dots, \gamma_5$ ,  $\phi'$ ).  $\theta'$  indicates the ease of H abstraction from  $A_1$  by  $\mu_2$  and  $\beta_1$  radicals, and  $\hat{k}'$  is a cross-coupling parameter which compares the propensity of  $\beta_1$  radicals to abstract H from  $A_2$  with that of  $\mu_2$  radicals to abstract H from  $A_1$ .  $\phi'$  describes relative time constants for H abstraction from the shuttle molecule by  $\mu_1$  and  $\beta_1$  radicals, respectively.

Application of Eq. 5 to coal liquefaction reaction families suggests several chemistry-driven simplifications. In many cases  $\beta$  scission is fast relative to H abstraction ( $M_1 \rightarrow 0$ ) which permits the simplification of Eq. 5 to:

$$E_1 = \frac{(1 + \hat{k}' \theta' S_2)}{(1 + \hat{k}' S_2 (\gamma_3 + \gamma_5 \hat{k}' S_2))^{\frac{1}{2}}} \quad (6)$$

In this instance  $\beta_1$  and  $\mu_2$  are the most abundant reaction intermediates. For the reasonable limiting case of equal termination rate constants save the statistical factor of 1/2 for self collision, the denominator simplifies to a perfect square and allows  $E_1$  to be written as:

$$E_1 = \frac{(1 + \hat{k}' \theta' S_2)}{(1 + \hat{k}' S_2)} \quad (7)$$

## Thermochemical Constraint

Further inspection of the controlling dimensionless groups  $\hat{k}'$  and  $\theta'$  shows them to be relative rate constants for a family of hydrogen abstraction reactions. The Evans-Polanyi relation  $E^* = E_0 + \alpha\Delta H_R^1$  for exothermic reactions (EXO) [2] should then provide a reasonable estimate of  $E_1$  in terms of reaction enthalpies and, ultimately, comparative bond strengths [3-9]. The dependence of these dimensionless groups on the relevant bond strengths is illustrated in Table 1, where  $\theta'$  is shown to be a function of  $d_{\beta_1-H}^0$  and  $d_{\mu_2-H}^0$  and  $\hat{k}'$  a function of  $d_{\beta_1-H}^0$ ,  $d_{\mu_2-H}^0$  and  $d_{\mu_1-H}^0$ .

Eqs. 6 and 7 for  $E_1$ , and the expressions in Table 1 for  $\theta'$  and  $\hat{k}'$ , allow illustration of the dependence of  $E$  on  $d_{\mu_2-H}^0$ ,  $d_{\beta_1-H}^0$ , and  $d_{\mu_1-H}^0$ . For a model where coal species are lumped as pseudo component 1, and with the chain transfer solvent as pseudo component 2, it is reasonable to consider  $\beta_1H$  and  $\mu_1H$  as fixed by the coal type and  $\mu_2H$  to be a design parameter. This renders  $E_1$  dependent on  $d_{\mu_2-H}^0$  and  $T$  for a given coal. This dependence is illustrated in Figure 3 for  $T = 400^\circ C$  and  $d_{\beta_1-H}^0 = 87$  kcal/mol, the bond strength for fission of toluene,  $\beta_1H$ , into  $H$  and  $\beta_1$ . Inspection of Figure 3 reveals an extremum in the dependence of  $E_1$  on  $d_{\mu_2-H}^0$ . For low  $d_{\mu_2-H}^0$ , the easily formed  $\mu_2$  radicals are also very stable. Here  $\mu_2-H$  acts as an inhibitor and lowers the rate. At the high  $d_{\mu_2-H}^0$  extreme, highly reactive  $\mu_2$  radicals are formed only with great difficulty. In the limit  $d_{\mu_2-H}^0 \rightarrow \infty$  the additive acts as an inert diluent, and  $E_1 \rightarrow 1$ . In an intermediate regime of  $d_{\mu_2-H}^0$  the enhancement  $E_1 > 1$ . Thus Figure 3 summarizes the homogeneous equivalent of the classic Balandin Volcano curve illustrating the principle of Sabatier.

The effect of unequal termination rate constants (Eq. 6) is illustrated in Figure 4. When, for example,  $\mu_2$  radicals terminate with one one-thousandth the rate constant of  $\beta_1$  radicals ( $\gamma = 0.001$ ), the enhancement is amplified by a factor of about 4.

## Sensitivity to Parameters

Eq. 7 allows more careful delineation of the conditions for enhancement and the location of the maximum of Fig. 3. Clearly  $E_1 > 1$  for  $\theta' > 1$ , or  $d_{\mu_2-H}^0 > d_{\beta_1-H}^0$ . This indicates that the formation of a less-stable  $\mu_2$  radical, relative to the  $\beta_1$  radical, will increase the rate relative to neat pyrolysis. Likewise, for  $\theta' < 1$ , the rate will decrease. But the magnitude of the effect will depend upon the rate of forming the  $\mu_2$  radicals, as shown by the derivative of  $E_1$  with respect to  $\hat{k}'S_2$ . i.e.,

$$\frac{\partial(E_1)}{\partial(\hat{k}'S_2)} = \frac{(\theta' - 1)}{(1 + \hat{k}'S_2)^2} \quad (8)$$

This is positive for  $\theta' > 1$  and negative for  $\theta' < 1$ . Thus the group  $\hat{k}'S$  attenuates the effect dictated by the value of  $\theta'$ . Finally, the curves parametric in  $d_{\mu_1-H}^0$  in Figure 3 intersect at  $\theta' = 1$ , which corresponds to  $d_{\mu_2-H}^0 = d_{\beta_1-H}^0$ , for all values of  $d_{\mu_1-H}^0$ .

Relevant coal model compound data are summarized in Table 2. The enhancement of dibenzyl ether (DBE),  $d_{\mu_1-H}^0 = 78.85$  kcal/mol and  $d_{\beta_1-H}^0 = 87$  kcal/mol) was observed in each of diphenylmethane, triphenylmethane, fluorene, dihydroanthracene, dihydrophenanthrene, and bibenzyl. The chain transfer solvents span a range of both C-H bond strengths [3-10] and termination rate constants. For example, triphenylmethyl radicals are known to be persistent due to steric hindrance to self collision. In this case,  $\gamma_5 \rightarrow 0$  and  $\gamma_3 \ll 1$ , and therefore the effect on DBE pyrolysis is predicted by the uppermost curve of Fig. 4.

Actual coal liquefaction data are consistent with the existence of an optimal chain transfer solvent. McMillen's analysis of the coal conversion data of Curtis [11] in terms of the C-H bond dissociation energy of the liquefaction solvent is summarized in Figure 5. McMillen's observation that the 'optimal' solvent was not that which most easily donated hydrogen (low  $d_{\mu_2-H}^0$ ) supported the hypothesis that the traditionally accepted view of coal liquefaction comprising bond scission and radical capping was incomplete. The likelihood of radical hydrogen transfer (RHT) as a mechanism for the fragmentation of strong bonds was noted. The behavior in Figure 5 is also consistent with the notion of an optimal chain transfer solvent. This suggests that the chain transfer scheme of Fig. 1 may contribute to the overall observable kinetics of coal liquefaction. Further delineation of the contributions of chain transfer, fission, RHT, etc. awaits more detailed accounting of the differences between coal and its model compounds.

<sup>1</sup> For endothermic reactions (ENDO)  $E^* = E_0 + (1 - \alpha)\Delta H_R$

## Conclusions

In summary, kinetic coupling of reaction cycles involving coal and solvent species can result in the presence of an optimal solvent for coal liquefaction. The present analysis permits qualitative prediction of this behavior using the hybrid molecular/lumped chain transfer scheme outlined in Fig. 1. Model compound data are consistent with these predictions.

## References

1. McMillen, D. F., R. Malhotra, G. P. Hum and S.-J. Chang. *Energy & Fuels* 1987, 1, 193-198.
2. Evans, M. G. and M. Polanyi. *Trans. Faraday Soc.* 34, 11, 1938.
3. Stein, S. E. "A Fundamental Chemical Kinetics Approach to Coal Conversion", in *New Approaches in Coal Chemistry*, Blaustein, Bockrath and Friedman, eds. ACS Symp. Ser. 169, Washington D. C., 1981.
4. Benson, S. W. *J. Chem. Ed.* 42 (9) 1965, 502.
5. Bockrath, B., E. Bittner, and J. McGrew. *J. Am. Chem. Soc.* 1984, 106, 135-138.
6. Benson, S. W. *Thermochemical Kinetics*, 2nd ed., John Wiley and Sons, Inc., New York, 1969.
7. McMillen, D. F. and D. M. Golden. *Ann. Rev. Phys. Chem.* 1982, 33:493-532.
8. Billmers, R., R. L. Brown and S. E. Stein. *Int. J. Chem. Kin.* 21, 375-386 (1989).
9. Ogier, W. C., D. F. McMillen and D. M. Golden. *Int. J. Chem. Kin.* (1982).
10. McMillen, D. F., R. Malhotra, S.-J. Chang, W. C. Ogier, S. E. Nigenda and R. H. Fleming. *Fuel* 1987, 66, 1611.
11. Curtis, C. W., J. A. Guin and K. C. Kwon. *Fuel* 63 1404, 1984.

## Acknowledgment

We are grateful for the support of this work by Amoco Oil Company and the Delaware Research Partnership Program.

Table 1: Thermochemical Relationships

Dimensionless Group [D]	- RT ln D = ΔE*		
	EXO/EXO	ENDO/EXO	EXO/ENDO
$\theta' = \frac{k'_{21}}{k'_{11}}$	$[(1 - \alpha)d_{\mu_2H}^0 - \alpha d_{\beta_1H}^0 - (1 - 2\alpha)d_{\mu_1H}^0]$	$[\alpha(d_{\beta_1H}^0 - d_{\mu_2H}^0)]$	—
$\hat{k}' = \frac{k'_{12}}{k'_{21}}$	$[\alpha(d_{\beta_1H}^0 + d_{\mu_1H}^0 - 2d_{\mu_2H}^0)]$	$[\alpha d_{\beta_1H}^0 - d_{\mu_2H}^0 + (1 - \alpha)d_{\mu_1H}^0]$	$[\alpha d_{\mu_1H}^0 - d_{\mu_2H}^0 + (1 - \alpha)d_{\beta_1H}^0]$

Table 2: Experimental Observations of DBE Enhancement in Chain Transfer Solvents

Solvent	E	$d_{\mu_2H}^0$	Explanation	Conclusions
Diphenylmethane	0.8	84±2	( $\theta' = 0.57$ )	$\gamma_5 \sim 0.25$
Triphenylmethane	1.5	75±4	$\gamma < 1$ due to steric hindrance ( $\theta' = 0.025$ )	$\gamma_5 \sim 0.0003$
Fluorene	1.3	81	$\gamma < 1$ due to steric hindrance ( $\theta' = 0.33$ )	$\gamma_5 \sim 0.3$
Dihydroanthracene	0.40	77±2	( $\theta' = 0.077$ )	$\gamma_5 \sim 0.04$
Dihydrophenanthrene	0.37	83	( $\theta' = 0.47$ )	$\gamma_5 \sim 2$
Bibenzyl	0.65	85±3	( $\theta' = 0.69$ )	$\gamma_5 \sim 1.5$

Figure 1

### Coal Liquefaction Reaction Families

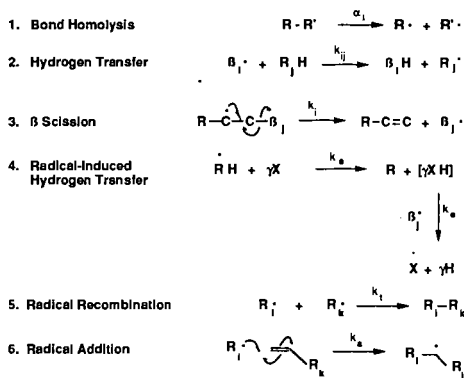
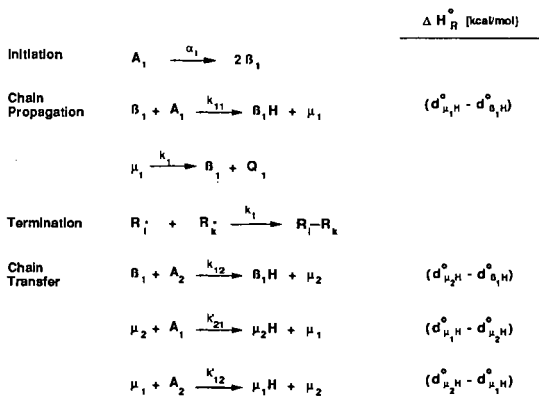


Figure 2

### Rice-Herzfeld Pyrolysis Mechanism

Including Chain Transfer Elementary Steps



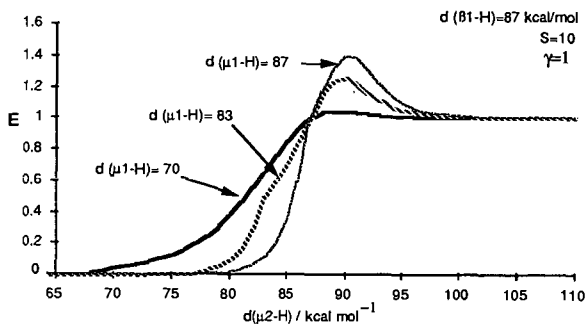


Figure 3 Rate Enhancement due to Hydrogen Transfer Solvent

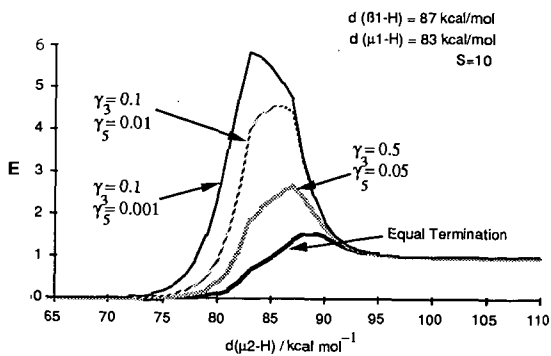


Figure 4 Rate Enhancement due to Chain Transfer Solvent:  
Effect of Unequal Termination Rate Constants

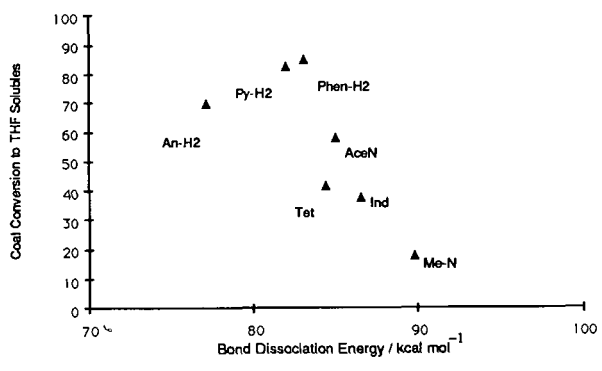


Figure 5 Coal Liquefaction Efficiency

## LASER PYROLYSIS OF AN ENTRAINED STREAM OF COAL PARTICLES

Michael W. Smith, Donald F. McMillen,  
Ripudaman Malhotra, and Robert M. Platz

Chemical Kinetics Department, Chemistry Laboratory  
SRI International, Menlo Park California, 94025-3493

**KEYWORDS:** Coal Pyrolysis, Laser-heated, PCAH additives.

### INTRODUCTION

In the search for efficient ways to convert coals to liquid fuels or other hydrocarbon products, the relative simplicity of pyrolysis has for a long time been recognized as a very attractive feature. However, char yields are typically high and volatile products are generally dominated by light hydrocarbons and tars that can be extremely difficult to upgrade. Efforts to guide research directed toward improved yields in pyrolysis processes have been hampered by the acceptance of a traditional mechanism that is, at best, incomplete (1).

In order to contribute to an improved understanding of the chemical and physical processes that control the formation of volatiles during coal pyrolysis, we have developed an apparatus for pyrolyzing coal particles entrained in cold gas with a CW infrared laser. (2) This approach results in very rapid in-depth heating of the coal to a steady-state temperature, which is determined by the balance between radiative input to the particle and the sum of convective and radiative heat losses to the cold gas. The advantages of this pyrolysis mode are that (i) it provides a very rapid heat-up to a steady state temperature and thus a close approximation to the idealized temperature-jump experiment; (ii) initially produced volatiles are evolved into a cold-gas atmosphere such that secondary reactions obscuring the nature of the original volatiles producing chemistry will tend to be minimized; and (iii) substantial quantities of coal are pyrolyzed making subsequent analysis of the tars and chars possible, something which is not possible with a single-particle approach. The difficulties of the approach involve the necessity to provide very constant flow rates and particle loadings and laser illumination that is constant with time and space in the heated region and is also reasonably omni-directional; the difficulties also involve the inescapable reality that even a narrow physical and aerodynamic particle size distribution will still result in some range of particle velocities, residence times, and steady-state temperatures.

A particular goal of this work is to use entrained-flow laser pyrolysis as one of the tools to explore the benefits that may be achieved by treating coals before pyrolysis with small amounts of high-boiling additives. The rationale for such an approach, along with some preliminary results using conventional heating methods, has been reported previously (3). In brief, in pyrolysis, meeting the stoichiometric and kinetic requirements of bond cleavage is especially crucial: not only is there no solvent to supply hydrogen as there is in liquefaction, but any hydrogen fed to the reaction zone is known (4) to be relatively ineffective at short reaction times and temperatures below  $\sim 700^{\circ}\text{C}$ . Therefore, it may be possible to achieve substantially increased yields of condensable volatiles, if pre-treatment with partially hydrogenated coal tars can (i) supply a small amount of critically needed hydrogen in a kinetically accessible form, and (ii) increase the efficiency with which the indigenous coal hydrogen can itself be shuttled from hydrogen-rich portions of the coal structure to more hydrogen-poor regions to aid in bond cleavage. Figure 1 summarizes the way by which polycyclic aromatic hydrocarbons (PCAH) tend to increase H-utilization efficiency in light of recently described chemistry (5-7): PCAH can serve to recover hydrogen atoms that have been transferred to positions where no linkage cleavage can occur. This recovery helps to re-direct hydroaromatic hydrogen from light hydrocarbon formation (ring-reduction and cracking) to cleavage of inter-cluster linkages.

## LASER PYROLYSIS TECHNIQUE

### Particle Flow

Schematic diagram of the laser-pyrolysis apparatus is shown in Figure 2. The coals are ground under nitrogen (or in the case of the Argonne -100 mesh samples, taken directly from the vials), wet-sieved, and dried for 18 hours under vacuum at 65°C. Several grams of the 270/230 mesh fraction (nominal 53 to 63  $\mu\text{m}$ ) are loaded into the hopper of a rotating-disc dust-feeder which feeds a fluidized bed, using argon as the entrainment gas. This bed in turn feeds the inlet of the 3-mm id ejector tube, the outlet of which is just downstream of an aluminum honeycomb flow straightener, and 3 to 5 mm upstream of the region where the IR laser beam crosses the axis of particle flow. The length of the illuminated region can be varied from 3 to about 20 mm. Condensable volatiles are either ejected from the pyrolyzing coal particles as an aerosol, or quickly form one when they hit the cold argon stream. Several mm downstream of the heated zone, the tar-aerosol and char particle stream enter a collector with an 8-mm id and a conical interior that smoothly decreases to 3 mm. The flow then passes through a miniature cyclone designed to collect particles larger than ca. 10  $\mu\text{m}$ . The tar aerosol (typically 0.2 to 0.3  $\mu\text{m}$  diameter), and any other small particles, pass through the cyclone and are collected on one of a pair of filters in a parallel-flow filter arrangement.

The char-tar separation is typically very good: microscopic examination shows the cake on the final filter to consist of tawny yellow tar aerosol particles, entirely free of black coal- or char-particles of any size. The cyclone contained all the char, with small amounts of tar aerosol attached to some of the char particles, evidently as the result of collisions within the cyclone. Since the aerosol particles were ca. 0.3  $\mu\text{m}$ , as compared with the ca. 50- $\mu\text{m}$  char particles, the mass fraction of tar contaminating the char was very low; typically less than 5%. This tar contamination could easily be removed from the char by a quick THF wash, either before char analysis, or for purposes of correcting the % yield of tar.

### Gas Flow Control

The flow control system leading to and from the laser pyrolysis apparatus consists of four streams: the ejector- and collector- flows, and the ejector- and collector- sheath flows. Because flow through the ejector tube (ca. 50 cc/min) is not controllable directly, but is constrained to be equal to the sum of the collector- and the collector-sheath- flows minus the ejector sheath flow, and the two sheath flow are each about 5 liters/min, small percentage changes in either of the sheath flows would result in a large percentage change in the ejector flow. Therefore, fine positive control of the sheath gas is maintained by routing ca. 97% of their flow through single-stage regulators and over a fixed flow-control orifice. The remaining 3% is shunted through a pair of 0 to 500-cc/min mass flow controllers (Tylan). The flows are adjusted to control the ejector gas flow at the desired volumetric flow, typically set so that the ejector and its sheath flow have nearly equal space velocities.

### Laser Beam Manipulation

The beam from a Coherent Model 41 CW CO<sub>2</sub> laser is passed through an 8-mm orifice in a graphite disc to remove the fringes, and is then directed to the cell by two flat and one slightly concave (20-m radius of curvature) copper mirrors. Immediately in front of the pyrolysis cell, the beam is focused through a point using a 1-in focal length zinc selenide lens, and allowed to expand into a channel integrator consisting of polished aluminum plates bolted together to form a channel having a 6.5-mm square opening. The divergent radiation that exits this channel is then imaged with a second lens through the KCl window in the pyrolysis cell and onto the axis of particle flow. The "beam" diverges after passing through the particle stream, and is re-imaged back on the flow axis by a concave copper mirror on the back side of the cell. The radiation that is not absorbed by the second pass diverges as it exits through the KCl window and is absorbed by a graphite beam block.

As shown schematically in Figure 3, the channel integrator converts the Gaussian profile of the laser beam into a profile that, on a microscopic scale, is flat across the entire image. Fresnel diffraction results in a series of peaks and valleys in the intensity, but these are on a microscopic

scale, with the peak-to-peak distance being ca. 200  $\mu\text{m}$ , and are suitably averaged by retro-reflection under conditions where the stream of particles is optically thin.

### Pretreatment of Coals and Product Analysis

The additive used in this work was a partially hydrogenated coal tar. The field ionization mass spectrum of the parent tar is shown in Figure 4. The spectrum clearly indicates that the tar is composed almost entirely of polycyclic aromatic hydrocarbons, with the most prominent PCAH structure being pyrene. In the spectrum obtained after hydrogenation (not shown), examination of the various M+2 and M+4 peaks shows that the degree of hydrogenation increases with increasing ring size. For example, ~22% of the pyrene, but 37% of the di-benzopyrenes were converted by the mild hydrogenation to di- or tetra- hydroaromatics. The coals were loaded with 8 to 10% of the hydrogenated tar, using tetrahydrofuran (THF) as the solvent employing the technique of incipient wetness to minimize preferential deposition of the additive at the particle surface and/or THF-extraction of soluble materials from the coal. The THF was removed by drying in a vacuum oven at 65°C for 18 hours. Some pyrolysis experiments were performed with THF-only treated coals to serve as appropriate blanks.

The primary analytical technique used thus far for examination of the tars and the chars has been field ionization mass spectrometry (FIMS). The use of the instrument at SRI has been extensively described in the literature (8); a series of unit-resolution mass spectra are recorded as the sample is heated in a temperature-programmed inlet (typically at 3°C/s, up to 450°C). From these data, the temperature evolution profile of any nominal mass or group of masses can be plotted, including a vacuum evaporation - or micro distillation- curve representing the sum of all volatiles. Although nominal mass provides no direct identification of the molecular formula of the particular molecular ion, in the low molecular weight range (m/z 50-150), and for prominent peaks at certain characteristic masses above that range, inspection can usually provide very reliable identification (8).

## RESULTS AND DISCUSSION

### The Impact of Pretreatment on Tar Yields

Figure 5 shows the impact of the tar pretreatment under laser-pyrolysis conditions, and for comparison, Figure 6 shows the impact observed under vacuum TGA conditions. (All of the yields were based on the assumption that the tar added in the pretreatment was itself fully volatilized.) Under the laser-pyrolysis conditions used thus far, the pretreated Pittsburgh No. 8 (Argonne) showed a substantial increase in tar yield (20%), but the pretreated Illinois No. 6 and Wyodak coals (Argonne), gave average corrected yields that were actually significantly lower than those for the untreated (but dried) coal. On the other hand, pyrolysis under TGA conditions resulted in 31 and 11% increases in yields of total volatiles for the pretreated Wyodak and Illinois No.6 coals, respectively, as well as an increase of 24% for the pretreated Pittsburgh No. 8 (Clovis Point Mine, and PSOC coals 1098 and 1099, respectively). The pretreated and the blank coals were not exactly identical in the two sets of pyrolysis experiments. However, for the reasons discussed below, we believe that the smaller benefit and less consistent improvement obtained under laser pyrolysis conditions resulted primarily from the fact that the final pyrolysis temperatures in the laser pyrolysis were more than 200°C higher. We therefore project that improving the yield-enhancing impact of the pretreatment entails pushing the laser-pyrolysis conditions further towards lower temperatures and longer times.

Since the amount of hydrogen actually supplied by the hydroaromatics added in the pretreatment is very small, it is important that this hydrogen be used with maximum efficiency, and that the added PCAH operate with maximum effectiveness in promoting the use of indigenous hydrogen. In order to meet these criteria, it is necessary to reach the temperature region of widespread radical reactions (i.e., 400 to 500°C), as these reactions are what bring about the H-atom transfer that results in hydrogenolysis. However, as the temperature increases, the PCAH in the reaction mixture are less and less able to recover hydrogen transferred to positions bearing no linkages (1,7). Optimum temperatures for conversion will thus be a compromise between reactivity and efficiency in hydrogen utilization.

We based our initial choice of conditions for the TGA pyrolyses that might constitute such a compromise on the work of Fong and Howard (9) on the evolution of volatiles and extractables

during coal pyrolysis. These authors report data showing that the yield of pyridine extractables generally goes through a maximum at the temperature at which the rate of volatiles production is highest. In general terms, this coincidence reflects the long recognized fact that in pyrolysis, an initially formed "bitumen" undergoes a disproportionation into a relatively hydrogen-rich volatiles fraction and a hydrogen-poor char fraction. As the temperature at which this disproportionation occurs is passed, the volatiles-forming reactions become progressively more dominated by gas-forming reactions such as dealkylation of small side chains, decarbonylation, and dehydrogenation, and production of large organic volatiles becomes no longer possible. Thus the maximum opportunity for influencing the "disproportionation" process so as to increase the volatiles, and decrease the char will likely come at the point where the natural volatiles formation rate is the greatest, and before rapid H<sub>2</sub> formation squanders whatever hydroaromatic hydrogen is available in the additive or in the coal structure itself. We speculate that the best use of a hydrogen-donor additive in a pyrolysis process, where there is no large confining pressure, will be made by going very rapidly to this temperature region, and then holding the temperature there.

In the rapid heating (1000°C/s) studies of Fong (9), the maximum volatiles formation rate occurred at a nominal temperature of about 600°C, but at the maximum heating rate achievable in the TGA apparatus used in this work (< 7°C/s), the volatiles formation rate was maximum at about 450°C. Therefore, we tested the impact of additives by raising a furnace, previously heated to 900°C, around the quartz tube containing the sample, and when a temperature of 450°C was reached, quickly lowering the furnace. Since the quartz tube cooled slowly compared to the rate at which it was heated, this procedure approximated the desired regimen, but the heating rate was slow enough that blank experiments with the tar additive loaded onto charcoal showed that a large fraction of the tar additive vaporized by the time the pretreated coal reached 450°C.

By comparison, the laser-pyrolysis, with a heating rate of about 10,000°C/s, should bring the pretreated coal to ca. 500°C while most of the additive is still within the coal matrix. Since the temperature of maximum volatiles formation in a linear heating-rate experiment is a function of heating rate, we expect the optimum temperature with laser-heating to be 100 to 200°C above that for the slower heating-rate pyrolysis. Unfortunately, the data shown in Figure 5 were generated when the residence time or "hold time" at maximum temperature was only ~0.1 s, and substantial tar formation is not observed in this short a reaction time unless the final temperature is above 700°C. We chose an upward flow in the pyrolysis cell to move the particles as slowly as practical. However, the distributions of aerodynamic particles sizes used thus far have not been narrow enough to allow successful entrainment at space velocities less than ca. 10 cm/s above the nominal settling velocity of 50-µm coal particles. We anticipate that the use of coal particles having a narrower aerodynamic size distribution, as well as a narrow physical size distribution, will enable us to improve the entrainment and increase the residence time to 0.5 to 1 second, and thus to lower the final pyrolysis temperature substantially.

### Characteristics of Laser-Pyrolysis Tars

The tars produced by pyrolysis of the coals in a stream of cold gas, and as collected on the final filter, consist of agglomerates of light yellow spheres, quite evenly sized at about 0.2 to 0.3 µm. Although they contain substantial amounts of rather low boiling materials (e.g., phenol, cresols, etc.), these aerosol particles are not very sticky at room temperature, and do not coalesce when scraped of the filter with a spatula. Upon exposure to air at room temperature, they turn black in several hours.

Several samples of the laser pyrolysis tars have been subjected to FI mass spectrometry. Figure 7 shows the spectra obtained for the tars from the Argonne Pittsburgh No. 8 and Wyodak coals. The volatility of the tars, under the FIMS analysis conditions (heated to 450°C at 3°C/s under a vacuum  $\leq 10^{-6}$  Torr) ranges from 57% for some of the Illinois No. 6 tars, to 90% or above for the Pittsburgh No. 8 and Wyodak tars. Since any fossil fuel material that has been through a distillation process (whether atmospheric or vacuum) is typically completely volatile (> 95%) in FIMS analysis, either a substantial part of the Ill. No. 6 tar is ejected as an aerosol without ever being in the vapor phase, or retrograde reactions converted a substantial fraction into non-volatile materials. Since the tars are ejected into a cold, inert atmosphere, where the cooling rate is in excess of 1000°C/s, we judge that any retrograde reactions that did not occur before the tar left the hot coal particle would be unlikely to occur after leaving. Thus the FI mass spectral analyses that are discussed below should be considered representative of the tar as it left the coal particle.

The yields of tars produced in the laser pyrolysis appear, as shown in Table 1, to be about 1.5 times larger than those obtained by Khan et al. (10) in a hot-gas, entrained-flow reactor (hot-tube EFR reactor) with a final temperature of 1100°C. However, uncertainty over what fraction of materials detected in the vapor state (e.g., "olefins") in the work of Khan would be found in the tar from the laser pyrolysis precludes a definitive comparison at this time. Therefore in this report we will focus on some of the differences in the character of the tars produced from the Argonne Pittsburgh No. 8 and Wyodak coals using each of these two rapid-heating entrained-flow pyrolysis techniques. (We reiterate that laser-pyrolysis has no process implications as such. The use of an IR laser in laboratory studies has value insofar as it leads to an increase in fundamental understanding and/or in the ability to improve yields in technologically important processes.)

In general terms, the tars from the Pittsburgh coal are rather similar, whereas those from the Wyodak show some marked differences. For example, in the Pittsburgh tars, the fractions constituted by cresols, dihydroxybenzenes, and the sum of alkylbenzenes and tricyclic alkanes are equal within 30%. However, in the Wyodak tars, the percents of dihydroxybenzenes and the most abundant acyclic alkanes are three and two times larger, respectively, in the laser-pyrolysis tar than in the hot-tube tar. Thus, in the tar that was evolved into a cold gas stream, the abundance of what is presumably the most retrogression-prone class of phenolics -- dihydroxybenzenes -- is substantially higher. What is perhaps more surprising is that the concentration of certain alkanes is also higher in the laser pyrolysis tars. Although there is hardly enough evidence yet to draw a definitive conclusion, a possible rationalization is that when the dihydroxybenzenes (or their precursors) undergo retrograde reactions, they tend to take the some of the alkanes (or their precursors) with them.

A still more striking comparison is that between the FI mass spectra of the laser-pyrolysis tar and that produced from the in-situ pyrolysis of the Wyodak coal in the temperature-programmed inlet of the mass spectrometer (Py-FIMS); the latter is shown in Figure 8. In the spectrum of the laser-pyrolysis tar (Figure 7b) the highest peak among the phenolics ( $m/z$  124, methyl-dihydroxybenzene) and the highest peak of the acyclic alkanes show intensities that are within 40% of each other, whereas in the Py-FIMS, the intensity of  $m/z$  124 is three times that of  $m/z$  268. Because any volatiles produced during Py-FIMS are evolved into a high vacuum, there is negligible opportunity for secondary gas phase reactions; therefore, any increased retrograde reaction under Py-FIMS conditions must be a result of a heating rate that is about three thousand times slower. At this point we cannot say whether the relative enhancement of such retrograde processes is an inherent result of reaction at lower temperatures during the slow heating, or merely reflects a greater chance for retrograde reaction during the slower transport of volatiles once they are generated within the coal.

Comparison of the temperature evolution curves for the most abundant single-ring monohydric and dihydric phenols (xyleneols and methyl dihydroxybenzenes) reveals a rather striking difference between the tars from the two entrained flow techniques. Figures 9 and 10 show that in the laser-pyrolysis tar essentially all of the material in both classes is preexisting in the tar. In the tar generated in the hot-tube reactor on the other hand, most of the monohydric phenols and a good part of the dihydric phenols are pyrolytically generated on the hot probe during the FIMS analysis, as seen from the fact that they are observed at much higher temperature. The difference between the two types of tars is even more pronounced than it appears in Figures 9 and 10, since what is plotted there is the fraction of the total observed in each case for each molecular ion. As shown in Table 1 and discussed above, for the Wyodak coal, the total amount of dihydric phenols in the laser pyrolysis tar is 3.3X higher than that seen in the EFR tar.

The above differences cannot be attributed entirely to a different distribution of volatiles between gases and tars in the two pyrolysis techniques. Since the hot-tube reactor tars were produced by heating the coal to 1100°C and the tars were originally evolved into a hot nitrogen stream, one might have expected the relatively low-boiling phenols to have been much more "distilled" out of the tars during the collection, and a greater fraction of those low molecular phenols that were seen might be expected to have been formed by pyrolysis on the hot FIMS probe. However, in three of the four curves shown, the situation with the laser pyrolysis tars was not merely that there were more preexisting phenols, but that there was essentially no phenol generation during analysis of the laser-pyrolysis tars. Thus we are forced to say that even though one might have expected the higher temperature, longer residence time, and hot-gas atmosphere in the EFR to have produced tars that were more "evolved" and therefore more refractory, they were

not more refractory. It could be that the greater opportunity for oxidative coupling reactions provided by the hot-gas environment of the hot-tube reactor provides coupling products of dihydroxyaromatics that subsequently gave monophenols on the heated FIMS probe. This scenario would be consistent with the substantially lower levels of dihydroxybenzenes seen in the Wyodak hot-tube tars, and also with the higher total tar yields observed in the laser pyrolysis.

In summary, although the chemistry responsible for formation and evolution of oxygenates in coal tars is still largely unknown, the above data from laser pyrolysis in a cold-gas atmosphere are helping to delineate the factors that control the types and amounts of phenolic structures present in pyrolysis products. At this stage, we can make the following tentative conclusions:

- The laser-pyrolysis tar yields appear to be higher than from those produced in hot-tube pyrolysis of the same coals at equal or greater severity.
- The differences between entrained-flow laser-pyrolysis tars and entrained-flow hot-tube pyrolysis tars are much greater for Wyodak coal than for Pittsburgh No. 8 coal.
- The laser-pyrolysis tars contain substantially more low-molecular weight monophenolic and diphenolic structures than do the entrained-flow hot-tube pyrolysis tars.
- These phenolics, which undergo facile oxidation, are presumably responsible for the initial pale yellow tars turning black upon exposure to air.

## REFERENCES

1. D. F. McMillen, R. Malhotra, S. E. Nigenda, *Fuel*, **1989**, *68*, 380.
2. D. F. McMillen, R. Malhotra, M. W. Smith, "Cleavage and Crosslinking of Polymeric Coal Structures during Pyrolysis," DOE Quarterly Report, Contract No. DE-AC21-87MC23286, August 1989.
3. R. Malhotra, G. A. St. John, D. S. Tse, D. F. McMillen, *Am Chem Soc, Div Fuel Chem. Preprints*, **1988**, *33(2)*, 257.
4. J. B. Howard, "Fundamentals of Coal Pyrolysis and Hydrolysis," in *Chemistry of Coal Utilization, Second Supplementary Volume*, M. A. Elliott, Ed., John Wiley and Sons, New York, 1982, p. 665.
5. D. F. McMillen, R. Malhotra, S.-J. Chang, W. C. Ogier, S. E. Nigenda, R. H. Fleming, *Fuel*, **1987**, *66*, 1611.
6. R. Malhotra and D. F. McMillen, "A Mechanistic Numerical Model for Coal Liquefaction Involving Hydrogenolysis of Strong Bonds. Rationalization of Interactive Effects of Solvent Aromaticity and Hydrogen Pressure," , submitted to *Energy and Fuels*.
7. D. F. McMillen, R. Malhotra, and D. S. Tse, "Interactive Effects Between Solvent Components: Possible Chemical Origin of Synergy in Liquefaction and Coprocessing," , submitted to *Energy and Fuels*.
8. See, for example: M. M. Boduszynski, *Energy and Fuels*, **1987**, *1*, 1
9. W. S. Fong, W. A. Peters, and J. B. Howard, *Fuel*, **1986**, *65*, 251.
10. M.R. Khan, M. A. Serio, R. Malhotra, and P.R. Solomon, *Am. Chem. Soc. Div. Fuel Chem. Preprints*, **1989**, *34(4)*, 1054.

Table 1  
 YIELDS OF TAR AND SELECTED PHENOLIC AND ALIPHATIC COMPOUNDS  
 IN LASER- AND HOT-TUBE<sup>1</sup>-COAL PYROLYSIS

Coal	Pyrolysis Technique/ Run No.	T <sub>final</sub> °C	% Tar Yield <sup>2</sup>	Tar/ Char	% FIMS <sup>3</sup> Volatility	% Total Ion Intensity <sup>4</sup>			
						m/z			
						122	124	260	268
WYODAK (Argonne)	LP/6-8-89-3	750	17.4	0.28	90	0.18	0.77	0.43	0.63
Pitts No. 8 (Argonne)	LP/6-13-89-2	925	27.4	0.64	92	0.11	0.11	0.38	0.24
ILL No. 6 (Argonne)	LP/5-26-89-1	880	29.2	0.57	71	0.13	0.29	0.36	0.34
WYODAK (Argonne)	HT	1100	7.71	0.18	86	0.067	0.23	0.31	0.32
Pitts No. 8 (Argonne)	HT	1100	21.84	0.46	63	0.075	0.057	0.18	0.30

<sup>1</sup>Data taken from the hot-tube entrained-flow pyrolysis results in Reference 10.

<sup>2</sup>In LP, % tar yield is derived from the collected weights of tar and char, by assuming the same gas yield reported in the 1100°C, hot-tube pyrolyses of reference 10. This gas yield will be an over-estimate, because of both the lower final coal temperatures of the LP runs and the cold gas atmosphere in the laser pyrolysis.

<sup>3</sup>Wt. % volatilized from probe at 450°C under high vacuum.

<sup>4</sup>m/z 122 corresponds to methyl cresols, 124 to methyl dihydroxybenzenes, 260 nominally to tetra-cyclic alkanes and alkyl-benzenes, and 268 nominally to acyclic alkanes. The % ion intensity values do not exactly equal mole %, owing to differences in sensitivity factors. However, the relative % changes in intensity values from one sample to another are expected to be reliable.

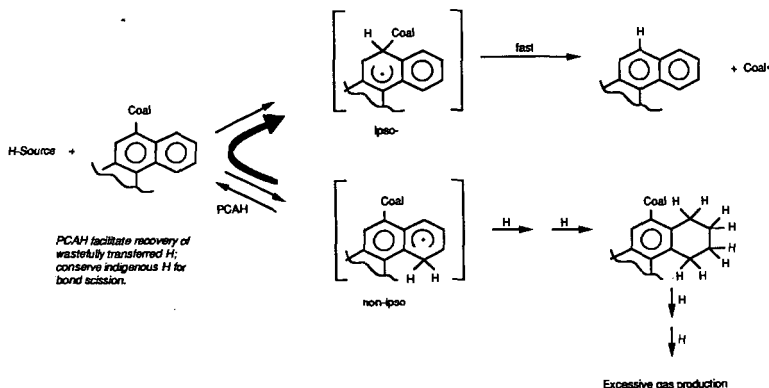


Figure 1. Rationale for Using Additives Rich in Polycyclic Aromatic Hydrocarbons (PCAH).

Premises: 1. Significant contribution of Induced bond cleavage.

2. Factors enhancing IBS also tend to minimize retrogressive reactions.

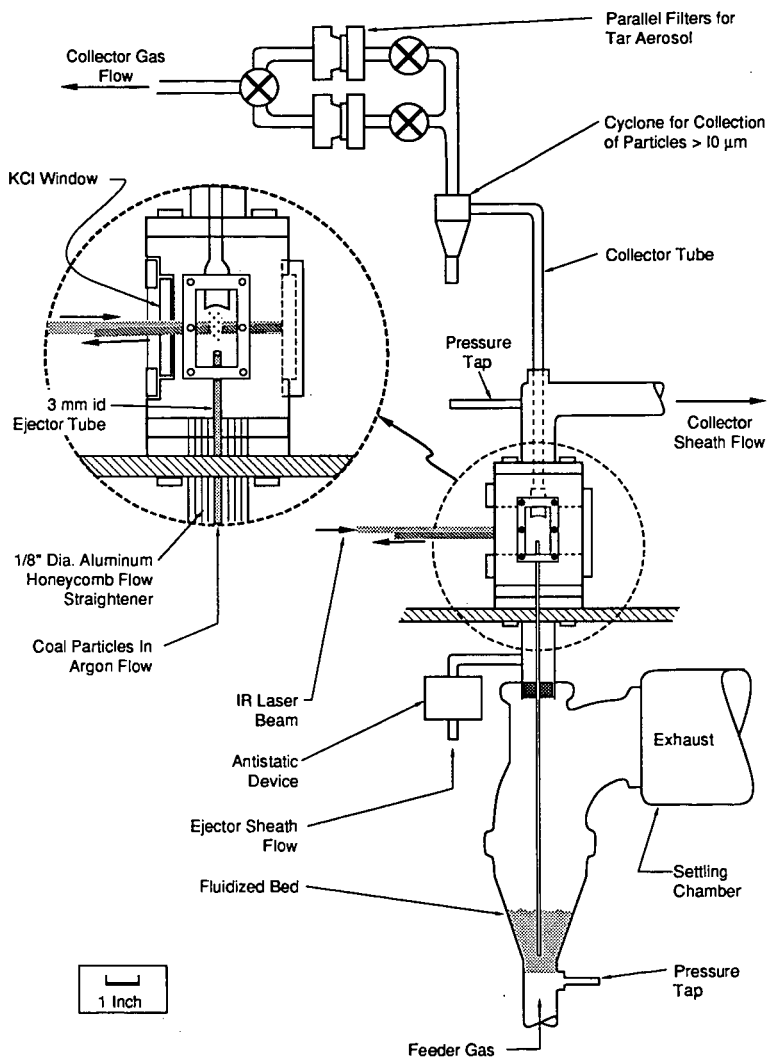


Figure 2. Schematic of entrained-flow laser pyrolysis apparatus.

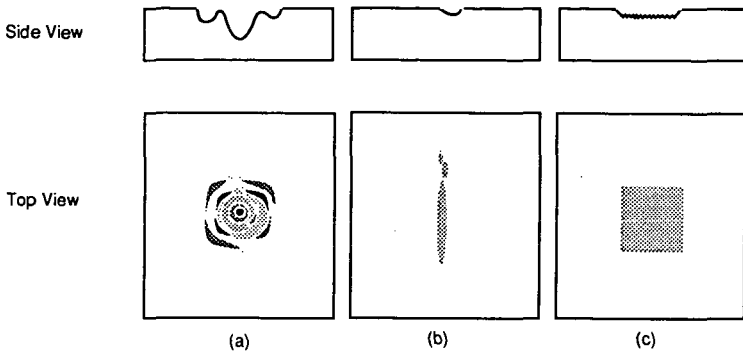


Figure 3. Schematics of burn patterns produced in acrylic pieces using (a) apertures, (b) beam expander, or (c) channel integrator in the optical configuration.

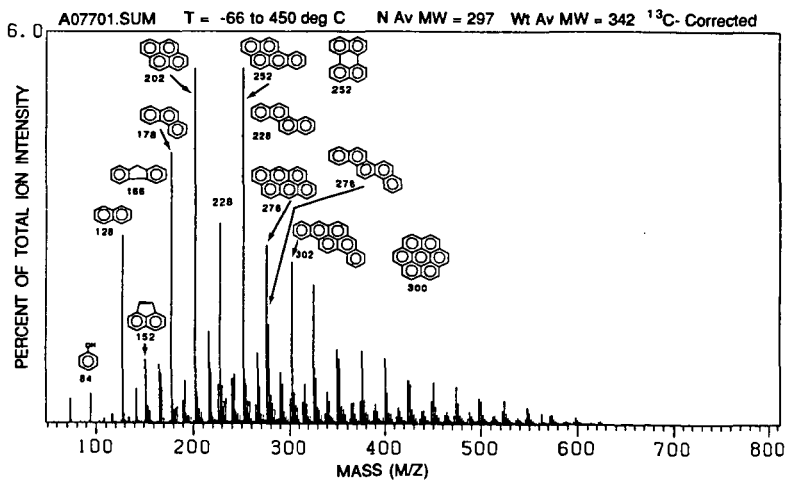


Figure 4. Field ionization mass spectrum of the coal tar prior to hydrogenation. Note that the tar is rich in PAH essentially devoid of alkyl substitution.

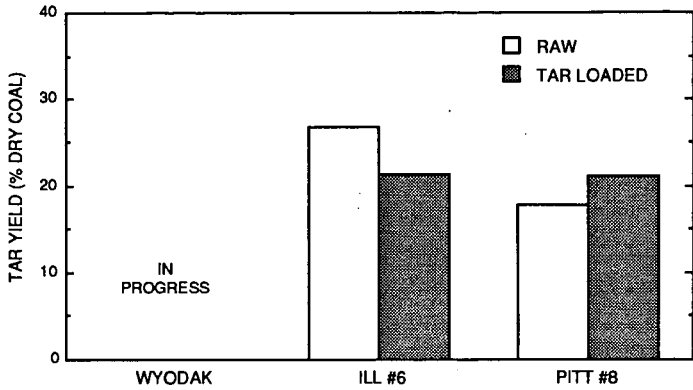


Figure 5. Effect of loading hydrogenated coal tar on the tar yield during laser pyrolysis. Maximum temperature of about 880°C for the ill. #6 coal and 840°C for Pitt. #8 coal.

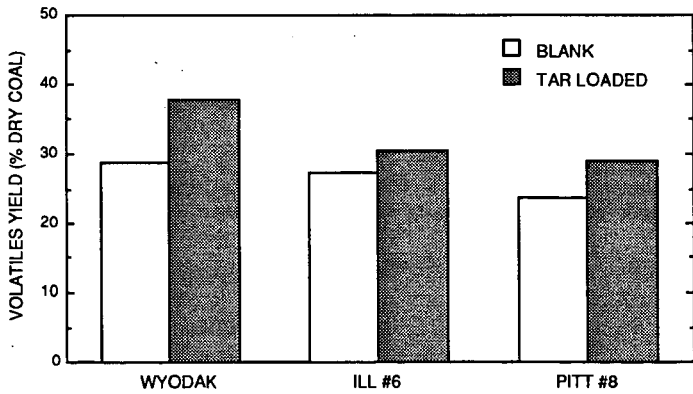
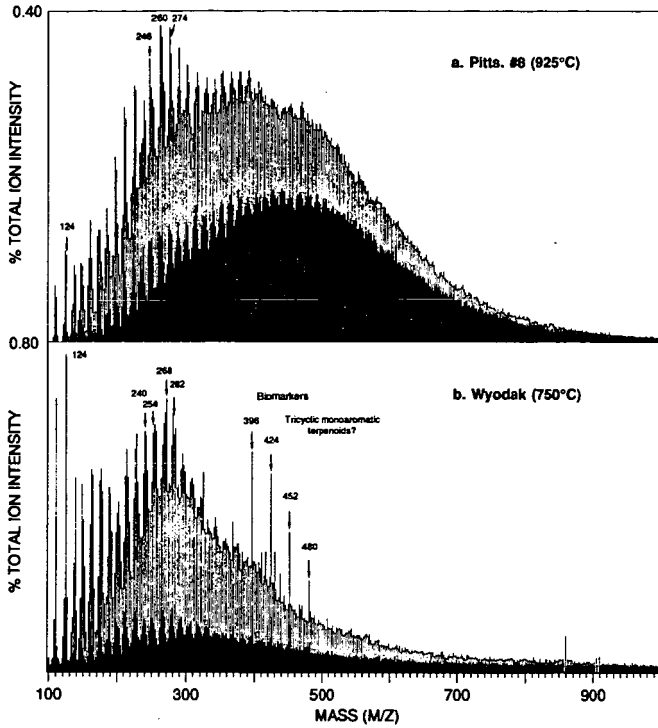


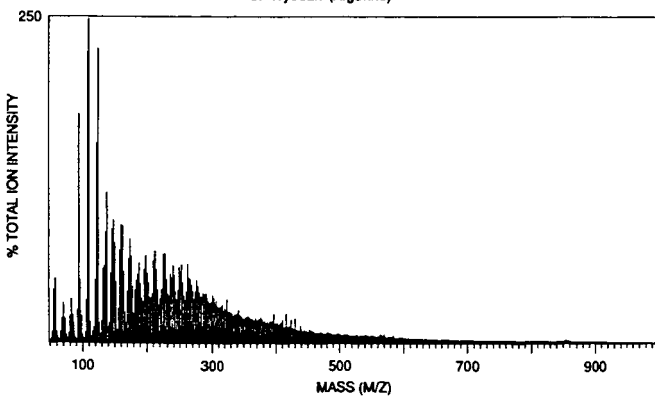
Figure 6. Effect of loading hydrogenated coal tar on volatiles yield during vacuum pyrolysis to a maximum temperature of about 450°C.



RA-4159-3

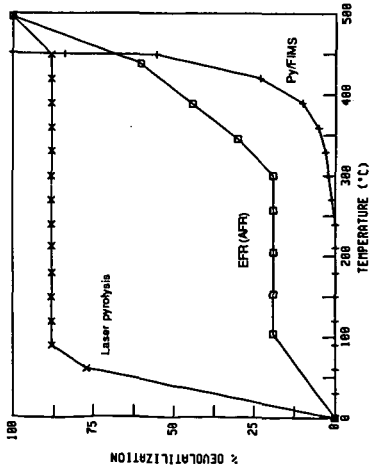
Figure 7. FI mass spectra of laser pyrolysis tars.

- a. Pittsburgh No. 8 (Argonne)
- b. Wyodak (Argonne)



RA-4159-4

Figure 8. Py-FIMS of Wyodak coal (Argonne Premium Coal Sample Program).



466

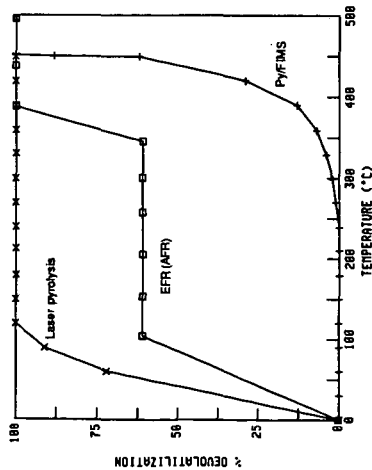


Figure 9. Temperature evolution profile of phenolics during FIMS analysis of laser-pyrolysis tar and tar from entrained flow pyrolysis in a hot tube (EFR), compared with the evolution during in-situ pyrolysis in the FI-mass spectrometer (Py-FIMS) of the Argonne Pittsburgh No. 8 coal. (a) monohydric phenols (m/z 122); (b) dihydric phenols (m/z 124)

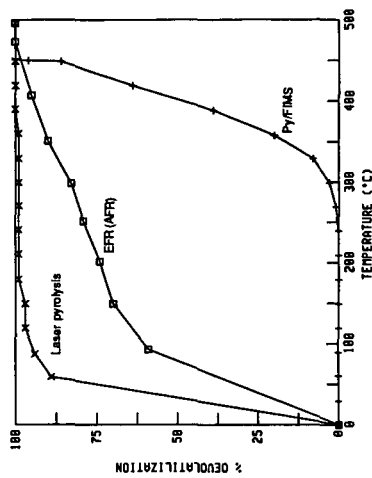
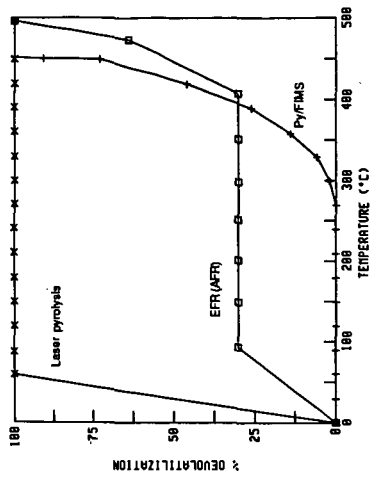


Figure 10. Temperature evolution profile of phenolics during FIMS analysis of laser-pyrolysis tar and tar from entrained flow pyrolysis in a hot tube (EFR), compared with the evolution during in-situ pyrolysis in the FI-mass spectrometer (Py-FIMS) of the Argonne Wyodak coal. (a) monohydric phenols (m/z 122); (b) dihydric phenols (m/z 124)

## CHARACTERIZATION OF COAL BY PYROLYSIS

A. Björkman and P. Simonsen  
Technical University of Denmark  
Lyngby, Denmark

### 1. Introduction

Coal characterization is an old subject. The heating value is a major important figure from an economic point of view. The common classification in ranks, however, has been associated with the coking properties and is usually based on the volatile matter content. Its value for the firing (and gasification) of coals is limited. One indirect method - vitrinite reflection is based on petrographic correlation. Also DTA and TG measurements are studied, but have not gained much use as yet.

The annual report 88/89 of IEA Coal Research gives some comments on the matter, stating that characterization should identify properties, that are critical to the performance of the coal. There is a need for better evaluative tests, based on modern techniques, but it is considered unlikely that methods can be devised in the near future, which are both specific, good for all coals and still simple.

Considering these methods and other characterization measurements, which are mainly analytical, it may be stated, that no method does really try to relate measured properties of coal with its burning characteristics, except for the somewhat primitive "drop-tube burning". Studies of the behaviour of coal particles in flames - usually contrived as some pyrolysis/gasification model - can be considered as characterization but may not easily produce figures for inherent coal properties.

The suggested approach, presented here, emphasizes pyrolytic properties of coal. A small sample is subject to a rapid well controlled laser-induced pyrolysis, followed by an equally controlled gasification, using a microbalance, to estimate the reactivity of the char, formed by the pyrolysis. The principal aim is not to contribute to the fundamental understanding of coal burning but to add - by the use of advanced equipment - to the empirical comprehension of burning properties of coal.

The purpose of the proposed measurements is thus related to the pyrolysis and gasification, which occurs during practical firing, where the time and intensity of pyrolysis may vary considerably between coal particles. The way a particle responds to pyrolysis is known to influence the char reactivity and may thereby determine the final burning (gasification). The approach presented here is apparently not attempted before.

The use of a very small sample is necessary to achieve a rapid pyrolysis with a laser beam, which in turn necessitates the use of a microbalance for the gasification step.

### 2. Equipment and procedure

#### Sample preparation

Coal powder (< 270 mesh) is pressed to a thin disc (< 0.1 mm) and cut to a circular specimen (4.5 mm), which is laid in a tiny quartz glass crucible and its weight recorded. It was established experi-

mentally, that the thickness of the specimen must be restricted to a maximum thickness of about 1 mg.

#### Rapid pyrolysis

The sample crucible is placed in a pyrolysis chamber (Fig. 1), which is flushed with pyrolysis atmosphere (usually He), and possibly pressurized. A glass window allows radiation of the sample with a laser beam, and a portion of the resulting gas may be sampled through a rubber septum, using a syringe.

A Neodym/YAG laser has been used, giving a beam, coaxial with sample and having the same width. The beam energy could be increased up to 14 J and given 1 to 20 ms duration. The pyrolysis gas was analyzed in a Perkin Elmer 8500 gaschromatograph with double detectors, combined to monitor for  $H_2$ , CO,  $CH_4$  (conjunct),  $C_2H_2$ ,  $C_2H_4$ ,  $C_2H_6$  and  $C_3H_6$ .

About 90% of the tar formed did deposit on the crucible wall, but no attempt was made to analyze or characterize this product. It would have been a difficult undertaking as such and could not be accommodated in the project.

#### Reactivity rating

The char disc (about 1 mg) from pyrolysis can easily be transferred to a clean crucible. It is vital that this crucible is handled carefully to avoid any generation of static electricity. The char is covered with a thin layer of quartz wool to assure that no char (or ash) is lost.

The gasification is made in a (locally built) apparatus, seen in Fig. 2, which is for the most part selfexplaining. A Satorius electronic ultramicrobalance (type 4436 MP8) has been used. It is important that the filament (steel + Pt), which carries the char crucible, is centered to avoid any contact to the furnace wall. It is also important to avoid any movement of the balance, when the hanging furnace is heated, which explains the use of an expansion joint. A small stream of nitrogen is used to protect the balance and to keep an unchanged atmosphere around the counterweight.

A partly perforated mixing section at the furnace top protects the filament and gives complete mixing of the two gas streams. Temperatures up to 950°C for  $H_2O$  or  $CO_2$  could be used but most experiments were run (with  $O_2/Ne$ ) at about 430°C. The temperature variation in the furnace chamber could be kept within 1°C.

After insertion of quartz crucible, the gasification is started with extended flushing of the furnace with  $N_2$  before turning on the heating. The temperature rise was normally quite rapid, but not until after about 2 hrs. the temperature became stable and the reactant gas could be admitted. The gasification media ( $O_2$ ,  $H_2O$ ,  $CO_2$ ) were diluted with  $N_2$ .

During the introductory phase of the experiments it was found to be proper to normalize the amount of char gasified at any time to the maximum amount possible. This latter value was found by raising the temperature of the oven 200°C in a flow of nitrogen, whereafter the oxidation is completed within few minutes to constant weight giving the ash figure.

### 3. Experimental results

Of the introductory/guiding experiments only a few need to be reported. Reproducibility of the two-step procedure was found to be quite satisfactory. The rate of gasification did not change when the flow of reactant gas was reduced to half, and the rate seems to be directly proportional to the  $O_2$  concentration (25 and 50%). Rate values at comparable conditions in the temperature range 408–438°C gave activation energies in the region 120–150  $\text{kJ}\cdot\text{mol}^{-1}$ , indicating that reaction rate only is rate-controlling.

A comparison of the relative rating of two coal samples is shown in Figures 3 to 5, using  $O_2$  (65%),  $H_2O$  (29%) and  $CO_2$  (50%). When the differences in curve heights are compared at the same degrees of gasification, the  $H_2O$  and  $CO_2$  ratings are nearly the same, while the "separation" is somewhat larger for  $O_2$ .  $H_2O$  is, however, more reactive than  $CO_2$ . The use of  $O_2$  is preferred, since the lower temperature is lenient to the furnace.

Using one coal sample, the influence of pyrolysis time at the same laser energy input (12 J) on rate of gasification was measured (Fig. 6). While the amount of pyrolysis residue (char) did not vary much, it is evident, that the reactivity of the char gets considerably higher, when pyrolysis time is short. This effect is likely to increase the spread of burning times in a PF flame.

The effect of laser energy input at constant pulse length (1 ms) was also studied. As seen in Fig. 7 the samples with the smallest amount of energy start at a lower degree of pyrolysis but are somewhat more reactive, why the final level of gasification gets to be more or less the same.

In another study with a set pulse time the ratio of energy to specimen weight was kept constant (Fig. 8). It resulted in almost identical gasification curves.

The composition of the pyrolysis gas varies somewhat with the laser-pulse duration as shown in fig. 7. These values may not be important for combustion performance but could give an indication of pyrolysis properties. When the level of laser energy was varied at constant pulse length the following relative amounts ( $\mu\text{l}$ ) were formed:

Energy, J	1	2	5	10
$H_2$	32	88	122	139
CO	9	31	57	81
$CH_4$	1.2	1.4	1.7	2.3
$C_2H_4$	0.43	0.46	0.73	1.15
$C_2H_2$	1.9	5.5	19.6	3.6

The rise in amounts was particularly strong in the lowest range of energy increase, except for  $C_2H_2$ .

From the curves shown so far and several others it can be inferred, that the (relative) amount of "post-pyrolysis" is proportional to the reactivity of the char, expressed as the initial slope of gasification curve.

In the Figures 10 to 13 some pyrolysis and gasification curves are given for the following 4 coal samples within the same rank, the figures being in %:

Origin	H <sub>2</sub> O	Ash	Volatiles
Australia	2.2	16.1	37.3
Mozambique	2.8	10.1	40.0
South Africa	2.9	13.3	29.9
Poland	2.6	17.2	38.4

It may be stated generally from the "reactivity curves", that the new type of characterization does discriminate between different coals. The differences appear as ultimate levels of (normalized) residue and as response at changes in pyrolysis parameters. It would be of interest to understand how these differences may be explained, but the important matter is to relate the observations to the performance of the coals in practical burning.

Fig. 13 also illustrates the deviation in behaviour, when the pyrolysis is done by heating the coal specimen slowly in the gasification oven. Evidently the slow carbonization yields a reactive char, which has almost the same "gasification profile" as the char from a low energy laser pulse (1 J) of short duration (1 ms). However, in characterization laser pyrolysis is more realistic and easier to control.

Though the use of CO<sub>2</sub> as gasification medium is less attractive, it is of fundamental interest to check the influence of characterization parameters in comparison to O<sub>2</sub>. It was found as a main observation, that the difference in reactivity, resulting from short and long pulse lengths, seems to be considerably smaller on CO<sub>2</sub> gasification.

Several experiments were made with different atmospheres and increased pressures in the pyrolysis chamber. On the whole, the effects observed were rather insignificant. Also a splitting of the laser energy into several consecutive pulses seems to give additional information of interest. *Title*

A few experiments with particles of different ranges in the coal powder, used to press the disc specimen, indicate some differences in the reactivity of the produced chars. Evidently, the particle size distribution should be controlled in accurate work.

Finally two series of "characterization experiments" were carried out, one with coals of different ranks, the other a comparison with results, produced by the Danish service and research institute dkTEKNIK.

The first series comprised one subbituminous coal (West Canada), two bituminous coals (South Africa), one "in between" these ranks (Columbia) and, as the last, anthracite. The laser energy was kept constant while two pulse lengths (1 and 20 ms) was used. The results are shown in Figures 14 and 15. The 1 ms experiments give a clear discrimination between the ranks, and the two bituminous coal appear to be identical. However, the 20 ms experiments do distinguish between these two coals, while the ranking order of the most reactive coal chars gets "mixed". Generally the new characterization method appears to be quite efficient.

The second series illustrates the only comparison with results from practice, identified so far. The three coals involved have the following conventional data:

Coal from	Ash,%	Volatiles,%	H <sub>i</sub> kcal/kg	Softening temp.,°C
Poland	16.1	36,0	7749	1190
South Africa	12.8	28,8	7783	1340
Mozambique	17.6	36.9	7690	?

Petrographic figures show substantial differences in vitrinite and inertinite contents. The DTH/DTC/TG data seem to differ moderately and do not offer an easy interpretation. The following test results are at hand (only two coals being used in PF firing):

Coal from	Drop tube % burnt	Ignition, combustion	Not burnt in ash,%
Poland	96,1	very good	2
South Africa	87,8	rather good	6
Mozambique	94,4	-	-

The overall dkTEKNIK results grade the samples in the order: Poland, Mozambique, South Africa. The pyrolysis/reactivity results, as shown in Fig. 16 give the same order. A detailed comparison does not seem possible.

#### 4. Summary

The results obtained do meet the prospects of a new possibility for coal characterization, in that the proposed principle seem to have a definite potential of practical interest. The method displays good reproducibility and reflects also minor differences in coal properties. The number and ranges of significant parameters appear to be limited, and standardization to optimal conditions, e.g. with regard to laser requirements, should be possible, using simplified equipment.

We have been invited by the European Common Market Authorities to examine the possible development of a commercial apparatus with the support of consultants with experience of such endeavours.

Lyngby, December 1989

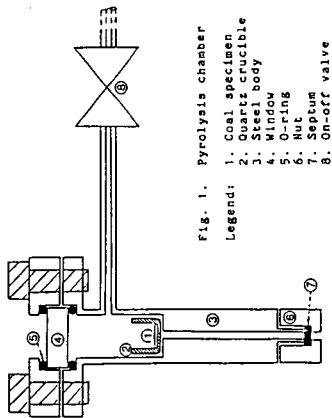


Fig. 1. Pyrolysis chamber

- Legend:
1. Coal specimen
  2. Quartz crucible
  3. Stopper body
  4. Window
  5. O-ring
  6. Nut
  7. Septum
  8. On-off valve

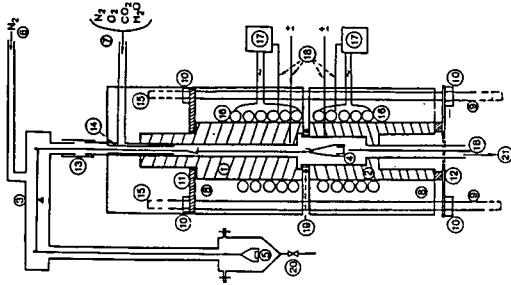
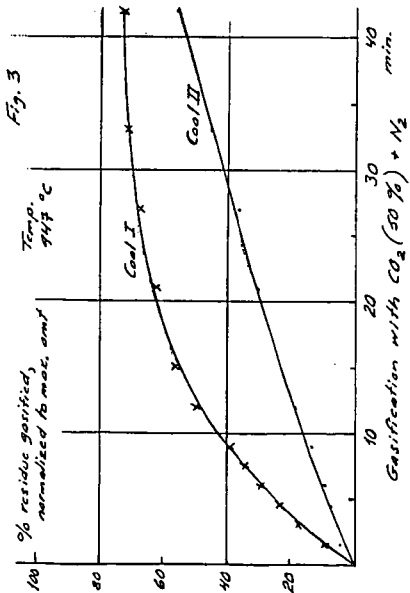
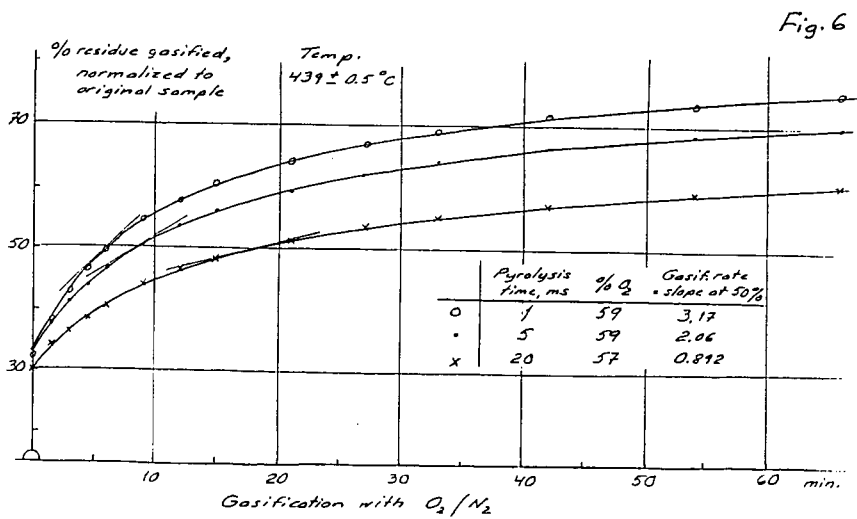
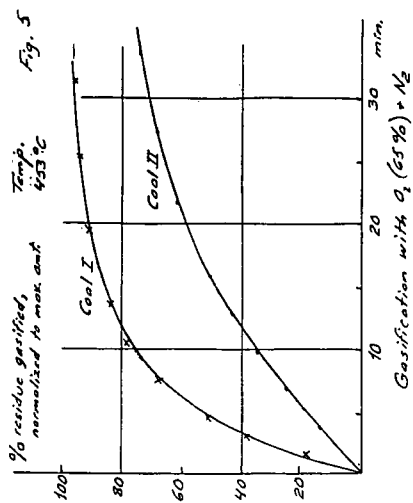
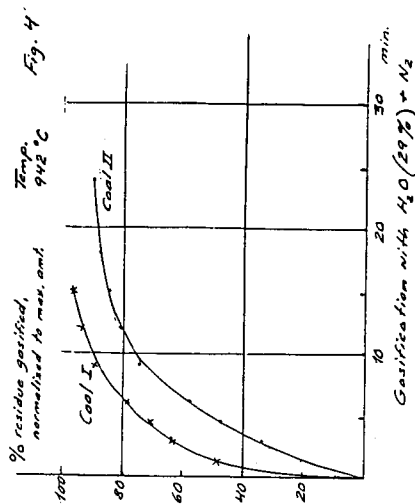


Fig. 2. Reactor furnace and microbalance

- Legend:
1. Reactor body, upper part
  2. Reactor body, lower part
  3. Micro balance
  4. Steel bars (to keep reactor parts together)
  5. Weighing pan (carrying crucible with coal specimen)
  6. Microbalance inlet (for protection of balance)
  7. Inlet for  $N_2$ ,  $O_2$ ,  $CO_2$ ,  $H_2O$
  8. Insulation
  9. 4 steel bars (to keep reactor parts together)
  10. Bolting nuts
  11. Top plate
  12. Top plate (springy material)
  13. Expansion joint
  14. Mixing section
  15. Prolonged bars (acting as hanging support)
  16. Heating coil
  17. Temperature controls
  18. Thermocouples
  19. Packing
  20. Vent
  21. To cooler and chromatograph





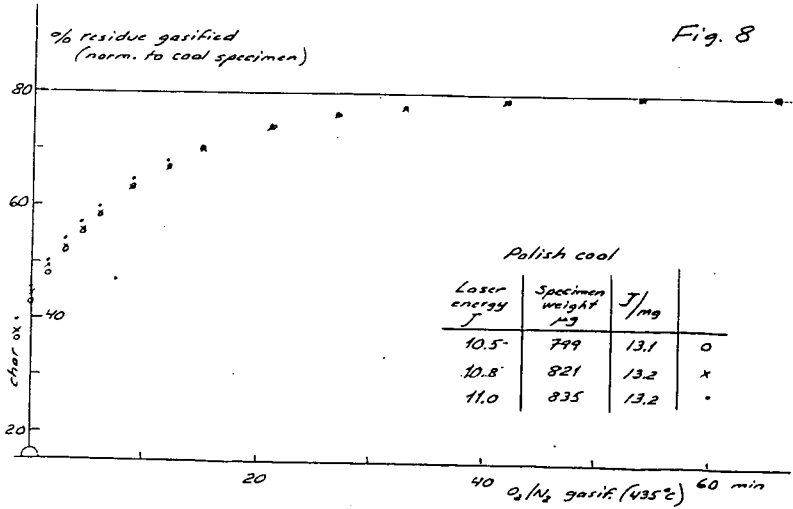
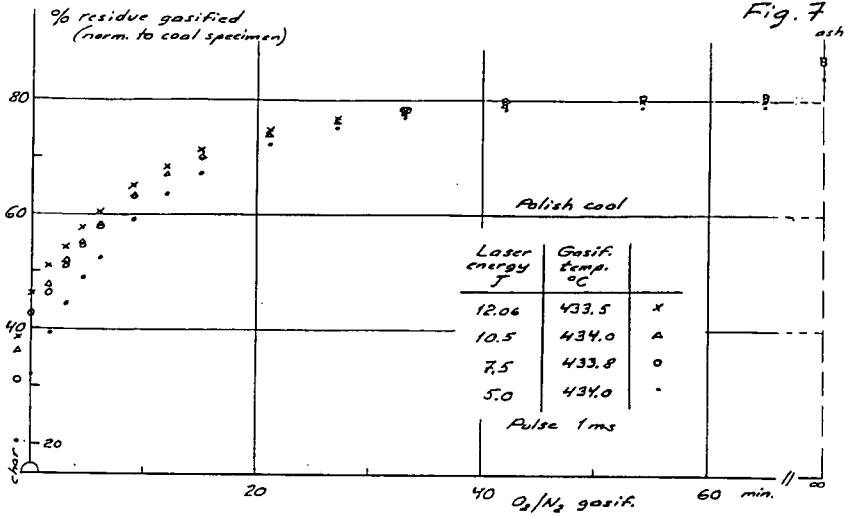
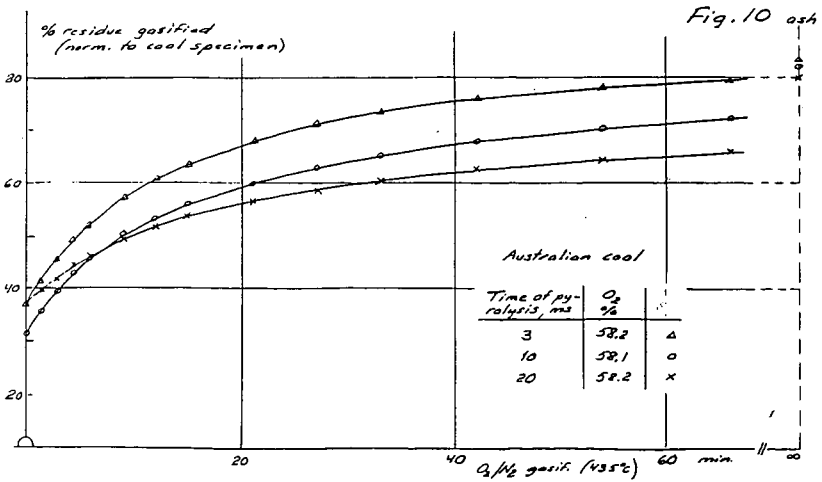
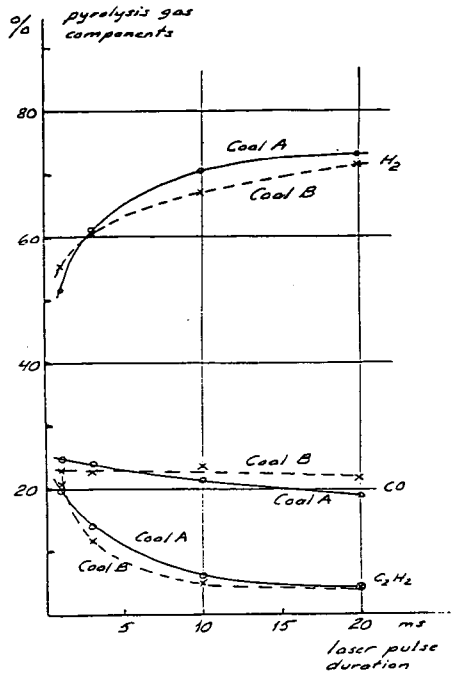
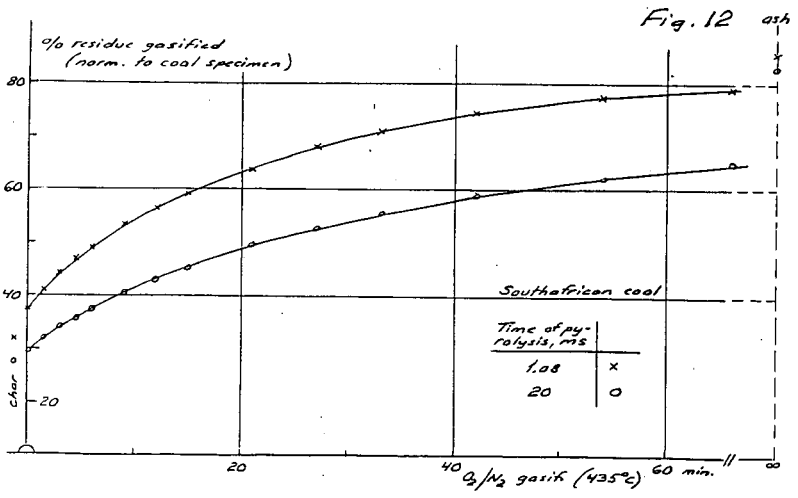
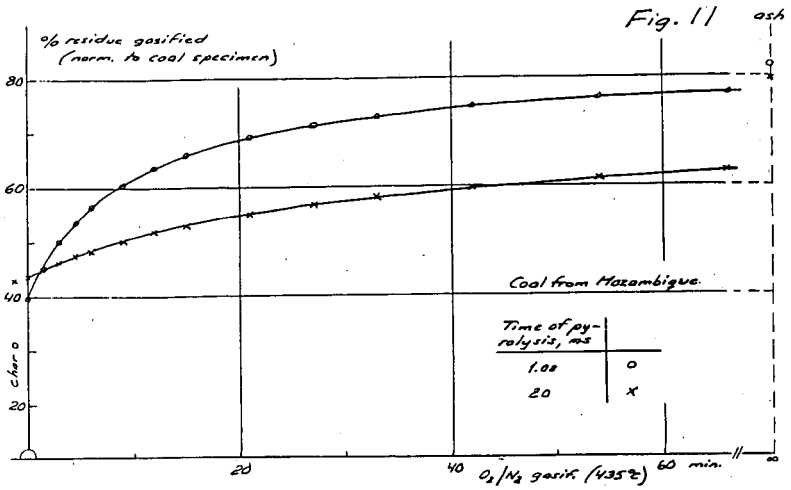
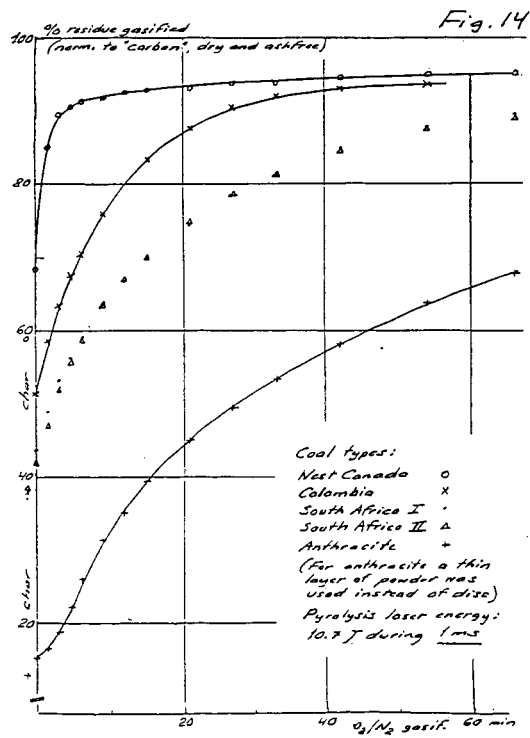
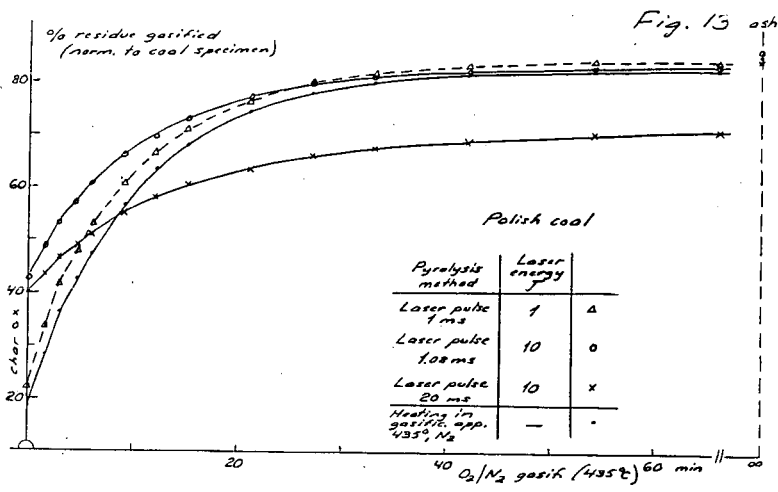
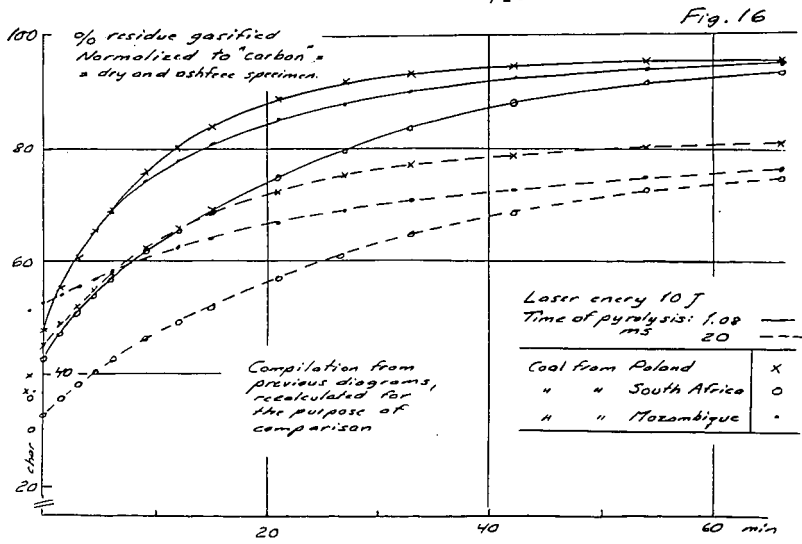
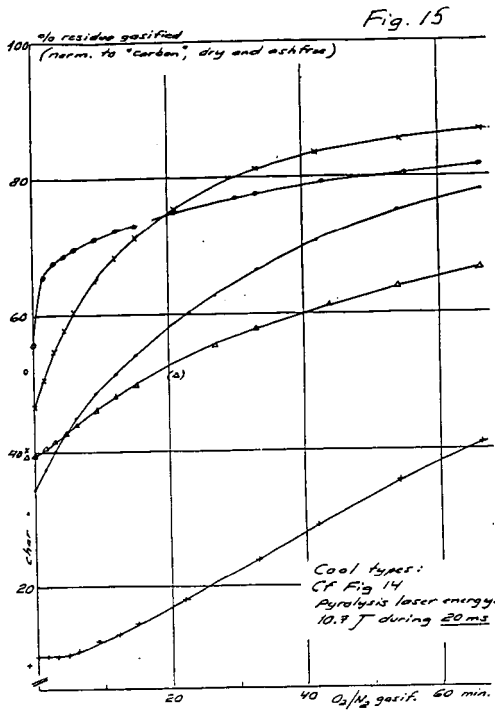


Fig. 9









## ADVANCES IN THE FG-DVC MODEL OF COAL DEVOLATILIZATION

P.R. Solomon, M.A. Serio, D.G. Hamblen, Z.Z. Yu, and S. Charpenay  
Advanced Fuel Research, Inc., 87 Church Street, East Hartford, CT 06108

**KEYWORDS:** Coal, Pyrolysis, Modeling, Network, Kinetics

### INTRODUCTION

The FG-DVC general model for coal devolatilization, which combines a functional group (FG) model for gas evolution and a statistical depolymerization, vaporization, and crosslinking (DVC) model for tar formation, has previously been presented (1). The FG model describes the evolution of gases from sources in the coal, char and tar. The DVC model describes the decomposition and condensation of a macromolecular network representation of coal under the influence of bond breaking and crosslinking to predict (using Monte Carlo statistical method) the molecular weight distribution of the network fragments. The crosslinking reactions are related to the evolution of CO<sub>2</sub> at low temperature and CH<sub>4</sub> at moderate temperature (2). Tar is formed from the light fraction of the network fragments which vaporizes and is transported by the light gases.

As discussed in Ref. 1, the FG-DVC model was based on a number of simplifying assumptions which provided a good first approximation of the devolatilization process. Included in the approximations were the assumptions that: i) the coal molecular structure could be described as substituted aromatic ring clusters of various sizes linked into a macromolecular network or present as guest molecules, ii) tar consists of fragments of that network and so has a similar composition. (except for a higher hydrogen content due to a larger number of methyl groups), iii) kinetics are independent of coal rank, iv) transport is controlled by the vapor pressure of tar fragments in the escaping gases.

Since the presentation of the original FG-DVC model, a number of improvements have been made. First we have added a second class of material, polymethylenes, to the macromolecular network. These polymethylenes can form a large part of the tar in low rank coals and so make the tar dissimilar to the parent structure (which is primarily the aromatic ring clusters). Second, the molecular weight distribution of macromolecular network fragments has been used as the basis for a theory of viscosity (3). This theory is quite sensitive to the accuracy of the kinetic rates. Consequently, third, rank dependent kinetics have been added to the model (3,4). Fourth, we have tested the tar transport theory by comparing its predictions on molecular weight distributions to measurements made with a Field Ionization Mass Spectrometer (FIMS). The results suggest that the vapor pressure law (5) used in the original model (1) appears to fit the data in its dependence on molecular weight and temperature, but was about a factor of 10 too low in its vapor pressure. Finally, we are exploring the use of percolation statistics as an alternative to the Monte Carlo calculations. An approximation is presented which includes the evolution of tar molecules and is based on a previously presented two coordination number percolation theory (6).

### MODEL IMPROVEMENTS

#### Polymethylenes

Varying amounts (typically 0-9%, but in some cases as high as 18%) of long-chain aliphatics (polymethylenes) have been reported in pyrolysis products by Nelson (7) and by Calkins and coworkers (8-11) and references quoted therein. The chains appear alone and attached to aromatic nuclei. The presence of these polymethylenes makes the tar more aliphatic than the parent coal. Also, for most coals, there is a low temperature tar peak which results from the vaporization of unattached small polymethylenes plus small aromatic ring clusters. This vaporization peak is illustrated in Fig. 1. Polymethylene chains can also crack or be released into the second tar peak. Further cracking of this material under more severe devolatilization conditions produces ethylene, propylene, and butadiene from which the concentration of polymethylenes may be determined (11). Originally, the polymethylenes were included in the FG model as part of the aliphatic functional group pool, which is assumed to decompose to produce gas products, not tar. This leads to predicted H/C ratios in the tar for low rank coals which are lower than those measured by Freihaut et al. (12).

Polymethylenes have now been added to the DVC part of the model as a second class of material whose molecular weight distribution and functional group composition are different from the main macromolecular network. The starting coal molecule now includes a distribution of oligomer sizes for polymethylenes and other guest molecules (with the chemical composition of the network). The vaporization of these molecules produces a peak which matches the early vaporization peak as shown in Fig. 1. We also account for polymethylenes which are attached to the coal matrix and removed by bond breaking by including them as species in the FG model. Those polymethylenes are then added to the tar after vaporization.

The model requires a value for the total polymethylene content in the coal. Calkins determined that the yields of ethylene, butadiene, and propylene correlated well with the polymethylene content (11). It was decided that this is the most general and fruitful approach to take and we have used the coals which are in our set and Calkins' set to calibrate the method. As a first approximation, we arbitrarily chose to use polymethylene = 0.7 (C<sub>2</sub>H<sub>4</sub>). This gave -CH<sub>2</sub>- contents slightly above Calkin's values, but within 15% of Calkin's. The model also assumes that 50% of the polymethylenes are small enough to vaporize and are included in the oligomer pool while the other 50% are not and are included in the FG pool.

A prediction for the total tar yield including polymethylenes is compared in Fig. 1 with measurements from a TG-FTIR experiment (13-15). The agreement is good. Comparisons between the predicted and measured (12) tar hydrogen compositions are shown in Fig. 2. The prediction is good for high rank coals and shows the correct trend with rank. The tar hydrogen composition is, however, overpredicted for lower rank coals. This is due to the fact that the model underpredicts, for these coals, the tar yield at high heating rates. The relative contribution of polymethylene is then more important. By improving the tar prediction with adjustments of DVC parameters, we should be able to obtain more accurate values of the tar hydrogen composition.

#### Viscosity Model

We have developed a model for coal fluidity as an extension of the FG-DVC model (2). The FG-DVC model predicts the yield of liquids (all fragments released from the network) produced during heating of the coal. The fluidity is dependent on the relative amounts of the liquid, and solid (the remaining network) and on the fluidity of the liquid component. The fluidity of the liquid component depends on the average molecular weight of the liquid and on the temperature. The details of the fluidity model and comparisons to literature values of viscosity are presented in Ref. 3. Excellent agreement has been obtained between the model predictions for fluidity and low temperature fluidity measurements of Oxley and Pitt (16), Fitzgerald (17), and van Krevelen (18).

Recently, we have applied the model to predict the fluidity data for the Argonne premium samples obtained using a Geissler plastometer (19). To properly predict the fluidity we found that the rank independent kinetics were no longer accurate enough. Rank dependent rates for bond breaking, low temperature crosslinking, and moderate temperature crosslinking were determined using the evolution rates for tar, CO<sub>2</sub>, and CH<sub>4</sub> in a TG-FTIR experiment as discussed in the next section. Their rank dependent rates were used to make the predictions of viscosity.

Figure 3 compares the measured and predicted viscosity for Upper Freeport coal. Figure 4 shows the predicted and measured values for the temperature of the initial softening point (where the plastomer first reads 1 DDM), the temperature of maximum fluidity, the maximum fluidity value, and the solidification temperature (where the plastometer last reads 1 DDM). The agreement is good, generally within  $\pm 10^\circ\text{C}$  for the temperature predictions and within a factor of 5 for the fluidity maximum.

#### Rank Dependent Kinetics

As discussed above, in order to fit the fluidity data, the tar formation, carbon dioxide, and methane kinetic rates had to be adjusted from those used in the original model which were rank independent (1,20). These rates control the bridge breaking, low temperature crosslinking and moderate temperature crosslinking rates, respectively. The rank dependent rates were chosen by fitting the TG-FTIR data at 30°C/min and the Geissler fluidity data (19) at 3°C/sec.

In addition to this study, an independent investigation was made of the rank dependence of the pyrolysis kinetics by doing experiments in a TG-FTIR reactor over a series of heating rates (3, 30, 50, 100°C/min) for the Argonne coal set (4).

The rank dependences of the rate constants for bridge breaking, (or tar evolution) and CH<sub>4</sub> evolution at 450°C determined from analyzing the TG-FTIR data at several heating rates and from fitting the FG-DVC model to fluidity data at 3°C/min and the tar and methane evolution data at 30°C/min are shown in Fig. 5. The two methods agree fairly well and show a systematic variation in rates with the coal's oxygen concentrations. The rates for tar evolution or bridge breaking vary by about a factor of 10 if the Pocahontas coal is excluded, which is consistent with previous results for coals from the same range of ranks (21). If the Pocahontas is included, the rank variation for the tar evolution or bridge breaking rates is about a factor of 25. The rates for tar evolution are consistent with those obtained by Burnham et al. (22) for total hydrocarbon evolution from Rock Eval analysis of the same coals.

### Tar Transport Model

The tar transport model assumes that the tars reach their equilibrium vapor pressure in the light gases and evolve with these gases as they are transported through the pores or by bubble transport. The details of the model are presented in Ref. 1. We have used the vapor pressure correlation of Suuberg et al. (5) for the equilibrium vapor pressure. Since this vapor pressure law is a function of molecular weight and temperature, we tested the accuracy of our model in predicting the evolution of tar fragments of specific molecular weight as a function of temperature.

The experimental data used was obtained from FIMS analysis, where the FIMS apparatus is in line with a probe used to heat the sample. The FIMS analysis was performed by Ripudaman Malhotra at SRI International on coals, which pyrolyze in the apparatus (coal FIMS), and on already formed coal tar, which vaporizes in the apparatus (tar FIMS). We divided the tar oligomers (from both data and theory) into five different bins: 50-200 amu, 201-400 amu, 401-600 amu, 601-800 amu, and > 800 amu. The evolution with temperature of each bin is then plotted.

Tar FIMS - We found good agreement between the tar FIMS data and our simulation (Fig. 6). A small mismatch is present for large molecular weight oligomers (> 800 amu), where the maximum of rate evolution occurs later in the simulation. The peak is also narrower, i.e. the temperature range of evolution is shorter than found experimentally. The vaporization of smaller oligomers is, however, well predicted. This validates the temperature and molecular weight dependence of the vaporization law (5) used in the model but not the absolute magnitude of the vapor pressure.

Coal FIMS - We compared the results of the simulation with coal FIMS data for two coals, Pittsburgh No. 8 and Wyodak. We found the best agreement when the Suuberg et al. correlation (5) is multiplied by ten. For the Pittsburgh No. 8, the theory gave an accurate prediction for the evolution temperature of low molecular weight oligomers, as well as the relative amounts of all oligomer classes (Fig. 7). It, however, predicted higher evolution temperatures for high molecular weight oligomers (> 600 amu), while the data showed a unique temperature of maximum evolution rates ( $T_{max}$ ) for all molecular weights. A shift to higher  $T_{max}$  with higher molecular weight is consistent with the fact that large oligomers need higher temperatures to vaporize, as confirmed by the tar FIMS data. Since coal FIMS data doesn't present this feature, we suspect some additional limitations occur as the fluid coal melt resolidifies.

The simulation for Wyodak coal gave a good prediction for the evolution of all molecular weight classes oligomers, including large ones (Fig. 8). The data (Fig. 8b) shows that the evolution of high molecular weight oligomers occurs slightly before the smaller oligomers. This also suggests the presence of additional limitations. In our simulation for low rank coals, the peak position is regulated by the low temperature cross-linking rate (which reduces the number of large oligomers which can vaporize) rather than by the vaporization law.

In order to obtain a better prediction for Pittsburgh No. 8, we considered additional transport limitations related to the reduction in the fluidity of the coal. However, none of the simple modifications tried gave a significant improvement in the model for both low and high rank coals. The current model gives good predictions for the relative amounts of the oligomers in each size classification. It also predicts accurately the evolution temperature of low molecular weight (< 600

amu) oligomers. The vapor pressure dependence on temperature and molecular weight is also validated by the good prediction of the tar FIMS data. The present model, therefore, uses the original FG-DVC transport assumption (1) with the Suuberg et al. vapor pressure correlation (5) multiplied by ten.

### Percolation Theory

The statistical Monte Carlo method used in our FG-DVC model has been quite successful in predicting the depolymerization and crosslinking processes of the coal macromolecular network. However, the method has a few drawbacks. First, it is computationally time-consuming compared with other statistical methods. Second, its statistical nature presents a certain degree of fluctuation in the final results. The latter becomes increasingly significant and poses some difficulties for the modeling of coal fluidity and swelling.

To address these problems, attempts have been made to use the mathematics of percolation theory as an alternative to Monte Carlo calculations (6,23,24). Percolation theory gives closed-form solutions for a Bethe lattice. Keeping in mind that an actual coal network contains some different features from the Bethe lattice (e.g. the Bethe lattice has no loops), we made use of some basic concepts of percolation theory while we further modified the mathematics of this theory to describe vaporization processes in coal devolatilization.

One of the key parameters of percolation theory is the coordination number,  $\sigma + 1$  which describes the possible number of bridge attachments per ring cluster (monomer). A linear chain has  $\sigma + 1 = 2$ , while a rectangular "fish net" has  $\sigma + 1 = 4$ . The higher the coordinator number, the more bridges must break to create network fragments. In attempting to apply percolation theory to the FG-DVC model (6), it became obvious that the single coordination number lattice used in most applications of percolation theory was not appropriate to describe coal network decomposition. It appears from solvent swelling data (25-29) and NMR data (30), that coal begins as a chain-like material with crosslinks every 2 to 8 ring clusters, i.e.,  $\sigma + 1$  between 2.2 and 2.5. So, its decomposition requires a low coordination number. However, crosslinking processes can occur at elevated temperature to increase the coordination number. Therefore, we extended the mathematics of percolation theory from a one-dimension probability computation into a two-dimensional probability computation to describe the coal network as a lattice with two bond types per cluster, i.e., two coordination numbers. This modified theory is referred to as the two- $\sigma$  model (6).

Two important new features in our two- $\sigma$  percolation theory are: (i) tar vaporization and (ii) molecular weight distribution of monomers. These features are basically treated the same way as in the original DVC model. The molecular weight of monomers is described by a probability distribution, which allows for the fact that monomers are made of various multi-ring structures. Tar molecules are removed out of the coal network using Suuberg's modified vaporization law. Molecular weight distributions of tar and char are kept track of during pyrolysis by a bookkeeping of the vaporization process in each mass bin. The percolation theory gives the mass fraction of all n-mers during pyrolysis. Combining this with a given molecular weight distribution of monomers, one can obtain the mass fraction of coal in each mass bin, which consists of two components: char and tar. Tar vaporization is computed for each mass bin. Tar in each mass bin monotonically increases and reduces the amount of char available for vaporization in the same bin until the char bin is emptied. Figure 9 shows the comparison of predicted tar yields between the Monte Carlo method and the modified percolation theory. Also, a two- $\sigma$  prediction of the fluidity for the same coal is included in Fig. 3. The Monte Carlo and two- $\sigma$  predictions agree reasonably well with each other and with the data.

### **CONCLUSIONS**

This paper describes a number of improvements and extensions of the FG-DVC model of coal devolatilization.

- 1) Polymethylenes have now been included in the model. They account for part of the low temperature vaporization peak observed for some coals, and for the increase in the H/C ratio of coal tar observed for low rank coals.

- 2) A fluidity model has been added to the FG-DC model. The fluidity is dependent on the relative amounts of the liquid and solid, and on the fluidity of the liquid component. The fluidity of the liquid component depends on the average molecular weight of the liquid and on the temperature. The model accurately predicts the measured fluidities for the Argonne coals using rank dependent kinetics.
- 3) Rank dependent kinetics for tar formation, CO<sub>2</sub> formation and CH<sub>4</sub> formation have been obtained for the Argonne coals by fitting the fluidity data. These agree with rates obtain by fitting data from a TG-FTIR experiment at several heating rates and with the rates obtained by Burnham et al. (22) for the same set of coals.
- 4) The tar transport model used in the original FG-DVC model (i.e., the tars reach their equilibrium vapor pressure in the light gases and evolve with these gases as they are transported through the pores or by bubble transport) was examined by comparing the temperature and molecular weight predictions for tar evolution measured in a FIMS analysis. The original assumptions give reasonably good fits to the data if the Suuberg et al. vapor pressure correlation (5) is multiplied by ten.
- 5) A new two- $\sigma$  percolation theory was developed with an approximation for tar evolution. The predictions of this model agree with the predictions using Monte Carlo statistics and with the data.

#### ACKNOWLEDGEMENT

The work was supported under Department of Energy, Morgantown Energy Technology Center Contract No. DE-AC21-86MC23075. Richard Johnson is the Project Manager.

#### REFERENCES

1. Solomon, P.R., Hamblen, D.G., Carangelo, R.M., Serio, M.A., and Deshpande, Energy & Fuel 2, 405, (1988).
2. Solomon, P.R., Serio, M.A., Deshpande, G.V., and Kroo, E., "Crosslinking Reactions During Coal Conversion", Energy & Fuels, accepted for publication (1990).
3. Solomon, P.R., Best, P.E., Yu, Z.Z., and Deshpande, G.V., ACS Div. of Fuel Chem. Preprints, 34, (3), 895, (1989).
4. Serio, M.A., Solomon, P.R., Yu, Z.Z., and Deshpande, G.V., "An Improved Model of Coal Devolatilization", presented at the Int. Conf. on Coal Sci., Japan, (1989), see also Serio, M.A., Solomon, P.R., Yu, Z.Z., and Basilakis, R., ACS Div. of Fuel Chem. Preprints, 34, (4), 1324, (1989).
5. Suuberg, E.M., Unger, P.E., and Lilly, W.D., Fuel, 64, 956, (2985).
6. Solomon, P.R., Best, P.E., Yu, Z.Z., and Deshpande, G.V., ACS Div. of Fuel Chem. Preprints, 34, (4), 1280, (1989).
7. Nelson, P.F., Fuel, 66, 1264, (1987).
8. Calkins, W.H., Hagaman, E., and Zeldes, H., Fuel, 63, 1113, (1984).
9. Calkins, W.H., Tyler, R.J., Fuel, 63, 1119, (1984).
10. Calkins, W.H., Fuel, 63, 1125, (1984).
11. Calkins, W.H., Hovsepian, B.K., Drykacz, G.R., Bloomquist, C.A.A., and Ruscic, L., Fuel, 63, 1226, (1984).
12. Freihaut, J.D., Proscia, W.M., and Seery, D.J., ACS Div. Fuel Chem. Preprints, 33, (2), 262, (1988).
13. Carangelo, R.M., Solomon, P.R., and Gerson, D.G., Fuel, 65, 960, (1987).
14. Whelan, J.K., Solomon, P.R., Deshpande, G.V., and Carangelo, R.M., Energy & Fuel, 2, 65, (1988).
15. Solomon, P.R., Serio, M.A., Carangelo, R.M., Basilakis, R., Gravel, D., Baillargeon, M., Baudais, F., and Vail, G., "Analysis of the Argonne Premium Coal Samples by TG-FTIR", Energy & Fuel, submitted for publication (1989).
16. Oxley, G.R. and Pitt, G.J., Fuel, 37, 19, (1958).
17. Fitzgerald, D., Fuel, 35, 178, (1956).
18. Van Krevelen, D.W., Coal, Elsevier, Amsterdam, (1961).
19. These data were provided by George Engelke of Commercial Testing and Engineering, Co.

20. Serio, M.A., Hamblen, D.G., Markham, J.R., Solomon, P.R., *Energy & Fuels*, **1**, 138, (1987).
21. Solomon, P.R., and Hamblen, D.G., "Pyrolysis," in Chemistry of Coal Conversion, Plenum Press, (R.H. Schlosberg, Ed.), New York, 1985, Chapter 5, p. 121.
22. Burnham, A.K., Oh, M.S., Crawford, R.W., and Samoun, A.M., *Energy & Fuel*, **3**, 42, (1989).
23. Niksa, S. and Kerstein, A.R., *Fuel*, **66**, 1389, (1987).
24. Grant, D.M., Pugmire, R.J., Fletcher, T.H., and Kerstein, A.R., *Energy & Fuels*, **3**, 175, (1989).
25. Green, T, Kovac, J, Brenner, D., and Larsen, J., in Coal Structure, (R.A. Myers, Ed.), Academic Press, NY, Chapter 6, p. 199, (1982).
26. Sanada, Y. and Honda, H., *Fuel*, **45**, 295, (1966).
27. Lucht, L.M. and Peppas, N.A., *Fuel*, **66**, 803, (1987).
28. Larsen, J.W. and Kovac, J., *ACS Symposium Series*, **71**, 36, (1978).
29. Lucht, L.M. and Peppas, N.A., *ACS Symposium Series*, **169**, 43, (1981).
30. Solum, M., Pugmire, R.J., and Grant, D.M., *Energy & Fuels*, **3**, 40, (1989).

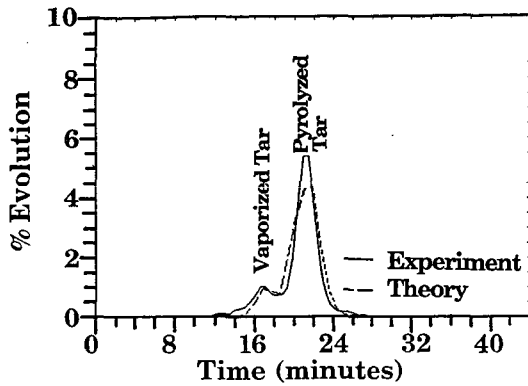


Figure 1. Comparison of FG-DVC Model Predictions for Tar Evolution Rate from Upper Freeport Coal with TG-FTIR Data.

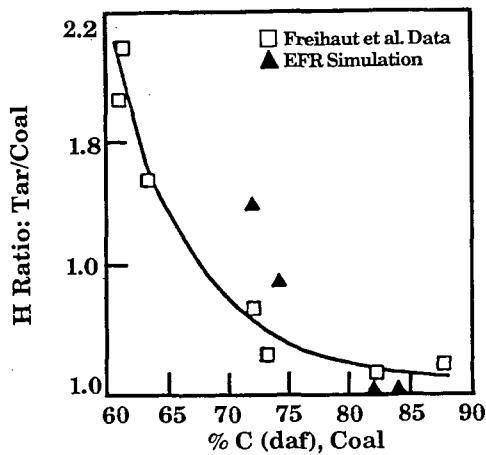


Figure 2. Ratio of % H in Tar to % H in Coal as a Function of Coal Rank. (from Freihaut et al. (12)).

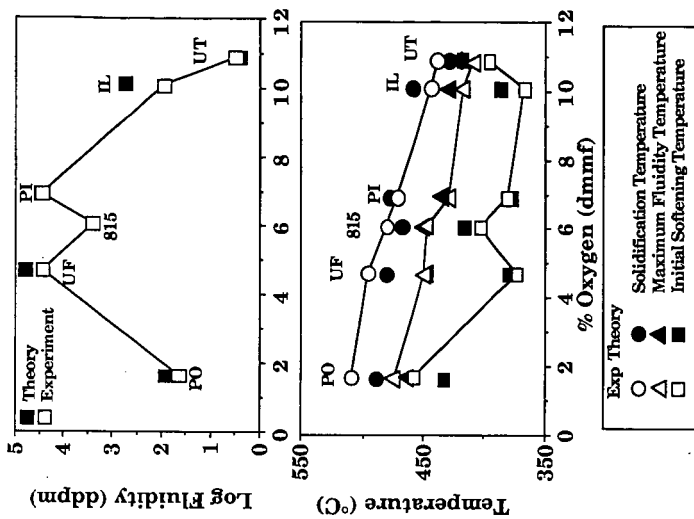


Figure 4. Fluidity Behavior as a Function of Coal Rank: Theory and Experiment. a) Maximum Fluidity Values and b) Fluidity Temperatures.

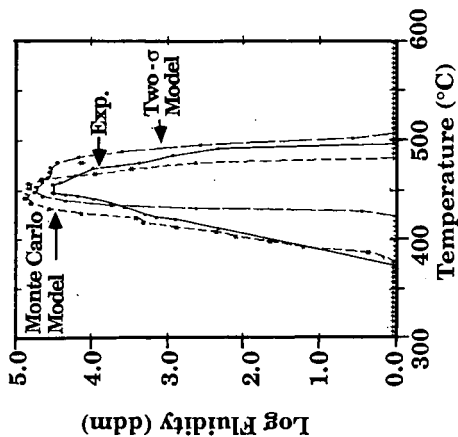


Figure 3. Fluidity of Upper Freeport Coal: Experiment (solid), Monte Carlo Theory (dashed) and Percolation Theory (lon dashed).

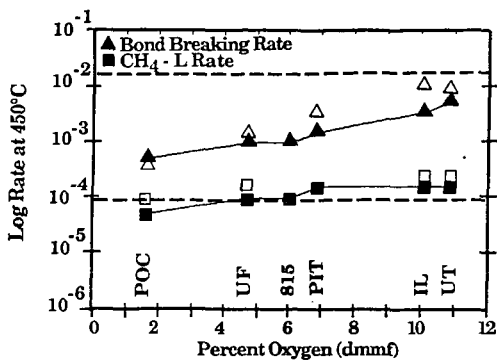


Figure 5. Rank Dependence of Kinetic Rates for Argonne Coals. Open Symbols: From Analysis of TG-FTIR Data at Four Heating Rates. Closed Symbols: From Fitting Fluidity Data at 3°C/min and TG-FTIR Data at 30°C/min. Dashed Lines: Rank Independent Rates used in Original FG-DVC Model.

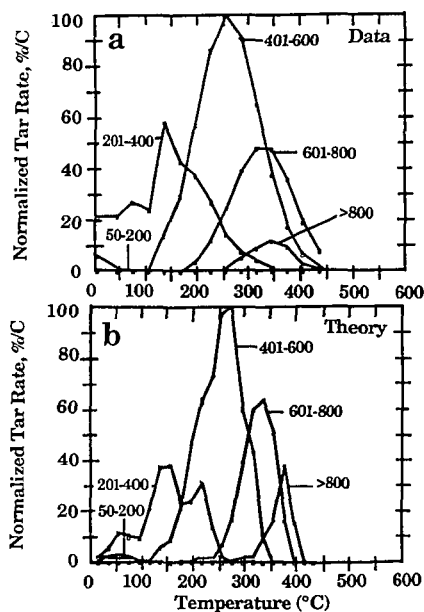


Figure 6. Comparison of a) FIMS Data and b) Theory for Pittsburgh No. 8 Coal Tar.

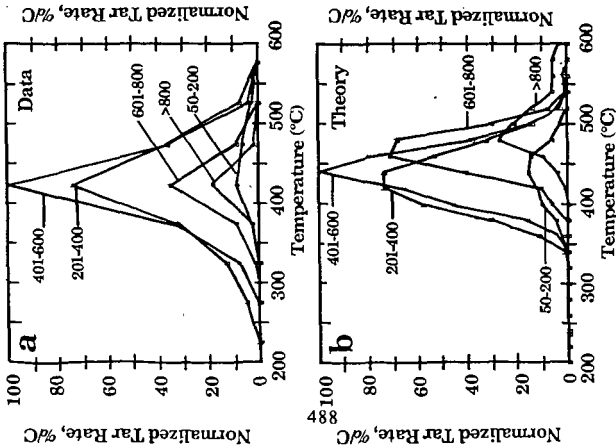


Figure 7. Comparison of a) FIMS Data and b) Theory for Normalized Tar Rate for Pittsburgh No. 8 Coal Pyrolyzed in the FIMS.

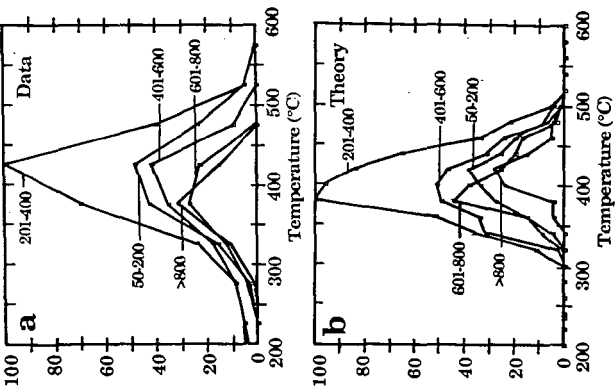


Figure 8. Comparison of a) Data and b) Theory for Normalized Tar Rate for Wyodak Coal Pyrolyzed in the FIMS.

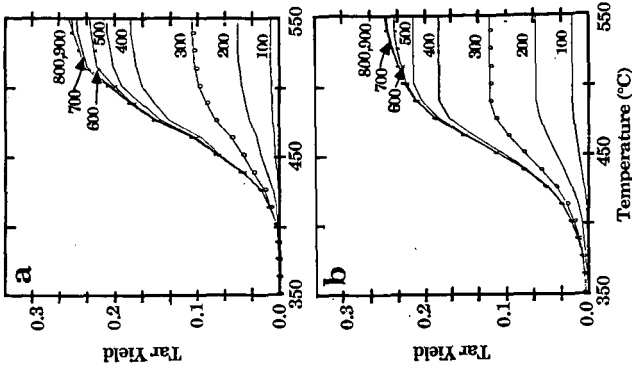


Figure 9. Comparison of Tar Molecular Weight Distribution Predicted with: a) Monte Carlo Method and b) Two- $\sigma$  Percolation Theory.

## MINERAL MATTER EFFECTS IN COAL PYROLYSIS

Insoo Bae, Majed Anani, Waleed Maswadh, Yongseung Yun, Henk Meuzelaar and Joel DuBow

Center for Micro Analysis and Reaction Chemistry, University of Utah  
214 EMRL, Salt Lake City, Utah 84112

KEYWORDS: pyrolysis, coal, minerals

### INTRODUCTION

Coal pyrolysis is a fundamental first step in combustion processes [1]. Yet coals exhibit a wide variation in pyrolysis behaviors. The origins of these wide variations are, for a given set of experimental conditions, both structural and compositional in nature. Because of its thermochemical and catalytic properties, mineral matter plays an important role in both the thermodynamics (product mixes, activation energies) and kinetics of coal pyrolysis [2]. The issue is further complicated by the manner in which mineral matter is distributed in various coals. While many classifications are possible, grouping into three classes is most common [3]. These classes are: (1) discrete minerals such as clays, oxides (basic and acidic) and sulfides; (2) organometallic matter such as ion-exchangeable cations; and (3) dispersed trace elements and compounds. A considerable body of research exists for studying equilibrium and non-equilibrium effects of the various forms of coal minerals on coal combustion [4,5,6].

In the present paper the mineral matter effects on coal pyrolysis are being analyzed using an approach whereby observable spectroscopic (TG/MS) differences in the pyrolytic decomposition between fresh coal and demineralized coal are reconstructed from the sum of mineral matter effects on pyrolysis arising from adding back, singly and in pairs, individual minerals in various forms.

### EXPERIMENTAL TECHNIQUE

A low rank coal, Beulah Zap lignite was chosen because of its readily exchangeable cations, the strategic and technological importance of the huge Northern Great Plains lignite resource, and its availability as a standard reference coal through the Argonne National Laboratory Premium Coal Sample Program (ANL-PCSP).

Prior to sample preparation, coal is freezer stored under Ar or N<sub>2</sub> at -30 to -90 C so that oxidation is prevented. A standard HCl/HF acid wash is used to demineralize the coal. This has been shown not to alter coal structure [6], but does influence the number of reactive sites and surface reactivity in the coal [8,9].

Subsequently, cations and/or minerals are added back into the coal following demineralization. The cations are added using titration techniques and the sulfide or oxide minerals, as well as the clays, added by physical mixing. The titration results agree within +/- 10% of ICP/AES (Inductively Coupled Plasma/Atomic Emission Spectroscopy) determinations. Figure 1 shows the comparison of the titration ion concentration with the ICP/AES measurements.

Following sample preparation, pyrolytic decomposition is studied. Thermochemical kinetics are obtained using a home-built thermogravimetry/mass spectrometry (TG/MS) system [10] in conjunction

with PAS (photoacoustic spectroscopy) using an MTEC model 200 PAS cell and Perkin Elmer Model X1760 FTIR system. The yield of char or ash is quantified using TGA and mineral concentrations are quantified using ICP/AES. Data for each run are replicated three times, and a minimum of three heating rates per sample composition are run in order to evaluate the kinetic parameters using one of three statistical kinetic programs.

## EXPERIMENTAL RESULTS

**Sample Preparation**-- Figure 2 demonstrates the effectiveness of the concentrated HF/HCl demineralization procedure. The ICP/AES data show that 95% of the mineral matter was removed. Furthermore, TG/MS data, as exemplified in Figures 3a and 3b, indicate that major structural transformations do not occur as a result of demineralization.

Minerals were subsequently added to the demineralized coal by physical mixing or by ion exchange titration. Figure 4 shows FTIR data including the computed difference between fresh (Figure 4a) coal and demineralized (Figure 4b) coal FTIR spectra. Figure 4c shows the difference between FTIR spectra for fresh Beulah Zap coal and demineralized Beulah Zap. The peaks at 1090  $\text{cm}^{-1}$  are particularly significant for cations and mineral phases. Note the strong similarities between the calculated difference spectrum in Figure 4c and the measured spectrum of ash obtained by low temperature ashing (Figure 4c). The effect of adding calcium is also given. The peaks for hydrogen replacement of cations and for the existence of mineral phases are consistent with known ion exchange and mineral substitution mechanisms.

**Coal Pyrolysis** - The effects of demineralization and of adding 2.6% Fe to demineralized Beulah Zap on specific products of devolatilization are shown in selected, time- and temperature-resolved mass spectral data in Figure 3.

Figure 3a-d shows the influence of demineralization (followed by adding iron chloride to demineralized coal) upon the DTG curve, the total ion count signal and the time (or temperature)-resolved ion profiles for  $\text{H}_2^+$  ( $m/z$  2),  $\text{CO}^+$  ( $m/z$  28), and  $\text{H}_2\text{O}^+$  ( $m/z$  18). The main features of the DTG profiles are replicated in the total ion count profiles. The mass spectral profiles for fresh and demineralized coal exhibit peak shifts in both temperature and amplitude. For iron, the concurrent sharp fall off of  $\text{H}_2\text{O}$  accompanied by a sharp rise in  $\text{H}_2$  (which is doubly activated) and  $\text{CO}$  is strongly suggestive of a water-gas-shift reaction. Moreover, the activation energies, based on first order kinetics, are similar for  $\text{H}_2$  and  $\text{CO}$ . Both calcium and iron affect the hydrogen generation kinetics.

**Kinetics** - A number of kinetic parameter-fitting models were evaluated for devolatilization kinetic parameter determination. The techniques of Yun (1989) and Burnham (1989) [11,12] are specifically focussed on distributed activation energy models. However, not all the reactions are necessarily uncoupled parallel first order reactions. The apparent activation energies and reaction order may be estimated from leading edge or TG/MS line profiles. Table 1 shows the computed activation energies for  $\text{H}_2$  and  $\text{CO}$ . The hydrogen generation curve may arise from a number of possible mechanisms. The experimental data for DMBZ+ 2.6%  $\text{FeCl}_3$  are indicative of two distinct reactions. The apparent activation energy of 42.2 K cal/mole is apparently increased by the contribution of lower temperature reactions (water-gas-shift and main pyrolysis reaction).

The existence of catalytic effects of mineral matter is reinforced by the thermochemical kinetic data enumerated in Table II. The fresh Beulah Zap coal activation energy is the highest and hence pyrolysis proceeds at the fastest rate. The lowest activation energy is for demineralized Beulah Zap

coal, while the activation energies for demineralized Beulah Zap samples with added iron and calcium lie in between.

## CONCLUSIONS

Marked effects of iron and calcium cation content on the hydrogen, water, and carbon monoxide generation rates during pyrolysis were observed. In addition, the potential for PAS-FTIR spectroscopy in quantitative applications to coal spectra was demonstrated on fresh demineralized and remineralized coal. Demineralization and selected remineralization affect the rate of gas evolution in general and of hydrogen and carbon monoxide in particular. This is in good agreement with published literature data [13,14,15].

## ACKNOWLEDGEMENTS

This work was sponsored by the Advanced Combustion Engineering Research Center. Funds for this Center are received from the National Science Foundation, the State of Utah, 23 industrial participants and the U.S. Department of Energy.

## REFERENCES

1. Howard, J.B., "Fundamentals of Coal Pyrolysis and Hydrolysis," pp. 665-784, Chemistry of Coal Utilization, Elliott, M.A., (ed.), Wiley-Interscience, New York, 1981.
2. Gavalas, G., Coal Pyrolysis, Elsevier Publ. Co., New York, 1984.
3. Morgan, B.A., and Scaroni, A.W., "Cation Effects During Lignite Pyrolysis and Combustion," pp. 255-266, The Chemistry of Low Rank Coals, American Chemical Society, Washington, D.C., 1984.
4. Badin, E.J., Coal Combustion Chemistry Correlation Aspects, pp. 40-45, Elsevier, Amsterdam, 1984.
5. Lahaye, J., and Prado, G., "Porous Morphology of Coal: Its Transformation During Pyrolysis," pp. 159-177, Fundamentals of the Physical-Chemistry of Pulverized Coal Combustion, Martinus Nijhoff Publishers, Dordrecht, 1987.
6. Vorres, K., Mineral Matter and Ash in Coal, ACS Symposium Series, 1986.
7. Boni, A.A., "Transformation of Inorganic Coal Constituents in Combustion Systems," DE-AC22-86PC90751, 1989.
8. Jenkins, R.G., Walker, P.L., "Analysis of Mineral Matter in Coal," in Analytical Methods for Coal and Coal Products, Chapter 26, Academic Press, 1978, pp. 265-292.
9. Franklin, H.D., Cosway, R.G., Peters, W.A., and Howard, J.B., "Effects of Cations on the Rapid Pyrolysis of a Wyodak Subbituminous Coal," Ind. Eng. Chem. Process Des. Dev., 22:39-42, 1983.

10. Yun, Y., Meuzelaar, H.L.C., "Simultaneous Thermogravimetric and Mass Spectrometric Observations on Vacuum Pyrolysis of Argonne PCSP Coals," ACS Preprints, Div. Fuel Chem., Vol. 33(3), 1988, pp. 75-84.
11. Yun, Y., and Maswadeh, W., Meuzelaar, H.L.C., Simmleit, N., Schulten, H.R., "Estimation of Coal Devolatilization Modeling Parameters from Thermogravimetric and Time-Resolved Soft Ionization Mass Spectrometric Data," ACS Preprints, Div. Fuel Chem., Vol. 34(4), 1989, pp. 1308-1316.
12. Burnham, A.K., oh, M.S., and Crawford, R.W., "Pyrolysis of Argonne Premium Coals: Activation Energy Distributions and Related Chemistry," Energy and Fuels, 3(1): 42-55, 1989.
13. Scaroni, A.W., Walker, P.L., and Jenkins, R.G., "Effect of Surfaces on the Yield of Volatiles from Coal," Fuel, 60:558-560, 1981.
14. Yamashita, H., Ohtsuka, Y., Yoshida, S., and Tomita, A., "Local Structures of Metals Dispersed on Coal 1," Energy and Fuels, 3(6):686-692, 1989.
15. Morgan, M.E., and Jenkins, R.G., "Role of Exchangeable Cations in the Rapid Pyrolysis of Lignites," pp. 213-226, The Chemistry of Low Rank Coals, American Chemical Society, Washington, D.C., 1984.

TABLE I  
ACTIVATION ENERGIES FOR HYDROGEN AND CO

Coal Sample*	Mass Peak	Activation Energy (kcal/mol)	Observed Temp. Range (K)
FRBZ	m/z 2 (H <sub>2</sub> +)	36.8	800-1200
	m/z 28 (CO+)	22.7	800-1200
DMBZ + 2.6% Fe	m/z 2 (H <sub>2</sub> +)	42.2	800-900
	m/z 28 (CO+)	35.2	800-1200

\* FRBZ = Fresh Beulah Zap  
DMBZ = Demineralized Beulah Zap

TABLE II  
ACTIVATION ENERGIES BASED ON TG WEIGHT LOSS DATA

Coal Sample*	E <sub>a</sub> (kJ/mol)	Chosen % Conversion	Heating Rate Used
FRBZ	213 ± 43.68	30, 32, 34, 36, 38, 40	5, 10, 25, 50
DMBZ	102.79 ± 32.72	15, 18, 21, 24	5, 10, 25
DMBZ + Fe	131.94 ± 51.40	30, 32, 34, 36, 38	10, 25, 50
DMBZ + Ca	144.44 ± 40.67	30, 32, 34, 36, 38, 40	10, 25, 50

\* see Table I

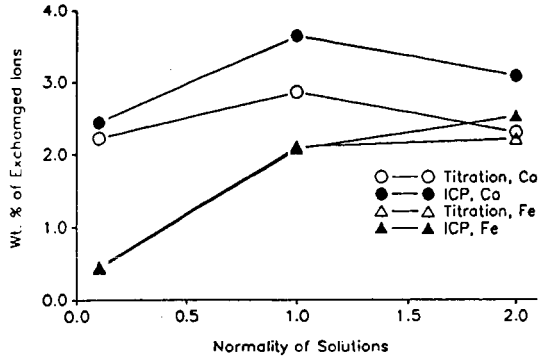


Figure 1. Ion exchange was accomplished via titration and verified by ICP/AES. The iron substitution data are nearly identical, indicating a more effective exchange than for calcium. The concentration in the coal tends to saturate above 1N solutions.

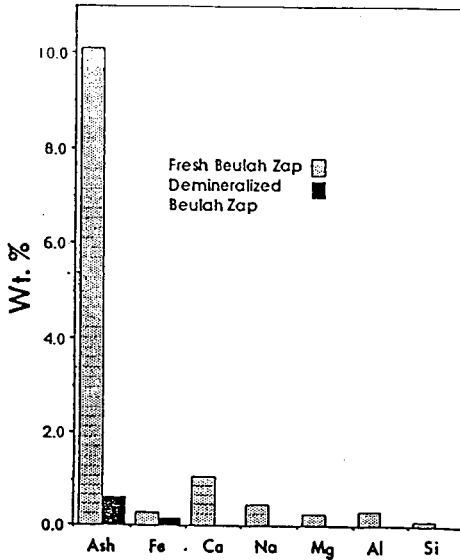
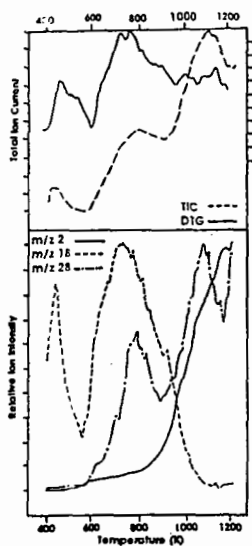
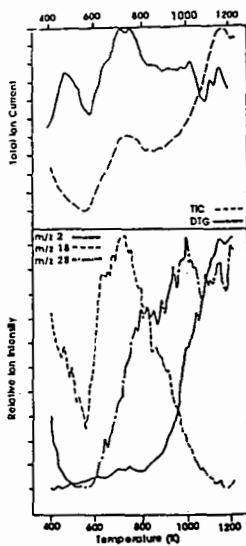


Figure 2. ICP-AES data for fresh and demineralized Beulah Zap coal. While the efficiency for mineral removal varies by element, the demineralization is seen to remove about 95 percent of the total mineral matter.

a. Fresh Beulah Zap



b. Demineralized Beulah Zap



c. as b + 2.6% Fe

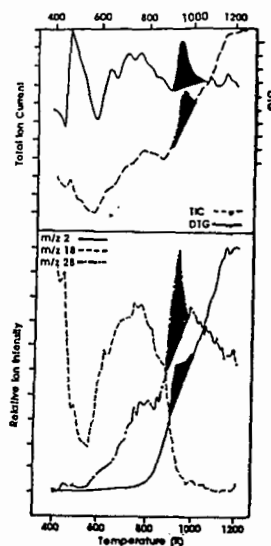


Figure 3. Selected thermogravimetric weight loss, total ion count and mass spectral profiles for  $\text{H}_2\text{O}$ ,  $\text{CO}$  and  $\text{H}_2$  is demineralized and remineralized Beulah Zap coal. Of note are the duplication of the main DTG features in the total ion count and the evidence in Figure 4c (see shaded areas) of water-gas-shift reactions (falling water concentration with concurrently rising hydrogen and  $\text{CO}$  concentrations). The iron cations shift the hydrogen profile to lower temperatures with accompanying rapid rise in  $\text{CO}$ . The activation energies for  $\text{H}_2$  ( $m/z$  2) in Table I are indicative of two interacting reactions for hydrogen generation, e.g., water-gas-shift and crosslinking.

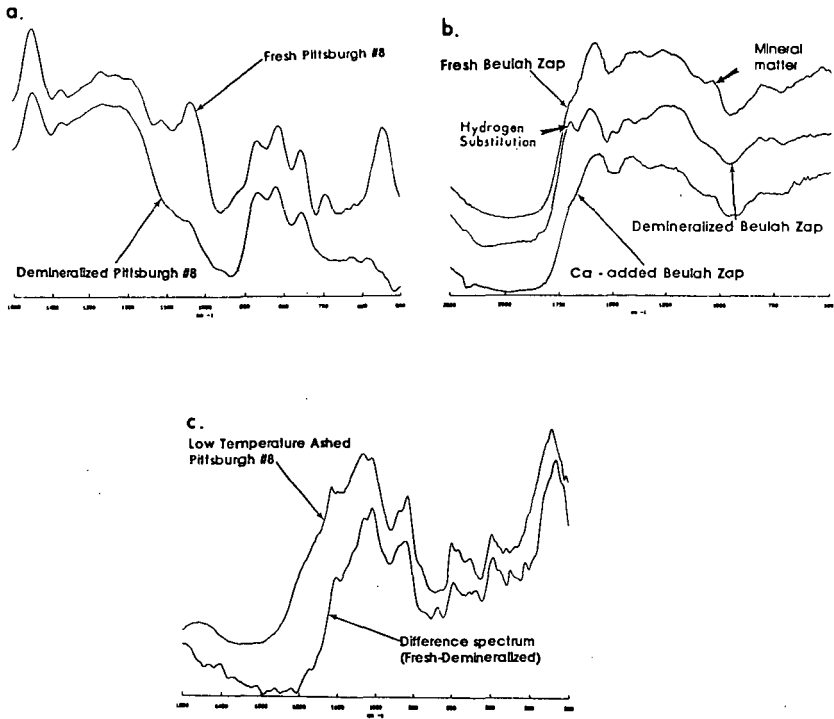


Figure 4. Photoacoustic FTIR spectra for fresh and demineralized Pittsburgh #8 and Beulah Zap coals. Of particular note in Figure 4a and c are the strong similarities between the computer difference spectra (between fresh and demineralized coal) and the ash spectra. Figure 4b shows the verification of calcium ion exchange in Beulah Zap coal through the FTIR spectral shifts at 1690  $\text{cm}^{-1}$  and 1050  $\text{cm}^{-1}$  between fresh, demineralized and Ca-added coals.

## ANOMALOUS SIDE CHAIN CLEAVAGE IN ALKYLAROMATIC PYROLYSIS

H. Freund, M. G. Maturro, W.N. Olmstead, R.P. Reynolds, and T.H. Upton  
Corporate Research  
Exxon Research and Engineering Co.  
Route 22 East  
Annandale, NJ 08801

**Keywords:** Alkylpyrene thermal chemistry, Side chain cleavage, Radical hydrogen transfer.

### INTRODUCTION

In reactions of hydrocarbons, alkylaromatic side chain cleavage occurs as the result of thermal or acid catalyzed cracking chemistry. In general, acid catalysis leads to direct bond cleavage at the aromatic ring whereas thermally promoted bond breaking gives primarily substituted aromatics.<sup>1</sup> The formation of a core aromatic by a thermal process is expected only at higher temperatures and in low yield due to the need for hydrogen atoms.

The thermal chemistry of simple alkyl substituted aromatics has been extensively studied both experimentally<sup>2</sup> and mechanistically<sup>3</sup> over a wide range of temperatures in the gas and liquid phase. Selectivity and conversion can generally be explained by the classical Rice-Hertzfeld chain mechanism,<sup>4</sup> involving initiation, chain propagation and termination steps.

Typically, thermal cleavage of an alkyl group at the ring for most systems studied (1 and 2 ring alkylaromatics) is observed only at relatively high temperature. It occurs by ipso hydrogen atom attack followed by cleavage and rearomatization by loss of the alkyl side chain.<sup>5</sup>

Recently, for the alkylpyrene system, extensive direct side chain cleavage has been observed for liquid phase, low temperature (375-425°C) pyrolysis (43% yield of pyrene at 400°C and 180 min.).<sup>6</sup> Pyrene formation was reported to be the result of autocatalysis. This yield of core aromatic is much greater than that found for single ring aromatics.<sup>2</sup> Detailed mechanistic interpretation of this work is obscured by the high levels of conversion and formation of higher molecular weight residues.

In this paper, we wish to report the results of a combined theoretical and experimental study which we believe does provide experimental confirmation of a direct cleavage path. In support of this conclusion, we present an analysis of the possible reaction pathways.

### EXPERIMENTAL SECTION

The model compound used in the pyrolysis studies, 1,20-di(1-pyrenyl)icosane (1) was obtained from Molecular Probes Inc., Eugene, Oregon and used without further purification. The material was 99 % pure by high temperature gc.

Nuclear Magnetic Resonance spectra were recorded using a Brüker AM-360. Peak positions were referenced to tetramethylsilane (TMS) and all spectra were run in CDCl<sub>3</sub>. Products were analyzed by gc using either a HP 5890 equipped with an FID detector (column 30M x 0.32mm I.D. SPB-5, cross-linked methyl silicone, 0.25μ) operated in the splitless mode or a Carlo Erba HT SIM-DIST (high temperature simulated distillation) GC. Mass spectral analyses were conducted using an HP5995 GC/MS with RTE-6 Data Station equipped with a column identical to that described above for the HP5890.

A Perkin Elmer TGS-2 Thermogravimetric System was modified and operated to achieve heatup rates up to 20 times faster than it was designed for. The reactor and balance mechanism were enclosed and continuously purged with helium. The TGA thermocouple was calibrated using high temperature Curie Point metals as recommended by Perkin Elmer.

Flash Pyrolysis studies were carried out using a commercial pyroprobe instrument (Chemical Data Systems, Inc. CDS 122 Pyroprobe) equipped with an electrically heated platinum coil on the end of an

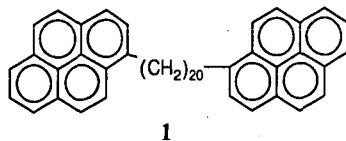
insulated probe. In a typical experiment, the nonvolatile model compound of interest was coated on the wire by placing a small amount of the organic material onto the coil and then heating until the material melts and formed a thin film on the surface. The probe was then fitted with a glass tube sealed at one end, and the pyrolysis chamber was purged with helium. The coil was then rapidly heated to temperature (600 to 1000°C max.) at the maximum rate possible (nominally 20,000 °C per sec) and maintained at temperature for the desired reaction time. Products collected on the inside surface of the air cooled tube and were washed down the tube with solvent and analyzed by gc, gc/ms, and <sup>1</sup>H NMR spectroscopy.

A detailed chemical kinetic model for the pyrolysis of 1 was constructed using an abbreviated set of reactions from the modeling of butylbenzene.<sup>3</sup> The thermochemistry was changed to reflect the increased stability of the 4-ring benzylic like radical relative to the one ring case. Stein and Golden estimate this to be 8 kcal/mole.<sup>7</sup>

## RESULTS AND DISCUSSION

### Pyrolysis Experiments

We have conducted pyrolyses using open reactor configurations and flash pyrolysis methods. The model used was 1,20-di(1-pyrenyl)eicosane (1) (bp. ~620°C, estimated from gc simulated distillation).



When 1 was pyrolyzed in an open reactor (TGA) at 425 and 512°C, the sample weight loss was monitored as a function of time. The products were collected and analyzed by high temperature GC. Liquid product recovery was nearly quantitative (99%) plus a 3% yield of a nonvolatile residue (total mass recovery 102 % for the 425°C sample. For the 512°C sample, liquid and residue yield were 94 and 2% respectively (total mass recovery 96%).

GC results show some starting material in the volatile liquids (32 % at 427 °C and 9 % at 512°C) and the formation of a substantial amount of pyrene and its paired pyrolysis product, 1-eicosylpyrene as well as the usual series of paired alkyl and terminal alkenylaromatics. This confirms the importance of an anomalous direct side chain cleavage pathway in alkylpyrene pyrolysis. It also indicates the extent of volatilization of 1 under the TGA experimental conditions.

In figures 1a and b, a schematic representation of the product selectivity data is given for the 427 and 512 °C runs. The plots clearly show the general pairing of products when an internal carbon-carbon bond is cleaved. Comparison of the plots demonstrates the suppression of pyrene production at high temperature. This is consistent with the sealed tube data in reference 6. Table I quantifies these trends for the alkylpyrenes, includes flash pyrolysis data for 1 at 575°C, and includes product selectivities for butylbenzene at 505°C for comparison.

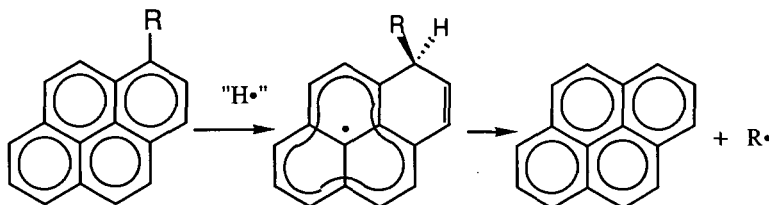
The proton NMR spectrum for the products derived from flash pyrolysis at 425°C is shown in figure 2 with an enlargement of the olefin region. The four multiplets on the right of this region are unambiguously assigned to the terminal hydrogens of vinylpyrene and the olefinic hydrogens of the series of terminal olefins (chain length greater than C<sub>2</sub>) substituted on pyrene.<sup>8</sup> The downfield multiplet is assigned to the beta hydrogen of an alkyl substituted vinylpyrene (see fig. 2b). Its chemical shift and coupling pattern are consistent with the trans isomer. Figure 2b shows a comparison of the experimentally observed adsorption and a spectral simulation.<sup>9</sup> Using standard literature coupling constants,<sup>10</sup> excellent agreement is obtained.

Formation of the internal olefin discussed above provides a candidate for the missing source of hydrogen needed for side chain cleavage. Confirming support for this hypothesis was obtained by tracking the formation of this species relative to pyrene at different temperatures. The ratios for pyrene to vinylpyrene and internal olefin to vinylpyrene are 0.46 and 0.41 (575°C max.) and 0.24 and 0.21 (800°C max.)

respectively.<sup>11</sup> These values clearly show that formation of the internal olefin is coupled to pyrene formation.

### Mechanistic Interpretations

In the general case, three mechanistic possibilities exist for the conversion of an alkylpyrene to pyrene and an alkane. They are distinguished by the following elementary reaction features: 1) ipso hydrogen atom addition, 2) bimolecular radical hydrogen transfer, RHT (transfer of hydrogen from a location beta or, in the general case, distant from the site of highest spin density at alternate carbons),<sup>12,13</sup> and 3) a multistep path with internal hydrogen transfer. All are assumed to involve the intermediacy of an adduct formed from the addition of a hydrogen atom to position 1 of the 1-substituted pyrene. The resulting species from this addition is a very stable polycyclic aromatic  $\pi$ -radical and is formally a vinyl substituted perinaphthyl radical (2). It is also expected that this intermediate will fragment rapidly to give the parent pyrene and an alkyl radical. The critical mechanistic steps concern the formation of 2.



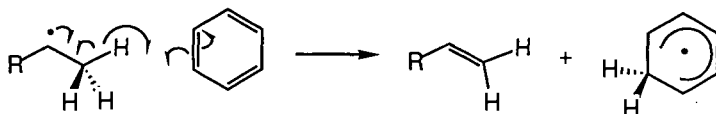
2

### *Ips*o Hydrogen Atom Addition

The production of pyrene and *n*-C<sub>20</sub>-pyrene decrease with increasing temperature. Previous experimental and modeling results on butylbenzene show an increase in benzene production by ipso hydrogen atom addition with increasing temperature. Kinetic modeling results in this work also show that an ipso hydrogen atom addition would yield an increase in side chain cleavage with increasing temperature. Since the experimental results are opposite this trend, we believe that free hydrogen atoms are not the primary cause of the cleavage.

### Radical Hydrogen Transfer (RHT)

Examination of the radical hydrogen transfer pathway from a thermochemical kinetic perspective requires a knowledge of the intrinsic reaction barriers and the heats of formation of the intermediates. For the proposed direct radical hydrogen transfer mechanism, little information exists concerning the barrier heights for this process.

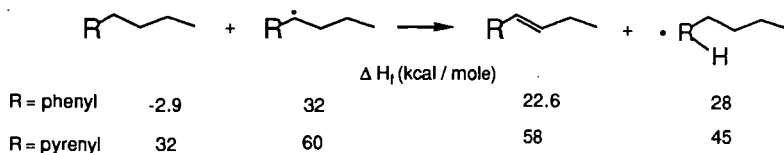


An estimate of the barrier for radical hydrogen atom transfer (RHT) can be calculated from literature rate constants for a nearly degenerate case ( $\Delta H = 0$ ) involving transfer of hydrogen from a 2-ethyl-9-hydroanthryl to anthracene.<sup>14</sup> Using a typical bimolecular pre-exponential factor, an  $E_a$  value of 18 kcal/mol is obtained.

From the above discussion, a key piece of information required to assess the viability of RHT as a mechanistic alternative is a quantitative estimate of the pyrene-derived vinylperinaphthyl radical stabilization energy. Estimates of hydrogen atom addition heats to a series of polycyclic aromatic systems have been reported. Unfortunately, large disagreement exists for the pyrenyl and phenanthryl ring systems. For perinaphthyl radical, estimates of resonance stabilization range from 22 to 47 kcal/mole

depending on the form of resonance-structure theory used.<sup>15</sup> To resolve this critical issue for our own work we have developed a linear free energy correlation using the reliable heats of hydrogen atom addition<sup>15,16</sup> and the reported rates of methyl<sup>17</sup> and trichloromethyl<sup>18</sup> radical addition to a series of polycyclic aromatic hydrocarbons. Given an appropriate reaction heat, a reliable estimate of perinaphthyl radical stabilization energy can be computed from known or easily estimated quantities. The vinyl perinaphthyl radical stabilization energy is estimated to be 46.7 kcal/mole which is close to the high range value estimated by Stein<sup>15</sup> ( $\Delta H_1(\text{perinaphthyl}) \sim 32\text{-}47$  kcal/mole) using Herndon's methods<sup>16</sup> for perinaphthyl itself.

For simplicity the butylpyrene system is used in all thermochemical estimates instead of 1. Given a stabilization energy of 47 kcal/mole for the vinyl-perinaphthyl system, a reaction heat can be calculated for bimolecular radical hydrogen transfer for the pyrenyl and phenyl systems.



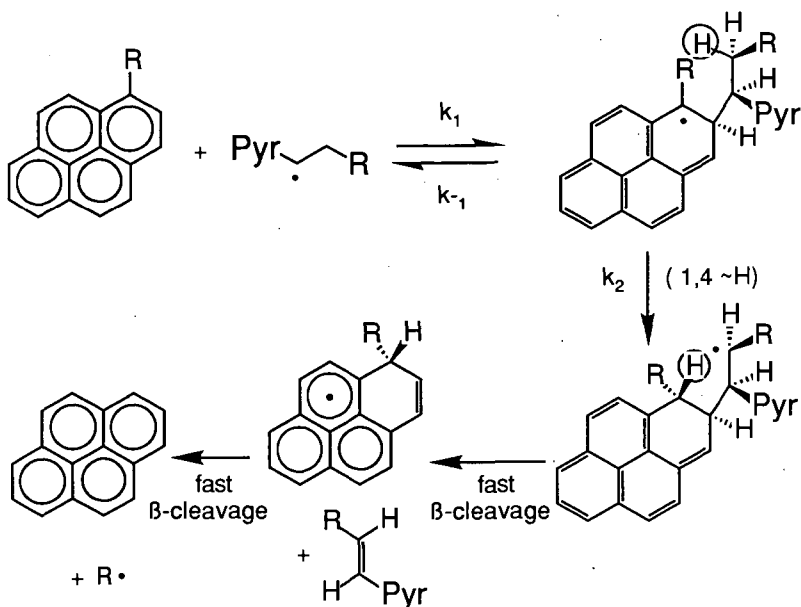
An enthalpy of 21 kcal/mole is obtained for the butylbenzene system while the overall reaction with butylpyrene gives a  $\Delta H_{\text{rxn}}$  of 11 kcal/mole. In both cases the reaction gives a delocalized radical and an internal olefin conjugated to an aromatic ring. Summing the barrier estimate for remote hydrogen transfer (RHT) calculated from Stein's work ( $E_a = 18$  kcal/mole) and all of the reaction enthalpy for the butylpyrene case gives a total barrier of 29 kcal/mole for this elementary step (RHT). This value would be an upper limit since all of reaction enthalpy would not be felt at the transition state. To put this value in perspective, note that the typical activation energies for thermoneutral hydrogen transfer are in the range of 10-13 kcal/mole. The reaction transferring a hydrogen atom from the highly stabilized benzylic radical in a pyrene system to form a secondary unstabilized radical is about 20 kcal/mole endothermic, leading to an activation energy in the range of 30-33 kcal/mole. Hence a process with a 29 kcal/mole activation energy for this radical hydrogen transfer should be quite competitive with conventional hydrogen transfer. Indeed, these values would suggest that at higher temperatures, if hydrogen transfer were rate limiting, conventional hydrogen transfer would begin to win out over this new reaction, leading to the observed temperature dependence of the selectivity.

To derive an estimate of the RHT barrier from the TGA data of the pyrolysis of 1, the existing model for butylbenzene pyrolysis was modified. Changes were made to make the model appropriate for butylpyrene (adjustment for increased radical stabilization by pyrene) and the inclusion of RHT hydrogen transfer step (see experimental section). The kinetic parameters for this reaction were adjusted to match the experimental measurements. This yielded a barrier of 25 kcal/mole [ $k = 3.5 \times 10^{11} e^{(-25000/RT)}$  cc/mole-sec] which is close to the above estimated value of 29 kcal/mole.

For the single ring aromatic case, the large reaction enthalpy and intrinsic barrier (21 + 18 = 39 kcal/mole) suggests that remote hydrogen transfer will not occur in that system and explains why little cleavage at the ring is observed experimentally.

#### Multistep Pathway

The third mechanistic possibility for side chain cleavage at the pyrene ring involves a sequence of elementary steps: addition, intramolecular hydrogen transfer and cleavage to products. The scheme shown below details these steps for alkyipyrene side chain cleavage.



We estimate that the reaction enthalpy for addition and for the subsequent hydrogen transfer to be quite endothermic ( $\sim 24$  and  $14$  kcal/mole, respectively). Using a steady state analysis of the initial addition adduct and typical intrinsic barriers with these reaction enthalpies leads to a product production rate which is many orders of magnitude less than the observed rate constant for pyrene formation extracted from kinetic modeling. Hence, no multistep mechanism that we can envision competes with the remote hydrogen transfer pathway.

## CONCLUSION

From our experimental work and modeling, we conclude that alkylpyrene side chain cleavage at the aromatic ring is unusual in two ways: First, it involves the specific structure of the pyrene system in that ipso addition of a radical generates a highly stable vinyl perinaphthyl radical and second, the critical, perinaphthyl like, intermediate is formed by a remote hydrogen transfer reaction. We estimated the heat of formation of the critical intermediate described above, and this supports a perinaphthyl radical stability of  $47$  kcal/mole, which is at the high end of literature values.

Product studies have revealed the formation of an internal olefin conjugated to pyrene during pyrolysis of model alkylpyrene which is produced in concert with pyrene. This provides confirming evidence for the source of hydrogen needed to effect bond cleavage. This information plus thermochemical analysis limits the mechanistic possibilities to a process that must involve direct bimolecular radical hydrogen transfer.

## REFERENCES

1. Hansford, R.C. in Farkas, A. Ed., *Physical Chemistry of Hydrocarbons*; Academic Press: New York, 1953, 224-226.
2. a) Rebick, C. in W.A. Pryor, Ed., *Frontiers of Free Radical Chemistry*; Academic Press: New York, 1980, 117-137.; b) Savage, P.E.; Klein, M.T. *Ind. Eng. Chem. Res.* **1987**, *26*, 374 and *ibid.* **1987**, *26*, 488.

3. Freund, H.; Olmstead, W.N. *Int. J. Chem. Kinetics* **1989**, *21*, 561-574.
4. Kossiakoff, A.; Rice, F.O. *J. Am. Chem. Soc.* **1943**, *65*, 590.
5. Robaugh, D.; Tsang, W. *J. Phys. Chem.* **1986**, *90*, 4159.
6. Savage, P.E.; Jacobs, G.E.; Javanmardian, M. *Ind. Eng. Chem. Res.* **1989**, *28*, 647.
7. Stein, S. E.; Golden, D.M. *J. Org. Chem.* **1977**, *42*, 839-841.
8.  $^1\text{H}$  NMR: Vinylpyrene terminal olefins (trans H, 5.98 ppm,  $J_{\text{trans}} = 17.4$  Hz,  $J_{\text{gem}} = 1.2$  Hz; cis H, 5.60 ppm,  $J_{\text{cis}} = 11$  Hz,  $J_{\text{gem}} = 1.2$  Hz); aliphatic chain olefins (terminal H's, 5.02-4.87 ppm, dd with allylic coupling, non terminal H, 5.79 ppm, multiplet).
9. Brüker spin system simulation software "PANIC", Parameter Adjustment in NMR by Iterative Calculation, 1985 version.
10. Typical coupling values were used in the simulation and gave peak positions and intensities nearly identical with the observed pattern; For the beta vinyl hydrogen in the internal olefin,  $J_{1,2}$ (trans olefinic coupling) = 15 Hz,  $J_{2,3}$ (olefinic to  $\text{CH}_2$ ) = 5.8 Hz =  $J_{2,4}$ ; Gorden, A.J., Ford, R. A. *"The Chemist's Companion"*; John Wiley & Sons; New York, **1972**, 269.
11. The pyrene to vinylpyrene ratio was obtained by gas chromatographic analysis while the internal olefin to vinylpyrene ratio was obtained by integration of the olefinic region of the  $^1\text{H}$  NMR spectrum (see figure 2).
12. McMillen, D.F.; Malhotra, R.; Chang, S.-J.; Ogier, W.C.; Nigenda, S.E.; Fleming, R.H. *Fuel* **1987**, *66*, 1611-1620.
13. Metzger, J.D. *Angew. Chem. Inter. Ed. Engl.* **1986**, *25*, 80.
14. Billmers, R.; Griffith, L. L.; Stein, S.E. *J. Phys. Chem.* **1986**, *90*, 517.
15. Stein, S. E. in R.H. Schlosberg, Ed., *The Chemistry of Coal Conversion*; Plenum Press: New York, **1985**, 13-44.
16. Hemdon, W.C. *J. Org. Chem.* **1981**, *46*, 2119.
17. Levy, M.; Szwarc, M. *J. Am. Chem. Soc.* **1955**, *77*, 1949.
18. Kooymann, E. C.; Farenhorst, E. *Trans. Faraday Soc.* **1953**, *49*, 58.

Figure 1a: Product Selectivities at 427°C Pyrolysis of 1

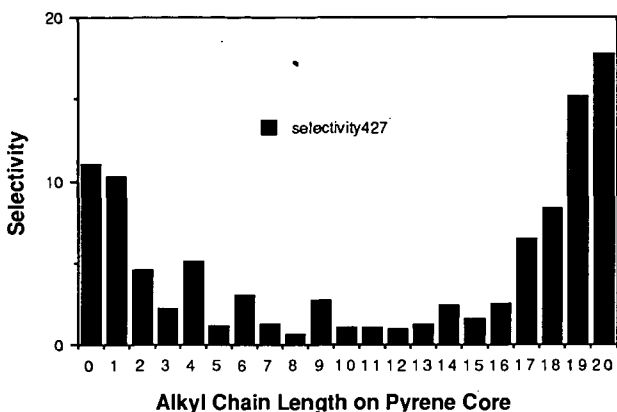


Figure 1b: Product Selectivities at 512°C Pyrolysis of 1

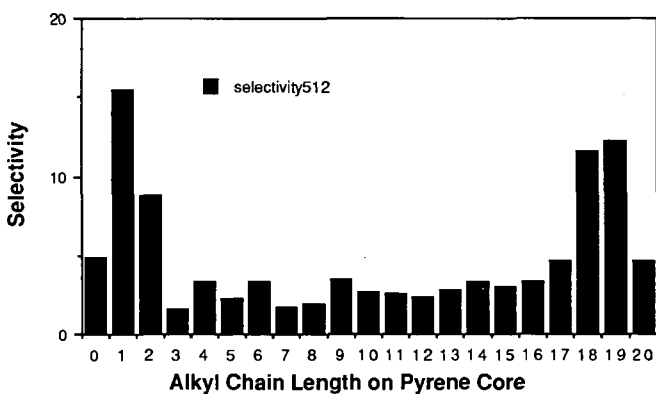


Figure 2a:  $^1\text{H}$  NMR Spectrum (360 MHz) of Flash Pyrolysis (575°C max.) with Expansion and Blow-up of Olefinic Region.

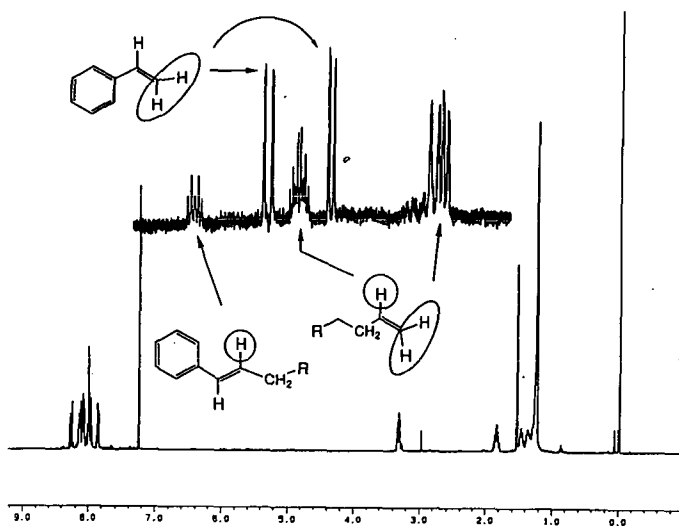


Figure 2b: Comparison of Measured and Simulated Proton NMR Spectrum of  $\text{H}_2$  in the Internal Olefin Product.

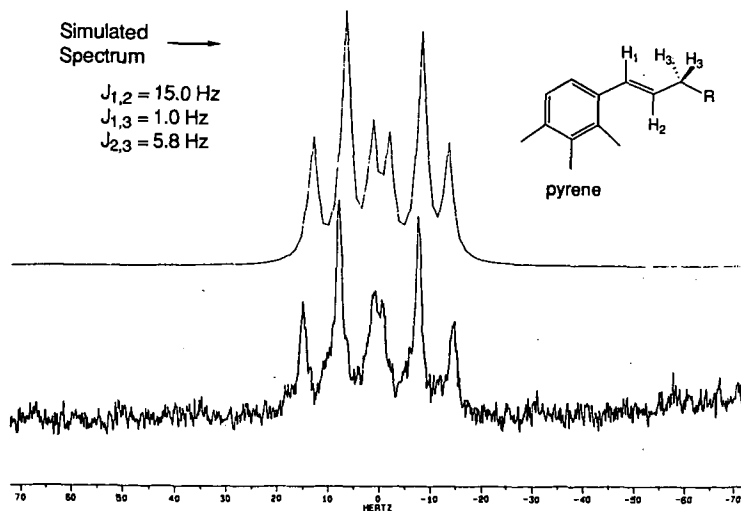


Table 1: Product Selectivities For Sealed Tubes (Savage et al.), OpenReactor (TGA), and Pt Wire (Flash Pyrolysis) Relative to Methylpyrene. Single Ring Data is for Butylbenzene.

	Savage et al.		TGA		Pt Wire	Single Ring Gas Phase
Pyrene	4.3	2.7	1.1	0.32	0.19	0.05
Methylpyrene	1.0	1.0	1.0	1.0	1.0	1.0
C2-pyrene	0.35	0.55	0.44	0.57	0.54	2.2
Temp. (°C)	375	425	425	510	575	505
Citation	ref. 6		this work		this work	ref. 2a

## PYROLYSIS OF PLASTIC COALS: PORE STRUCTURE DEVELOPMENT AND CHAR REACTIVITY

Andreas Matzakos and Kyriacos Zygourakis  
Department of Chemical Engineering  
Rice University  
Houston, Texas 77251-1892

**Keywords:** Coal pyrolysis, macropore structure of chars, char reactivity in oxygen.

### INTRODUCTION

Complex morphological transformations accompany the chemical reactions occurring during the pyrolysis of coals. The structural changes are particularly evident during the pyrolysis of plastic coals. Such coals soften as they are heated up, and the evolving volatile gases form bubbles that swell the coal particles and lead to the formation of highly cellular internal macropore structures.

The macropore structure of chars becomes a major factor in determining char reactivity during gasification processes that take place at elevated temperatures and are, therefore, diffusion-limited. Under such conditions, the accessibility of pores to the gaseous reactants has a strong effect on gasification rates. Low utilization of the surface area associated with the micropores is expected and the reactions occur mostly in the larger macropores that are close to the particle exterior. As the reaction proceeds, however, walls of closed pores will burn away exposing surface area previously unavailable for reaction and leading to substantial particle fragmentation. The opening of closed porosity, the formation of a progressively more tortuous particle exterior and the fragmentation of the original particles can lead to large enhancements of the observed gasification rates.

This study presents some of our recent experimental results on the effect of pyrolysis conditions on the macropore structure of coal chars and on their reactivity during combustion with oxygen. The variables we consider are the pyrolysis heating rate, the final heat treatment temperature (HTT), and the soak time at HTT. Pyrolysis and gasification experiments are carried out on (i) a thermogravimetric reactor that provides accurate measurements of volatile evolution and combustion rates and (ii) a microscope hot-stage reactor that allows direct observation of pyrolyzing and burning particles under a microscope. The combination of these two techniques allows us to observe and interpret some interesting transient phenomena such as self-ignition and fragmentation of char particles. Our analysis pays particular attention to combustion at high temperatures where the heterogeneous reactions take place in the regime of strong diffusional limitations.

### EXPERIMENTAL PROCEDURES

The coal used was the Illinois #6 from the Argonne premium coal sample collection. Coal particles in the 28-32 mesh (500-595  $\mu\text{m}$ ) range were pyrolyzed in a thermogravimetric reactor (Perkin Elmer TGS-2) with a custom-built furnace and computer-controlled heater. For each run, a coal sample of about 1 mg (8-10 particles) was pyrolyzed in nitrogen atmosphere. Pyrolysis experiments were carried out at the following conditions: Heating rates: 0.1, 1 and 10  $^{\circ}\text{C}/\text{s}$ ; Final heat treatment temperature (HTT): 700, 800 and 900  $^{\circ}\text{C}$ ; and Soak Time at HTT: 0 and 3 minutes.

The char particles were reacted with oxygen immediately after the pyrolysis stage. The pyrolyzed samples were rapidly cooled from the HTT to 250  $^{\circ}\text{C}$  and a mixture consisting of 20% oxygen and 80% nitrogen was introduced in the reactor. After a few minutes, the samples were rapidly

ramped to the final combustion temperature which varied from 400 °C to 550 °C. The gravimetric capabilities of our reactor allowed us to also obtain a proximate analysis of the volatile and ash content of the coal samples.

A data acquisition and control computer continuously monitored the weight of the samples during both the pyrolysis and combustion stages. The same computer controlled the temperature of the TGA and operated the mass flow controllers that set the gas flow rates. Temperature control was very accurate. During the entire temperature program, the average squared error in temperature was of the order of 1 °C. Raw data (sample weight and temperature vs. time) were stored on a computer disk for later analysis. The weight vs. time data were interpolated with B-splines (using a least squares approximation) and the interpolant was differentiated to obtain the reaction rates.

A microscope hot-stage reactor (Glass and Zygourakis, 1988) was also used for visual observation of the coal particles during the stages of pyrolysis and combustion. The experiments were recorded in video tape and specific images were later digitized on a digital image processor. From the digital images, time resolved measurements of particle swelling were obtained.

## RESULTS AND DISCUSSION

### Pyrolysis

The experiments on the microscope hot-stage reactor showed that the coal particles swell considerably and that the swelling increases with increasing heating rates. Although we did not characterize in detail the macropore structure of the chars produced during the experiments reported here, our swelling measurements indicate that the char particles have very open cellular macropore structures similar to those quantified via digital image analysis in our earlier studies with the same parent coal (Zygourakis, 1988). As we expected, the heating rate strongly affected the swelling (and therefore the macroporosity) of the char particles.

By continuously monitoring the weight loss of the pyrolyzing coal samples, the instantaneous volatile release rates were obtained and analyzed to elucidate the effects of heating rate. Figure 1a shows the weight loss rates for several runs at two different heating rates. The results for 0.1 and 10 °C/s indicate very good reproducibility and the maximum pyrolysis rate is observed in a rather narrow temperature range for each heating rate. There is, however, a significant shift of this maximum towards higher temperatures as shown in Figures 1a, 1b and Table 1.

Heating rate (°C/s)	0.1	1.0	10
Temperature (°C)	410-425	460-480	510-545

This shifting of the maximum to higher temperatures with increasing heating rates suggests that such experiments can be used to determine the kinetic constants of devolatilization rates. For example, if we assume that the rate of devolatilization can be described by the following simple model

$$\frac{dV}{dt} = k_0 e^{-\frac{E}{RT}} (V^* - V) \quad (1)$$

where  $V(t)$  is the fraction of the original coal sample lost up to time due to the release of volatiles and  $V(t) \rightarrow V^*$  as  $t \rightarrow \infty$  (see Anthony and Howard, 1976). If we set  $\theta = (V^* - V) / V^*$ , Equation (1) becomes

$$\frac{d\theta}{dt} = -k_0 e^{-\frac{E}{RT}} \theta \quad (2)$$

At the temperature  $T_m$  where the maximum devolatilization rate is observed

$$\frac{d^2\theta}{dt^2} = 0 \Rightarrow \exp\left[-\frac{E}{RT_m}\right] = \frac{E q}{k_0 R T_m^2} \Rightarrow \ln\left(\frac{T_m^2}{q}\right) = \left(\frac{E}{R}\right) \frac{1}{T} + \ln\left(\frac{E}{R k_0}\right)$$

where  $q$  is the constant pyrolysis heating rate. The semi-log plot of Figure 2 shows an excellent correlation ( $R=0.9998$ ) and yields  $E = 43.4$  kcal/mole and  $k_0 = 2.09 \times 10^{11}$ . These numbers are in good agreement with other data in the literature. An analysis of these data using a more detailed pyrolysis model is currently under way. Although the weight loss rate changes significantly during the pyrolysis stage, our data show that most of the weight loss occurs during a period when the pyrolysis rate is almost constant. Since the pyrolysis occurs under nonisothermal conditions, this observation agrees with the previous model.

A final observation (Figure 3) is that the amount of released volatiles appears to increase slightly with increasing heating rates. This observation is in agreement with the theoretical predictions (Fletcher et al., 1989) of the chemical percolation devolatilization (CPD) model and the experimental observations of Gibbins-Matham and Kandiyoti (1987). We should note, however, that video microscopic observations of coal particles pyrolyzing at high heating rates show "vigorous bubbling" as volatiles are emitted from the softened coal. This raises the possibility that the escaping volatiles may carry away small fragments of the coal.

### Combustion

The combustion rates were computed from the weight vs. time data  $m(t)$  according to the formula

$$r(t) = \frac{1}{m(t)} \frac{dm(t)}{dt} \quad (3)$$

where  $m(t)$  is the mass of the sample at time  $t$ .

Figures 4a and 4b show the evolution of reaction rates with conversion for several char samples prepared at a heating rate of 1 °C/s and three different heat treatment temperatures (HTT): 700, 800 and 900 °C. Soak time at the HTT for all these samples was 3 minutes. The experimental gasification data at 450 °C show the expected char reactivity pattern. Chars produced at a HTT of 700 °C are more reactive than chars produced at higher HTT (800 and 900 °C) and the char reactivity (as measured by  $r(t)$ ) increases continuously with conversion. These observations are in agreement with earlier studies on char combustion (see, for example, Serio et al., 1989) indicating an increase in the molecular order of chars produced at high HTT due to enhanced annealing of the organic and mineral components and the microporosity of the chars. They also agree with theoretical models for gasification in the kinetic control regime where the active surface area associated with the micropores is easily accessible to the reactants (see, for example, Zygorakis and Sandmann, 1988). These and similar models predict that the intrinsic reaction rate will follow an increasing pattern due to the increasing accessibility and specific surface area of the enlarging micropores.

The experimental reactivity curves at 550 °C reveal a different behavior. Figure 4b shows that the reaction rate increases sharply and in a rather "discontinuous" fashion in the early stages of gasification with sharp maxima spanning a conversion range of approximately 10%. After one (or more) such maxima, the reaction rate settles at a fairly constant plateau for the remainder of the reaction. Similar maxima but with smaller amplitude and width can be seen in the reactivity curves of Figure 4a.

We carried out a systematic analysis to make sure that these sharp maxima were not artifacts due to measurement errors or to the interpolation of the numerical data. Figure 5 shows the raw weight and temperature as well as the computed reaction rate for curve A of Figure 4b. By carefully analyzing these and other similar data we concluded that the sudden and sharp drop of the sample weight cannot be due to errors in weight measurements or failures of our controller to maintain constant sample temperature.

We have also carefully analyzed our procedure for obtaining the reaction rates. Usually, our data acquisition system will collect about 300 data points during the pyrolysis stage of each run and 300-3,000 data points during the combustion stage (depending on the reaction temperature). The collected weight vs. time data are interpolated in the least-squares sense ( $L^2$  norm) using B-splines and this polynomial approximation is then differentiated to obtain the observed reaction rate according to Eq. (3). It is essential to determine the appropriate order of polynomials and number of breakpoints to use for the interpolation of the raw weight data. If high order polynomials are used, the reactivity curves will be smoothed out and fine details will be lost. Also, the curves will be very noisy if a large number of breakpoints is used. Our choice of polynomials was dictated by the form of our data that indicated the reaction rate is continuous in time but not necessarily smooth (i.e. it has a discontinuous first derivative). Such behavior has also been observed by Sundback et. al. (1984) who attributed it to particle fragmentation. Our earlier studies (Zygourakis and Sandmann 1988, Zygourakis 1989) indicate that these jumps may also be caused by the opening of large internal pores during combustion in the diffusion-limited regime (high temperatures). Therefore, we decided to use C-1 quadratics for the interpolation instead of the more often used C-2 cubic splines. This assumes that the reaction rate is a linear function of time at each interval and can exhibit sharp maxima and minima which would be smoothed out with a cubic spline. The number of intervals is in most cases larger than 30 and our software allows for dynamic placement of the breakpoints in regions with rapidly changing sample weight, a feature that improves our ability to resolve fine details of the reactivity curve. Since we always have more than 20 data points in each subinterval, any noise disturbances cannot significantly influence our results.

The microscope hot-stage reactor provided the last piece of conclusive evidence that helped us determine the cause of the observed "spikes" in the reactivity curves. Visual observation revealed that some particles ignited, usually during the very early stages of gasification at the higher temperatures (e.g. 550 C). Ignited particles were then rapidly consumed. The width of the spikes corresponds to about 10% total conversion and, thus, spike should be attributable to the ignition of one of the 8-10 particles loaded in our reactor for each run.

All this evidence strongly suggest that the sharp spikes in the reactivity curves are due to **particle ignition**. After the ignited particles are completely consumed, the reaction rate remains almost constant for a wide range of conversion. This behavior is in (at least qualitative) agreement with our gasification models that assume that the macropore structure is the major rate-determining factor in the regime of diffusional limitations (high temperatures). While at first only the outer macropores are available for reaction, closed macropores open up as the reaction front reaches them and the observed reaction rate remains relatively constant.

The jumps observed during reaction in the kinetic control regime may also be caused by a progressive opening of large macropores that makes previously closed micropores accessible to the reactive molecules and creates sharp maxima in the reaction vs. conversion curves. We should also note here that **char particles treated at lower HTT are more likely to ignite at 550 °C.**

Figures 6a and 6b show that longer soaking times at the HTT decrease the reactivity of the char samples. Our results also strongly indicate that the longer soaking time (3 mins) rendered the chars much less likely to ignite at 550 C.

Finally, Figures 7a and 7b provide the strongest evidence of the significant effects of the macropore structure on char reactivity. As we have previously established (Zygorakis, 1988), high pyrolysis heating rates lead to increased particle swelling, large vesicular macropores and higher macropore surface areas. These structural characteristics should lead to (a) more reactive chars when combustion is carried out at high temperatures and (b) reactivity vs. conversion patterns exhibiting sharply increasing rates followed by regions of slowly decreasing or almost constant gasification rates. Figures 7a and 7b clearly show that the chars produced at 1 and 10 C/s are more reactive, exhibit the reactivity patterns that are clearly attributable to their macropore structure and ignite more easily during combustion at 550 °C (Figure 7b). When combustion takes place at 450 °C, the reaction rates do not appear to be significantly influenced by the pyrolysis heating rate and, therefore, by the macropore structure. Still, the reactivity curve for the char produced at a pyrolysis heating rate of 10 °C/s shows some "jumps" whose small amplitude seems to indicate that they are caused by macropore opening (e.g. cenosphere structures) rather than by particle ignition.

## CONCLUSIONS

In agreement with literature data, our results show that high heat treatment temperatures and longer soak times result in significant declines in reactivity caused by the increased molecular order of the chars. More importantly, however, the preliminary results presented here clearly indicate that the pyrolysis conditions have strong effects on the macropore structure and, consequently, on the reactivity of the produced chars. They also provide some new insights into the transient phenomena associated with particle ignition and macropore opening during combustion in the diffusion-limited regime of high temperatures.

## ACKNOWLEDGMENT

The authors gratefully acknowledge the support for this work provided by the Department of Energy under contract DE-FG22-87PC79930 (James R. Longanbach, Project Manager).

## REFERENCES

- Anthony, D.B and Howard, J.B., *AIChE J.*, **22**(4), 625 (1976).
- Fletcher, T.H., Kerstein, A.R., Pugmire, R.J. and Grant, D.M., *ACS Div. of Fuel Chem. Preprints*, **34**(4), 1272 (1989).
- Gibbins-Matham, J. and Kandiyoti, R., *ACS Div. of Fuel Chem. Preprints*, **32**(4), 318 (1989).
- Glass, M.W and Zygorakis, K., *Rev. Sci. Instrum.*, **59**(4), 580 (1988).
- Serio, M.A., Solomon, P.R., Bassilakis, R. and Suuberg, E.M., *ACS Div. of Fuel Chem. Preprints*, **34**(1), 9 (1989).
- Sundback, C.A., Beer, J.M., and Sarofim, A.F., *20th Intern. Symp. on Combustion*, Ann Arbor, MI, p. 1495 (1984).
- Zygorakis, K. and Sandmann, C.W., Jr., *AIChE J.*, **34**(12), 2030 (1988).
- Zygorakis, K., *ACS Div. of Fuel Chem. Preprints*, **33**(4), 1272 (1988).
- Zygorakis, K., *ACS Div. of Fuel Chem. Preprints*, **34**(1), 202 (1989).

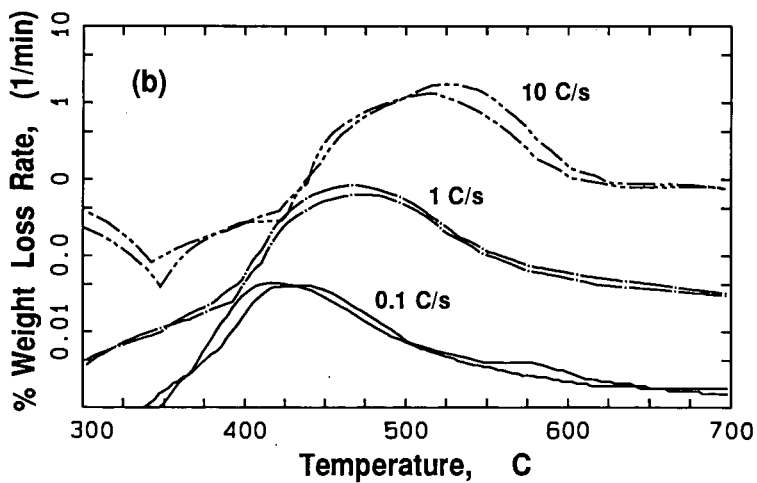
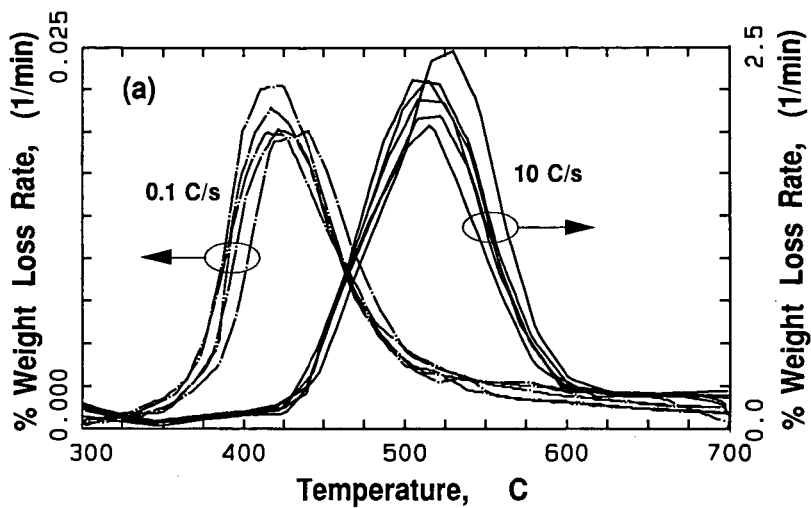


Figure 1: Experimental devolatilization rates for several pyrolysis runs performed at three different heating rates.

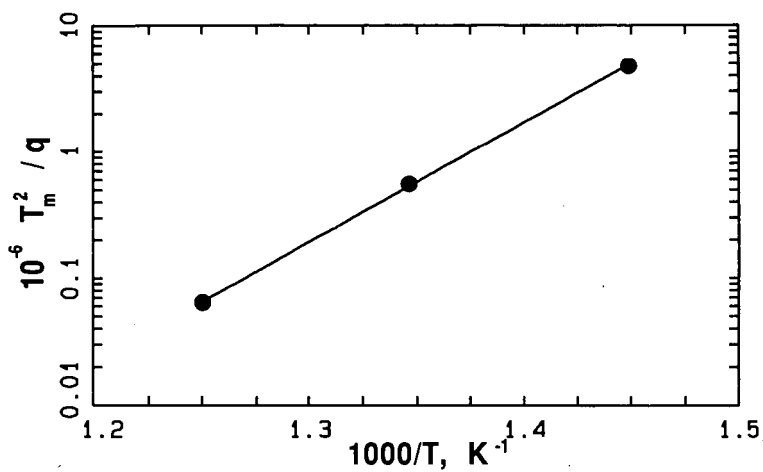


Figure 2: Plot for determining the kinetic constants of the pyrolysis model of Equation (1).

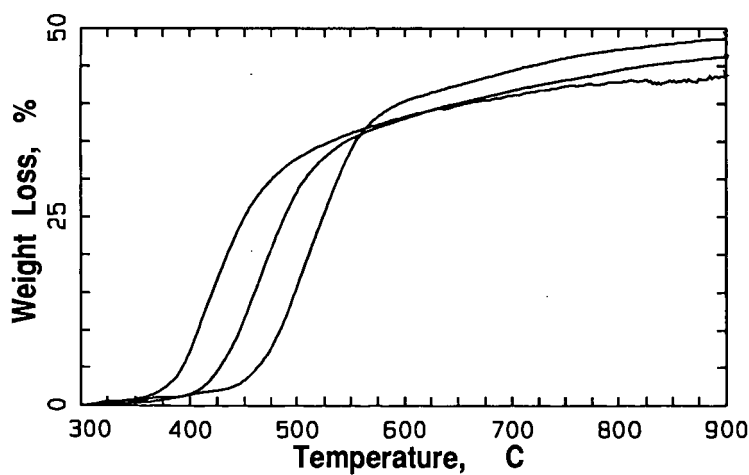


Figure 3: The effect of pyrolysis heating rate on the total amount of released volatiles.

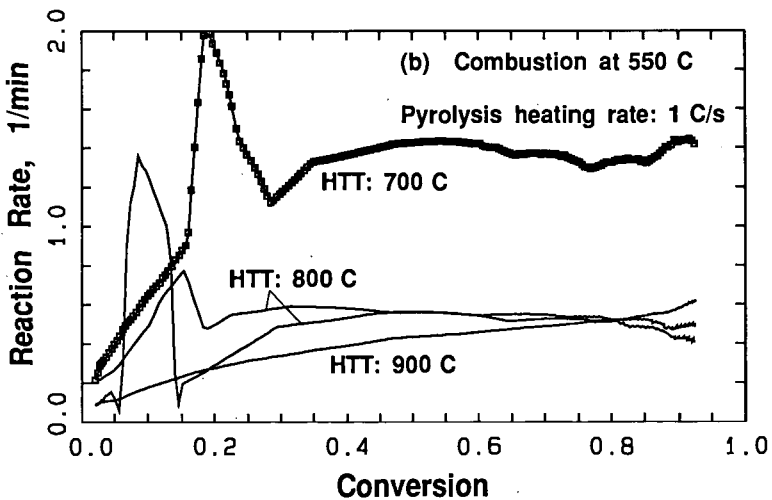
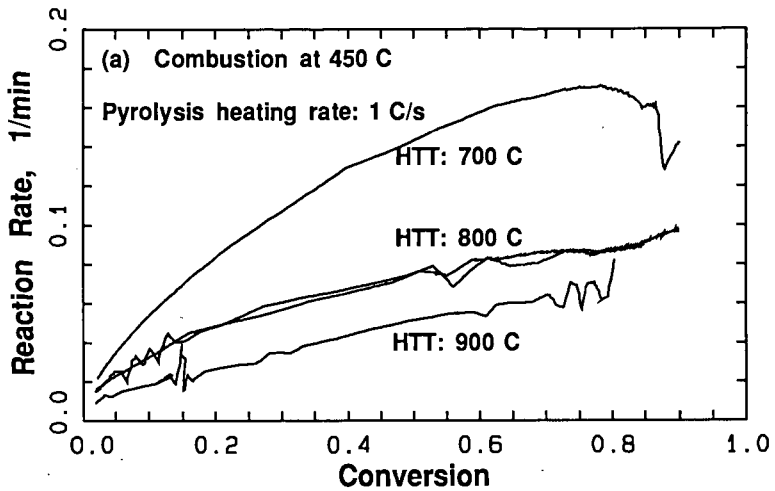


Figure 4: The effect of heat treatment temperature on the reactivity vs. conversion patterns for Illinois #6 chars gasified with oxygen at (a) 450 and (b) 550 °C (Soaking time at HTT: 3 minutes).

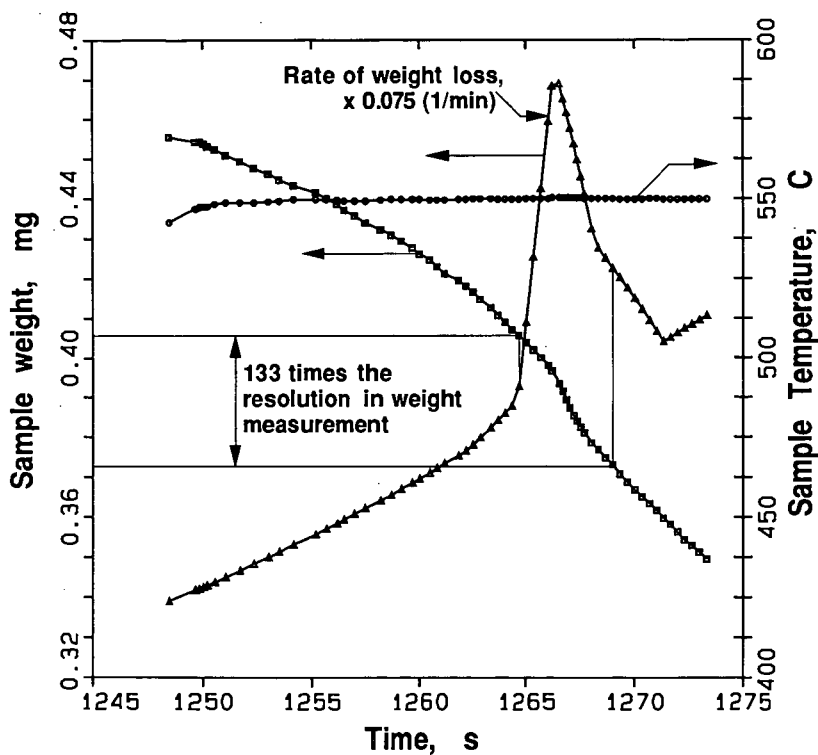


Figure 5: Raw data (sample weight and temperature vs. time) and computed reaction rate for a small part of curve A of Figure 4b.

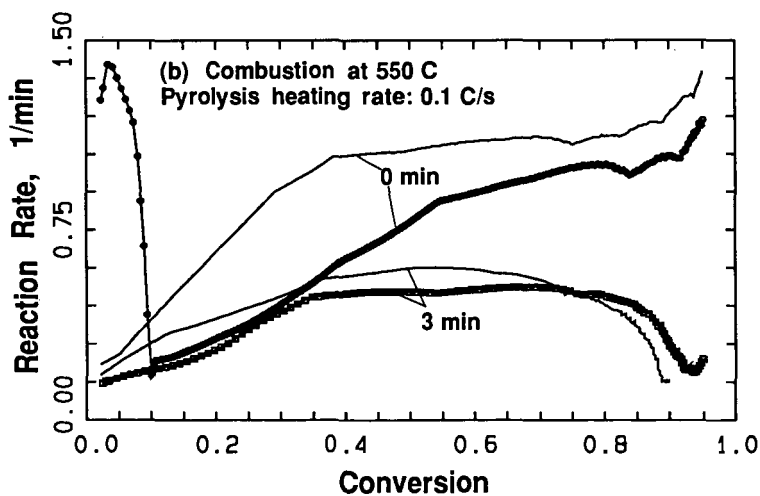
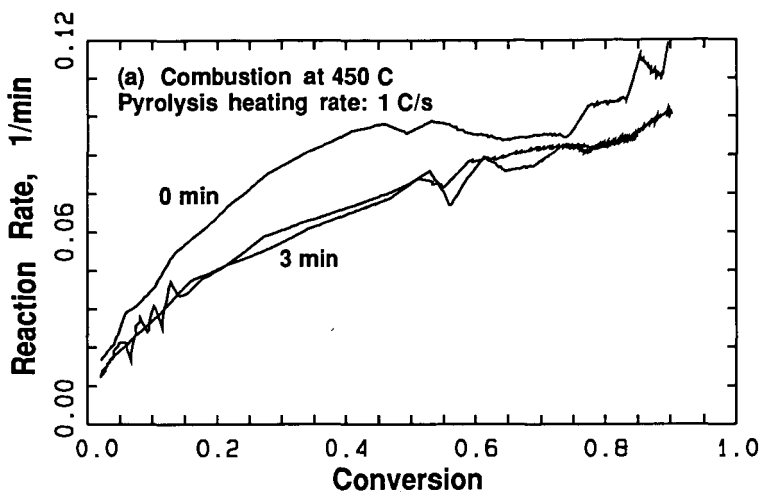


Figure 6: The effect of soaking time on the reactivity vs. conversion patterns for Illinois #6 chars gasified with oxygen at (a) 450 and (b) 550 °C (Heat treatment temperature: 700 °C).

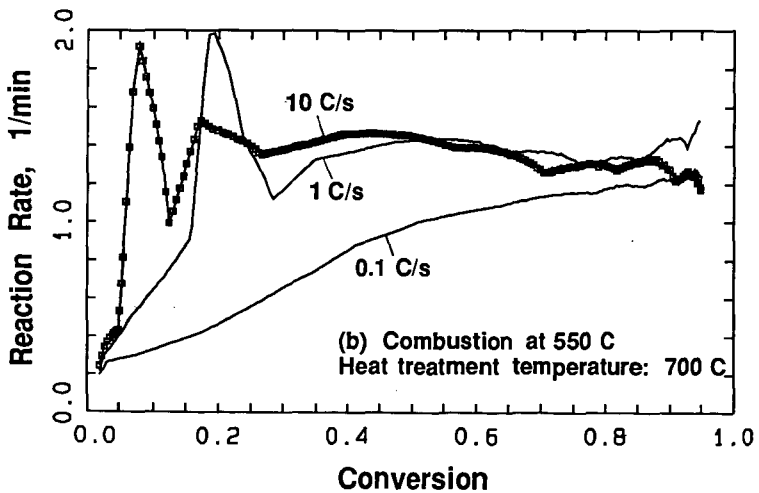
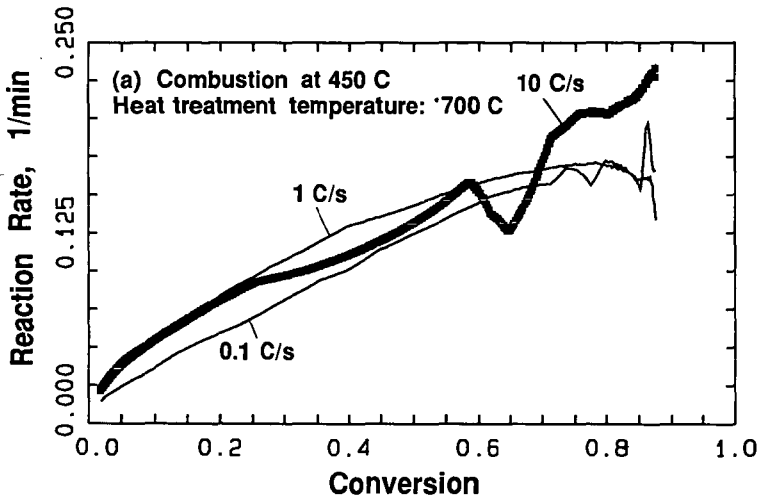


Figure 7: The effect of pyrolysis heating rate on the reactivity vs. conversion patterns for Illinois #6 chars gasified with oxygen at (a) 450 and (b) 550 °C.

PERCHLOROETHYLENE EXTRACTION OF SULFUR AND  
SULFUR COMPOUNDS FROM COAL

David H. Buchanan and Linda C. Warfel

Chemistry Department  
Eastern Illinois University  
Charleston, IL 61920

Keywords: Elemental sulfur, Pyrite oxidation

ABSTRACT

Perchloroethylene (PCE) is an excellent solvent for extracting elemental sulfur ( $S^0$ ) from bituminous coal. The same amount of  $S^0$  is extracted within one hour at reflux (120°C) or 72 hours at 27°C. Extractions at 120°C also remove 1-2 weight % organic material within 30 minutes. Additional heating increases the amount of organic material extracted but decreases the concentration of  $S^0$  in solution due to reactions between sulfur and coal. The elemental sulfur content of ten different mid-western coal samples varies with the sulfatic sulfur content, consistent with the view that both elemental sulfur and sulfate in coal come from weathering of pyrite. The nature of the organosulfur compounds extracted by PCE and by THF has been studied by Sulfur Sensitive Gas Chromatography and GC/MS as described in an accompanying paper by K. Vorres.

INTRODUCTION

Previous studies have shown that hot perchloroethylene (PCE) extracts significant quantities of elemental sulfur ( $S^0$ ) from several mid-western coals. Narayan reported that 1.6%  $S^0$  by weight was recovered from an Indiana refuse coal and speculated that organic sulfur in coal may in fact exist as insoluble polysulfides which are converted to soluble orthorhombic sulfur ( $S_8$ ) by hot PCE.(1) S. Lee and H. Leeche have reported that ASTM organic sulfur is reduced in the PCE-insoluble product coals after PCE extraction and they have qualitatively identified  $S^0$  in the extracts.(2)(3) However, other studies have shown that little or no  $S^0$  is found in most US coals using other methods.(4)(5)(6) Removal of significant amounts of organic sulfur from coal by simple solvent extraction would be an important contribution to pre-combustion desulfurization.

We have shown that only small amounts of  $S^0$  are extracted by PCE from Illinois coals and that only weathered coals contain extractable  $S^0$ .(7) For at least one coal, pyrite oxidation was shown to be the source of the  $S^0$  extracted.(8) IBC-107 is an Illinois No. 6 coal in which the forms of sulfur have characteristic stable sulfur isotope ratios (SSIR,  $^{34}$ ). In this coal, the SSIR for the organic sulfur is 1.9‰, for sulfatic sulfur 13.2‰ and for pyritic sulfur 24.0‰. The elemental sulfur isolated from this coal had an SSIR value of 19.8‰, showing that it was derived from the pyritic rather than the organic fraction of the sulfur in this coal.(8)

Temperature and contact time were found to be important variables for both the reduction of organic sulfur and yield of  $S^0$  by PCE extraction.(1-3)(7) Long term heating of weathered coal with PCE reduces the yield of  $S^0$ .(9) We now report on the effect of temperature on the extraction of  $S^0$  from coals and on the isolation and chromatographic fractionation of organic compounds extracted by PCE. Because early reports on PCE extraction emphasized the isolation of only elemental sulfur, it is important to note that organosulfur compounds are also present in PCE extracts. The identification of organosulfur compounds in these extracts is discussed in the accompanying paper by Vorres.(10)

## EXPERIMENTAL PROCEDURES

Coal samples used were Illinois Basin Coal Sample Program (Illinois State Geological Survey - ISGS) IBC-101, -201, -501, and -701; Argonne Premium Coal Sample Program coal No. 3 plus an oxidized version of this coal; an Ohio 5/6 coal from Horizon Coal Co. (C.J. Kulik) and an Indiana Refuse coal (R. Narayan). Unless otherwise noted, all coal samples and solid products were dried to constant weight at 0.1 Torr., 100°C in an Abderhalden apparatus before use or before final weights were determined. Samples were supplied as either -60 or -100 mesh material and were not further reduced in size. Ultimate analyses and ASTM Forms of Sulfur analyses of the actual samples of all feed coals and solid products were performed under the supervision of Dr. Chusak Chaven at the ISGS.

HPLC grade PCE (Aldrich) was fractionally distilled before use to remove traces of a UV-active material which interfered with the UV detector used in the HPLC determination of elemental sulfur. Elemental sulfur for preparation of analytical standards and reactions with coal was sublimed immediately before use to remove traces of amorphous sulfur which did not completely dissolve in PCE.

The Soxhlet extraction method developed for PCE is slightly modified from that reported earlier.(11) A thermometer or thermocouple probe was arranged to measure the temperature inside the extraction thimble in the upper one third of the coal mass. An electric heating tape (Brisket) was wrapped around the glass barrel holding the thimble and the PCE inside was maintained at a slow boil (120°C) during the extraction. Under these conditions, any constriction in the siphon tube of the apparatus interrupted smooth cycling of hot solvent. Solvent was added to the apparatus and brought to temperature and the coal sample added to the solvent in the thimble. At the end of the extraction, the contents of the thimble were vacuum filtered on a 0.45 µm PTFE membrane filter. In batch extraction experiments, a weighed sample of dry coal was quickly added to a measured volume of well-stirred PCE in a round-bottom flask maintained at a known temperature with an electrically heated oil bath. Product coal was recovered by hot filtration in which the filter funnel and filter paper were heated by boiling PCE vapors from the receiver flask. A thermometer was suspended such that the temperature of the slurry in the filter was measured and maintained above 118°C.

Product coals were recovered by washing with hot 80% methanol/water, filtration and vacuum drying or by steam distilling PCE away from the coal residue. Aliquots of the solvent extracts were analyzed for elemental sulfur by HPLC after passage through a dry-packed Florisil chromatography column (1cm x 30cm) to remove organic compounds which interfere with the analysis. Column flow was adjusted to 1 drop per second and sample eluted with additional pure PCE. The second milliliter to elute from the column was collected for HPLC analysis on a 4.6 x 250 mm C<sub>18</sub> reversed phase HPLC column using a mobile phase of 95% methanol/water at 1.5 mL/minute with UV detection at 290 nm. The method was calibrated with standard solutions of sublimed S<sup>0</sup> in distilled PCE. The calibration samples were also passed through a Florisil clean-up column.

PCE and THF extracts were fractionated for GC/MS studies by published methods.(12)(13) Solvent-free extracts were chromatographed on alumina using hexane, benzene, chloroform and THF/10% ethanol in sequence. PAC fractions (benzene) were re-chromatographed on silica gel impregnated with PdCl<sub>2</sub>.

## RESULTS AND DISCUSSION

Yields of elemental sulfur extracted are given in Table 1 along with ASTM Forms of Sulfur analyses. A less complete version of this data set has been presented elsewhere.(7)(9) Linear least-squares correlations between weight percent elemental sulfur extracted by PCE and weight percent sulfatic sulfur (ASTM) are

shown below the data. Since  $S^0$  is both produced and consumed during pyrite oxidation, the numerical value of the relationship is probably not a simple ratio of reaction rate constants. The significance of the data is that  $S^0$  is only found in weathered coals, and then in amounts proportional to sulfatic sulfur which is widely conceded to arise from pyrite oxidation. These results, taken with the stable sulfur isotope ratio study, (8) make a strong case for pyrite oxidation as the only source of  $S^0$  necessary to explain PCE extractions.

The reduction in ASTM organic sulfur in the product coals (PCE-insoluble residues) ranged from 2 to 24% by weight. Total sulfur material balances (product coal, PCE extract and wash solvent, if any) ranged from 87 to 102%, with most values from 92 to 96% by weight, Table 2. To date, only coal 0560 has given an organic sulfur reduction above 11%. Because of the many errors in ASTM organic sulfur values, it is important to determine how all of the sulfur in the feed coal is distributed among the product fractions and not just report an apparent loss of sulfur from one fraction.

Our preliminary studies (7) and others (2) (3) have shown that extractions at 90-110°C recover less  $S^0$  than those in which the temperature is carefully maintained at 120°C, the boiling point of PCE. Additional heating at 90 - 115°C decreases rather than increases the yield of  $S^0$  extracted. The studies summarized in Figures 1 and 2 show this behavior to derive from two competing processes - rapid solution of  $S^0$  by processes proceeding even at 27°C, and retrograde reactions between sulfur and coal which occur only at the higher temperature.

Figure 1 shows that the same yield of  $S^0$  is obtained from IBC-101 coal in a batch extraction after 72 hours at 27°C as was obtained under optimum Soxhlet extraction conditions, 3 hours at 120°C. At 120°C, the maximum yields in batch extractions occur at one half hour. Figure 2 shows the decrease in concentration of  $S^0$  remaining in solution when approximately 12 g of APCSP No. 3 coal or a heavily oxidized fraction of that coal (E0935, Table 1) was heated with 1.7 millimoles of elemental sulfur in 150 mL of PCE at 120°C for 816 hours under nitrogen. A control experiment minus the coal did not lose appreciable amounts of sulfur during that time. The initial increase in  $S^0$  concentration for E0935 is due to solution of the  $S^0$  originally present. A plot of  $\ln[S^0/S^0_{int}]$  vs time for the premium coal was linear through four half lives and gave an apparent first-order rate constant of  $9.7 \times 10^{-7} \text{ sec.}^{-1}$  for the disappearance of sulfur.

Conditions which maximize the yield of  $S^0$  do not maximize the yield of organic compounds also extractable from coal. PCE extracts 1-2% by weight organic material from coals. The solvent-free extracts have elemental compositions similar to toluene extracts of the same coals, (11) as expected for a non-polar, non-swelling solvent. We measured the volumetric swelling ratio of IBC-105 coal in PCE to be 1.03 at 25° and 1.06 at 90°C. The total sulfur content of the PCE extract of IBC-105 is 2.1%, essentially the same as the ASTM organic sulfur content of the feed coal. Sulfur contents of PCE extracts of weathered coals are greater than that value by the amount of elemental sulfur extracted. In order to characterize organosulfur compounds removed by PCE, several extracts were fractionated on alumina (12) and on Pd impregnated silica gel. (13) Typical recoveries of fractionated extracts for both PCE (non-polar) and THF (polar) are shown in Table 3. Recovery data show that considerable polar material, especially from the THF extract, remains bound to the column. Stripping the column with pyridine followed by methanol did not raise the total recoveries above 73% for PCE extracts or 40% for THF extracts. Elemental sulfur, when present, elutes with the AHC fraction, in which it was detected by both HPLC and GC/MS. Both fractionated and un-fractionated extracts were analyzed by Sulfur Sensitive Gas Chromatography and Gas Chromatography/Mass Spectrometry at Argonne National Laboratory. The results of that study are discussed in the following paper. (10) The organosulfur compounds identified to date are typical of those

reported by others for non-polar extracts of bituminous coals.(13)(14)

#### CONCLUSIONS

PCE is an excellent solvent for the extraction of elemental sulfur from coals in that the process is quickly completed and very little organic material is lost from the feed coal to the solvent. However, only weathered coals contain elemental sulfur which is the result of pyrite oxidation. PCE extraction does not remove more than 10% true organic sulfur from most coals. Elemental sulfur dissolved in PCE reacts with coal at 120°C to become bound to the coal an effect which may explain why exhaustive extractions with other solvents have failed to yield elemental sulfur.

#### ACKNOWLEDGMENT

We thank Drs. Carl W. Kruse, Conrad Kulik, Ramani Narayan and Karl S. Vorres for samples, Dr. Chusak Chaven and Mr. Kenneth Coombs for experimental assistance, and the Electric Power Research Institute and Illinois Coal Development Board for financial support through the Center for Research on Sulfur in Coal.

#### REFERENCES

1. Narayan, R.; Kullerud, G.; Wood, K.V. Prepr. Pap.- Am. Chem. Soc., Div. Fuel Chem., 1988, 33(1), 193. This coal was mis-identified in the pre-print. We thank Dr. Leon Stock for calling this correction to our attention.
2. Lee, S.; Kesavan, S.K.; Lee, B.G.; Kulik, C.J. Fuel Sci. Technol. Internat., 1989, 7, 443.
3. Leehe, H. in Proceedings: Fourteenth Annual EPRI Fuel Science Conference, EPRI, (1989), in press. Proceedings: 1987 Workshop on Coal Structure, EPRI Report, (1988), ER-6099-SR.
4. White, C.M.; Lee, M.L. Geochim. Cosmochim. Acta, 1980, 44, 1825.
5. Duran, J.E.; Mahassay, S.R.; Stock, L.M. Fuel, 1986, 65, 1167.
6. Schicho, R.N.; Brown, S.H.; Olson, G.J.; Parks, E.J.; Kelly, R.M. Fuel, 1989, 68, 1368.
7. Buchanan, D.H.; Coombs, K.J.; Murphy, P.M.; Chaven, C.; Hackley, K.C.; Kruse, C.W. in Proceedings: Fourteenth Annual EPRI Fuel Science Conference, EPRI, (1989), in press.
8. Hackley, K.C.; Buchanan, D.H.; Coombs, K.J.; Chaven, C.; Kruse, C.W. Fuel Process. Technol. in press.
9. Buchanan, D.H.; Coombs, K.J.; Chaven, C.; Kruse, C.W.; Hackley, K.C. in Proceedings: Third International Conference on Processing and Utilization of High-Sulfur Coals, Elsevier, in press.
10. Vorres, K.S. Prep. Pap.- Am. Chem. Soc., Div. Fuel Chem., 1990, 35( ),
11. Buchanan, D.H.; Osborne, K.; Warfel, L.C.; Mai, W.; Lucas, D. Energy Fuels 1988, 2, 163.
12. Later, D.W.; Lee, M.L.; Bartle, K.D.; Kong, R.C.; Vasilaros, D.L., Anal. Chem. 1981, 53, 1612.
13. Nishioka, M., Energy & Fuels 1988, 2, 214.
14. White, C.M.; Douglas, L.J.; Schmidt, C.E.; Hackett, M., Energy & Fuels 1988, 2, 220.

Table 1

## ASTM FORMS OF SULFUR AND S° EXTRACTED BY PCE FOR WEATHERED COALS

EIU #	Sample Bank #	% S° by PCE	% Total S	% Sulfatic ASTM	% Pyritic ASTM	% Org S (Diff)
HERRIN SEAM ILLINOIS No. 6						
0930	APCSP-3	0.000	4.83	0.010	2.47	2.35
0630	IBC-105	0.0006	4.24	0.010	2.60	1.63
0620	IBC-105	0.037	4.46	0.373	2.26	1.83
0650	IBC-105	0.1085	4.31	0.77	1.45	2.17
E0935	APCSP-3	0.127	4.67	0.934	1.83	1.91
OTHER ILLINOIS/INDIANA COALS						
0300	IBC-101	0.034	4.23	0.127	1.40	2.70
0410	IBC-102	0.199	3.22	0.466	1.88	0.87
0710	IBC-107	0.032	3.77	0.272	0.71	2.79
RN20	INDREFUSE	1.54	11.7	5.96	4.46	1.28
0560	OHIO 5/6	0.058	3.44	0.381	1.18	1.83

ALL 10 SAMPLES: % S° = 0.260\*[% Sulfatic S] - 0.028  $r^2 = 0.993$

HERRIN SEAM: % S° = 0.140\*[% Sulfatic S] - 0.0048  $r^2 = 0.994$

Table 2

## DECREASE OF ORGANIC SULFUR IN PRODUCT COALS AND TOTAL SULFUR MASS BALANCE

Sample Number	Wt% PCE Extract	Wt% Coal Product	Wt% Organic Sulfur in Product	% OS Lost	Mass Balance Sulfur
0410	1.57 %	97.5 %	0.88 %	1.34 %	93.3 %
0560	1.70	98.8	1.44	24.00	97.7
0620	1.77	99.8	1.70	7.28	91.2
0630	1.64	97.3	1.53	8.70	95.2

FRACTIONATION SCHEME

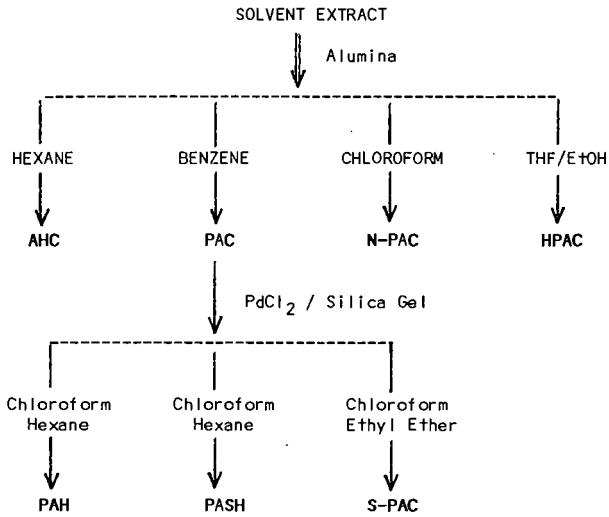


Table 3

FRACTIONATION OF PCE AND THF EXTRACTS

Sample Number	Extract Solvent	Wt % of Extract in Alumina Column Fractions			
		AHC	PAC	N-PAC	HPAH
0560	PCE	20.90 %	22.15 %	16.82 %	8.20 %
0630	PCE	7.24	14.79	15.73	21.54
0930	PCE	8.87	17.28	15.41	28.28
0630	THF	1.44	4.47	3.54	27.88
0930	THF	3.17	3.80	5.06	15.75
		Wt % of PAC in Silica Gel Column Fractions			
		PAH	PASH	S-PAC	
0630	THF	79.69	15.66	14.97	

## Wt % S Extracted vs Time

### Effect of Temperature

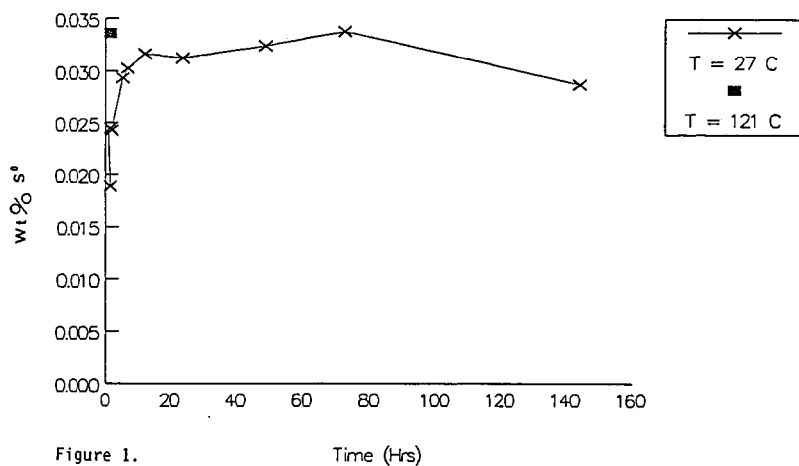


Figure 1.

## [Sulfur] in PCE vs Time

T = 120°C

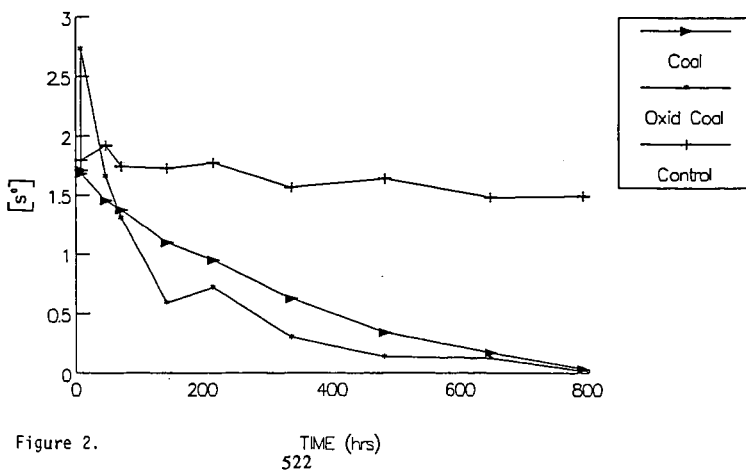


Figure 2.

TIME (hrs)

## Sulfur Species in Perchloroethylene and Other Coal Extracts

Karl S. Vorres  
Chemistry Division, Building 211  
Argonne National Laboratory  
Argonne, IL 60439

Keywords: Sulfur, Premium coal samples, Solvent extraction

### INTRODUCTION

Earlier work (1,2,3) has indicated that elemental sulfur can be removed from coal by the use of perchloroethylene (tetrachloroethylene). The unique ability to remove the elemental form of the sulfur has led to considerable interest in the process and mechanism of action. Under joint CRSC-EPRI sponsorship, an effort has been made to understand the species that can be removed by extraction with perchloroethylene (PCE). The effort involved the extraction of a set of coals at Eastern Illinois University by Prof. David Buchanan and coworkers, and the related effort to identify the species in the extract by the use of gas chromatography-mass spectrometry at the Argonne National Laboratory (ANL). This paper reports on the analytical work on the extracts.

### EXPERIMENTAL

Extracts were prepared and sent in glass vials to ANL. The contents of the vials were dissolved in solvents and studied in one of two systems.

The first system was a gas chromatograph equipped with a Hall Effect Conductivity Detector (HECD). This detector was selected because it can be made to be sensitive to sulfur-containing species and will permit establishing the number of species in very dilute concentrations. The HECD was mounted on a Tracor Model 540 gas chromatograph, and attached to a strip chart recorder. A J&W DB-5 column (30 m, .25 mm id) was used. The typical run started at 85 C for 4 minutes and then the temperature was increased at 10 C/minute to 320 C and held there for up to 30 minutes before cooling. The attenuator on the recorder was reset as needed to keep the peaks on the chart. The settings were recorded on the chart. A series of standards was run to provide retention time values for comparison with the observed peaks.

The HECD measures the conductivity of a sample which has been oxidized (in this case to  $\text{SO}_2$ ) and introduced into a stream of purified methanol. This can be calibrated with standards of varying concentration to obtain quantitative data. The instrument is extremely sensitive to contamination from halogen containing-materials.

The system was calibrated for the amount of sulfur in the individual species by preparing different concentrations of thiophenol and making several runs to establish the response in terms of peak height per unit of mass of sulfur in the compound. The response was  $5 \times 10^{-12}$  grams of sulfur per one millivolt peak.

The second system was a Hewlett Packard GC/MS, model 5970B, which was set up using the same type of J&W DB-5 column used in the Tracor instrument. The same time-temperature profile used with the HECD system was employed to be able to compare the results on a common basis. At the beginning of each day the autotune procedure was used to assure that the instrument was performing to meet the manufacturer's specifications. A blank run was then carried out to check on performance of the chromatograph system and to check on the cleanliness of the solvent.

In a typical run, the chromatogram was displayed, data were saved, and analyzed later. The portion of the chromatogram to study was selected and the characteristics of the peaks to be included were specified. A macro was developed to analyze the mass spectral data for use with the Hewlett Packard computer system. Then for each peak the relative abundance for each mass was tabulated. The data were then checked against the library of about 133,000 spectra for the best matches. A graphical representation of the 4 best matches was printed together with a table of the 20 best matches. A numerical value of the "quality" of the match was included. A standard algorithm for this quality, developed earlier by McClafferty and coworkers, was used.

Initially the gas chromatograph was programmed to have a temperature increase of 10 C/minute for data acquisition. It became evident from the GC/MS results that a number of extracts contained many constituents. A precision temperature profile which used a 4 C/minute heating rate was then used to provide for better resolution of the peaks and improved identification of the species.

The coals used and samples derived from them included

Series 9391, 7107, 7111 and 7112

These extracts were prepared from Illinois #6 samples of the Argonne Premium Coal Sample Program (APCS) and the isotopically labelled sulfur sample of the Illinois Basin Coal Sample Program (IBCSP).

APCS #3, pristine, PCE extract, EIU #9391  
IBCSP #7, oxidized, PCE extract, EIU #7107  
IBCSP #7, light organics from EIU 7107, EIU #7111  
IBCSP #7, heavy organics from EIU 7107, EIU #7112

Series 9395 and 9397

These samples were prepared from APCS #3, a pristine starting material.

Tetrahydrofuran extracts and fractionated on an alumina column to give the following EIU sample numbers

EIU # 9395 AHC Aliphatic hydrocarbons  
EIU # 9395 PAC Neutral polycyclic aromatic hydrocarbons  
EIU # 9395 N-PAC Nitrogen polycyclic aromatic hydrocarbons  
EIU # 9395 HPAH Hydroxy polycyclic aromatic compounds  
EIU # 9395 Py Pyridine eluent  
EIU # 9395 MeOH Methanol eluent

Perchloroethylene extracts

EIU # 9397 AHC  
EIU # 9397 PAC  
EIU # 9397 N-PAC  
EIU # 9397 HPAH  
EIU # 9397 Py

Series 6320

These samples were prepared from IBCSP #5, unoxidized. These samples came from the same block of coal used for APCS #3.

These samples were extracted with THF and fractionated on an alumina column to give the following EIU sample numbers:

6320 AHC  
6320 PAC  
6320 N-PAC  
6320 HPAH  
6320 Py

The 6320 PAC fraction was further separated on a silica gel/PdCl<sub>2</sub> column to give:

6320 PAH  
6320 PASH  
6320 S-PAC, passed over a silica column.

Sample 6269

A PCE extract of oxidized IBCSP #5 was given the sample number 6269.

Sample 6201-38

IBCSP #5, oxidized, PCE extract was sample number 6201-38.  
6201-38 untreated with NiCl<sub>2</sub>  
6201-38 treated with NiCl<sub>2</sub>

Sample 5618

A THF extract of oxidized Ohio 5/6 coal is 5618. The sulfatic sulfur = 0.38%.

In addition to the extracts a number of standard compounds have been run in both instruments. For the HECD, this provided a set of retention times for checking the identity of compounds. For the GC/MS this provided a means of checking the mass spectra as well as retention times.

#### RESULTS AND DISCUSSION

A number of species were found with the HECD in the extracts. Retention times and peak heights were noted such that comparisons could be made later with GC/MS data.

Calibration data with thiophenol indicated that a peak of 1 mv was equivalent to an injection of one microliter containing  $5 \times 10^{-12}$  grams of sulfur. From this the percent of sulfur in the original extract due to these peaks has been calculated.

The data obtained with the HECD indicate that there are many sulfur species in the extracts. Peaks of retention times close to those for sulfur and dibenzothiophene have been observed. The number of sulfur species observed with this detector significantly exceeds the number that have been identified with the GC/MS. However the concentration of these species is so small, that their peaks are lost in the background of the GC/MS traces. The effort to quantify the peaks gave an indication of the amount of sulfur species that were present in the extracts examined with the HECD. The concentration of sulfur species identified in the extracts is usually such that they would account for at most 0.014% S in the sample extract. The organic sulfur content of the samples is at least 2%.

The GC/MS work indicates that the peaks observed are typical of the aliphatic (n-alkanes) and aromatic (substituted naphthalenes) species present in coal samples. In addition a number of substituted thiophenes, benzothiophenes, dibenzothiophene, thiazoles, benzothiazoles and elemental sulfur have been observed

in different samples. The most frequently observed and most abundant is dibenzothiophene. These data are consistent with the observations of Winans et al (10) on the existence of a number of heteroatom containing species in this sample.

In the HECD studies, the 9397 aliphatic hydrocarbon (AHC) extract contained two peaks close to those for sulfur in a total of 11 peaks. Elemental sulfur does elute with this fraction.

According to earlier reports elemental sulfur is not found in extracts of pristine coal samples (4). The results of this study are consistent with the earlier work. Elemental sulfur was seen in a PCE extract of an oxidized coal. This sample showed three forms of elemental sulfur differing in their molecular weights as the hexamer, heptamer and octamer. As expected the retention times increased with the molecular weight. Each comes off of the column at a reproducible retention time, and has a mass spectrum consistent with the particular polymer size. It is significant that the elemental sulfur is found in the oxidized sample which was later extracted with PCE, but not in the pristine samples.

The PCE does extract a series of species which on fractionation are typical of the fractions from better solvents. A range of n-alkanes was seen in the 9397 AHC fraction in addition to the tetramethyl longer chain hydrocarbons. The ability of PCE to remove some organic sulfur compounds from pristine samples is seen in the compounds identified from 9397 PAC. These compounds included three different substituted benzothiophenes and dibenzothiophene. The nitrogen-containing polycyclic fraction also had dibenzothiophene in it along with a possible isothiazole. The hydroxy polycyclic aromatic fraction had a small number of peaks, but they included substituted derivatives of benzenethiol, thiophene, benzothiazole and benzothiophene. In the latter case the quality of the matches were all low, but represent best choices from the available data.

The extracts which were analyzed without fractionation seemed to have too low a concentration of sulfur species for them to be observed. After fractionation, with the associated concentration of these species, the sulfur species were observed. The 9391 was a whole coal extract of pristine APCS #3 and showed almost no indication of a sulfur compound. The 9397 extract fractions showed evidence of sulfur compounds in three of the fractions (PAC, N-PAC and H-PAH). There were 10 peaks in the three fractions representing 9 compounds.

The THF fractions from the same pristine APCS #3 (9395 series) with sulfur compounds in them were essentially the same with the addition of the MeOH eluent. However there were fewer peaks observed (5) representing only 4 compounds. By comparison the PCE was more effective in solubilizing sulfur species. Only one was observed in both series (dibenzothiophene). The other compounds were different in the two series.

Those fractions with more sulfur species in the 9397 series were also observed to have more sulfur species peaks in the HECD studies than the other fractions. The PAC fraction in 9397 had 4 compounds while the HECD showed 53 peaks, and the N-PAC fraction had two compounds while the HECD showed 12 peaks.

Some species were identified which are associated with solvents as preservatives (2-6 bis(1,1dimethylethyl)4 phenol and its oxidation product (1,1 dimethylethyl) 4 methoxy phenol. PCE extracts sometimes had hexachlorobutadiene in them as a product of reaction of two PCE molecules. Others are associated with pump oils such as 1,2 benzenedicarboxylic acid and its esters.

A number of isomers exist for some common compounds in these samples. A number of dimethyl naphthalene isomers were indicated. The difference in quality for these is too small to assign a retention time to a specific isomer. In several cases the compound has simply been listed as dimethyl naphthalene. Since these are not sulfur compounds, the specific identification of these species was not crucial to the study.

#### CONCLUSIONS

1. Small quantities of a number of organic sulfur compounds are extracted from Illinois Basin coals by both perchloroethylene and THF. The amounts are much less than the total organic sulfur in the coal.
2. Elemental sulfur is found in some of the extracts. These extracts are from oxidized coal samples.
3. The elemental sulfur is found in the form of three oligomers with six, seven or eight atoms per molecule.
4. The organic sulfur compounds identified include substituted thiophenes, benzothiophenes, dibenzothiophene, thiazoles, benzothiazoles and possibly others in concentrations lower than were detected with the GC/MS.

5. The concentrations of sulfur species in whole coal extracts was too low to be observed with the GC/MS, but the concentration in the various chromatographic fractions did permit identification of sulfur species in some of the fractions.

6. The PCE extracted different sulfur compounds than the THF did, and extracted a larger number of them.

7. The fractions (PAC, N-PAC, HPAH) which contained sulfur compounds from PCE extractions also contained these types of compounds in the THF extractions.

8. The PCE and THF extracts contained a range of aliphatic and aromatic compounds common to Illinois #6 coal.

#### ACKNOWLEDGMENTS

The sponsorship of the Electric Power Research Insititute is gratefully acknowledged. The principal investigator is grateful for the assistance of P. Sean Smith with the measurements made with the HECD system, to R. L. McBeth for assistance with the preparation of some of the samples, and to Ken Anderson for developing the macro for evaluation of the peaks with the GC/MS. He is also indebted to David Buchanan of EIU and his staff (especially Linda Warfel) for discussions and preparation of the original extracts.

#### REFERENCES

1. R. Narayan, G. Kullerud, and K. Wood, Preprints, Fuel Chem. Div., Am. Chem. Soc., 33 (1) 193-199 (1988).
2. Leehe, H., EPRI Workshop, May, 1988.
3. S. Lee, S. K. Kevasan, B. G. Lee, A. Ghosh and C. J. Kulik. Fuel Science and Technology Int'l, 7 4 443-468 (1989).
4. J. E. Duran, S. R. Mahaysay and L. M. Stock, Energy & Fuels, 2 (2) 163-170 (1986).

## ANION EFFECTS ON CALCIUM CATALYSIS OF LOW-RANK COAL CHAR-STEAM GASIFICATION

R.C. Timpe and R.E. Sears

University of North Dakota  
Energy & Environmental Research Center  
P.O. Box 8213, University Station  
Grand Forks, ND 58202

### ABSTRACT

Limestone (primarily  $\text{CaCO}_3$ ) has been shown to be an excellent bed material in a fluidized-bed reactor operated at 700-800°C and atmospheric pressure for the steam gasification of coal. It not only maintains its physical integrity under these conditions but also has shown catalytic effects on a subbituminous coal-steam reaction that are comparable with the effects of an alkali salt. The study reported in this paper concerns the effect, if any, of calcium-associated anions on the reaction kinetics of the coal char-steam reaction. Velva lignite and Wyodak subbituminous coals to which  $\text{CaO}$ ,  $\text{CaSO}_4$ , limestone, or  $\text{Ca}(\text{C}_2\text{H}_3\text{O}_2)_2$  had been added, were charred in a thermogravimetric analysis unit (TGA) and then were immediately reacted with steam at the temperature and pressure conditions described above. Both coals showed less catalytic effect for limestone and calcium sulfate than for the other two additives. The rate for the Wyodak char-steam reaction increased steadily over 700-800°C with calcium oxide whereas the Velva rate increased rapidly to the maximum between 700-750°C. Apparent activation energies along with surface analyses of selected samples to determine catalyst dispersion and form will be presented.

### INTRODUCTION

Gasification of coal has been shown by many researchers to be greatly enhanced by the addition of alkali or alkaline-earth compounds to the reaction mixture. In the case of the alkali compounds, the excellent catalytic effect of carbonates, hydroxides and bicarbonates, and the somewhat lesser effect of chlorides and sulfates of potassium and sodium are well documented. However, the reasons for the large differences in catalysis that occur with changes in anion have not been satisfactorily explained, and those reasons have been the focus of only limited study, since the negative aspects of using potassium and sodium minerals as catalysts make them impractical to use under present processing conditions. The major drawback to using potassium is the relatively high cost of its catalytically active minerals. Although sodium compounds are plentiful in mineral deposits (trona, nahcolite, sodium chloride) and therefore relatively inexpensive, the inherent problems, such as fouling and agglomeration, associated with having sodium in a reactor make them unsatisfactory additives. Limestone, largely calcium carbonate, has been shown to have a catalytic effect on the reaction between low-rank coal char and steam at temperatures of 700-800°C and ambient pressure in a continuous process unit (CPU)(1). This mineral is not only inexpensive and causes few reactor problems, but also is, in fact, a viable candidate for bed material in fluidized-bed reactors and is promoted by some researchers as an in-bed sulfur-capture material. The question as to the importance of the carbonate, if any, on the activity of the catalyst was addressed in this study by substituting other calcium compounds for limestone in two previous thoroughly-studied char-steam reactions. The answer to the question was expected to provide some understanding of the effect of the anion on the reactivity of the char-steam reaction.

Table 1 shows the elemental analyses of the ash of the raw coals. Both of the coals reacted had a high calcium content.

#### EXPERIMENTAL

Laboratory reactivity testing was carried out at 700, 750, and 800°C and ambient pressure on a DuPont 951 Thermogravimetric Analysis (TGA) module interfaced with a DuPont 1090 Thermoanalyzer data station. Approximately 40 milligrams of -60 x 0 mesh raw coal containing 10 wt% catalyst was devolatilized in vitro, followed immediately by reaction of char carbon with steam as previously reported (2). The reactivity parameter,  $k$ , was calculated for 50% carbon gasification in each test.

Pilot-scale data was obtained from experiments carried out in a nominal 30-lb/hour CPU operating at ambient pressure and temperatures similar to those reported for the TGA experiments (1).

#### CALCIUM CATALYST SCREENING

Wyodak subbituminous and Velva lignite char-steam reactions were carried out using four calcium-containing catalysts, calcium oxide, calcium sulfate, limestone, and calcium acetate, at 700, 750, and 800°C and atmospheric pressure. The choice of limestone is obvious (see Introduction). Calcium oxide was chosen because it has been reported to be the predominant species responsible for catalysis of the gasification reaction (3). Calcium acetate was selected since it is water soluble and, upon heating, decomposes into calcium carbonate and acetone. Since calcium sulfate is insoluble and does not readily decompose at the temperatures of this study it was the final choice. The Arrhenius energy of activation,  $E_a$ , and the correlation coefficient,  $r_2$ , for the Arrhenius plot, along with the reactivity parameter of each of the reactions is reported in Tables 2 and 3. In addition,  $k$  values calculated from CPU data are also given for experiments where limestone was used as bed material. There appears to be a significant difference in the catalysis of the Wyodak char-steam reaction among the materials tested.

TABLE 1

XRFA RESULTS OF ASH PREPARED FROM AS-RECEIVED VELVA LIGNITE AND WYODAK SUBBITUMINOUS COALS USED IN HYDROGEN PRODUCTION TESTS

Element	Velva Ash % Elemental	Wyodak Ash % Elemental
Silicon	5.57	11.44
Aluminum	5.00	7.55
Iron	12.73	12.45
Titanium	0.38	0.76
Phosphorous	0.20	0.55
Calcium	25.49	14.80
Magnesium	6.52	3.53
Sodium	0.45	0.92
Potassium	0.00	0.00
Sulfur	4.68	5.47
Oxygen (Diff.)	38.98	42.53
Ash	6.94	9.05

TABLE 2  
 REACTIVITY PARAMETER FOR WYODAK CHAR-STEAM REACTIONS CATALYZED  
 WITH VARIOUS CALCIUM-CONTAINING SUBSTANCES.

TEMP, C°	Uncat.	Limestone		CaO	CaSO <sub>4</sub>	Ca(Ac) <sub>2</sub>
		k, in g/hr/g				
		TGA	CPU			
700	1.33	1.26	1.60	3.80		
750	3.28	3.01	3.53	6.36	2.77	4.33
800	7.33	3.86	38.98	15.74		
E <sub>‡</sub>	35.45	23.35	65.64	29.34		
r <sup>2</sup>	1.00	0.92	0.95	0.97		

TABLE 3  
 AVERAGE REACTIVITY PARAMETER FOR VELVA CHAR-STEAM REACTIONS  
 CATALYZED WITH VARIOUS CALCIUM-CONTAINING SUBSTANCES.

TEMP, °C	Uncat.	Limestone		CaO	CaSO <sub>4</sub>	Ca(Ac) <sub>2</sub>
		k, in g/hr/g				
		TGA	CPU			
700	2.40	4.95	2.24	6.89		
750	4.95	6.84	5.45	8.01	4.75	6.80
800	6.89	6.95	49.13	10.86		
E <sub>‡</sub>	22.05	7.14	63.57	9.38		
r <sup>2</sup>	0.97	0.81	0.96	0.95		

## RESULTS AND DISCUSSION

Dispersion of catalyst over the organic matrix is a major consideration when studying gasification and catalyst effects (4,5).

Each of the catalysts studied was applied by admixing 10 wt% with coal. Impregnation was not used so as to preserve the integrity of the anion on contact with the raw coal. Of the four calcium catalysts chosen, two (acetate and oxide) were soluble in water and two were not. In coal with 30+% moisture, water-soluble catalyst can disperse into water-filled micropores as well as over the moist surface of particles. In addition, the CaO forms a base, Ca(OH)<sub>2</sub>, when dissolved in water enabling it to better penetrate the coal structure. However, since the water-insoluble catalysts (carbonate and sulfate) were applied as <150 um particles, they were limited to a finite number of contact surfaces and were probably excluded from most micropores. The variation in solubility that results in differences in catalyst dispersion accounted for some of the effects noted in the study.

The uncatalyzed char-steam reactions had rate constants,  $k$ , which were slightly higher at 700°C and 750°C for Velva than for the Wyodak char. This was attributed to catalysis caused by the higher inherent calcium content of the Velva coal. The Velva coal has 33% more calcium and magnesium than the Wyodak coal on a mole-of-element/gram-of-coal basis. The inherent sodium content of the Wyodak, albeit small, was more than twice as great as that of the Velva but probably too small to give obvious rate increases. Silicon and aluminum, which are known catalyst killers, were nearly three times and two times as abundant, respectively, in Wyodak as they were in Velva. However, at 800°C the Wyodak  $k$  was slightly higher than that of the Velva, probably because of limitations due to physical effects such as mass transport rather than chemical reactivity (6).

The catalyst effects observed in this study varied between the two coals. The CaO gave reactivities which were similar for the two coals at 700°C and 750°C but was 1.5 times greater for the Wyodak than for the Velva at 800°C. The limestone-catalyzed reactions had reactivities that were two-fold greater for the Velva than for the Wyodak at each temperature. The calcium acetate-catalyzed Velva char-steam reactivity at 750°C was 1.5 times larger than that of Wyodak. The calcium sulfate appeared to have no positive catalytic effect at 750°C with either coal char.

The catalytic effect of the calcium on the char-steam reaction for each coal varied substantially with the associated anion. With the Wyodak coal little positive effect was observed for the limestone at the three temperatures tested, and no positive effect, and perhaps even some inhibition, was observed for the calcium sulfate at 750°C. The calcium oxide doubled the reactivity of the Wyodak, but it must be realized that a 10 wt% loading of this material provides 7 wt% calcium whereas the other catalysts tested contributed <4 wt% of the element. Calcium acetate also increased the reactivity of the Wyodak at 750°C even though 10 wt% provides only 2.8 wt% calcium.

With the Velva coal, limestone exhibited catalysis at the lower two temperatures. Calcium oxide, as with the Wyodak coal, enhanced the reaction at all three temperatures. At 750°C calcium sulfate did not catalyze the reaction but the acetate conferred as much catalysis as the limestone at the same temperature.

The Arrhenius energy of activation,  $E_a$ , varied greatly with calcium catalyst in this suite of tests. Wyodak, even in the presence of additive, had a much higher energy requirement for reaction than the Velva.

A comparison of the rate constants obtained using limestone catalyst on the TGA with those of the Continuous-Process-Unit (CPU) showed good agreement at 700°C and 750°C but lack of agreement at 800°C. The fluidized bed provided for improved heat transfer and mass transport compared to the fixed bed of the laboratory unit. In addition, the temperature of the reported 800°C experiment in the CPU was actually 10 to 15 degrees hotter than that of the bench-scale experiments. The limestone used in this experiment undergoes a thermally induced transition at 800°C as shown by Differential Thermal Analysis (DTA) resulting in what appeared by Scanning Electron Microscope (SEM) to be fragmentation of the limestone particles and the subsequent wider dispersion of catalyst. Thus the difference in rate constants for the two reactors at 800°C was probably due to a relatively large TGA sample size which resulted in transport limitations and the lower TGA reaction temperature. The deviation of the correlation coefficient ( $r^2$ ) from 1.00 could also be an indication of those limitations, although from this study there is no basis for ruling out a change in mechanism.

## CONCLUSIONS

- Calcium catalysis of char-steam reactions of low-rank coals is affected by the associated anion.
- Rate constants determined by TGA are comparable with those obtained with the 30-lb/hr CPU.
- Water-soluble calcium compounds are better low-rank coal reaction promoters than those that are insoluble.
- Calcium inherent to the coal does not necessarily affect catalysis by calcium additives.

## ACKNOWLEDGEMENTS

The authors gratefully acknowledge the support of the U.S. Department of Energy and the Morgantown Energy Technology Center. We also wish to acknowledge Ron Kulas for his assistance with laboratory work.

## REFERENCES

1. Sears, R.E., S.J. Cisney, M.K. Heidt, M.A. Musich, R.C. Timpe, "Production of Hydrogen From Low-Rank Coals", Annual Technical Report to USDOE-METC for April 1, 1988-June 30, 1989, UND Energy and Environmental Research Center, Grand Forks, ND, 1989.
2. Timpe, R.C., R.E. Sears, W.G. Willson, E.A. Sondreal, "Production of Hydrogen From Low-Rank Coals: Char Properties and Reactivity", Topical Report to USDOE-METC on Grant DE-FC21-86MC10637, UND Energy and Environmental Center, Grand Forks, ND, 1989.
3. Radovic, L.R., P.L. Walker, Jr., R.G. Jenkins, Fuel, (1983), 62, 209.
4. Linares-Solano, A., O.P. Mahajan, P.L. Walker, Jr., Fuel, (1979), 58, 327.
5. Radovic, L.R., P.L. Walker, Jr., R.G. Jenkins, Fuel, (1983), 62, 849.
6. Veraa, M.J., A.T. Bell, Fuel, (1978), 57, 194.

## Characterization of Syncrude Sludge Pond Tailings\*

Abdul Majid<sup>1</sup>, V.J. Boyko<sup>1</sup>, Bryan D. Sparks<sup>1</sup>, John A. Ripmeester<sup>1</sup> and H. Kodama<sup>2</sup>

1. Division of Chemistry, National Research Council of Canada, Ottawa, Ontario, K1A 0R9 Canada
2. Chemistry and Biology Research Institute, Ottawa Ontario, K1A 0R6 Canada

Key Words: Oil Sands, Tailings, Characterization, agglomeration.

The hot water process used by Suncor and Syncrude to extract bitumen from the Athabasca Oil Sands produces large volumes of tailings slurry. The fine grained sludge component of this waste is the most troublesome because of its stability and poor compaction potential. The sludge apparently owes its stability substantially to a complex interaction between organic coated amorphous particles, clays and bitumen. In this study we have investigated the nature of both the minerals and the associated organic matter present in a thickened, aqueous tailings sludge sample, from the Syncrude Canada Limited plant. An oil phase agglomeration technique was used to remove free bitumen and associated oil wettable solids from the sludge. On standing, the treated sludge, unlike a comparable blank, separated into settling and non-settling fractions. The solids from these fractions were analyzed by; X-ray diffractometry, Inductively Coupled Plasma Atomic Emission Spectrometry, Solid State MAS <sup>29</sup>Si and <sup>27</sup>Al NMR spectroscopy in an attempt to characterize the inorganic minerals present. The oil phase solids showed considerable enrichment in heavy metals compared to the other solids. The findings of this study could be helpful in providing some insight into the nature of tailings pond sludge, a problem which poses the most imminent environmental constraint to future use of the "hot water" process.

### INTRODUCTION

Two commercial oil sand extraction plants in Alberta generate vast quantities of tailings slurry as a result of the hot water extraction of bitumen from tar sands.<sup>1-3</sup> The fine-grained sludge component of this waste is the most troublesome because of its stability and poor compaction potential. The reason for the intractability of the sludge has been the subject of considerable study.<sup>1,3-7</sup> Based on some recent studies, it is generally believed that toluene insoluble organic matter (IOM) associated with certain

---

\*Issued as NRCC No. 30798

largely amorphous solids could be partly responsible for the stability and incompressibility of the oil sand slimes.<sup>2,5-7</sup> It is believed that the IOM causes particle surfaces to develop some hydrophobic character, allowing particle bridging, possibly through the medium of residual bitumen, thereby setting up a gel structure.<sup>7,8</sup> Another reason for the stability of oil sands sludge is said to be the presence of fine clay platelets which, with their differential edge and force-wetting properties, can also assist in the stabilization of suspensions<sup>2,9</sup>.

In our previous work, we have isolated and characterized insoluble organic matter from a number of oil sand tailings streams obtained from both the Suncor and Syncrude plants.<sup>6,7</sup> More recently we have fractionated sludge from the main Syncrude Canada Ltd. tailings pond. After removal of the emulsified bitumen by an oil phase agglomeration technique the sludge solids separated into settling and non-settling fractions. The insoluble organic matter associated with the fines present in the non-settling portion of the sludge was concentrated by an acid dissolution scheme<sup>6</sup> and then characterized using elemental analysis and solid state <sup>13</sup>C NMR spectroscopy<sup>10</sup>. In this communication we, report the analysis of inorganic mineral fractions using X-ray diffractometry, Inductively Coupled Plasma Atomic Emission Spectrometry, and <sup>29</sup>Si and <sup>27</sup>Al NMR Spectroscopy.

## EXPERIMENTAL METHODS

### Sample

Aqueous sludge from the 17 m level of the Syncrude tailings pond<sup>11,12</sup> was provided to us by Drs. R. Schutte and L. Danielson of Syncrude Canada Ltd. in 4-litre jugs. Prior to further sub-sampling, the samples were thoroughly mixed by vigorous manual agitation.

### Oil Phase Agglomeration Treatment

A countra-rotating stirring device (grease kettle) was used to remove bitumen from the sludge<sup>10,13</sup> using vacuum still bottoms as the oil collection phase. After removal of bitumen the aqueous sludge was fractionated as shown in Figure 1. The aqueous phase was transferred into a 500 mL beaker and the contents allowed to gravity settle for one week. The suspension was then decanted off to leave the settled solids. Water was evaporated at 100°C to obtain the solids from the supernatant liquor. The dried solids fraction from the suspension was demineralized using HCl and HF in order to concentrate the organic matter associated with the mineral fines<sup>6</sup>.

### NMR Measurements

$^{29}\text{Si}$  MAS NMR spectra (spinning rate  $\approx 3.5\text{kHz}$ ) were recorded at 59.60 MHz on a Bruker MSL-300 NMR spectrometer (magnetic field 7.1 T). About 4,000 free-induction decays (FIDs) were accumulated at a repetition time of 2s. Chemical shifts are given in ppm with respect to tetramethylsilane (TMS).

$^{27}\text{Al}$  MAS NMR spectra were recorded at 78.172 MHz on the same instrument using a repetition time of 1s. The number of free-induction decays accumulated were 6 for solids VI and 145 for the other two samples.  $^{27}\text{Al}$  chemical shifts were measured with respect to solid  $\text{Al}(\text{H}_2\text{O})_6^{3+}$ .

Mineral Composition. Mineral (crystalline) composition of the samples was determined semi-quantitatively by comparing their X-ray diffraction (XRD) peak intensities with those of standards. XRD patterns were recorded using a SCINTAG PAD V automated powder diffractometer equipped with a graphite monochromator, using  $\text{CoK}\alpha$  radiation ( $\lambda = 1.7902\text{\AA}$ ). The amount of each of the minerals in the samples was estimated by multiplying the peak intensity of the characteristic reflection for the respective mineral by the intensity factor for that mineral, determined from XRD data for a set of standard mixtures. The standards were measured under identical experimental conditions, including sample preparation radiation source and diffraction geometry. The amount of poorly-crystalline components (X-ray amorphous) was expressed by the difference of 100 and the total % of crystalline components.

Heavy Metal Analysis. Quantitative Inductively Coupled Plasma Atomic Emission Spectroscopic methods (ICP-AES) were used to analyze the ash for Ti, Zr, Cu, Ni, Cr, Mn, Al, Ca, Fe and Mg.

## RESULTS AND DISCUSSION

The separated solids fractions were treated according to the scheme shown in Figure 2. The non-settling portion was leached with HCl and HF in order to concentrate the insoluble organic matter associated with this fraction. Table I lists the semi-quantitative X-ray diffraction analysis of the mineral matter fractions shown in Figures 1 and 2. The following conclusions are obvious from examination of the data in Table I.

1. The proportion of amorphous material was higher in the suspended solids than in the sediment.

2. Solids obtained from the washing of the oil phase had the lowest quantity of amorphous material and the highest quartz content of all the solids fractions.
3. The proportion of mica and kaolinite clays in the sediment was higher than in the non-settling solids.
4. There is an unexpected discrepancy in the determination of amorphous material in the ashed and unashed samples of solids II and III.

These results suggest that removal of bitumen has a marked effect on the structure of sludge, freeing the bulk of the crystalline minerals and allowing them to freely settle out. Also, the remaining suspended solids, associated with larger amounts of amorphous material and insoluble organic carbon (IOC), were found to settle more readily, although slowly, from the treated sludge than from the untreated sludge. This suggests that bitumen present in the sludge interacts with some component of the sludge solids to form a structure which is capable of entrapping particles that would otherwise settle.

Table II lists the elemental analyses of ashed solids obtained from the fractionation of Syncrude sludge. Solids III obtained by washing the oil phase, after sludge treatment, contained the lowest concentrations of heavy metals which is consistent with the very high quartz content found in these solids. Solids IV (suspension solids) had higher concentrations of Al, Mg and Zr but lower concentrations of Cr and Mn than solids II from the sediment. Concentrations of Ti, Fe and Ca in the two fractions was similar. Whereas solids IV from the suspension comprise a large proportion of both the X-ray amorphous material and the elements Al, Mg and Zr it seems likely that these components are directly associated.

Leaching of the suspension solids IV with dilute HCl dissolved the Ca and Mn almost quantitatively plus the greater part of the Fe, Al, Mg and Cr. However, Ti and Zr appeared to resist dissolution by HCl as seen from the enrichment of these elements in the HCl extracted solids V.

Treatment of solids V by HF produced a solution with Al as the major element followed by Fe, Ti and Zr. Minor constituents in the HF solubles included Mg, Ca, Cr and Mn.

Table III lists the elemental distribution among solids fractions VI to VIII. It is obvious from this data that the bulk of the Ti and Zr has been unaffected by treatment with HCl and HF with over 60% of these elements being insoluble. Thus it seems likely that Ti and Zr are strongly complexed with the IOM and that these complexes are not readily decomposed by the acid treatment.

Almost quantitative dissolution of Ca and Mn in HCl was achieved, suggesting that these elements are not complexed to IOM but are present as inorganic minerals. Al, Fe, Mg and Cr exhibit an intermediate solubility, indicating that they could be present as a mixture of free inorganic minerals and as complexes with the IOM.

#### Solid State $^{29}\text{Si}$ and $^{27}\text{Al}$ MAS NMR

The  $^{29}\text{Si}$  MAS NMR spectrum of non-settling solids from suspension (Figure 3a) shows a sharp resonance at 92 ppm from TMS with a very weak shoulder around -88 ppm. These features fall in the  $^{29}\text{Si}$  chemical shift range of layer structured phyllosilicate ( $Q^3$ ) minerals<sup>14</sup>. Examples of these minerals include trioctahedral silicates like serpentine and dioctahedral aluminosilicates like pyrophyllite and kaolinite.

The  $^{27}\text{Al}$  MAS NMR spectra of dried sludge and suspension solids from clean sludge are shown in Figures 3b and 3c respectively. Both spectra consist of a single peak at -4 ppm with respect to  $[\text{Al}(\text{H}_2\text{O})_6]^{3+}$  as an external reference. This suggests that Al in these samples is exclusively in octahedral coordination.

On treatment of suspension solids with 6M-HCl  $\approx$  30% of the material leached out. Infrared and DC-Arc spectrographic analysis of this material was consistent with  $\text{AlCl}_3 \cdot x\text{H}_2\text{O}$  being the major component and Zn, Fe species as trace amounts. Figure 3d is the  $^{27}\text{Al}$  MAS NMR spectrum of this material. The spectrum consists of a single sharp peak at -1 ppm indicating the presence of octahedral Al alone.

#### CONCLUSIONS

1. The suspension solids separated after oil phase agglomeration of Syncrude sludge contained a higher proportion of X-ray amorphous material than the settled solids. The suspension solids also had a higher concentration of Al, Mg and Zr suggesting that these elements were associated with the amorphous solids.
2. The resistance of Ti and Zr towards dissolution by HCl and HF suggests that these metals could be complexed with insoluble organic matter (IOM).
3. Al, Fe and Cr appear to be present as a mixture of soluble inorganic minerals and as insoluble complexes with IOM.

4. Solid state  $^{29}\text{Si}$  NMR spectrum of the suspension solids suggested the presence of phyllosilicate minerals, conforming to the minor amounts of kaolinite detected by X-ray diffractometry.
5. Solid state  $^{27}\text{Al}$  NMR spectra indicated that Al in these samples was exclusively in the octahedral coordination.

#### REFERENCES

1. Camp, F.W., Can. J. Chem. Engin. 55, 581 (1977).
2. Kessick, M.A., J. Can. Pet. Techn. 77, 49 (1979).
3. Hall, E.S. and Tollefson, E.F. Can. J. Chem. Engin. 60, 812 (1982).
4. Kessick, M.A. Proc. Surf. Phenom. Enhanced Oil Recovery, 559, (1981).
5. Ripmeester, J.A. and Sirianni, A.F., J. Can. Pet. Techn. 2, 131 (1981).
6. Majid, A. and Ripmeester, J.A., Fuel 65, 1714 (1986).
7. Majid, A. and Ripmeester, J.A., ACS-Symposium Series 344, "Metal complexes in Fossil Fuels: Geochemistry, Characterization and Processing" pp 290-306 (1987).
8. Ignasiak, T.M.; Zhang, Q.; Kratochvill, B.; Maitra, C.; Montgomery, D.S. and Strausz, O.P., AOSTRA J. Res. 2, 21 (1985).
9. Young, R.N. and Sethi, A.J., J. Can. Pet. Technol. 76, 76 (1978).
10. Majid, A., Sparks, B.D. and Ripmeester, J.A. Fuel (in press).
11. Danielson, L.J. Syncrude Canada Limited, Internal Report 1989.
12. MacKinnon, M.D. Syncrude Research Report 1988, 88-9.
13. Sirianni, A.F., Capes, C.E. and Puddington, I.E., Can J Chem. Eng. 1969, 47, 166.
14. Lippma, M.G., Samoson, A., Engelhardt, G. and Grimmer, A.R., J. Phys. Chem. 88, 1518 (1984).

Table 1 Semi-quantitative X-ray Diffraction Analysis of Mineral Matter Fractions from Syncrude Sludge Pond Tailings\*

Fraction No.†	Description	Concentration Range (wt. %)			
		Mica	Kaolinite	Quartz	X-ray Amorphous
-	Dried Untreated Sludge				
	Un-ashed	10-25	10-25	10-25	40
	Ashed	10-25	10-25	10-25	40
1	Sediment from Untreated Sludge				
	Un-ashed	10-25	10-25	25-40	25-40
2	Sediment from Clean Sludge				
	Un-ashed	10-25	10-25	25-40	25-40
	Ashed	10-25	25-40	25-40	1-10
3	Washings from Recovered Bitumen				
	Un-ashed	1-10	1-10	40	10-25
	Ashed	10-25	1-10	40	1-10
4	Suspension Solids from Clean Sludge				
	Un-ashed	1-10	1-10	1-10	>40
	Ashed	1-10	1-10	1-10	>40
5	HCl Treated Suspension Solids from Clean Sludge				
	Un-ashed	1-10	1-10	1-10	>40
	Ashed	1-10	1-10	1-10	>40

\* In addition to the amount of major minerals listed in the table, small amounts of the following minerals were also detected in some of these fractions:

Interstratified Minerals minor amounts (1~10%) in Fractions 1,2 and dried sludge;  
 Microcline , trace (<1%) in Fraction 1; Plagioclase, trace (<1%) in dried sludge;  
 Lepidocrocite minor quantities in dried sludge, and Siderite in minor quantities in Fraction 2

† According to Figure 1 and 2

Table II The Elemental Composition of the Mineral Portion of Various Fractions from Syncrude Sludge Pond Tailings (Figures 1 and 2)

Fraction No.†	Yield (g/100 g sludge)	Ash (wt %)	C (wt%)	Elemental Analysis (wt. % of ash)*							
				Ti	Fe	Al	Ca	Mg	Zr‡	Cr‡	Mn‡
1	2.0	94.2	3.7	0.5	2.2	8.8	0.18	0.41	180	88	620
2	11.5	94.3	3.7	0.56	2.9	10.3	0.25	0.41	130	220	950
3	1.6	83.3	3.0	0.40	0.5	3.5	0.02	0.12	100	33	52
4	13.0	92.4	5.8	0.50	2.4	12.5	0.25	0.72	230	120	410
5	9.0	88.9	7.9	0.73	1.4	7.3	0.011	0.22	330	67	21
6	2.2	100**	1.9	2.05	3.6	16.3	0.06	0.1	930	190	53
OPS	0.1	70	17.3	1.7	10.5	7.4	N.D.	N.D.	660	7200	N.D.

† Figures 1 and 2 as ppm

N.D. not determined

\* Cu and Ni in all fractions other than OPS were below the detection limit of the instrument. Concentration in OPS: Ni - 0.23%; Cu - 490 ppm; V - 190 ppm

\*\* Analyzed as un-ashed samples

Table III Elemental Distribution by Repeated Acid Leaching of Non-settling Solids from Syncrude Sludge

Fraction	Elemental Distribution (wt. % of amount in solids IV)*							
	Ti	Fe	Al	Ca	Mg	Zr	Cr	Mn
Solids VI; HCl Solubles	2.8	61.1	61.1	97.1	79.6	4.4	62.8	96.6
Solids VIII, HF Solubles	75.10	27.5	23.9	4.4	2.5	74.1	29.0	2.4
Solids VII**	22.1	11.5	15	-	17.9	21.5	8.2	1.0

\* HCl Solubles =  $\frac{y-x}{y} \times 100$  where  $y$  = Elemental amounts in solids IV calculated as:

Elemental concentrations from Table II x 0.13 (yield fraction) x 0.924 (ash fraction)

X = Elemental amounts in solid V calculated as:

Elemental concentrations from Table II x 0.09 (yield fraction) x 0.889 (ash fraction)

HF Solubles =  $\frac{z}{y} \times 100$  where  $z$  = Elemental considerations from Table II x 0.022 (yield fraction)

\*\* calculated by difference

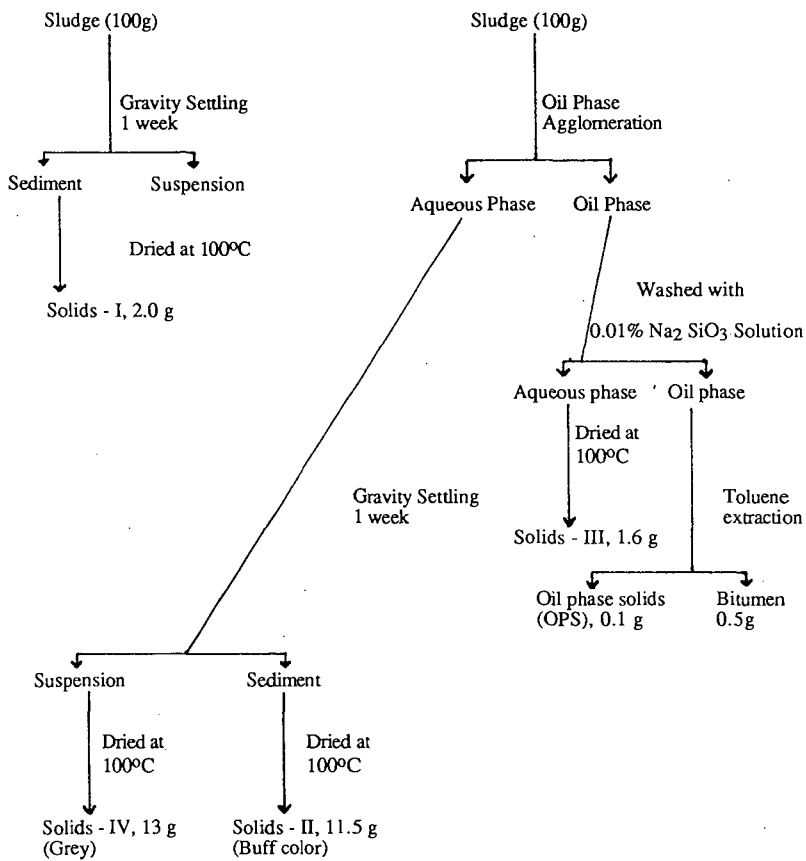


Figure 1. Fractionation scheme for Syncrude Sludge Pond Tailings.

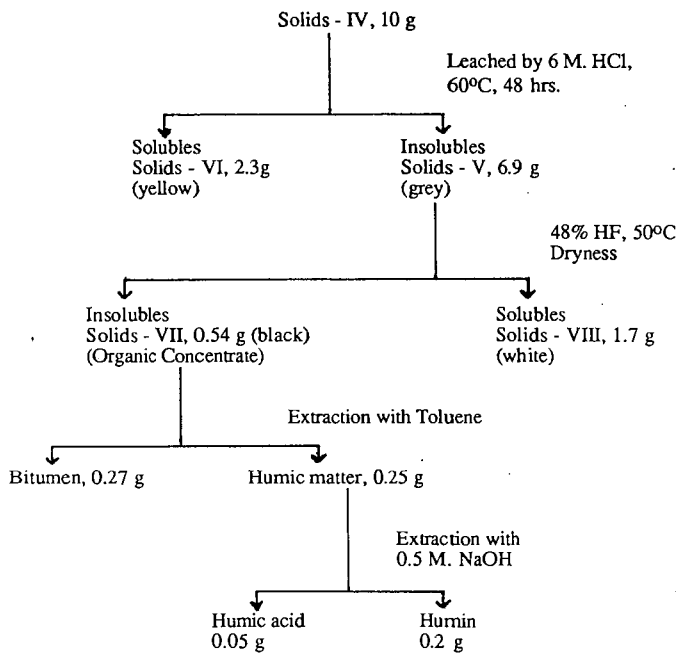


Figure 2. Flow sheet for the treatment of non-settling solids by successive acid leaching and extraction of humic acids

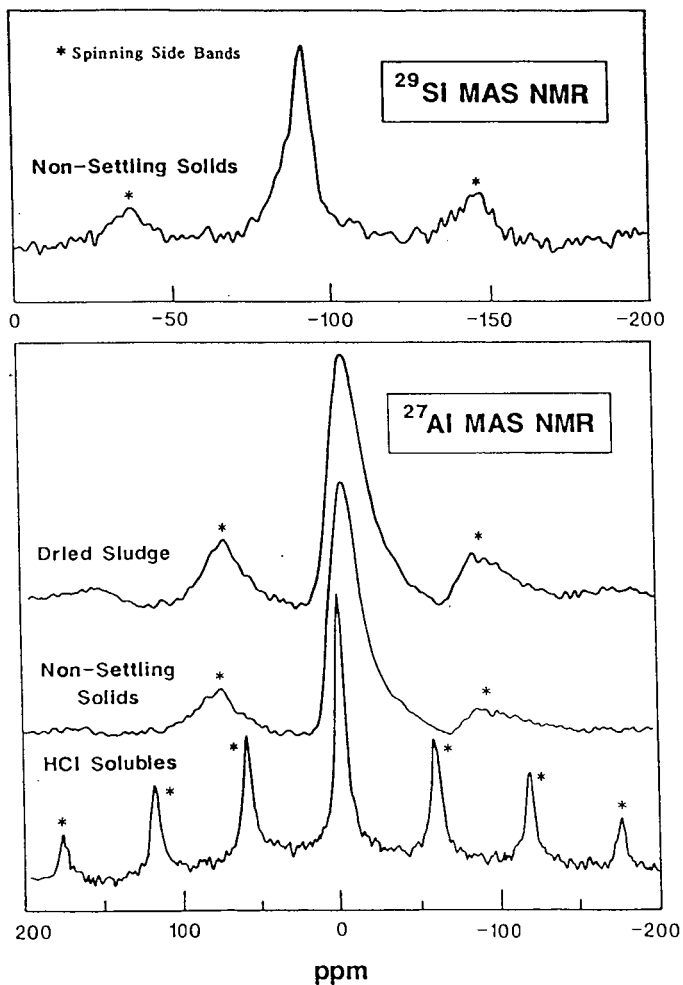


Figure 3a)  $^{29}\text{Si}$  MAS NMR spectrum of suspension solids.

b-d)  $^{27}\text{Al}$  MAS NMR spectra of b) dried Syncrude Sludge, c) suspension solids from clean sludge and d) HCl solubles from suspension solids.

**THE LUBRICITY PROPERTIES OF JET FUEL  
AS MEASURED BY THE BALL-ON-CYLINDER LUBRICITY EVALUATOR**

Bruce H. Black  
GEO-Centers, Inc., Ft. Washington, MD 20744  
Dennis R. Hardy  
CODE 6181, Naval Research Laboratory, Washington, DC 20375-5000  
and  
Margaret A. Wechter  
Southeastern Massachusetts University, North Dartmouth, MA 02747

**KEYWORDS:** Lubricity, Jet Fuel, BOCLE

**ABSTRACT**

In recent years the quality of petroleum feedstocks used by refineries has decreased. This has necessitated the use of severe refinery processes in order to produce jet fuels of high thermal stability and cleanliness. Unfortunately these processes remove the compounds that are responsible for a fuel's inherent lubricity. As a result, fuel lubricated engine components are experiencing greater wear and mechanical failure. The Ball-on-Cylinder Lubricity Evaluator (BOCLE) was developed to predict a fuel's tendency to cause lubricity related problems. This paper discusses the influence of trace polar species on lubricity, the use of additives to increase lubricity, changes in a fuel's lubricity during storage, and inadequacies of the BOCLE. Finally, a suggested long term solution to lubricity problems by hardware modifications will be discussed.

**INTRODUCTION**

The incidence of lubricity related problems in commercial and military jet aircraft has increased over the past twenty years. This is a result of the need for more severe refinery processes to remove trace fuel species that adversely affect thermal stability and water removal by coalescence.<sup>1-4</sup> These processes also remove trace polar species that are responsible for a fuel's inherent lubricity properties.

Lubricity is a qualitative description of the relative abilities of two fluids, with the same viscosity, to limit wear and friction between moving metal surfaces.<sup>2,4</sup> It may be the most critical fuel property degraded by refinery processes.<sup>3,5</sup> The continued use of low lubricity fuel can lead to a decrease in the operational lifetime of fuel lubricated engine components. This leads to increased maintenance costs and down-time of aircraft. Furthermore, the use of low lubricity fuel has been implicated in the loss of certain military aircraft.

In the late 1960s, it was serendipitously found that a pipeline corrosion inhibitor had a significant effect on lubricity enhancement. The additive's original intended purpose was to decrease corrosion to fuel handling systems and transfer lines.<sup>4</sup> The additive is effective as a corrosion inhibitor due to its surface-active nature. The active

ingredient in most corrosion inhibitors is a dimeric organic acid, usually dilinoleic acid (DLA). It is the surface-active nature of the dimeric acid that causes the corrosion inhibitor to be an effective lubricity enhancer.

The use of a corrosion inhibitor as a lubricity enhancer is now required in all military JP-4 and JP-5 jet fuel.<sup>7</sup> Unfortunately the additive can hinder water removal by coalescence. In other cases a fuel may have adequate lubricity initially and would preclude the use of the additive. Currently there is no lubricity specification for either commercial or military jet fuel. This has been due primarily to the lack of a test method; hence, the mandatory addition of the additive to assure adequate lubricity.

During the past fifteen years considerable effort has been made to develop a mechanical method to measure fuel lubricity. The current and most widely accepted method is the Ball-on-Cylinder Lubricity Evaluator (BOCLE). The lubricity of a fuel is determined by the measurement of an oval wear scar on a ball that has been in contact with a rotating cylinder partially immersed in a fuel sample under controlled conditions.<sup>8</sup> The reported value is the average of the major and minor axes of the oval wear scar in millimeters. Two limitations to this method are: First, the BOCLE is run at 25°C, a temperature that is not characteristic in aircraft environments. Second, the test is limited to a measurement of boundary lubrication, a lubrication regime not characteristic of currently used aircraft fuel pumps.<sup>9,10</sup>

In the United Kingdom a second method is being used. This method, developed and used exclusively by Shell Research, Ltd., is known as the Thornton Aviation Fuel Lubricity Evaluator (TAFLE). This consists of a stationary cylinder loaded onto a rotating cylinder both of which are completely immersed in the fuel sample. Measurements can be obtained at both ambient and elevated temperatures. This test also measures scuffing load which is generally characteristic of fuel system failures.<sup>9,10</sup>

## EXPERIMENTAL

Reagents- HPLC grade uninhibited tetrahydrofuran (THF) and HPLC grade methylene chloride were obtained from Fisher Scientific. JP-5 and Jet A jet fuel samples were obtained from the Naval Air Propulsion Center (NAPC). JP-4 jet fuel samples were obtained from Wright-Patterson Air Force Base (WPafb). Carboxylic acid standards were obtained from a variety of sources including; Aldrich Chemical Company, Inc., LaChat Chemicals, Inc., and PolyScience, Inc. Trimethylsilyl ester derivatives of the carboxylic acids and jet fuel base extracts were prepared using Power Sil-Prep obtained from Alltech Associates, Inc.

Equipment and Materials- For HPLC analyses, samples were analyzed using a Beckman-Altex Microspherogel high resolution, size exclusion column, Model 255-80 (50A pore size, 30 cm x 8.0 mm i.d.). Uninhibited THF was used as a mobile phase. The THF was periodically purged with dry nitrogen to inhibit the formation of hazardous peroxides. The injector was a Rheodyne loop/valve Model 7125. A Beckman Model 100-A HPLC pump was used for solvent delivery with a Waters Model 401 differential refractometer

for detection. A Varian Model 9176 strip chart was used to record peaks. A Fisher Accumet pH Meter Model 610A and a Fisher Standard Combination Electrode Catalog Number 13-639-90 were used for pH adjustments.

Gas Chromatography/Mass Spectrometry (GC/MS) analyses were performed using a Hewlett-Packard Model 5890 GC coupled to a Finnigan MAT ion trap detector. An all glass GC inlet was used in combination with a 0.2 mm x 50 m OV-101 fused silica capillary column. Data were collected using an IBM AT Personal Computer with ITDS software (version 3.0).

BOCLE analyses were performed using an InterAV Model BOC 100. The cylinders used were Timken Rings Part Number F25061 obtained from the Falex Corp., Aurora, IL. The test balls used were 12.7 mm diameter, Swedish Steel, Part Number 310995A obtained from SKF Industries, Allentown, PA.

**Methods-** HPLC analyses of fuel extracts were performed using a previously developed method.<sup>11-13</sup> This involved the extraction of 100 mL of jet fuel with an equal volume of 0.2 M NaOH. The aqueous phase was drained and acidified with concentrated HCl. The acidified aqueous phase was subsequently back-extracted with 100 mL of HPLC methylene chloride which was then drained and allowed to evaporate. The residue was dissolved in 2.0 mL HPLC THF for analysis.

BOCLE measurements were performed according to the method described in appendix Y of the Aviation Fuel Lubricity Evaluation published by the Coordinating Research Council, Inc.<sup>8</sup>

## RESULTS

Figure 1 is an HPLC chromatogram of a base extract from a typical JP-5 jet fuel. The active ingredient of the lubricity enhancer additive, DLA, has an elution volume of 5.85 mL. The DLA component has a molecular weight of 562. This material is prepared by a 1,4- cycloaddition (Diels-Alder) reaction of two linoleic acid molecules. The product is a monocyclic compound with a molecular weight twice that of linoleic acid. It possesses two carboxylic acid moieties which are the points of attachment to the active surface sites.

The peak that elutes at approximately 5.4 mL corresponds to trilinoleic acid (TLA). The TLA component, which is also a product of the Diels-Alder reaction, has a molecular weight of approximately 840. It may possess either a partially unsaturated fused dicyclic ring structure or two isolated partially saturated cyclohexyl rings.

The components with elution volumes of approximately 6.5 mL and 7.0 mL correspond to naturally occurring base extractable materials. These peaks are designated regions 3 and 4 respectively. These peaks can be clearly seen in Figure 2. The components that elute in what are designated regions 3 and 4 are believed to play a significant role in the inherent lubricity of jet fuel as measured by the BOCLE. Earlier work has shown a relation between the presence of these components and BOCLE measured lubricity.<sup>14-15</sup> In general, as the concentration of components that

elute in regions 3 and 4 increase, the lubricity of a fuel sample measured by the BOCLE increases.

While performing routine analyses of jet fuel samples, an interesting change in the fuel samples was noted. A series of JP-5 field samples were analyzed for base extractable material. After nine months of ambient storage, these same samples were analyzed a second time. It was found that the amount of base extractable material that elutes in regions 3 and 4 had increased. Table 1 lists the peak heights of regions 3 and 4 before and after nine months of ambient storage. ◊

BOCLE analyses were run to determine if there had been a concomitant change in lubricity. Since these were actual field samples of JP-5 jet fuels and, therefore, contained the mandatory lubricity enhancer additive, these fuel samples were all considered to be high lubricity fuels originally. It was found, however, that lubricity had increased. Previous work with an early version of the BOCLE yielded similar results. The lubricity of eight additive-free JP-5 and Jet A fuel samples were measured before and after 18 months of ambient storage. The change in wear scar diameter measurements for these fuels are listed in Table 2. It can be seen that the lubricity had increased in most cases. The wear scar diameters measured are smaller than those that would be measured on the current version of the BOCLE. This is a result of a metallurgical change in the cylinders to increase repeatability and reproducibility.

The increase in base extractable material with a concomitant increase in BOCLE measured lubricity is probably a result of oxidative changes in the fuel. Free radical autoxidation mechanisms are well known and readily occur in some fuels. These mechanisms can lead to the formation of trace levels of carboxylic acids that are known to enhance BOCLE measured lubricity.

The relation between lubricity and fuel composition is of great interest. Attempts have been made to correlate a number of fuel properties to lubricity measurements with little or no success. Early work performed by Grabel showed that straight chain carboxylic acids were among the most effective lubricity enhancers at very low concentrations.<sup>16</sup> The effect of straight chain carboxylic acids on boundary lubrication is well known and well documented. It's not surprising that an corrosion inhibitor based on carboxylic acids is also an effective lubricity enhancer. Grabel attempted to correlate the total acid number of a fuel to its lubricity as measured by the BOCLE. It was found that there was a relation, however, it would not serve as a adequate prediction of a fuel's lubricity. The conclusion is that there are acids that contribute substantially to the total acid number that are not involved in lubricity.

Combined gas chromatography/mass spectrometry (GC/MS) was used to identify components present in regions 3 and 4. With the knowledge of the effect of carboxylic acids on BOCLE measurements, comparison between fuel extracts and carboxylic acid standards were made. Both the fuel extracts and standards were derivatized to form their trimethylsilyl analogs to facilitate GC/MS analysis. After analysis of a standard mixture of derivatized carboxylic acids, a variety of fuel extracts were analyzed. Carboxylic acids were found to be present at low concentrations. These

were identified by both GC retention time and by their mass spectra. To aid in identification, multiple ion detection was also used for samples with overlapping peaks. The specific alkanolic acids found ranged from heptanoic acid (C<sub>7</sub>) to undecanoic acid (C<sub>11</sub>). The total concentration of the alkanolic acids varied with different samples. In most cases the total concentration was on the order of a few parts per million. Previous work has shown that as little as 2 ppm of added alkanolic acids can significantly improve BOCLE measured lubricity.

In addition to the acids, the majority of the species present in the fuel extracts were substituted alkyl phenols. Earlier work by Grabel has shown that these materials are not effective lubricity enhancers at low concentrations. At higher concentrations they may, however, contribute to BOCLE measured lubricity.

#### SUMMARY

The BOCLE is a useful tool in the laboratory for jet fuel lubricity measurements. Its limitations, however, must be recognized. The test is performed at 25°C, well below the operating temperature of aircraft fuel systems. Compounds that exhibit a beneficial influence on lubricity in the BOCLE test may fail at higher temperatures. The BOCLE analysis is performed in a different lubrication regime than is found in current aircraft fuel systems. This may lead to erroneous conclusions about a fuel's ability to impart lubricity in actual fuel systems. For instance, the BOCLE measured lubricity of a fuel is not influenced by the presence of sulfur compounds. Jet fuel lubricity as measured by the TAFLE, indicates that sulfur compounds increase the load limit of a fuel before scuffing occurs. This means that the BOCLE may fail a fuel that is capable of high loads in an actual fuel pump.

Lubricity related problems have been associated with only certain specific aircraft. The use of the lubricity enhancer additive has been found to adequately alleviate these problems. Other aircraft have not been found to exhibit any lubricity related problems. One may ask why there is a concern about lubricity. In the past the Navy has had problems with lubricity as a result of shipboard fuel handling practices. As JP-5 fuel is depleted from shipboard storage tanks, seawater is pumped in for ballasting. Seawater has been shown to effectively remove the lubricity enhancer additive by forming dicationic salts of the DLA.<sup>12,13</sup> This results in jet fuel with inadequate lubricity.

Another cause for recent lubricity problems is the lack of a lubricity specification. Additives used for lubricity enhancement are used, not for their ability to enhance lubricity, but their ability to inhibit corrosion. Of the additives qualified for use in jet fuel<sup>17</sup>, some are not effective surface active lubricity enhancers.

Two recommendations as an approach to short term and long term lubricity concerns are as follows: First, delete the additives from the Qualified Products List that are not found to enhance lubricity. Of the additives remaining, select those additives that are most effective for lubricity enhancement, are most cost effective, and are readily available.

Second, design aircraft components that are not affected by the continued use of low lubricity fuel. Long term problems with jet fuel lubricity should be approached by hardware modification not by the continued use of additives.

#### REFERENCES

(1) Vere, R.A.; Soc. Automot. Eng., SAE Reprint Number 690667, National Aeronautic and Space Engineering and Manufacturing Meeting, Los Angeles, CA, 1969; pp. 2237-2244.

(2) Moses, C.A., Callahan, T.J., Cuellar, Jr., J.P., Dodge, L.G., Likos, W.E., Naegeli, D.W., Valtierra, M.L.; "An Alternative Test Procedure to Qualify Fuels for Navy Aircraft," Final Report, Naval Air Propulsion Center Contract Number N00140-80-C-2269, Report Number NACP-PE-145C; Southwest Research Institute, San Antonio, TX, 1984.

(3) Petrarca, Jr., J.; "Lubricity of Jet A-1 and JP-4 Fuels," NTIS Number AD-784772; Report Number AFAPL-TR-74-15, Air Force Aero Propulsion Laboratory, Wright-Patterson AFB, OH, 1974.

(4) Goodger, E., Vere, R.A.; Aviation Fuels Technology; MacMillan Publishers Ltd.: Houndmills, Basingstoke, Hampshire, England, 1985; pp. 80-82.

(5) Biddle, T.B., Meehan, R.J., Warner, P.A.; "Standardization of Lubricity Test," Report Number AFWAL-TR-87-2041, Air Force Wright Aeronautical Laboratories, Aero Propulsion Laboratory (AFWAL/POSF), Wright-Patterson AFB, OH, 1987.

(6) Master, A.I., Weston, J.L., Biddle, T.B., Clark, J.A., Gratton, M., Graves, C.B., Rone, G.M., Stoner, C.D.; "Additional Development of the Alternative Test Procedure for Navy Aircraft Fuels," Naval Air Propulsion Center Contract Number N00140-84-C-5533, Report Number NACP-PE-160C; United Technologies Corporation, Pratt and Whitney, West Palm Beach, FL, 1987.

(7) Military Specification, MIL-T-5624M, Turbine Fuel, Aviation, Grades JP-4 and JP-5, 25 March 1988.

(8) Coordinating Research Council; "Aviation Fuel Lubricity Evaluation," CRC Report Number 560, CRC Inc., Atlanta, GA, 1988.

(9) Report of the Ministry of Defence (PE), Aviation Fuel Committee Lubricity Steering Group, March 1985 to October 1987.

(10) Report of the Ministry of Defence (PE), Aviation Fuel Lubricity Steering Group, Summary of Activities: November 1987 to October 1988.

(11) Black, B.H., Wechter, M.A., Hardy, D.R.; J. Chromatogr., 1988, 437, 203-210.

(12) Hardy, D.R., Black, B.H., Wechter, M.A.; J. Chromatogr., 1986, 366, 351-361

(13) Wechter, M.A.; "Quantitative Determination of Corrosion Inhibitor Levels in Jet Fuels by HPLC," Final Report, Naval Research Laboratory Contract Number N00014-85-M-0248; Southeastern Massachusetts University, North Dartmouth, MA, 1986.

(14) Black, B.H., Hardy, D.R.; Preprints of the Division of Fuel Chemistry, American Chemical Society, Vol. 34, No. 2, 1989, pp. 573-580.

(15) Black, B.H., Hardy, D.R.; Preprints of the Division of Fuel Chemistry, American Chemical Society, Vol. 34, No. 2, 1989, pp. 581-588.

(16) Grabel, L.; "Lubricity Properties of High Temperature Jet Fuel," Report Number NAPTC-PE-112, Naval Air Propulsion Test Center, Trenton, NJ, August 1977.

(17) QPL-25017-14, Qualified Products List of Products Qualified Under Military Specification MIL-I-25017, Inhibitor, Corrosion/Lubricity Improver, Fuel Soluble (Metric), 1984; U.S. Air Force, ASD/ENES, Wright-Patterson AFB, OH.

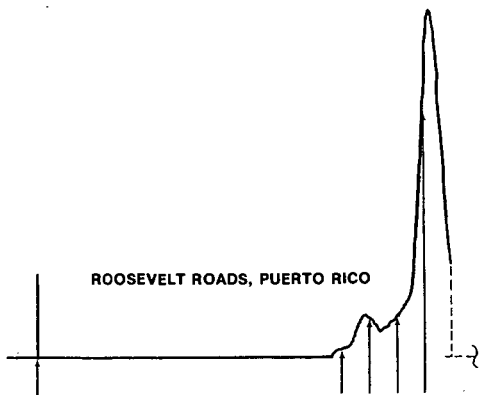


FIGURE 1



FIGURE 2

HPLC CHROMATOGRAMS OF JP-5 FIELD SAMPLES

TABLE 1

SAMPLE	Reg. 3 Pk Hgt		Reg. 4 Pk Hgt	
	Before	After	Before	After
Roosevelt Roads	14.5	28.0	128.0	55.0
Guantanamo Bay	11.0	28.0	25.0	200
Diego Garcia	20.0	22.0	22.0	65.0
Iorlaki, Japan	4.0	4.0	3.5	11.0
Gatun, Panama	12.0	15.0	24.0	250
Cartagena, Spain	5.0	12.0	8.5	29.0
Azorea	7.5	7.0	6.5	13.0

CHANGE IN CONCENTRATION OF BASE EXTRACTABLE MATERIAL AFTER NINE MONTHS OF STORAGE

TABLE 2

SAMPLE	ORIGINAL WSD	REMEASURED WSD
1	0.28 mm	0.23 mm
2	0.32 mm	0.28 mm
3	0.28 mm	0.27 mm
4	0.43 mm	0.28 mm
5	0.31 mm	0.34 mm
6	0.62 mm	0.36 mm
7	0.53 mm	0.38 mm
8	0.52 mm	0.41 mm

CHANGE IN WEAR SCAR DIAMETER MEASUREMENT FOR ADDITIVE-FREE JET FUELS AFTER 18 MONTHS OF STORAGE

## THE INTERACTION OF A METAL DEACTIVATOR WITH METAL SURFACES

John A. Schreifels

Department of Chemistry, George Mason University, Fairfax, VA 22030

Robert E. Morris<sup>a</sup>, Noel H. Turner<sup>b</sup> and Robert L. Mowery<sup>b</sup>

<sup>a</sup>Navy Technology Center for Safety & Survivability, Code 6180

<sup>b</sup>Surface Chemistry Branch, Code 6170

Chemistry Division, U.S. Naval Research Laboratory  
Washington, D.C. 20375-5000

Keywords: metal deactivator, thermal stability, JFTOT

### INTRODUCTION

In modern aircraft fuel systems, the fuel is used as a heat transfer medium to dissipate heat from the avionics and hydraulic systems. Under these conditions, the fuel can undergo autoxidation. Autoxidation of jet fuel can result in the formation of insoluble gum and sediment which can impair operation of the jet engine. In addition, hydroperoxides which form during autoxidation have been known to attack certain elastomeric fuel system components. Thus, the thermal oxidation stability of the fuel becomes an important consideration. Trace quantities of certain transition metals will catalyze fuel autoxidation. Dissolved copper has been shown to be the most reactive (Pederson, 1949; Smith, 1967). Copper contamination of fuels can and does occur, particularly in shipboard fuel handling systems from contact with copper lines, brass fittings, admiralty metal, and other copper-bearing alloys.

Metal deactivator additives (MDA) were developed to counteract the catalytic activity of dissolved metals. These additives (N,N'-disalicylidene-1,2-propanediamine and N,N'-disalicylidene-1,2-cyclohexanediamine) can act as polydentate ligands for copper (Pederson, 1949). Chelate complexes derived from similar hydroxyaromatic Schiff bases are known to be thermally stable (Marvel, et al., 1956). The military specification, MIL-T-5624, allows for the addition of up to 5.8 mg MDA per liter in JP-4 and JP-5, while the ASTM specification for aviation turbine fuels, D1655-85a, (Annual Book of ASTM Standards, 1987) allows up to 5.7 mg per liter.

Laboratory scale tests, such as the Jet Fuel Thermal Oxidation Tester (JFTOT), have been relied upon to evaluate the thermal oxidation stability of aviation fuels. In the ASTM Method for assessing thermal oxidation stability of aviation fuels (Annual Book of ASTM Standards, 1988), the fuel is passed once over the outside of a resistively heated aluminum tube (the heater tube) at a flow rate of approximately three ml/min. In previous work (Morris, et al., 1988; Morris and Turner, in press), we have observed that the addition of a metal deactivator resulted in significant reductions in deposits on 304 stainless steel JFTOT heater tubes from 280 to 310°C.

In tests conducted with an injector feed-arm simulator, metal deactivator reduced deposit formation in two fuels by two and fourteen fold respectively onto clean steel surfaces (Kendall and Earls, 1985). However, after an induction period,

rapid deposition ensued at a rate similar to that observed in the absence of MDA. From this it was concluded that MDA passivated the clean steel surface towards thermal deposits, but was ineffective once the surface became coated with an organic deposit (Kendall, et al., 1987). The effectiveness of MDA in JFTOT testing of metal-free hydrotreated fuels was also attributed to passivation of the clean metal surface of the JFTOT heater tube (Clark, 1988).

The strong influence exerted by MDA in JFTOT testing has raised questions about the applicability of the method for ranking fuels with respect to thermal oxidation stability in the presence of metal deactivators. If MDA produces a disproportionately strong inhibition of deposition in the JFTOT, then fuels ranked stable may form insolubles during use. We have thus directed our efforts at ascertaining the various mechanisms by which MDA can act, particularly in accelerated stability testing. One objective of this study was to determine to what extent interactions with metal surfaces of the test apparatus govern the effectiveness of metal deactivators. This paper describes an examination of metal surfaces exposed to MDA solutions to determine under what, if any, conditions metal passivation can occur.

#### EXPERIMENTAL

X-ray photoelectron spectroscopy (XPS) was used to determine the presence of a continuous layer of MDA on metal surfaces. Analyses were performed using a Surface Science Instruments SSX-100-03 X-ray Photoelectron Spectrometer. Quantitative estimates of the surface composition were obtained using the analysis program supplied with the spectrometer. The base pressure was at least  $2 \times 10^{-8}$  torr for all samples analyzed. Fourier transform infrared spectroscopy (FTIR) was performed with a Digilab FTS-15/90 Fourier transform infrared spectrometer. Secondary ion mass spectroscopy (SIMS) was performed in a static mode with a time of flight instrument constructed at the Naval Research Laboratory (Hues, et al., 1988). A pulsed alkali ion gun with a thermionic emitting source was used which produced 2-5 ns pulses of 13.0 keV cesium ions, resulting in an impact energy of 8.0 keV for positive ions.

In order to minimize the risk of surface contamination from trace impurities in a fuel, a model fuel consisting of n-dodecane (Philips 66, Pure grade, 99 mol% min.) was used. XPS analyses were conducted on flat metal coupons exposed to the model fuel and the model fuel containing MDA. N,N'-Disalicylidene-1,2-propylene-diamine (MDA) was obtained from Pfalz and Bauer and dissolved into the dodecane to obtain a final concentration of 5.8 mg/l. MDA-copper complex was prepared by combining equimolar quantities of MDA and copper(II) ethylacetoacetate in dodecane.

Coupons measuring 2.5cm x 1.2cm consisting of copper, 6061 aluminum and 304 stainless steel were used as substrates. All surfaces were ground to 4000 grit using silicon carbide paper with triply distilled water as the lubricant. Coupon samples used for (FTIR) were further polished with 0.05 micron alumina. The stainless steel samples examined by SIMS were 1cm x 1cm and were prepared as described above. After polishing, the coupons were rinsed with triply distilled water and allowed to air dry in acid cleaned glassware. Samples were immersed in either pure dodecane or dodecane containing MDA at room temperature for two and one half hours. Afterwards the samples were withdrawn from this solution and rinsed with HPLC grade n-heptane, covered with aluminum foil and analyzed

within an hour. Samples that were analyzed by SIMS and FTIR were also rinsed with low residue toluene (Baker).

Stainless steel and aluminum JFTOT heater tubes were also examined by XPS. JFTOT stressing was carried out with dodecane and solutions of MDA at 5.8 mg/l in dodecane at 260°C and 310°C for one hour. The tubes were washed with hexane immediately after a JFTOT experiment.

#### RESULTS AND DISCUSSION

XPS signal intensity ratios for carbon, nitrogen and oxygen cannot be utilized as a quantitative measure of the amounts of MDA on the surface and can only be used as a qualitative indication of the presence of MDA. Almost any surface that has been exposed to air will have adsorbed oxygen and carbon. It was thus necessary to rely on the intensity of the nitrogen signal alone as the most reliable indication of the presence of MDA on the surface since it is unique to that compound and is not present in the pure dodecane.

An XPS survey scan of the copper-MDA complex demonstrated that the surface binding energies were similar to those reported for a copper-Schiff base analog of MDA (Dillard, et al., 1974). It is clear from analysis of the observed peaks that all the expected elements are present. The nitrogen peak was quite intense relative to both the carbon and oxygen peaks. Although nothing definitive can be said from the spectrum about the relative atomic concentrations, the relative intensities of the carbon, nitrogen and oxygen peaks should give a reasonable indication of the expected intensity ratios for this chelate if it were present as a very thick film. Analysis of signal intensities from high resolution scans of these peaks allowed an estimation of the atomic concentration of the elements present. The calculated copper concentration was a factor of two higher than expected, while the atomic ratios of the other elements were what were expected. Although the exact reason for this discrepancy is not understood, the relative intensities of the peaks should provide a reasonable indication of the amount of MDA present on an uncontaminated surface.

Copper coupons: While it is not practical to attempt to remove all copper-bearing components from shipboard fuel delivery systems, MDA may play a role in inhibiting the dissolution of copper into the fuel. For this reason it was felt that MDA adsorption onto copper surfaces should be studied to provide an insight into the role it may play, if any, in passivating the exposed copper parts. Prepared copper coupons were exposed to dodecane and dodecane containing MDA at room temperature for 2.5 hours. The strips were then removed and rinsed with heptane (HPLC grade), mounted onto the XPS carousel and introduced into the vacuum system within two hours using a quick insertion system that is part of the apparatus. The XPS survey scan from the freshly cleaned copper surface, which was mounted as soon as it was air dried, had weak carbon and oxygen peaks and strong copper peaks, indicating that the sample preparation procedure used produced an acceptably clean surface. Exposure to the MDA solution had clearly increased the amount of carbon on the surface but no nitrogen was observed in the broad scan. This indicated that at most there could only be a very thin film of the MDA on this surface. Otherwise, the nitrogen intensity would be comparable with that found in the complex above. High resolution scans of the peaks for each element were obtained and the composition of the surface was estimated. The results of this are shown in Table I for the freshly polished

surface and after exposure to MDA. The carbon and oxygen levels, although still quite high, are small compared with those found from any other cleaning procedures that were tried. As expected, the calculated carbon contents on surfaces that were exposed to the organic solutions were higher than on the freshly cleaned surfaces. In addition, the quantities of carbon were about the same for the surfaces of both the sample exposed to pure dodecane and to MDA. Nitrogen levels were at or below the detection limit of 1-2 atomic percent. The lack of any nitrogen signal suggests that the formation of an MDA coating on the copper surface was not occurring, since XPS can easily resolve monolayer thicknesses.

Examination of the copper surface by FTIR revealed the presence of an organic acid on all samples exposed to the dodecane. The magnitudes of the C-H and C=O stretches that characterized the surface adsorbed acids were influenced by the MDA concentration. This may indicate some interactive effects between acids adsorbed on metal surfaces and the MDA.

**Stainless steel coupons:** The results from the XPS examination of 304 stainless steel coupons exposed to dodecane and dodecane containing 5.8 mg MDA/l for 2.5 hours at room temperature are shown in Table I. Higher levels of oxygen were found on the freshly cleaned stainless steel surface than on the copper surface, presumably because of the presence of metal oxides. Nitrogen content was at or below the limit of detection. FTIR analysis of stainless steel strips exposed to dodecane again revealed the presence of a carboxylic acid on the surface, from strong C-H and C=O absorptions. No changes in surface acid concentration were evident, nor was MDA detected on surfaces exposed to dodecane containing 5.8 mg MDA/l. Treatment of the dodecane with silica gel before use was sufficient to eliminate the presence of adsorbed carboxylic acids on the metal surfaces. The presence of a few parts per million of dodecanoic acid was confirmed by HPLC analysis of the base-extractable component of the dodecane. Thus, the acid adsorbed on the metal surface was most likely dodecanoic acid, derived from autoxidation of the dodecane.

In an effort to gain a more sensitive measure of the presence of MDA on the surface, SIMS analysis was performed on a stainless steel surface which had been exposed to neat dodecane and a dodecane solution of 5.8 mg MDA/l for 2 hours at room temperature. The positive secondary ions thus formed showed that indeed some MDA was present on the surface, while none was detected on the neat dodecane exposed blank. Since the surface had been rinsed with toluene, it is assumed that the MDA present was tightly bound to the surface. However, a more intense signal was obtained at 52 Daltons higher than the MDA peaks, suggesting that most of the MDA was bound to chromium. These findings demonstrate that after exposure of 304 stainless steel to a solution of MDA at room temperature, some MDA will be bound to the surface, predominantly at chromium sites. However, the coating is far from complete and would not significantly alter the surface reactivity towards deposition.

**Stainless steel JFTOT heater tubes:** While 6061 aluminum is the material most commonly used in the construction of JFTOT heater tubes, 304 stainless steel is often employed in research efforts involving the JFTOT apparatus. Furthermore, many fuel system components are constructed from stainless steel. XPS analyses were performed on selected areas of stainless steel JFTOT heater tubes used to stress samples of dodecane with and without 5.8 mg MDA/l in the JFTOT apparatus for one hour. Nitrogen on heater tubes heated at 260°C was near the detection

limit. The metal contents (i.e., Fe, Cr, Mn, etc.) on the tube surfaces were very low (Table II). Chromium levels were at or below the detection limit of 1 atomic percent, compared to a nominal level of 18% in the base metal. This indicates multilayer deposit formation was taking place regardless of whether MDA was present or not. At 310°C in the presence of MDA, similar results were obtained except that the carbon levels were higher. These findings demonstrate that within one hour of JFTOT testing, it is possible to produce multilayer coatings of carbonaceous thermal oxidation products on the stainless steel JFTOT heater tube surface from a relatively unreactive "fuel", i.e., dodecane.

Aluminum JFTOT heater tubes: XPS examinations of 6061 aluminum JFTOT heater tubes tested at 260°C for one hour in dodecane and dodecane with 5.8 mg MDA/l revealed that, in both cases, carbon levels were lower than on the stainless steel tube surfaces (Table III). There was no evidence of multilayer structure of thermally degraded dodecane over the full length of the tube. This substantiates earlier reports that while the liquid-phase chemistry is identical for both tube materials (Hazlett, et al., 1977), heavier deposits tend to form on stainless steel heater tubes (Faith, et al., 1971; Kendall, et al., 1987). Nitrogen was at or below the detection limit in both cases, however, slightly more nitrogen was evident on tubes heated in the MDA solution.

#### CONCLUSIONS

Surface analyses of copper, aluminum and stainless steel exposed to MDA in static solutions and in JFTOT testing, point towards a different mechanism than what would be expected if the surface were deactivated towards deposition by a contiguous layer of MDA. While these findings suggest that the surface contains some MDA, it is sparsely distributed. In addition, there may be some interactive effects between MDA and surface bound carboxylic acids. On stainless steel, it appears that the MDA is predominantly bound to chromium sites on the surface but this coating is also a fraction of a monolayer and thus would not significantly change the surface activity. There was no evidence that MDA was coating a pure copper surface.

In the JFTOT, there was more deposition onto the 304 stainless steel tubes than on the 6061 aluminum. If surface passivation was responsible for the strong response of the JFTOT to the presence of MDA, then one would expect to observe at least a monolayer of MDA on the tube surface over the entire test duration of two and one half hours. However, in this study, multilayer thermal oxidation deposits were produced on 304 stainless steel JFTOT tubes after only one hour of JFTOT testing at the specification test temperature, 260°C. Therefore, the time required for monolayer deposition of thermal oxidation products onto stainless steel heater tubes during JFTOT testing was well within the limits of the test.

While it does not seem likely that surface passivation is occurring in the JFTOT, there is still no doubt that MDA exerts a powerful inhibiting influence on thermal deposition and the question of validity of the JFTOT results in the presence of MDA remains to be answered. Measurements of oxidation of JFTOT effluent have shown inhibition by MDA in some cases and none in others. This suggests the possibility that the effects exerted by MDA in the JFTOT may be a consequence of interactions in the liquid-phase.

#### ACKNOWLEDGEMENTS

The authors wish to thank Dr. Stephen M. Hues of the Naval Research Laboratory, Chemistry Division, Code 6170 for conducting the SIMS analyses and Mr. Bruce Black of Geo-Centers, Inc. for the determination of acid in the dodecane. This work was funded by the Office of Naval Research and the Naval Air Propulsion Center.

#### REFERENCES

ASTM "Specification for Aviation Turbine Fuels". In Annual Book of ASTM Standards; ASTM: Philadelphia, 1987; part 23, ASTM D1655-f2a.

ASTM "Standard Method for Thermal Oxidation Stability of Aviation Turbine Fuels (JFTOT Procedure)" In Annual Book of ASTM Standards; ASTM: Philadelphia, 1988; vol. 05.02, ASTM D 3241-85.

Clark, R. H.; "The Role of Metal Deactivator in Improving the Thermal Stability of Aviation Kerosines". In Proceedings of 3rd International Conference on Stability and Handling of Liquid Fuels; R.W. Hiley, R.E. Penfold and J.F. Pedley, Ed., The Institute of Petroleum: London, UK, 1989, p. 283.

Dillard, J. G. and Taylor, L. T.; "X-Ray Photoelectron Spectroscopic Study of Schiff Base Metal Complexes". J. Elect. Spect. & Rel. Phenom., 1974, 3, 455.

Faith, L. E.; Ackerman, G. H.; Henderson, H. T.; Richie, A. W. and Ryland, L. B.; "Hydrocarbon Fuels for Advanced Systems". Shell Development Company, Air Force Report AFAPL-TR-70-71, Part III, 1972.

Hazlett, R. N., Hall; J. M. and Matson, M.; "Reactions of Aerated n-Dodecane Liquid Flowing over Heated Metal Tubes", Ind. Eng. Chem., Prod. Res. Dev., 1977, 16(2), 171.

Hues, S. M.; Colton, R. J.; Mowery, R. L.; McGrath, K. J.; and Wyatt, J. R.; "Determination of Hydrogen in Perfluorinated Polyalkylethers Using Time-of Flight Secondary Ion Mass Spectrometry, Infrared Spectroscopy, and Nuclear Magnetic Resonance Spectrometry". Appl. Surf. Sci. 1988, 35, 507.

Kendall, D. R. and Earls, J. W.; "The Assessment of Aviation Fuel Thermal Stability". Presented at the 25th IATA Aviation Fuel Subcommittee, September 17-18, 1985, Geneva.

Kendall, D. R.; Houlbrook, G.; Clark, R. H.; Bullock, S. P.; Lewis, C.; "The Thermal Degradation of Aviation Fuels in Jet Engine Injector Feed-Arms, Part I - Results from a Full-Scale Rig". Presented at the 1987 Tokyo International Gas Turbine Congress, October 26-31, 1987, Tokyo, Japan.

Marvel, C. S.; Aspey, S. A. and Dudley, E. A.; "Quadridentate and Sexadente Chelates. Some Preliminary Studies in their Preparation and Thermal Stability". J. Amer. Chem. Soc. 1956, 78, 4905.

Morris, R. E.; Hazlett, R. N.; McIlvaine, C. L. III; "The Effects of Stabilizer Additives on the Thermal Stability of Jet Fuel". Ind. Eng. Chem. R&D 1988, 27(8), 1524.

Morris, R. E. and Turner, N. H.; "Influences Exerted by Metal Deactivator on the Thermal Stability of Aviation Fuel in the Presence of Copper". Fuel Sci. & Tech. Int. (in press).

Pederson, C. J.; "Inhibition of Deterioration of Cracked Gasoline During Storage". Ind. Eng. Chem. 1949, 41, 924.

Smith, J. D.; "The Effect of Metals and Alloys on the Thermal Stability of Avtur 50". J. Aero. Eng. 1967, 33(4), 19.

Table I. Composition of Films Formed on Polished Flat Coupons Exposed to Dodecane and 5.8mg MDA/l Dodecane in Atomic Percent

Copper

Condition	C	O	Cu
Freshly Polished	39	27	35
Dodecane, 2.5 hrs	63	23	12
MDA/dodedane, 2.5 hrs	54	28	18

304 Stainless Steel

Condition	C	O	Fe
Freshly Polished	21	58	14
Dodecane, 2.5 hrs	46	37	8
MDA/Dodedane, 2.5 hrs	35	49	11

Table II. Composition of Films Formed on Stainless Steel JFTOT Tubes in Atomic Percent after Stressing for 1 Hour

Dodecane, 260°C			
Temp. (°C)	C	O	Fe
174-208	57	38	3
208-238	41	49	7
238-257	52	40	5
257-260	78	20	1

5.8 mg MDA/l in Dodecane, 260°C			
Temp. (°C)	C	O	Fe
174-208	56	38	2
208-238	43	46	4
238-257	48	42	4
257-260	82	18	0

5.8 mg MDA/l in Dodecane, 310°C			
Temp. (°C)	C	O	Fe
212-253	40	45	11
253-287	56	38	4
287-305	82	14	0
305-310	93	6	0

Table III. Composition of Films Formed on Aluminum JFTOT Tubes in Atomic Percent after Stressing for 1 Hour

Dodecane, 260°C			
Temp. (°C)	C	O	Al
141-193	31	47	20
193-232	29	47	21
232-256	32	46	18
256-260	28	48	19

5.8 mg MDA/l in Dodecane, 260°C			
Temp. (°C)	C	O	Al
141-193	31	45	19
193-232	33	43	18
232-256	34	43	19
256-260	44	36	17

HYDROCRACKING WITH NEW SOLID ACID CATALYSTS:  
LOW SEVERITY LIQUEFACTION PRODUCTS FROM LOW RANK COAL:

Edwin S. Olson, John W. Diehl, and Ramesh K. Sharma

Energy and Environmental Research Center  
University of North Dakota  
Grand Forks, ND 58202

Solid acid catalysts, prepared by supporting zinc chloride on silica gel and on acid-exchanged montmorillonite, were tested for catalytic hydrocracking of first stage liquefaction products from Wyodak subbituminous coal. Unsupported acid-exchanged montmorillonite was also tested. The reactions were carried out by heating the high molecular weight, THF-soluble, low-severity product with the supported zinc chloride catalyst in a microreactor at 400°C for three hrs with 1000 psig of hydrogen (repressurized at 1-hr intervals). These reactions gave good yields of distillates (53-68%), which exceeded those obtained with conventional hydrotreating catalysts under similar conditions. Coking or retrograde condensation reactions were minimal. The distillate compositions, determined by GC/FTIR/MS/AED, consisted of phenolics, one and two ring aromatics and hydroaromatics, and alkanes. The nonvolatiles were examined by elemental analysis, FTIR, NMR, and m.w. determinations by GPC and LALLS. The hydrotreated liquefaction products, both volatiles and nonvolatiles, showed a complete absence of organo sulfur compounds, as determined by the very sensitive helium afterglow discharge emission and elemental analysis.

Key words: Liquefaction, hydrocracking, solid acid catalyst

#### INTRODUCTION

The preparation of new catalysts for the production of a distillate with a low content of heteroatoms such as sulfur, oxygen, and nitrogen is a major goal in coal liquefaction. More than 50 years ago Eugene Houdry (1) reported that acid modified smectites can produce gasoline in high yields when used as petroleum cracking catalysts. In contrast to thermal cracking, catalytic cracking produces gasoline of higher octane rating (2). Many cracking catalysts are combinations of alumina and silica oxides, known to exhibit acidic properties (3). The mechanism of the acid-catalyzed cracking reactions is understood to involve carbonium ion intermediates (4). The catalytic cracking of cumene has been extensively used to characterize the acidity of various catalysts (5). Synthetic silica alumina catalysts or zeolites were more stable both structurally and catalytically, gave superior product distributions compared to naturally occurring clays, and, thus revolutionized the catalytic cracking (6-10).

Petroleum hydrocracking catalysts are not necessarily effective for coal liquefaction, however. Highly acidic catalysts may result in coking on the catalyst as well as in the equipment. Although molten zinc chloride effectively depolymerizes coals (11,12), significant hydrodesulfurization of aryl sulfur compounds is not affected by this reagent (13). Other disadvantages of zinc chloride are its difficulty of recovery and corrosive nature.

In a recent paper we reported a solid acid catalyst prepared by supporting zinc chloride on silica gel to be effective in hydrodesulfurization of diphenyl sulfide and dibenzothiophene (14). The preparation and characterization of three solid acid catalysts: 1) supporting zinc chloride on silica gel, 2) supporting zinc chloride on acid-exchanged montmorillonite, and 3) unsupported acid-exchanged montmorillonite have already been reported (14,15). In this paper, we report the catalytic

hydrotreatment of the first stage products from the low-severity liquefaction of Wyodak subbituminous coal with zinc chloride supported on silica gel and on acid-exchanged montmorillonite, unsupported acid-exchanged montmorillonite, and commercial Trilobe 60 HDN catalyst.

## EXPERIMENTAL

Zinc chloride on silica gel, zinc chloride on acid-exchanged montmorillonite, and unsupported acid-exchanged montmorillonite catalysts were prepared as described earlier (14,15). Total acidity and pKa's of the solid acid catalysts were determined by *n*-butyl amine titrations using Hammett indicators (16).

Analytical procedures; instrumentation:

Carbon, hydrogen, and nitrogen analyses were performed on Control Equipment Corporation Model 240XA Elemental Analyzer. Total sulfur was determined with a LECO Model 532 Sulfur Analyzer using ASTM D1551 method. Oxygen was determined by difference. The method of Vogel (17) was used for chlorine analysis.

<sup>13</sup>C NMR, CP/MAS solid state spectra were recorded on a Varian XL200 NMR spectrometer with Doty Scientific solids probe operating at 50.3 MHz. Infrared spectra were obtained in KBr on either a Perkin-Elmer Model 283 spectrophotometer or a Nicolet 205XB FTIR spectrometer equipped with a mercury cadmium telluride (MCTA) detector and a Nicolet 1280 computer with a fast Fourier transform coprocessor.

Quantitative GC/FID analyses were performed with a Hewlett-Packard 5880A gas chromatograph equipped with J&W 60 m x 0.25 mm (i.d.), 1.0 micron DB-1701 capillary column. *n*-Octadecane was used as the internal standard. Isotope dilution GC/MS were performed on a Finnigan 800 ITD ion trap detector with an HP-5890A gas chromatograph and a J&W 30 m x 0.32 mm (i.d.), 1.0 micron film of DB-5. Phenol, tetralin, and naphthalene were determined with the per-deuterated analogs as the respective internal standards. A 15 m x 0.25 mm (i.d.) 0.25 micron DB-5 column was used for the analysis of high boiling components. Quantitative analysis of organo sulfur compounds in the distillate was done by GC/AED.

Low severity liquefaction:

A slurry consisting of 904.5 g Wyodak coal (as received) and 1254.9 g of solvent (tetralin) was placed in a two-gallon reactor, and the reactor was sealed. The reactor was evacuated and charged with a mixture of 900 psig carbon monoxide and 100 psig hydrogen sulfide. The reactor was slowly heated to 384°C, and left at this temperature for one hour. At the end of the reaction, the reactor was cooled to room temperature, and the gases collected in a gas bag. The product slurry was separated into THF-soluble and insoluble fractions by extracting with THF. The THF-insoluble fraction was dried in vacuo at 110°C overnight, and weighed.

Preparation of solvent free low-severity product (LS-W) for second stage catalytic hydrotreatment :

A large batch of THF-soluble fraction was distilled under reduced pressure (2 torr) to remove solvents. The residue, a viscous oil, solidified upon cooling to room temperature (LS-W) was used for catalytic hydrotreatment. This product was analyzed by elemental analysis and the results are given in Table 1.

Catalytic hydrotreatment of LS-W:

In a typical run 1.0 g of LS-W and 0.50 g of the desired catalyst were placed in a tubing bomb (12-ml microreactor). The microreactor was evacuated and pressurized

with 1000 psig of hydrogen, and placed in a rocking autoclave heated to 400°C. The heating continued for three hours. At the end of the reaction period, the microreactor was cooled to room temperature, degassed, and opened.

The tubing bomb was attached to a set of three pre-weighed traps cooled in air, dry ice-acetone, and liquid nitrogen. The tubing bomb was slowly heated (3°C/min.) to 250°C, and heating was continued until distillation stopped. The distillate was weighed and dissolved in 10 ml of methylene chloride. The distillate was mixed with appropriate internal standards and analyzed by GC/FID and GC/FTIR/MS/AED. The undistilled residue was separated into THF-soluble and insoluble fractions by extracting with THF. These fractions were dried in vacuo and weighed. The mass balance data are given in Table 2.

In a separate reaction, the tubing bomb was depressurized and repressurized with 1000 psig of hydrogen at one hour intervals. The total heating time was three hours.

## RESULTS AND DISCUSSION

### Catalytic hydrotreating; Liquefaction:

#### Catalytic hydrotreating of LS-W with silica gel zinc chloride (SZC):

Hydrotreating of solvent free low severity liquefaction product from Wyodak coal (LS-W) was carried out to determine the catalytic activities of supported zinc chloride catalysts. The three-hour tests were performed with an initial (cold) hydrogen pressure of 1000 psig, which increased to 3000 psig at the final reactor temperature of 400°C. In one test, the microreactor was cooled and repressurized with hydrogen (1000 psig) after each hour, while in another test, no additional hydrogen was added over the three-hour experiment. In calculating the conversions for the reaction, it is necessary to consider that the low-severity starting material for the test consisted mostly of high molecular weight material, but did contain a small amount of tetralin and naphthalene derived from solvent used in the low severity liquefaction and a small amount of volatile coal-derived material. The yields in the hydrotreating tests were determined by measuring the amount of vacuum distillate and corrected by subtraction of the distillable material present in LS-W (20%) to obtain the actual yield.

The hydrotreatment of LS-W with silica gel-zinc chloride catalyst (SZC) in the three hour test without depressurizing and repressurizing with hydrogen gave a distillate yield of 35%. Subtraction of the LS-W volatiles resulted in an actual yield for the hydrotreating step of 15%. The most striking aspect of the composition of the distillate is the complete absence of sulfur containing compounds, as determined by the very sensitive helium afterglow discharge atomic emission detection. The GC/FTIR/MS data indicated that benzene, alkylbenzenes, cyclohexane, phenolics, tetralin, naphthalene, and a series of alkanes were the major components of the distillate.

The residue from the distillation was separated into THF-soluble and insoluble fractions. The THF-soluble fraction amounted to 54% of the weight of the starting material. This material had a hydrogen-to-carbon ratio of 1.01, identical to the starting LS-W product. <sup>13</sup>C NMR, CP/MAS spectrum shows a large increase in the hydroaromatic bond at 30 ppm. This data also indicates removal of phenolics, carboxylic acids and carboxylate groups during hydrotreating. Infrared spectrum shows a larger aromatic ring absorption at 1600 cm<sup>-1</sup>, which may have resulted from a change in the type of aromatic groups present. An increased aromatic content could have resulted from either cleavage and loss of alkyl groups to the distillate fraction or from condensation, dehydration, and dehydrogenation reactions to give

TABLE 1  
ELEMENTAL ANALYSES OF COAL LIQUEFACTION PRODUCTS

Catalyst	Produce	C	H	N	S	O	H/C
None	Wyodak (maf)	70.9	5.2	0.9	0.6	22.3	0.88
None	LS-W	82.9	6.9	1.1	0.71	8.3	1.00
*SZC	THF-S THF-I Dist.	87.3	7.35	0.68	0.14 0.84 0.0	4.53	1.01
SZC	THF-S THF-I Dist.	88.0	6.02	1.07	0.0 0.74 0.0	4.91	0.82
AM	THF-S THF-I Dist.	83.7	5.58	1.24	0.42 0.0	9.48**	0.80
AMSZC-B	THF-S THF-I Dist.	85.4	6.38	0.94	0.0 1.47 0.0	7.28	0.90

• Single H<sub>2</sub> pressurization  
\*\* Includes sulfur

TABLE 2  
CATALYTIC HYDROTREATING OF LS-W

CATALYST	LS-W (g)	PRODUCTS (%)		
		THF-I	THF-S	Distillate
*SZC	1.02	11.8	54.0	35.0
SZC	1.00	1.9	28.6	67.7
AM	1.00	20.0	46.0	28.0
AMZC-A	1.00	--	49.0	53.0
AMZC-B	1.00	--	41.0	62.0
HDN	1.00	14.3	49.61	35.0

• Single H<sub>2</sub> Pressurization

more aromatic structures. Experience with model compound hydrotreating with this catalyst (14) suggests that single rings are not hydrogenated, but naphthalenes, and polynuclear aromatics are readily hydrogenated (19). Thus the hydrotreating at 400°C appears to consist mainly of hydrocracking alkylaromatics and hydrogenation of multi-ring aromatics. Hydrotreating may predominate over hydrogenation, because of the higher concentration of single ring aromatics in the low-rank coals.

The THF-insoluble fraction from the experiment without repressurization consisted mainly of catalyst, but did contain organic material amounting to 12% of the starting LS-W. This material was also more aromatic than the original LS-W.

The hydrotreating of LS-W with silica gel-zinc chloride catalyst with repressurization of hydrogen at one-hour intervals gave a distillate yield of 68% (actual 48%). The composition of the distillate was similar to that of the product from the single pressurization with hydrogen. The THF-soluble fraction amounted to 24% of the starting material. As in the experiment discussed above, the infrared spectrum indicated this fraction to be more aromatic than the original LS-W. The THF-soluble fraction was essentially the recovered catalyst with only a small amount (<3%) of carbonaceous material.

#### Catalytic hydrotreating with montmorillonite-zinc chloride (AMZC):

Catalytic hydrotreating of LS-W with acid-exchanged montmorillonite (AM) and hydrogen depressurizing and repressurizing at one-hour intervals gave 28% distillate. Since, 20% distillate was already present in the LS-W, only 8% of the distillate was actually produced during the second stage of the reaction. The GC/MS data indicated the major components of the distillate to be tetralin, naphthalene, and phenols. Tetralin is more likely to be solvent-derived and naphthalene could either be solvent-derived, coal-derived or both. Other products in the distillate were cresols, benzene, alkylbenzenes, and alkylnaphthalenes. A significant portion of the starting material (20%) became insoluble in THF after the second stage reaction, which may be due to condensation reactions catalyzed by the acidity of the clay.

Catalytic hydrotreating with zinc chloride supported on acid-exchanged montmorillonite prepared from clay dried at 110°C in vacuo (AMZC-A) gave 53% distillate (actual 33%). The stability and catalytic activity of the catalyst was found to depend on the drying temperature of the clay. The zinc chloride supported catalyst that was prepared from clay dried at 250°C (AMZC-B), was not only more stable on long standing but also gave higher distillate yield, 62% (42% actual). The distillate yield with this catalyst was comparable to that obtained from silica gel-zinc chloride catalyst. Furthermore, no coking or enhanced aromatic residue was formed during catalytic upgrading.

#### Catalytic hydrotreatment with commercial Ni-Mo catalyst (HDN):

In order to evaluate the catalytic activity of the zinc chloride supported silica gel and acid-exchanged montmorillonite, reaction of low severity Wyodak (LS-W) product with commercially available HDN catalyst was carried out under the same conditions as described above, and the results compared. The distillate yield was only 35% (actual 15%), which is significantly lower than those obtained with zinc chloride supported on silica gel and acid-exchanged montmorillonite. The product distribution of the distillate was much the same as with supported zinc chloride catalysts. The THF-soluble fraction was 50% of the starting material. A significant amount of organic material became insoluble in THF, which may have been formed due to dealkylation or condensation reactions (15).

Catalytic hydrotreating: Desulfurization:

Table 3 shows the sulfur removal for four different catalysts. The distillates obtained from these reactions did not contain any sulfur as indicated by very sensitive helium afterglow atomic emission spectroscopy. Therefore, sulfur amounts in the recovered catalyst (THF-insolubles) and THF-soluble fraction were used to determine desulfurization during catalytic hydrotreating of LS-W. Elemental analysis of the THF-insoluble fraction gave 0.74% sulfur (0.0075 g S). This amount of sulfur is essentially the same as that present in the starting LS-W (0.0071 g). These data demonstrate that the catalyst is highly effective in removing sulfur from the bottoms as well as the distillate. The occurrence of zinc sulfide in the catalyst is expected (14) but has not yet been confirmed. However, only 73.6% sulfur was removed from LS-W in the test without hydrogen repressurization. These results suggest that hydrogen repressurization is needed for the efficient removal of organic sulfur from coal products. Acid-exchanged montmorillonite removed only 42.3% sulfur from LS-W. However, on supporting zinc chloride on acid-exchanged montmorillonite, the desulfurization activity of the clay was considerably increased.

TABLE 3  
SULFUR BALANCE

Catalyst	S(g)				% S Removed
	Reactant	Products			
	LS-W	Distillate	THF-S	Recovered Catalyst	
*SZC	0.0072	0.0	--	0.0053	73.6
SZC	0.0071	0.0	0.0	0.0074	100
AM	0.0071	0.0	--	0.0030	42.3
AMZC-B	0.0071	0.0	0.0007	0.0060	84.5

\* Single H<sub>2</sub> Pressurization

CONCLUSIONS

Comparing the results of hydrocracking of low-severity liquefaction Wyodak products with supported zinc chloride catalysts to the results with HDN catalyst shows that these supported catalysts give higher distillate yields and effectively remove organic sulfur under mild conditions. The strong acid hydrotreating catalyst (acid-exchanged montmorillonite) was not very effective in hydrotreating. The experiments showed that repressurizing the hydrogen is needed to sustain hydrogenation and prevent condensations at this temperature. These acid catalysts are effective in removing organic sulfur from coal-derived products.

ACKNOWLEDGMENT

This research was supported by Contract No. DOE FC-2186MC10637 from the U.S. Department of Energy. References herein to any specific commercial product by trade

name or manufacturer does not necessarily constitute or imply its endorsement, recommendation, or favoring by the United States Government or any agency thereof. The assistance of Jonathan Kautz is greatly appreciated.

#### REFERENCES

1. E. Houdry, and A. Joseph, Bull. Assoc. Fr. Tech. Pet., 117 1956 177.
2. V. Haensel, Adv. Catal., 3 1951 194.
3. F.M. Gayer, Ind. Eng. Chem., 29 1933 1122.
4. F.C. Whitmore, Ind. Eng. Chem., 26 1934 94.
5. A. Corma, B.W. Wojciechowski, Catal. Rev. Sci. Eng., 24(1) 1982 165.
6. C. Walling, J. Am. Chem. Soc., 72 1950 1169.
7. E.J. Demmel, A.V. Perella, W.A. Stover and J.P. Shambaugh, Proc. A.P.I. Div. Refining, 46 (1966) 165.
8. A.G. Oblad, Oil Gas J., 70 (13) 1972 84.
9. C.J. Plank and E.J. Rosinski, Chem. Eng. Prog. Symp. Ser., 73 (63) 1967 26.
10. C.J. Plank, E.J. Rosinski, and W.P. Hawthorne, Ind. Eng. Chem., Prod. Res. Dev., 3 1972 165.
11. D.P. Mobley and A.T. Bell, Fuel, 59 1980 507-510.
12. C.W. Zielke, R.T. Struck, J.M. Evans, C.P. Costanza, E. Gorin, Ind. Eng. Chem. Proc. Des. Dev., 5 1966 158-164.
13. R.T. Struck and C.W. Zielke, Fuel, 60 1981 795-800
14. R.K. Sharma, J.W. Diehl, and E. S. Olson, 3rd Int. Conf. on Proc. and Utilz. of High Sulfur Coals, Ames, Iowa, Nov. 14-16, 1989.
15. R.K. Sharma, J.W. Diehl, and E.S. Olson, ACS Div. of Fuel Chem., Boston, MA, April, 1990 (communicated).
16. K. Tanabe, Solid Acids and Bases, their catalytic properties, Academic Press, New York/London, (1970) 528.
17. A. Vogel, Textbook of Quantitative Inorganic Analysis, 4th edn., Longman Sci. and Tech. Group, Essex, Eng., (1978) 434.
18. E.S. Olson, and J.W. Diehl, Anal. Chem., 59 1987 443-448.
19. R.K. Sharma, E.S. Olson, and J.W. Diehl (Unpublished results).

## DISPERSED PHASE MOLYBDENUM CATALYST RECOVERY IN COPROCESSING

Donald Krastman, B.R. Utz, A.V. Cugini, R.G. Lett  
United States Department of Energy  
Pittsburgh Energy Technology Center  
Pittsburgh, Pennsylvania, 15236

Keywords: molybdenum recovery, cleaned coal, coprocessing

### INTRODUCTION

Dispersed-phase molybdenum catalysts are being used at PETC to enhance the simultaneous conversion of petroleum bottoms material and coal to distillate products. A series of tests were performed in micro-autoclaves, 1-liter semi-batch stirred autoclaves, and a 1-liter continuous unit aimed at maximizing the production of distillates while minimizing the catalyst requirements [1]. Similar product yield structures and conversions have been demonstrated using molybdenum concentrations from 200 ppm (based on coal weight) to 1000 ppm in the 1-liter continuous unit. Dispersed-phase catalysis using molybdenum may require catalyst recovery. This paper examines the potential for the recovery of a dispersed-phase molybdenum catalyst.

Molybdenum catalyst recovery schemes typically involve ashing the non-distillate process residue and converting the metals to their oxide form. Certain metal oxides are selectively solubilized by dissolution in ammonium hydroxide ( $\text{NH}_4\text{OH}$ ), including molybdenum, which forms water-soluble ammonium heptamolybdate. A recovery process patented by AMAX [2] involves mixing a gasifier residue with an alkali metal hydroxide, heating the mixture between 600°C and 800°C in the presence of air, adding water to the mixture, and then acidifying and ammoniating the aqueous solution to extract and selectively crystallize as ammonium heptamolybdate. Universal Oil Product Incorporated [3,4] (UOP) has recovered a dispersed vanadium catalyst by first performing a particle size classification of the reactor product with hydroclones, followed by calcination (ashing) of the solids at 500°C, and extraction with an ammonium hydroxide solution.

Earlier experiments at PETC [5] indicated that the nickel and vanadium, present as contaminants in the petroleum bottoms, appear to be incorporated into the carbonaceous material. Thus, these metals are also present in the bottoms material produced in dispersed-phase catalytic coprocessing along with the catalyst and coal mineral matter. The catalyst recovery procedure consisted of extracting the reactor product with tetrahydrofuran (THF), ashing the extract at elevated temperature, and extracting the ash with an ammonium hydroxide solution. Initial recovery experiments used the ASTM procedure for ashing coal [6]. The effects of ashing temperature, coal mineral matter, and the choice of hydroxides (strength of the base) on molybdenum recovery were examined.

### EXPERIMENTAL

Reagents were ACS grade and obtained from Alfa Chemicals. Coals used included an Illinois No. 6 (Burning Star Mine) hvBb coal that was ground to less than 75 microns, and a deep-cleaned Kentucky (Blue Gem Mine) hvAb coal that was ground to less than 7.5 microns and physically cleaned by the Otisca T-Process [7]. Analyses of the feed coals and the coal ash are presented in Table 1. Maya atmospheric tower bottoms (Maya ATB) was used as the vehicle. An analysis of the Maya ATB is

presented in Table 2.

The semi-batch 1-liter autoclave was charged with 150 grams of coal, 350 grams of oil, and 35 grams of 0.045 M ammonium molybdate solution. The unit was operated with a continuous gas stream ( $3\text{H}_2\text{S}:97\text{H}_2$ ) at a rate of 4 SCFH (113 standard liters/hr). Water and volatile products (light oils) from the reactor were condensed in a trap maintained at room temperature. The reactor was maintained at run temperature for 2 hours, cooled, depressurized, drained, and washed with methylene chloride to quantitatively recover the product. Typical heatup and cool-down times of the autoclave tests were two hours. All semi-batch experiments were performed using reactor conditions of 435°C, 2500 psig, and 2 hours residence time.

The catalyst recovery scheme is depicted in Figure 1. Reactor product was slurried with a 5:1 wt ratio of n-heptane and then decanted. The heptane insoluble residue was then washed/extracted with THF and pressure-filtered through a 0.45 micron Durapore® membrane filter, using a 142-mm Millipore Hazardous Waste Filtration System and 40 psig nitrogen. The THF-insoluble residue was vacuum dried and weighed. A portion of the insoluble residue was ashed in a Fisher Model 495 Programmable Ashing Furnace. The residue was heated at a rate of 5°C/min to 250°C, held for an hour at 250°C, heated to the final temperature (700°C, 675°C, 510°C), and held at temperature for 600 minutes.

Solubilizations of the ash were performed at 65°C for one hour. Five grams of ash were used for experiments conducted with residues produced from Illinois No. 6 coal. One or three grams of ash were used for experiments that were conducted with residues produced from Kentucky (Blue Gem) coal or coal-free experiments. The ash was first mixed with approximately 100 ml of deionized water. Ammonium hydroxide was then added to give a weight ratio of ammonia-to-molybdenum of 10:1 and the mixture diluted to 300 ml with additional deionized water. A magnetic stirrer provided agitation during the solubilization. A water-cooled condenser prevented some vapors from escaping. The suspension was then filtered hot in a 47-mm Millipore vacuum filtration apparatus using a water aspirator. The ammonium hydroxide-soluble filtrate was evaporated to dryness using a rotoevaporator. Both the soluble and insoluble filter cakes were dried in a vacuum oven.

Selected samples were examined by thermogravimetric analysis (TGA), scanning electron microscopy (SEM) energy dispersive analysis, X-ray diffraction, and inductively couple plasma emission spectroscopy (ICP). TGA was performed in a Perkin-Elmer TGS-2 Thermogravimetric system using a temperature profile of 5°C per minute in an air atmosphere. Samples were examined with an SEM equipped with an energy-dispersive spectrometer. ICP analysis was carried out at the University of Pittsburgh Applied Research Center (UPARC) using a Bausch and Lomb ARL Model S34000 system.

## RESULTS AND DISCUSSION

By ashing at 700°C and extraction with ammonium hydroxide, over 95 % of the molybdenum could be recovered from physical mixtures of coal ash, molybdenum trioxide, vanadium pentoxide, and nickel oxide. When experiments were performed using residues generated from continuous unit operations, only 50 percent of the molybdenum could be recovered in the ammonium hydroxide soluble extract. Since the melting point of  $\text{V}_2\text{O}_5$  is 695°C, the ashing temperature was reduced to 675°C. Recoveries

of molybdenum were still unsatisfactory. Consequently, a series of semi-batch experiments were performed using different feedstocks and dispersed molybdenum catalyst to produce samples that could determine the effects of ashing temperature, other metals present, and of coal ash constituents on catalyst recovery.

The first set of experiments, experiment A in Table 3, were performed with a THF-insoluble reactor product from liquefaction reactions conducted with Maya ATB and catalyst. The THF-insoluble residue was ashed at a temperature of 675°C producing a glassy solid. The glassy solid was difficult to remove from the crucible and extract with  $\text{NH}_4\text{OH}$ . SEM analysis indicated that the glassy solid was chemically homogeneous to a resolution of 1 cubic micron. X-ray diffraction analysis of the ash was unable to identify the major constituent of the ash.  $\text{MoO}_3$ ,  $\text{NaVMoO}_6$ , and  $\text{Fe}_4\text{V}_2\text{Mo}_3\text{O}_{20}$  were identified as minor constituents. The literature suggested [8] that vanadium-molybdenum complexes form at temperatures of 635°C and that lowering the ashing temperature to below 635°C would eliminate the formation of this complex and possibly the glassy solid.

The effect of ashing temperature on carbon removal from a THF-extracted reactor product was studied by TGA. The weight profile versus temperature indicated that carbon loss was occurring at temperatures as low as 510°C. By lowering the ashing temperature to 510°C, the ash obtained was the expected consistency and weight. Experiments were repeated at the lower ashing temperature of 510°C, (experiment B in Table 3), and the ash produced was a granular material rather than a glassy solid. X-ray diffraction analysis of the ash identified alpha- $\text{MoO}_3$  and  $\text{NaVMoO}_6$  as the major constituents of the ash. The unidentified major constituent observed at the higher ashing temperature (675°C) was not present. In an attempt to identify the compound present in the 675°C ash, a sample was ashed at 600°C. The 600°C ash sample contained the unidentified compound,  $\text{NaVMoO}_6$ ,  $\text{Na}_2\text{V}_2\text{Mo}_3\text{O}_{15}$ , and beta- $\text{MoO}_3$  as major constituents. Thus the molybdenum bound with the vanadium at 510°C is transformed to more complex structures at 600°C and possibly even more complex structures at 675°C which are inhibiting the recovery of molybdenum. Extraction of the 510°C ash residue with  $\text{NH}_4\text{OH}$  resulted in solubilization of the molybdenum and recoveries were greater than 90 percent. In these experiments, and all subsequent experiments, recoveries are defined as the percentage of molybdenum that is recovered in the basic solution. The range of values in Table 3 for molybdenum purity and ammonium molybdate recovery were from multiple experiments. Solubilized fractions were not selectively crystallized to recover the pure heptamolybdate salt.

The second set of experiments, experiments C and D in Table 3, were done to determine the effect that coal ash has on molybdenum recovery. Semi-batch liquefaction experiments were performed with Illinois No. 6 coal, Maya ATB, and catalyst. The THF-insolubles were ashed at a temperature of 510°C and extracted with  $\text{NH}_4\text{OH}$  but the recovery of molybdenum as a soluble species was only approximately 50 percent. X-ray diffraction analysis of the ammonium hydroxide-insoluble material indicated the presence of calcium molybdate. ICP analysis indicated a 1:1 molar ratio of calcium to molybdenum, consistent with the identification of calcium molybdate by X-ray diffraction.

Experiments were performed to determine if the formation of  $\text{CaMoO}_4$  was interfering with molybdenum recovery. Semi-batch experiments, experiment E in Table 3, were performed using a deep cleaned coal, Kentucky Blue Gem, containing 0.8 wt% ash, rather than the Illinois No.

6 coal containing 11.1 wt% ash. The purpose of using a deep-cleaned bituminous coal was to reduce the effect of the calcium (present in the coal mineral matter) on molybdenum recovery. The THF-insoluble residue was ashed and extracted with  $\text{NH}_4\text{OH}$  and the observed molybdenum recovery as a soluble species was now greater than 95 percent. The results of these experiments demonstrate that the calcium present in the mineral matter reacts with  $\text{MoO}_3$  in the ashing step to form  $\text{CaMoO}_4$ .  $\text{NH}_3$  does not appear to be a strong enough base to react with  $\text{CaMoO}_4$  to solubilize molybdenum.

Pure calcium molybdate was treated with  $\text{NH}_4\text{OH}$  at temperatures as high as  $90^\circ\text{C}$  but it was unreactive and not solubilized. Since ammonium hydroxide was ineffective, the stronger base, sodium hydroxide, was tested. Calcium molybdate was decomposed to form insoluble calcium hydroxide and soluble sodium heptamolybdate when treated with sodium hydroxide. These results demonstrate that stronger bases, such as sodium hydroxide, are capable of decomposing calcium molybdate and removing calcium as an insoluble salt. It also suggests that sodium hydroxide might be used as a substitute for ammonium hydroxide. Treatment of a solution containing sodium heptamolybdate with  $\text{NH}_4\text{OH}$  should result in the selective crystallization of ammonium heptamolybdate, the catalyst precursor.

A typical material balance for metals in a run made with cleaned Kentucky Blue Gem coal is indicated in Figure 2. Molybdenum present as ammonium heptamolybdate comprises 78 percent of the  $\text{NH}_4\text{OH}$ -soluble material. Analyses were not performed for the remaining constituents of the soluble fraction. Experiments with Illinois No. 6 coal typically did not yield as high an ammonium heptamolybdate concentration in the  $\text{NH}_4\text{OH}$ -soluble material. It is thought that some of the coal ash components are being solubilized with the ammonium hydroxide. Typically, for these experiments, molybdenum accounts for 50 percent of the  $\text{NH}_4\text{OH}$ -soluble material.

#### CONCLUSIONS

It has been demonstrated that molybdenum can be recovered from coal liquefaction coprocessing experiments. High recoveries of molybdenum required an ashing temperature of  $510^\circ\text{C}$  to avoid the formation of a refractory molybdenum-vanadium complex, which appeared to form at higher ashing temperatures ( $675^\circ\text{C}$ ) and inhibited molybdenum recovery. X-ray diffraction and elemental analyses of the ash produced from experiments that used coal indicate the presence of calcium molybdate in the ammonium hydroxide-insoluble material. Calcium molybdate that is formed from calcium in the coal mineral matter and the molybdenum catalyst is unreactive with ammonium hydroxide and inhibits the recovery of molybdenum. This was supported by conducting experiments with deep-cleaned coal wherein most mineral matter, to include calcium, had been removed. More than 90% of the molybdenum was recovered from deep-cleaned coal. Preliminary experiments have shown that stronger hydroxides, such as sodium hydroxide, react with calcium molybdate to form a soluble molybdate salt and would result in improved molybdenum recovery. As a result of optimizing the conditions, a recovery scheme has been developed that can recover the molybdenum when calcium has been removed from the feed coal. This scheme most likely will apply to raw coals using sodium hydroxide as a substitute for ammonium hydroxide.

#### ACKNOWLEDGEMENT

The authors thank Michael Ferrer for performing the TGA analyses, Don Martello for performing the SEM analyses, and Sidney Pollack and Elizabeth Fromell for performing the X-ray analyses.

#### DISCLAIMER

Reference in this report to any specific commercial product, process, or service is to facilitate understanding and does not necessarily imply its endorsement or favoring by the United States Department of Energy.

#### REFERENCES

- [1] Lett, R.G.; Cugini, A.V.; Utz, B.R.; Krastman, D.; Cillo, D.L.; Jin, G.T. U.S./Korea 6th Joint Workshop on Coal Utilization, Seoul, Korea, 1989.
- [2] Sebenik, R.F.; Hallada, C.J.; Barry H.F.; Tsigdinos, G.A. U.S. Patent 4,374,100, Feb. 15, 1983.
- [3] Gatsis, J.G.; Nelson, B.J.; Lea, C.L.; Nafis, D.A.; Humbach, M.J. Coal Liquefaction Co-processing, Topical Report Number 2 ,DE-AC22-84PC70002, Aug. 19, 1988.
- [4] Nafis, D.A.; Fullerton, H.E.; Gatsis, J.G., Miller, M.A. Sixth Annual International Pittsburgh Coal Conference, September, 1989.
- [5] Cugini, A.V.; Ruether, J.A.; Cillo, D.L.; Krastman, D.; Smith, D.N.; Balsone, V. Preprints, Div. Fuel Chem., Am. Chem. Soc. 33(1), 6 (1988).
- [6] ASTM D3174-82 "Standard test method for Ash in the Analysis sample of coal and coke from coal," 1988 Annual book of ASTM standards, 5.05, 1988.
- [7] Simmons, F.J.; Keller Jr., D.V. 10th International Coal Preparation Congress, Sept. 1986.
- [8] Strupler, N.; Morette, A.; in Phase diagrams for Ceramists 1975 Supplement, (Ed. K.R. Reser) The American Ceramic Society, 1975.

Table 1. Analysis of Feed coals.

	Illinois No. 6 Burning star	Cleaned Kentucky Blue Gem Mine
Ultimate Analysis, wt% (Moisture Free)		
Carbon	70.2	80.3
Hydrogen	4.8	5.1
Nitrogen	0.9	1.9
Sulfur	3.1	0.8
Oxygen(difference)	9.9	11.1
Ash	11.1	0.8
Major Elements in Ash		
SiO <sub>2</sub>	44.6	29.1
Al <sub>2</sub> O <sub>3</sub>	18.3	25.9
Fe <sub>2</sub> O <sub>3</sub>	21.9	25.1
TiO <sub>2</sub>	0.9	3.2
P <sub>2</sub> O <sub>5</sub>	0.1	0.4
CaO <sub>2</sub>	5.1	4.9
MgO <sub>2</sub>	0.6	1.4
Na <sub>2</sub> O	1.6	1.4
K <sub>2</sub> O	1.1	1.7

Table 2. Analysis of Vehicle oil.

	Maya ATB 650°F*
Ultimate Analysis, wt%	
Carbon	84.5
Hydrogen	10.6
Nitrogen	0.5
Sulfur	4.0
Oxygen(direct)	0.3
Ash	0.1
850°F (Vol%)	30
Heptane insols, wt%	20
Nickel (ppm)	70
Vanadium (ppm)	370

Table 3. Effect of extraction conditions on Molybdenum recovery.

Exp	Coal	Solvent	Ni+V gm	Mo gm	Ash temp °C	Ash gm	Recovery Mo in sols wt%	(NH <sub>4</sub> ) <sub>2</sub> Mo <sub>7</sub> O <sub>24</sub> Purity wt% sols
A	None	Maya	0.23	1.6	675	4.0	ND	ND
B	None	Maya	0.23	1.6	510	4.2	88	73
C	Ill. # 6	Maya	0.15	2.4	675	20.0	35	44
D	Ill # 6	Maya	0.15	1.0	510	18.5	49 - 57	34 - 38
E	Blue Gem	Maya	0.15	1.0	510	3.4	90 - 98	66 - 78

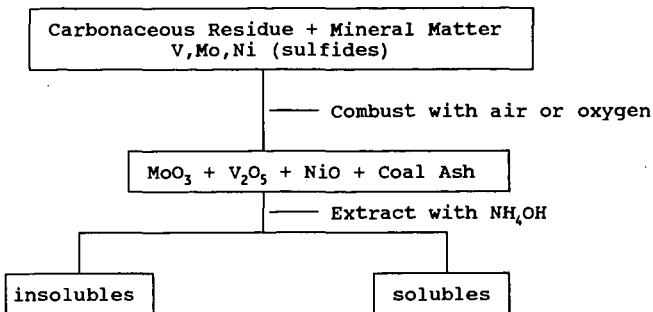


Figure 1. Catalyst Recovery in Coprocessing.

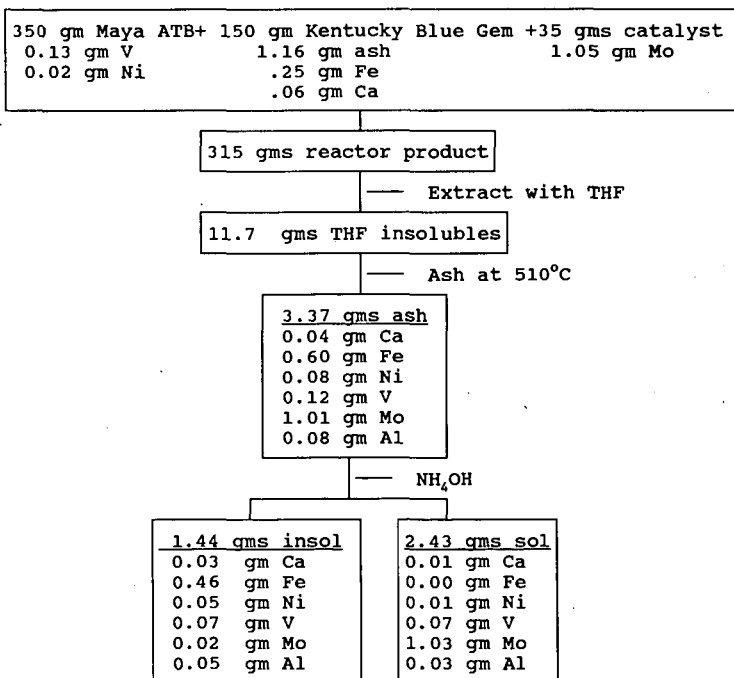


Figure 2. Catalyst Material Balance for Batch Run

CYCLIC OLEFINS AS NEW HYDROGEN DONOR COMPOUNDS  
FOR COAL LIQUEFACTION

Michael W. Bedell and Christine W. Curtis  
Chemical Engineering Department  
Auburn University  
Auburn, Al 36849

Keywords: Coal Liquefaction, Hydrogen Transfer, Donor Compounds

ABSTRACT

A new set of hydrogen donor compounds, cyclic olefins (CLO), has been evaluated to determine their effectiveness as hydrogen donors to coal. These cyclic olefins are hydroaromatic species which do not contain aromatic rings. The efficacy of these donors has been compared to conventional hydroaromatics. The CLO's under study are 1,4,5,8-tetrahydronaphthalene, also known as isotetralin, and 1,4,5,8,9,10-hexahydroanthracene. CLO's are much more reactive than their conventional hydroaromatic analogues, both in model reactivity studies and in reactions with Western Kentucky No. 9 coal. In this paper, the thermal and catalytic reactivity of the CLO's under nitrogen and hydrogen at coal liquefaction temperature is discussed. Results for the reactions of the CLO's and their conventional hydroaromatic analogues, e.g. tetralin, 9,10-dihydroanthracene, and octahydroanthracene, with Western Kentucky No. 9 coal are discussed.

INTRODUCTION

In both thermal and catalytic coal liquefaction reactions, hydrogen transfer reactions are important avenues by which hydrogen is transferred to coal and substantially increases the amount of coal conversion and upgrading. Hydrogen donors typically used are hydroaromatic and phenolic compounds (1-6). A new set of hydrogen donor compounds has been discovered that are much more effective than conventional hydroaromatics in transferring hydrogen to coal. These donors are cyclic olefins (i.e. hydroaromatic species which do not contain aromatic rings). An example is isotetralin, 1,4,5,8-tetrahydronaphthalene.

The efficiency of isotetralin for converting coal to THF solubles has been shown to be much higher than its conventional hydroaromatic analogue, tetralin (1). In reactions with Western Kentucky No. 9/14 coal, isotetralin converted 80.6% of the coal to THF solubles compared to only 58% for tetralin. This dramatic increase in coal conversion with isotetralin leads to the current investigation of cyclic olefins as hydrogen donors for coal liquefaction.

The objective of this research is to test cyclic olefins as donors for coal liquefaction. The cyclic olefins under study are 1,4,5,8,9,10-hexahydroanthracene (HHA) and 1,4,5,8-tetrahydronaphthalene, isotetralin (ISO). The first step in fulfilling this objective was to investigate the chemistry of these compounds. Both the thermal and catalytic reactivity under hydrogen and nitrogen atmospheres has been determined. The catalysts used were presulfided, pulverized NiMo/Al<sub>2</sub>O<sub>3</sub> and Mo/Al<sub>2</sub>O<sub>3</sub>. Secondly, these compounds were thermally reacted with Western Kentucky No. 9 coal under a nitrogen atmosphere to evaluate their hydrogen donability.

## EXPERIMENTAL

The reactivity and stability of the cyclic olefins were tested in a stainless steel tubing bomb reactor with a volume of 20 cc under the following conditions: 380°C, horizontal agitation at 425 cpm, 1250 psig nitrogen or hydrogen pressure at ambient temperature, reaction times ranging from 15 minutes to 1 hour, 2.0 g hexadecane as the diluent solvent, 3 weight percent CLO, and for catalytic reactions a total active metal loading of 3000 ppm. Two catalysts were used, Shell 324, NiMo/Al<sub>2</sub>O<sub>3</sub>, and Amocat 1B, Mo/Al<sub>2</sub>O<sub>3</sub>, to evaluate the catalytic reactivity of ISO at liquefaction conditions. Each catalyst was presulfided, pulverized, and sized between 100 and 200 mesh before being used.

The reactions of both CLO's and three conventional hydroaromatic donor compounds with Western Kentucky No. 9 were also performed. For this study the following reaction conditions were employed: 30 minute reaction time, 1250 psig nitrogen atmosphere at ambient temperature, 380°C reaction temperature, 2.0 g coal, 4.0 g total solvent mixture including 0.1-0.5 weight percent donable hydrogen of the model compound with the balance being fluorene as a diluent solvent, 700 cpm vertical agitation rate, stainless steel tubing bomb reactor of approximately 50 cm<sup>3</sup> volume.

The chemicals used were obtained from the following manufacturers and used as received: tetralin, 1,4,5,8,9,10-hexahydroanthracene, 1,2,3,4,5,6,7,8-octahydroanthracene, and 9,10-dihydroanthracene from Aldrich Chemical Co.; 1,4,5,8-tetrahydronaphthalene from Wiley Organics Inc.; Western Kentucky No. 9 coal from PSU/DOE sample bank.

For this work coal conversion is defined as

$$\text{conversion} = 1 - [ \text{IOM (maf)} / \text{coal charge (maf)} ] \times 100$$

In order to use this definition of coal conversion, both the moisture and ash contents were needed. The moisture content was 4.5 ± 0.6% and the ash 10.16 ± 0.14%.

## RESULTS AND DISCUSSION

### ISOTETRALIN SYSTEM

In the model reactivity studies, ISO was very reactive at the catalytic conditions studied; none was observed in the reaction products even at reaction times as short as 15 minutes. Two different presulfided hydrogenation catalysts were used: Shell 324, NiMo/Al<sub>2</sub>O<sub>3</sub>, and Amocat 1B, Mo/Al<sub>2</sub>O<sub>3</sub>. These catalysts were chosen because of their different hydrogenation activities with NiMo/Al<sub>2</sub>O<sub>3</sub> usually being more active. With ISO in the presence of NiMo/Al<sub>2</sub>O<sub>3</sub> and a hydrogen atmosphere, tetralin (TET) was produced as a major product, while no measurable amount of naphthalene (NAP) was formed. With increasing reaction times, less TET was produced, while more decalin (DEC) was formed. With the NiMo/Al<sub>2</sub>O<sub>3</sub> catalyst, the trans to cis isomer ratio was approximately 3 to 1. The DEC isomer ratio was independent of reaction time, within experimental error. With Mo/Al<sub>2</sub>O<sub>3</sub>, the predominant product formed was TET; cis and trans DEC as well as NAP was also formed, yielding approximately 20 weight percent DEC and one weight percent NAP. The trans to cis DEC isomer ratio was approximately 2.5 to 1 and was constant for reaction times ranging from 15 minutes to 1 hour. For ISO, NiMo/Al<sub>2</sub>O<sub>3</sub> was a more active hydrogenation catalyst than Mo/Al<sub>2</sub>O<sub>3</sub>, as evidenced by the greater amounts of DEC produced. The product slate was independent of time, within experimental error, for the reactions performed with the Mo/Al<sub>2</sub>O<sub>3</sub> catalyst under equivalent

conditions but varying reaction times; i.e. all the products were formed within the first 15 minutes yielding the same product slate regardless of reaction time.

The thermal reactivity study of ISO showed that all ISO was converted at reaction times of 15, 30, and 60 minutes. The product slate for the thermal reactions differed from that of the catalytic reactions. 1,2-dihydronaphthalene (1,2-DHN) and 1,4-dihydronaphthalene (1,4-DHN) were formed thermally, whereas catalytically they were not. In a nitrogen atmosphere, the predominant product was NAP, with other major products being 1,2-DHN 1,4-DHN, and a minor amount of TET. Approximately 55 weight percent NAP and 40 weight percent DHN's were produced. In a hydrogen atmosphere, the observed products were TET, 1,2-DHN, 1,4-DHN, and NAP. The product slate for the thermal reactions was time dependent. Although the same products were observed, different amounts of each were formed at different reaction times. With increasing reaction time, the amount of NAP produced increased while the amount of 1,2-DHN and 1,4-DHN decreased. The 1,2-DHN to 1,4-DHN isomer ratio varied widely with varying reaction times. At a reaction time of one hour, the 1,4-DHN produced was unexpectedly small; it is believed that 1,4-DHN was rehydrogenated to TET, which would account for the increased TET produced at this reaction time.

#### HEXAHYDROANTHRACENE SYSTEM

The thermal and catalytic reactivity of 1,4,5,8,9,10-hexahydroanthracene, (HHA) was also examined. As in the ISO reactions, NiMo/Al<sub>2</sub>O<sub>3</sub> was a more active hydrogenation catalyst than Mo/Al<sub>2</sub>O<sub>3</sub> in the HHA reaction system. With NiMo/Al<sub>2</sub>O<sub>3</sub>, the predominant products from HHA hydrogenation were isomers of fully hydrogenated anthracene, perhydroanthracene (PHA); the other major products were isomers of octahydroanthracene (OHA) with a minor amount of tetrahydroanthracene isomers (THA) observed. Increasing reaction times favored the formation of the more hydrogenated product PHA, while decreasing the amount of OHA produced. For all reaction times, HHA was totally converted, with either NiMo/Al<sub>2</sub>O<sub>3</sub> or Mo/Al<sub>2</sub>O<sub>3</sub>. With the Mo/Al<sub>2</sub>O<sub>3</sub> catalyst, the predominant product was OHA; other products in lesser amounts were PHA and THA. Increasing reaction times increased the amount of hydrogenated product formation. Both OHA and PHA production increased, while that of THA decreased.

In the thermal reaction system for HHA, under both nitrogen and hydrogen atmospheres, the predominant products were isomers of dihydroanthracene (DHA) with 9,10-dihydroanthracene being the major isomer observed. Lesser products included THA and anthracene (ANT). In a nitrogen atmosphere, a trace amount of HHA was observed at the end of the 30 minute reaction time. In a hydrogen atmosphere, with increasing reaction times, HHA recovery decreased. DHA formation decreased, while ANT and THA formation increased. After 60 minutes of reaction in a hydrogen atmospheres, a minor amount of OHA was formed.

#### COMPARISON OF CYCLIC OLEFINS AND CONVENTIONAL DONORS

The reactivity of the conventional hydrogen donor analogues, DHA, OHA, and TET were compared to that of HHA and ISO under equivalent reaction conditions.

With NiMo/Al<sub>2</sub>O<sub>3</sub> in a hydrogen atmosphere, ISO completely reacted, whereas, approximately 25% of TET remained unconverted. The products formed from ISO were TET and DEC, while those from TET were primarily DEC. However, it should be noted that the trans to cis DEC isomer ratio was the same for both compounds, (3 to 1), within experimental error, and that neither ISO nor TET formed NAP as product.

This suggests that ISO was converted to TET by some pathway before forming the more hydrogenated products. With Mo/Al<sub>2</sub>O<sub>3</sub> in a hydrogen atmosphere, ISO was also completely reacted, whereas, TET remained almost 95% unconverted. However, as was the case with NiMo/Al<sub>2</sub>O<sub>3</sub>, the trans to cis DEC isomer ratio was the same for both ISO and TET (2.5 to 1), within experimental error. This result also suggests that ISO was converted to TET prior to forming DEC.

In thermal reactions, ISO completely reacted under both nitrogen and hydrogen atmospheres. By contrast, TET reacted only slightly in nitrogen producing NAP and was less than 4% converted in a hydrogen atmosphere, forming 1,2-DHN and 1,4-DHN.

The reactions of DHA, OHA, and HHA with NiMo/Al<sub>2</sub>O<sub>3</sub> in a hydrogen atmosphere produced hydrogenated anthracenes as the predominant products. All three reactants formed PHA, OHA, and THA. DHA and HHA were completely converted to hydrogenated products, whereas OHA remained approximately 32% unconverted. With the Mo/Al<sub>2</sub>O<sub>3</sub> catalyst, HHA was completely converted, approximately 8% of the DHA remained unreacted, and 98% of the OHA remained unreacted. These comparisons show that catalytically, HHA was much more reactive than either of the conventional hydrogen donor compounds, DHA or OHA.

A comparison of the thermal reactions of HHA, OHA, and DHA showed that in a nitrogen atmosphere HHA completely reacted, the predominant product from HHA hydrogenation being DHA, with lesser amounts of THA and ANT being formed. By contrast, OHA did not react and DHA remained 95% unconverted, with ANT being the only product. In a hydrogen atmosphere more than 98% of HHA was converted, with the predominant product again being DHA. By comparison OHA did not react and only 8% of DHA was converted to dehydrogenated products. The results from the thermal reactions show that HHA was much more reactive than either OHA or DHA at 380°C under both hydrogen and nitrogen atmospheres.

To summarize, when ISO is compared to TET, it is important to note that both thermally, under nitrogen and hydrogen, as well as catalytically, ISO completely converted. By comparison TET did not react thermally, only converted 5% with Mo/Al<sub>2</sub>O<sub>3</sub> and converted 75% with NiMo/Al<sub>2</sub>O<sub>3</sub>. The comparison of the conventional analogues to HHA showed that DHA was only converted 10% in a thermal reaction system, converted 100% with NiMo/Al<sub>2</sub>O<sub>3</sub>, and converted 90% with Mo/Al<sub>2</sub>O<sub>3</sub>. In a thermal system, under both nitrogen and hydrogen, OHA did not react; with the NiMo/Al<sub>2</sub>O<sub>3</sub> catalyst, OHA was 68% reacted, while with the Mo/Al<sub>2</sub>O<sub>3</sub> only 2% converted. HHA was completely converted by both NiMo/Al<sub>2</sub>O<sub>3</sub> and Mo/Al<sub>2</sub>O<sub>3</sub>. In a thermal system under nitrogen, HHA was completely reacted and was more than 90% converted under hydrogen. Thus, ISO was more reactive than TET, and HHA was more reactive than either DHA or OHA.

#### REACTIONS WITH WESTERN KENTUCKY NO. 9 COAL

A series of thermal reactions using ISO, HHA, TET, OHA, and DHA with Western Kentucky No. 9 coal in a nitrogen atmosphere was performed. The results for coal conversion to tetrahydrofuran solubles (THFS) is presented in Table I. Each datapoint represented in Table I is the result of at least a duplicate analysis. These are two important aspects to this table. The first is the ranking of the five donor species at the equivalent loading of 0.5 weight percent donable hydrogen. The second is the comparison of HHA and OHA at three different levels of donable hydrogen, 0.5, 0.2, 0.1 weight percent. Important to note in the rankings of the donor species at 0.5 weight percent, is that the two cyclic olefins, HHA and ISO, yielded greater coal conversions than did their conventional

hydroaromatic analogues, TET, OHA or DHA. HHA produced an increase in coal conversion of approximately 12% over its nearest analogue DHA. HHA also showed more than 13% greater conversion than did OHA. ISO yielded approximately 14% greater conversion than did its conventional analogue, TET. All of these comparisons were made on an equivalent amount of donable hydrogen.

When the level of donable hydrogen was varied, HHA consistently converted more than did OHA, albeit, in decreasing differential amounts as the level of donable hydrogen decreased. This result implies that a deficiency of donable hydrogen occurred at these lower levels of donable hydrogen.

For each of the reactions, the THFS fraction was then further analyzed to determine the effect of the coal reaction on the amount of the model hydrogen donor compound that was present in the reaction products. Important to note from this analysis is that for a given hydrogen donor compound, as the level of donable hydrogen was decreased, the products shifted to less hydrogenated species.

A plot of coal conversion versus net grams of H donated from the hydrogen donor is represented in Figure 1. These values were obtained in the following manner. Net grams of hydrogen released (grams of H donated from model compound) - (grams of H going to form other hydrogen donor species). For these calculations, the only other H donor formed was OHA. The solid line shown is the linear best fit to all the data points. The general trend is that as coal conversion increased, the amount of hydrogen donated also increased.

#### SUMMARY

As seen in both the model compound reactions as well as reactions with Western Kentucky No. 9 coal, the new hydrogen donor compound, cyclic olefins, HHA and ISO, are much more reactive at model liquefaction conditions than either DHA, OHA, or TET. In the model compound reactivity studies, ISO was more reactive, both thermally and catalytically, than TET; HHA was more reactive, both thermally and catalytically, than either DHA or OHA. In reactions with Western Kentucky No. 9 coal in a nitrogen atmosphere, HHA produced an increase in coal conversion to THF solubles of greater than 12% compared to that obtained with OHA, and 12% greater conversion than that obtained with DHA. ISO produced an increase in coal conversion of approximately 14% more than obtained with TET.

#### REFERENCE

- (1) Curtis, C.W.; Guin, J.; Kwon, K.; "Coal Solvolysis in a Series of Model Compound Systems."; Fuel; 63, 1984.
- (2) Neavel, R.C.; "Liquefaction of Coal in Hydrogen Donor and Non-donor Vehicles"; Fuel; 55, 1976.
- (3) Utz, B.R.; Appell, H.R.; Blaustein, B.D.; "The Roles of Vehicles and Gaseous Hydrogen During Short Contact Time Coal Liquefaction"; Fuel; 65, 1986.
- (4) Kitaoka, Y.; Mikio, U.; Murata, K.; Ito, H.; Mikami, K.; "Effect of Catalyst and Vehicle in Coal Liquefaction"; Fuel; 61, 1982.
- (5) Bockrath, B.C.; "Chemistry of Hydrogen Donor Solvents"; Coal Science; Vol. 2, Academic Press, New York, NY; 1982

- (6) Franz, J.A.; Camaioni, D.M.; "Radical Pathways of Coal Dissolution in Donor Media During Reactions of Coal and Specifically Deuterated Tetralin"; Prep. Paper., ACS Div. Fuel Chem.; 1981, 26(1).

ACKNOWLEDGEMENTS

We gratefully acknowledge the support of the work by the Department of Energy under Contract No. UK DE-FC22-88PC88806.

Table I. Coal Conversion Summary for Western Kentucky No. 9

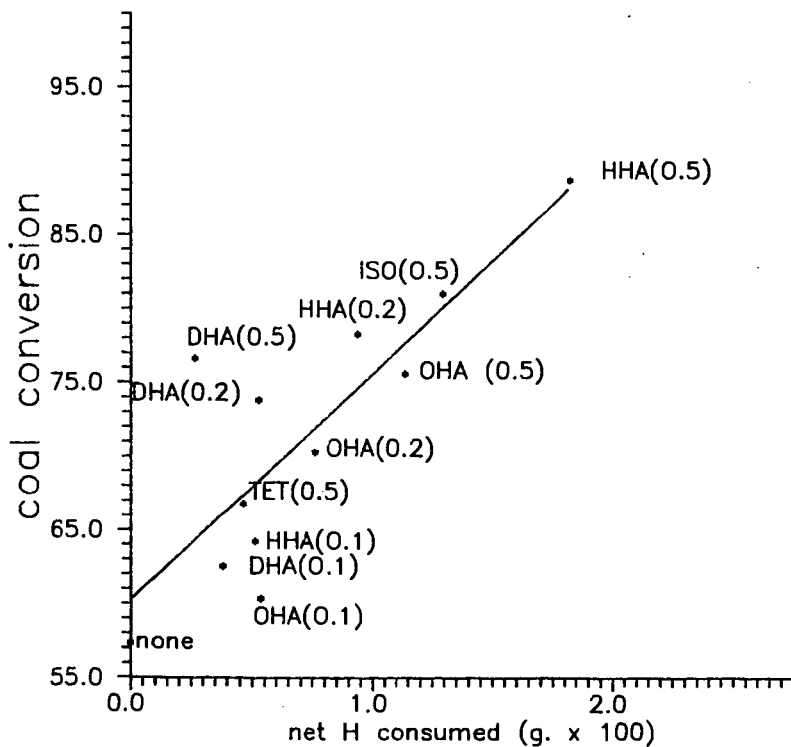
Donor Compound	Conversion* at		
	.5wt% DH	.2wt% DH	.1wt% DH
HHA	88.6(0.04)	78.2(0.5)	64.2(2.5)
ISO	81.0(0.9)		
DHA	76.6(0.8)	73.8(1.1)	62.5(1.2)
OHA	75.5(0.7)	70.2(2.7)	60.3(0.7)
TET	66.8(0.9)		
none	57.4(2.3)	57.4(2.3)	57.4(2.3)

\* conversion defined as  $1 - \frac{IOM(maf)}{coal(maf)}$   
and DH refers to donable hydrogen

\*\*All reactions at 380°C, 1250 psig (cold) N<sub>2</sub> atmospheres, 700 cpm, and 30 minute reaction time.

In the pairs of numbers above, the first is the conversion obtained. The second, in parenthesis, is the standard deviation for that data point.

Figure 1. COAL CONVERSION VERSUS HYDROGEN DONATED.  
 THREE LEVELS OF DONABLE HYDROGEN,  
 (0.5, 0.2, and 0.1 weight percent)



ACTIVATION OF METHANE BY TRANSITION METAL-SUBSTITUTED  
ALUMINOPHOSPHATE MOLECULAR SIEVES

V. A. Maroni, K. A. Williams, Hiep Hoa Nguyen, and L. E. Iton  
Argonne National Laboratory  
9700 South Cass Avenue  
Argonne, Illinois 60439.

Keywords: methane activation, molecular sieve, catalysis

ABSTRACT

Recent experiments in our laboratory have demonstrated that aluminophosphate molecular sieves substituted with cobalt and cobalt/silicon combinations and having the  $AlPO_4-34$  or  $AlPO_4-5$  structure activate methane starting at  $\sim 350^\circ C$ . Between 400 and  $500^\circ C$  the rate of methane conversion increases steadily with typical conversion efficiencies at  $500^\circ C$  ranging from 15 to 60%. The cobalt and silicon substituted  $AlPO_4-34$  structure (CoAPSO-34) produces ethylene, ethane, propylene, and propane in varying proportions, depending on reaction conditions. The cobalt-substituted  $AlPO_4-5$  (CoAPSO-5) produces propylene in very high yield, with ethane, ethylene, and propane also seen. Analogous aluminophosphate molecular sieves substituted with magnesium or silicon, but containing no transition metal (e.g., SAPO-34, MAPO-5), do not activate methane under the conditions described above. The activation mechanism is based on reduction of the cobalt(III) form of the molecular sieve to the cobalt(II) form with accompanying oxidative dehydrogenation of the methane. Reoxidation of the cobalt(II) form to the cobalt(III) form can be done either chemically (e.g., using  $O_2$ ) or electrochemically.

INTRODUCTION

In a recently published paper (1) we reported the finding that when Co(II) is substituted for Al(III) in the framework of certain aluminophosphate ( $AlPO_4$ ) molecular sieves and the resulting Co(II)-containing  $AlPO_4$  (CoAPO) is calcined in oxygen, the Co(II) is oxidized to Co(III). Further work with these Co(III)APOs showed that they possess strong oxidizing capability, and, for example, can convert methanol to formaldehyde (at  $25^\circ C$ ), NO to  $NO^+$  (at  $25^\circ C$ ), and  $H_2$  to  $2H^+$  (at  $>300^\circ C$ ). These results inspired the thought that Co(III)APOs might actually oxidize methane and in the process convert the activated species directly to light hydrocarbons by virtue of their known Bronsted acid catalyzed homologation capacity (2,3) and the product selectivity constraints imposed by their pore dimensions. Recent experiments in our laboratory (summarized below) have demonstrated that this is in fact the case.

EXPERIMENTAL

The synthesis methods used to prepare the aluminophosphate molecular sieve materials employed in this work have been discussed elsewhere (1). Reactions of methane on these molecular sieve materials and on several other metal oxides known to activate methane (e.g.,  $Sm_2O_3$ ) were carried out in a quartz tube reactor having an 8 mm inside diameter. The catalyst sample ( $\sim 1$  gram) was supported on a quartz fritted disk fused into the midsection of the quartz tube. The tube was mounted in an electrically heater furnace (with the sample in the middle of the heated zone) and attached to the gas handling system. The gases used in the experiments [99.999% He, 10%  $CH_4$  in Ar ( $C_{2+}$  hydrocarbons/ $CH_4 \approx 0.002$ ), and "zero" air, all supplied by Matheson Gas Products] were introduced at the bottom of the

reaction tube. A quartz-sheathed thermocouple was positioned inside the reaction tube just above the bed of catalyst material. Electrochemical activation was accomplished by inserting two coiled sections of platinum wire that were flattened to conform to the side wall of the reaction tube and then mounted in the tube so that they faced each other with a spacing of  $\sim 3$  mm.

In a typical experiment with a molecular sieve material, the sieve sample was calcined in "zero" air at  $550^\circ\text{C}$  in the reaction tube to burn off any remaining template ions (for a fresh sample) or carbonaceous residues (for a used sample). This calcining restored the cobalt-containing molecular sieves to the Co(III) form as described previously (1). After calcining, the reaction tube was brought to the desired temperature and purged of residual oxygen with flowing helium, then  $\sim 10$  cc (STP) of the 10%  $\text{CH}_4$  in Ar mixture was introduced at a rate of  $\sim 0.5$  cc/min. The reaction products, unreacted  $\text{CH}_4$ , and Ar coming out the top of the reaction tube were collected in a liquid nitrogen cooled loop. The loop was then isolated from the reaction tube and warmed up to room temperature; after which a gas sample was withdrawn through a septum port on the side of the loop (using a gas syringe) and injected into a gas chromatograph (GC) equipped with a flame ionization detector (FID). In some experiments injections were also made into a GC equipped with a thermal conductivity detector (TCD) to determine the amounts of  $\text{H}_2\text{O}$ ,  $\text{CO}$ , and  $\text{CO}_2$  that were produced relative to the amount of  $\text{CH}_4$  reacted.

Electrochemical activation studies were performed using a constant voltage power supply. Potentials in the range from 3 to 10 V dc were applied across the two platinum wire electrodes (described above). Gas handling procedures employed in the presence of an applied potential were the same as those used on air calcined molecular sieve samples, except that the sieve sample was fully reduced (deactivated) with  $\text{CH}_4$  between the calcining and helium purging steps. The voltage was applied during purging and maintained throughout the  $\text{CH}_4$  introduction step.

## RESULTS

Methane activation experiments were performed on the following aluminophosphate molecular sieve materials: CoAPSO-34 (P:Co:Si = 12:1:1.8), CoAPO-5 (P:Co = 24:1), MAPO-5 (P:Mg = 12:1), and SAPO-34 (P:Si = 6.7:1). The onset temperature for activation of  $\text{CH}_4$  by the cobalt-containing  $\text{AlPO}_4$  (i.e., where a few percent of  $\text{C}_{2+}$  products are observed relative to the  $\text{CH}_4$ ) occurs in the  $350$  to  $400^\circ\text{C}$  range. At  $500^\circ\text{C}$  the reaction proceeds more rapidly, and single pass conversions of  $\text{CH}_4$  to  $\text{C}_{2+}$  hydrocarbons ranging from 15 to 30% have been observed. In single pass experiments without electrochemical stimulation,  $\sim 1$  cc (STP) of methane deactivates almost all of the active sites in  $\sim 1$  gram of the CoAPSO-34 or CoAPO-5, and recalcination with  $\text{O}_2$  is required to reactivate the sieve material. Many air calcinings have been run on some samples of CoAPSO-34 without evidence of significant permanent loss of activity, but in most other cases we have observed steady decreases in activity with extended use. In the presence of applied dc potentials in the 3 to 10 V range, it is possible to activate the reduced form of the cobalt-containing molecular sieves [(HCo(II)APSO-34 and HCo(II)APO-5)] and achieve significant ( $\geq 15\%$ ) methane conversion to  $\text{C}_{2+}$  hydrocarbons in a single pass at  $500^\circ\text{C}$ . However, even electrochemically activated samples tend to exhibit reduced activity with extended use.

Identical experiments were performed on the silicon-substituted  $\text{AlPO}_4$ -34 (SAPO-34) and magnesium-substituted  $\text{AlPO}_4$ -5 (MAPO-5), wherein air calcination and electrochemical stimulation were employed in the same manner as was used with the CoAPSO-34 and CoAPO-5. None of these experiments gave any evidence of methane activation to  $\text{C}_{2+}$  hydrocarbons. A test of air-calcined  $\text{Sm}_2\text{O}_3$ , a known methane

activation catalyst at  $\geq 700^\circ\text{C}$  (4), failed to produce any  $\text{C}_{2+}$  products in our apparatus for temperatures up to  $580^\circ\text{C}$ , using methane only as a reactant (no oxygen co-feed).

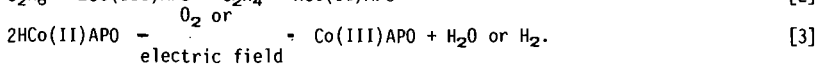
A summary of typical results from the experiments described above is given in Table I. Reproductions of FID gas chromatograms for the products of methane activation over an air calcined sample of CoAPSO-34, an electrochemically stimulated sample of CoAPSO-34, and an electrochemically stimulated sample of CoAPO-5 are shown in Figs. 1, 2a, and 2b, respectively. TCD gas chromatograms run on products from experiments where high yields of  $\text{C}_{2+}$  hydrocarbon were obtained typically showed relatively low levels of  $\text{CO}_2$  (a few percent at most) and hardly any CO. If care was not taken to remove oxygen (as  $\text{O}_2$ ) from the reaction environment prior to introduction of the methane, higher levels of  $\text{CO}_2$  and lower levels of  $\text{C}_{2+}$  hydrocarbons were normally observed, i.e., the yields of  $\text{C}_{2+}$  hydrocarbons and  $\text{CO}_x$  have tended to be inversely related to one another in the types of experiments described above.

Finally, we wish to note that electrochemical stimulation experiments done on samples of Co(II)-exchanged SAPO-34 (P:Co  $\leq 12$ ) and Co(II)-exchanged Y zeolite (Si:Co  $\sim 5$ ) at  $500^\circ\text{C}$  (using the same conditions as for the CoAPSO-34 and CoAPO-5 experiments) produced smaller (but nonetheless measurable) yields of the same products observed for CoAPSO-34 (see Table I). In the case of single pass experiments with Co(II)-exchanged Y zeolite, evidence of a few percent conversion of methane to  $\text{C}_{2+}$  hydrocarbons at  $500^\circ\text{C}$  was also seen for a sieve sample that was air calcined at  $550^\circ\text{C}$  prior to methane exposure.

#### DISCUSSION

The results presented in the preceding section give clear evidence that cobalt-substituted aluminophosphate molecular sieves have the capability to catalyze the coupling of methane to  $\text{C}_{2+}$  hydrocarbons at temperatures  $< 500^\circ\text{C}$ . The single pass yields which have exceeded 30% at  $500^\circ\text{C}$ , the high selectivity to  $\text{C}_{2+}$  hydrocarbons, the encouraging observation that molecular oxygen is not essential to the activation process, and the absence of large quantities of  $\text{CO}_x$  in the product stream represent a significant advance in the state-of-the-art for methane coupling using inorganic catalyst materials. The further finding that the cobalt-substituted molecular sieve can be maintained in the active state by an electric field allows for the development of continuous methane homologation processes using, e.g., packed or fluidized electrochemical bed reactors.

Data from comparative experiments -- CoAPSO-34 vs SAPO-34 and CoAPO-5 vs MAPO-5 -- show that cobalt is essential to the activation process. Prior work (1) indicates that the active state of the cobalt is tetrahedrally-coordinated Co(III) bound in framework metal atom positions of the molecular sieve. The overall reaction mechanism is believed to include the following steps:



The formation of  $\text{C}_3$  hydrocarbons could occur from reaction of methyl radicals ( $\text{CH}_3^\bullet$ ) with ethylene or from Bronsted acid catalyzed reactions involving

ethylene. All of the above reactions are believed to take place within the molecular sieve framework which selectively constrains the size and shape of the transition state species and the products.

Although we assume that the framework-bound cobalt is the active agent in this catalysis, there was evidence that air calcined and electrochemically stimulated beds of Co(II)-exchanged SAPO-34 and Co(II)-exchanged Y zeolite also produced detectable quantities of C<sub>2+</sub> hydrocarbons when exposed to methane at 500°C. This apparent catalytic activity of Co(II)-exchanged molecular sieves, which was actually predicted recently in the modeling work of Aparicio and Dumesic (5), is believed to occur by a mechanism that is separate from, but possibly related to, the one given above for framework-bound Co(II)/Co(III) in AlPO<sub>4</sub> molecular sieve structures.

The effectiveness of electrochemical stimulation as a redox activator was not unexpected in this work. There is increasing evidence (6) that molecular sieve materials are good ionic conductors at elevated temperature and have great potential for use in gas phase electrocatalysis applications. Also, Creasy and Shaw (7) recently demonstrated the electrocatalytic activity of CoAPSO-34 micro-electrodes in the presence of methane using cyclic voltammetry.

There are a number of aspects of the research findings described above that call for further, more detailed study. Other transition metals, such as manganese and iron, can be substituted into the framework of AlPO<sub>4</sub> molecular sieves (2,3) and these might also exhibit methane coupling activity. The fact that a variety of pore sizes and framework architectures are possible with AlPO<sub>4</sub> molecular sieves (2,3) should be exploited to determine the relationship between sieving properties and activity/selectivity. The optimum amount of transition metal substitution, the role (beneficial or otherwise) of non-redox type acid site creators (e.g., Si, Mg, Zn) in the framework, and the optimum balance between redox and non-redox framework metal atoms requires exploration. Factors such as framework demetalization, over-dehydrogenation (leading to soot formation), the need for oxygen potential control (to avoid destabilization of the framework structure), and the role of impurities (e.g., H<sub>2</sub>O) in the activation and ionic conduction processes all need to be elucidated. Foremost among the concerns stemming from our research to date are the causes of the gradual loss of catalytic activity observed for the CoAPSO-34 and CoAPO-5 sieve materials, and the implicit need for a methodology to identify/produce more stable, resilient transition metal-substituted AlPO<sub>4</sub> structures.

#### ACKNOWLEDGEMENT

This work was supported by the U. S. Department of Energy, Office of Basic Energy Sciences, Division of Advanced Projects, under contract W-31-109-ENG-38.

#### REFERENCES

- (1) L. E. Iton, I. Choi, J. A. Desjardins, and V. A. Maroni, *Zeolites* 9, 535 (1989).
- (2) R. J. Pellet, P. K. Coughlin, E. S. Shamsoum, and J. A. Rabo, in *Perspectives in Molecular Sieve Science*, W. H. Flank and T. E. Whyte, Jr., Eds., American Chemical Society Symposium Series No. 368 (1988) p.85.
- (3) E. M. Flanigen, R. L. Patton, and S. T. Wilson, in *Studies in Surface Science and Catalysis*, Vol. 37, P. J. Gobet, W. J. Mortier, E. F. Vansant, and G. Schulz-Ekloff, Eds. (Elsevier Publishers, Amsterdam, 1988) p. 189.

- (4) K. Otsuka, K. Jinno, and A. Morikawa, *J. Catal.* 100, 353 (1986).
- (5) L. M. Aparicio and J. A. Dumesic, *J. Molec. Catal.* 49, 205 (1989).
- (6) K. E. Creasy, *Electrochemical Society Extended Abstracts Vol. 89-2*, 972 (1989).
- (7) K. E. Creasy and B. R. Shaw, Department of Chemistry, University of Connecticut (work in progress).

Table I. Examples of Product Distributions from Typical<sup>a</sup> Methane Activation Experiments at 500°C

Molecular Sieve	Activation Method	Number of Passes	Product Distribution (Mole %)				
			CH <sub>4</sub>	C <sub>2</sub> H <sub>6</sub>	C <sub>2</sub> H <sub>4</sub>	C <sub>3</sub> H <sub>6</sub>	C <sub>3</sub> H <sub>8</sub>
CoAPSO-34	Air calcine	Single	65	15	12	1	7
	Electrochem.	Single	91	5	1	2	1
	Electrochem.	Multiple <sup>b</sup>	85	4	3	4	4
SAPO-34	Air Calcine	Single	99	— nil —			
	Electrochem.	Single	99	— nil —			
CoAPO-5	Air Calcine	Single	54	1	5	1	39
	Air Calcine	Multiple <sup>b</sup>	21	1	10	1	67
	Electrochem.	Single	58	2	4	4	32
MAPO-5	Air Calcine	Single	99	— nil —			
	Electrochem.	Single	99	— nil —			
Co(II)-EX <sup>c</sup> SAPO-34	Electrochem.	Single	98 <sup>d</sup>	0.5	0.4	0.3	0.3
Co(II)-EX <sup>c</sup> Y Zeolite	Electrochem.	Single	98	1	1	-	-
	Electrochem.	Multiple <sup>b</sup>	94	1	1	1	3

- (a) The data presented in this table were derived from averages of several of the better results obtained with each material.
- (b) In multiple pass experiments the unreacted methane and products from the first pass are recycled through the bed four or five additional times.
- (c) Indicates Co(II) exchanged molecular sieve material.
- (d) A fifth undetermined low molecular weight product was observed with Co(II)-exchanged SAPO-34. It was not acetylene, cyclopropane, or CO.

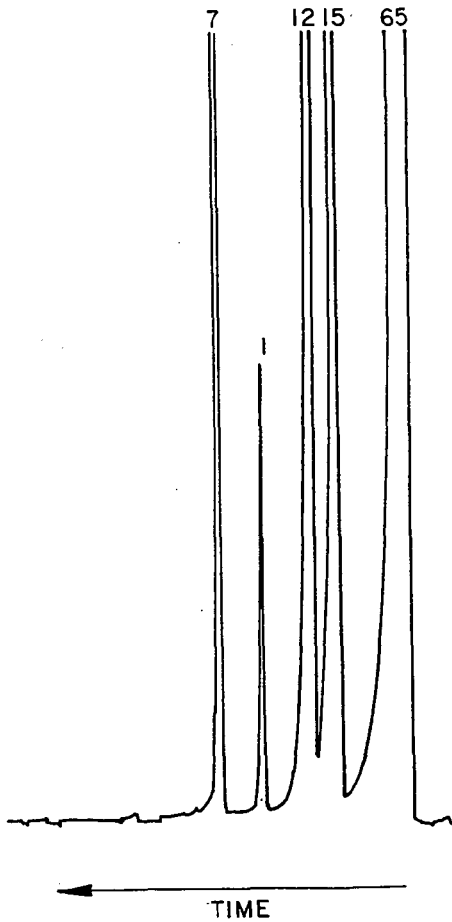


Figure 1. Gas chromatogram of the products from a typical single pass reaction of methane over air calcined CoAPSO-34 at 5000C. The numbers above each peak give the approximate mole percentages of each gas; i.e., 65% =  $\text{CH}_4$ , 15% =  $\text{C}_2\text{H}_6$ , 12% =  $\text{C}_2\text{H}_4$ , 1% =  $\text{C}_3\text{H}_8$ , and 7% =  $\text{C}_3\text{H}_6$ .

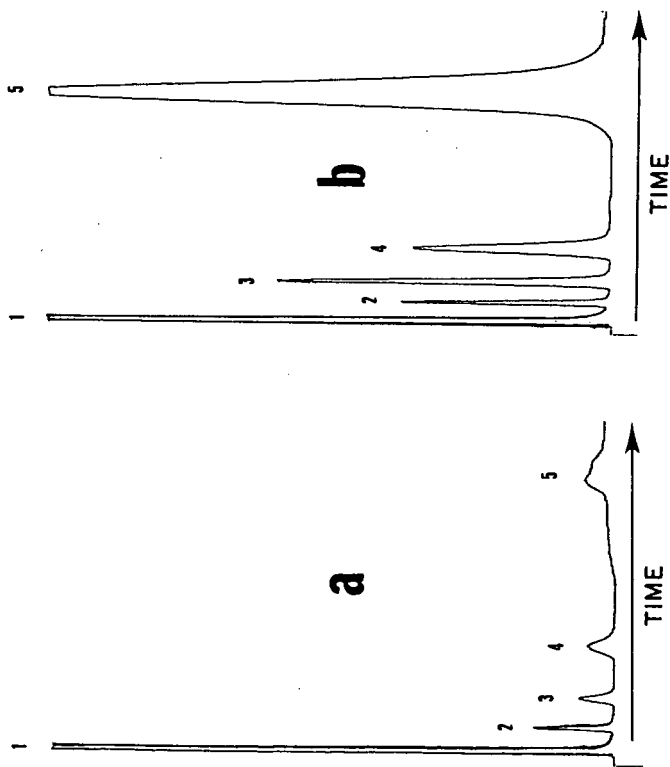


Figure 2. Results of single pass reactions of methane over electrochemically stimulated (10 V) CoAPSO-34 (insert a) and CoAPO-5 (insert b) at 5000C. Peaks 1 through 5 are  $\text{CH}_4$ ,  $\text{C}_2\text{H}_6$ ,  $\text{C}_2\text{H}_4$ ,  $\text{C}_3\text{H}_8$ , and  $\text{C}_3\text{H}_6$ , respectively.